UNIVERSITY OF TRENTO - Italy

International PhD Program in Biomolecular Sciences

Centre for Integrative Biology

30th Cycle

"Identification of REST-Regulated Molecular Circuitries and Targets Exploitable for hGSCs-Targeted Therapies"

Tutor

Prof. Luciano Conti

Laboratory of Stem Cell Biology

Centre for Integrative Biology, Università degli Studi di Trento

Ph.D. Thesis of

Jacopo ZASSO

Laboratory of Stem Cell Biology

Centre for Integrative Biology, Università degli Studi di Trento

Academic Year 2016-2017

Declaration of Original Authorship

I confirm that this dissertation is my own work and the use of all material from other sources has been properly and fully acknowledged.

Abstract

Glioblastoma (GBM) represents the most frequent and lethal cancer affecting the central nervous system for which no cure is currently available. The presence of Glioma Stem Cells (GSCs) has been proposed to be at the root of therapeutic failures due to their intrinsic abilities of escaping common treatments and relapsing the pathology. Thus, advances in therapeutic options may derive from the manipulation of mechanisms controlling the GSCs self-renewal, survival and functions. RE1-Silencing Transcription Factor (REST) is a master repressor of neuronal developmental programme in non-neuronal lineages, recently described as a main actor in the maintenance of the GSCs' tumorigenic competence as its knockdown strongly impairs GSCs stemness both *in vitro* and *in vivo*. However, REST is critical for restraining neuronal cellular identity in various tissues, so that a targeted therapy to this transcriptional repressor is likely to present numerous side effects.

Here, by taking advantage of a Tet-on system for the manipulation of REST expression in both human GSCs and Neural Stem Cell lines (hNSCs), we performed a transcriptomic profiling analysis in order to identify novel tumour-specific REST-regulated functions and molecular targets. Our analyses confirmed the previously reported roles of REST in neural tissues and enlightened novel REST functions in hGSCs, including the regulation of alternative hGSCs identity/state. Finally, analysis of hGSC-specific REST-regulated genes in GBM patients' dataset revealed an inverse correlation with glioma aggressiveness, thus establishing a hGSC REST score that might provide a useful prognostic tool.

Aim of the Research

The discovery of GSCs dramatically revolutionised the way GBM is conceived. The presence of cells with self-renewal abilities as well as the competence to originate the typical tumour heterogeneity, suggests that GBM mimics non-pathological tissues, having a pyramidal organisation with few slow-cycling stem cells as the truly responsible for cancer growth, and differentiated cancer cells with distinct neoplastic abilities composing the tumour bulk. The high rate of proliferation and the loss of DNA-repairing systems, sensitise differentiated cancer cells to common chemotherapeutics. However, such drugs are intrinsically inactive on more quiescent cells due to their mechanisms of action as well as the improved DNA-repairing activity and drugs efflux enzymes characterising hGSCs.

The discovery of cancer stem cells (CSCs) implies that standard GBM care is not aimed at targeting the tumorigenic stem compartment of GBM, and raises central questions in tumour biology: (i) how tumorigenic competence is established in cancer stem cells and (ii) how we could exploit this information in order to develop targeted and effective therapeutic options.

Previous studies suggest that pathways regulating multipotency in physiological hNSCs are also involved in sustaining GBM tumorigenesis. The Repressor Element 1 Silencing Transcription factor (REST) has been identified as master regulator of neuronal genes in non-neuronal cells, in order to restrict their expression to the nervous system. Tissue- and cell-specific functions of REST have been subsequently identified. In adult hNSCs, REST maintains self-renewal and represses neuronal differentiation in order to preserve the stem cell pool. Similarly, hGSCs multipotency is promoted by REST as its loss results in impairment of self-renewal and induction of differentiation and apoptosis processes leading to a significantly compromised tumor initiating capability. However, the mediators of REST's oncogenic competence in hGSCs are still very poorly characterised.

Aim of this project is to identify the molecular networks differentially regulated by REST in hGSCs and hNSCs, in order to (i) reach a deeper understanding of the role of REST in GBM, and (ii) isolate REST targets exclusively modulated in hGSCs as potential mediators of REST-induced tumorigenesis.

To achieve this purpose, the project has been subdivided in three sections:

i. *Generation and characterisation of hGSC and hNSC stable cell lines able to either knock-down or overexpress REST in an inducible way*. In order to identify the differential role(s) of REST in hGSCs and hNSCs, we generated stable tetracycline-inducible cell lines for the controlled REST overexpression or silencing. In these cells, we evaluated the kinetics of REST modulation achievable *in vitro*, and analysed the phenotypic alterations in hGSCs and hNSCs resulting either from REST overexpression or REST knock-down.

ii. *Characterisation of REST transcriptional activity in hGSCs*. The cells generated in previous section were used in gene expression analyses to identify differentially expressed coding transcripts in either REST overexpressing and REST knock-down hGSCs and hNSCs. By focussing particularly on hGSCs, we used a panel of bioinformatics tools to determine (novel) REST functions.

iii. *Identification of hGSC-specific REST-regulated targets*. In order to identify the REST targets selectively regulated in hGSCs, we compared the gene expression profile of REST-modulated hGSCs *versus* hNSCs and experimentally validated the list of hGSC-specific REST-regulated genes. Finally, we analysed the prognostic potential of the hGSC-specific REST-regulated genes in publicly available expression profile dataset of GBM patients.

Contents

INTRODUCTION 1

GLIOBLASTOMA MULTIFORME 2
1.1 BRAIN TUMOURS 2
1.2 GLIOBLASTOMA MULTIFORME 4
1.3 CLINICAL AND MOLECULAR CLASSIFICATION OF GLIOBLASTOMA 9
CANCER STEM CELLS OF GLIOBLASTOMA 15
2.1 THEORIES OF TUMOUR BIOLOGY 15
2.2 ADULT NEUROGENESIS AND NEURAL STEM CELLS 17
2.3 GLIOMA STEM CELLS 23
REPRESSOR ELEMENT 1 SILENCING TRANSCRIPTION FACTOR 26
3.1 DISCOVERY OF REST 26
3.2 MECHANISM OF ACTION OF REST 28
3.3 CONTROL OF REST EXPRESSION – FROM TRANSCRIPTIONAL TO POST-TRANSLATIONAL REGULATION 32
3.4 REST INVOLVEMENT IN STEM CELLS IDENTITY AND NEUROGENESIS 37
3.5 REST INVOLVEMENT IN CANCERS 40
3.6 REST IN GLIOBLASTOMA MULTIFORME 41

RESULTS 47

PREFACE 48
4.1 PREFACE 48
4.1 PINDUCER SYSTEMS FOR CONTROLLED REST EXPRESSION 49
GENERATION AND CHARACTERISATION OF HGSCS AND HNSCS SYSTEMS FOR INDUCIBLE SILENCING OF REST 51
5.1 GENERATION OF REST INDUCIBLE KNOCK-DOWN HUMAN GLIOMA STEM CELL LINES 51
5.2 GENERATION OF REST INDUCIBLE KNOCK-DOWN HUMAN NEURAL STEM CELLS 63
5.3 EFFECT OF REST LOSS OF FUNCTION ON HGSCS AND HNSCS PROPERTIES 65
GENERATION AND CHARACTERISATION OF HGSC AND HNSC SYSTEMS FOR INDUCIBLE OVEREXPRESSION OF REST 72
6.1 GENERATION OF REST INDUCIBLE OVEREXPRESSION HUMAN GLIOMA STEM CELL LINES 72
6.2 GENERATION OF REST INDUCIBLE OVEREXPRESSION HUMAN NEURAL STEM CELLS 79
6.3 EFFECT OF REST GAIN OF FUNCTION ON HGSCS AND HNSCS PROPERTIES 81
GENE EXPRESSION ANALYSIS OF REST MODULATED HGSCS AND HNSCS 88
7.1 COMPARING REST MODULATED HGSCS TO HNSCS REVEALS HGSCS SPECIFIC EFFECT OF REST 88
7.2 REST CONTROLS NEURAL MULTIPOTENCY THROUGH MODULATION OF NEURONAL DIFFERENTIATION, PROLIFERATION AND CELL METABOLISM 93
7.3 HGSC-SPECIFIC REST-REGULATED GENES REGULATES NEURONAL DIFFERENTIATION, PROLIFERATION AND CELL METABOLISM 101
7.4 REPRESSION OF HGSC-SPECIFIC REST REGULATED GENES IS ASSOCIATED TO POORER PROGNOSIS 105

CONCLUSIONS **108**

DISCUSSION **109**
8.1 HGSCS TARGETED THERAPY 109
8.2 REST CONTROLS DIFFERENTIATION AND QUIESCENCE MARKERS OF BOTH HGSCS AND HNSCS 110
8.3 REST ORCHESTRATES MULTIPLE PROCESSES TO REGULATE QUIESCENCE IN HGSCS 113
8.4 HGSC-SPECIFIC REST TARGETS REGULATE MULTIPOTENCY AND HAVE PROGNOSTIC RELEVANCE 116
8.5 FUTURE PERSPECTIVES AND CONCLUDING REMARKS 121

METHODS **124**

METHODS **125**
9.1 CELL CULTURES 125
9.2 PRODUCTION OF LENTIVIRAL PARTICLES CARRYING PINDUCER SYSTEMS 127
9.3 FLOW CYTOMETRY AND CELL SORTING 127
9.4 REAL-TIME QUANTITATIVE POLYMERASE CHAIN REACTION 128
9.5 IMMUNOBLOTTING 128
9.6 IMMUNOSTAINING 129
9.7 CELL PROLIFERATION ASSAY 129
9.8 MICROARRAY AND GENE EXPRESSION ANALYSES 130
9.9 STATISTICS 132
9.10 LIST OF PRIMERS 133
9.11 LIST OF ANTIBODIES 134

APPENDIX **135**

LISTS OF DIFFERENTIALLY EXPRESSED CODING GENES **135**

LIST OF ABBREVIATIONS **144**

BIBLIOGRAPHY **149**

SIDE PROJECT **169**

INDUCIBLE ALPHA-SYNUCLEIN EXPRESSION AFFECTS HUMAN NEURAL STEM CELLS' BEHAVIOR **170**
Preface 170
Authors contribution 170
Inducible Alpha-Synuclein Expression Affects Human Neural Stem Cells' Behavior 171

Introduction

Chapter 1

Glioblastoma Multiforme

Contents

1.1 BRAIN TUMOURS	**2**
1.2 GLIOBLASTOMA MULTIFORME	**4**
1.3 CLINICAL AND MOLECULAR CLASSIFICATION OF GLIOBLASTOMA	**9**

1.1 Brain tumours

Brain tumours constitute a heterogeneous family of neoplasia, characterised by abnormal and disorganised growth within the central nervous system (CNS). For simplicity, CNS tumours are classified according to the tissue of origin, with primary entities born within the CNS and secondary tumours deriving from the metastatic invasion by non-CNS derived cancers that occupy brain or spinal cord territories. Secondary brain tumours are the most common brain cancers in adults, having an incidence rate's ten times higher than primary brain tumours (**Subramanian et al., 2002**). These tumours most commonly derive from breast cancer, lung cancer, and melanoma (**Johnson and Young, 1996**) and, as subsidiary of malignant entities, they maintain the aggressiveness developed in the original site, causing neurological dysfunctions that result in important causes of both morbidity and mortality. Patients median survival following detection of brain metastases is only a year (**Subramanian et al., 2002**).

Primary brain tumours are the 17th most common group of cancers in the European Union, representing the 2% of the total tumour diagnosed, with an incidence of 42.547 new cases per year, corresponding to 6.9 per 100.000 people. They result in 4.9 per 100.000 individuals' mortality rate[1]. Even though they all derive from the CNS, primary brain tumours represent a heterogeneous group of malignancies each with a distinct natural history (**Buckner et al., 2007**). CNS tumour aggressiveness is evaluated according to the World Health Organisation (WHO) grading guidelines, first published in 1979 and reviewed periodically. Histological examinations of tumour specimens are used to identify tumour features concurring in defining tumour malignancy degree with the aim of helping the determination of the therapeutic regimen. These guidelines identify the following classes:

Grade I (or low grade) tumours: a biologically benign, circumscribed tumour possessing low proliferative potential, likely to benefit from surgical resection alone.

Grade II tumours (also considered low grade): incurable by surgery because of their infiltrative nature and sometimes tend to progress to higher grades.

Grade III tumours: fast growing malignant cancers showing nuclear atypia.

Grade IV tumours: high grade, mitotically active malignant cancers characterised by the presence of necrosis area and neo-angiogenesis, associated to rapid disease evolution and a very poor prognosis (**K.J., 1979; Louis et al., 2007**).

A third histopathological, classification of brain tumours according to the similarity with a putative cell of origin is historically considered to separate *gliomi* from *non-gliomi*, depending on the presence of predominant glial *versus* neuronal features and finally discern *gliomi* in astrocytic, oligodendroglial and astro-oligodendroglial lesions (**Table 1**).

[1] numbers for European Union - 27 states in 2012; rate is age standardised per 100.0000, both sexes. Sources: http://www.cancerresearchuk.org/ and http://eco.iarc.fr/

Tumour type	WHO grade	subtype
Astrocytic	I	subependymal giant cell astrocytoma
		Pilocytic astrocytoma
	II	Pilomyxoid astrocytoma
		Diffuse astrocytoma
		Pleomorphic xanthoastrocytoma
	III	Anaplastic astrocytoma
	IV	Glioblastoma
		Giant cell glioblastoma
		Gliosarcoma
Oligodendroglial	II	Oligodendroglioma
	III	Anaplastic oligodendroglioma
Oligoastrocytic	II	Oligoastrocytoma
	III	Anaplastic oligoastrocytoma
Neuronal and mixed neuronal - glial	I	Gangliocytoma
		Ganglioglioma
		Desmoplastic infantile astrocytoma and ganglioglioma
		Dysembryoplastic neuroepithelial tumour
	III	Anaplastic ganglioglioma
Embryonal	IV	Medulloblastoma
		CNS primitive neuroectodermal tumour (PNET)
		Atypical teratoid / rhabdoid tumour

Table 1.1 Summary of the main CNS tumours with classified for cell type and WHO grade according to Louis et al., 2007.

1.2 Glioblastoma multiforme

Glioma represents the most common brain tumour, accounting for the 70% of the intracranial neoplasia diagnosed every year in the adults (**Parsons et al., 2008**). Among these, *glioblastoma multiforme* (GBM), classified as WHO grade IV astrocytoma, and represent the most common glioma, comprising the 45.6% of the primary brain tumours. Glioma patients are generally diagnosed at 64 years and the median overall survival (OS) is 15 months from post-operative radiation and chemotherapy (**Stupp et al., 2005**). Only 5% of GBM patients survive over 5 years, and this measure decreases to 2% among patients older than 65 years, showing a survival inversely correlated with age (**Ostrom et al., 2014**). Even though 5% of GBM patients have a familial history of brain tumours, that is sometimes associated to the presence of other hereditary cancer syndromes, risk factors for GBM are

yet to be clearly defined (**Reuss and von Deimling, 2009; Weller et al., 2015**). Age is the main factor associated to the development of GBM, with an age-adjusted incidence of 0.15 per 100.000 in children rising to 15.03 per 100.000 in subjects aged 75-84 years. Males are slightly more affected than females (1.6:1) and whites than blacks (2:1) (**Ostrom et al., 2014**). The only environmental agents confirmed to increase the relative risk for glioblastoma is ionizing radiation of the brain (**Neglia et al., 2006; Ron et al., 1988; Sadetzki et al., 2005**). However, these do not include radiation scans performed according to diagnostic procedures (**Brada et al., 1992; Minniti et al., 2005**). The correlation between either the use of mobile phone or the exposure to electromagnetic fields and the development of brain tumours have been studied extensively, though with inconclusive results (**Ostrom and Barnholtz-Sloan, 2011**).

GBM mainly arise in cerebral hemispheres, mostly in the frontal (25.8%), temporal (19.7%), and parietal (12.2%) lobes while less than 5% of the cases arise in other brain area in the adults (**Figure 1.1A**) (**Ostrom et al., 2014**). Brainstem *gliomi* represents the vast majority in paediatric age (**Ostrom et al., 2015**). Despite the area of origin, high-grades *gliomi* are known for their extraordinary ability to invade neighbouring brain regions (**Furnari et al., 2007**), making GBM poorly curable by surgical resection. Secondary malignancies outside the brain have been reported to lungs, lymph nodes, bones, and liver, but represent rare cases, likely because of a poor adaptation of GBM cells to the metabolic and the immunological environment outside the CNS (**Fecci et al., 2014; Mashimo et al., 2014; Schweitzer et al., 2001**).

Overall, the clinical course of GBM is defined by tumour location and invasive dynamics within the brain parenchyma and there is no exemplary clinical presentation. Only rarely the disease remains stable over time. More frequently GBM exhibits suddenly, with a severe impact on the quality of life (**Keime-Guibert et al., 2007; Pérez-Larraya et al., 2011; Roa et al., 2004; Taphoorn et al., 2005**). GBM may manifest with headache, nausea, seizures, memory loss and confusion due the intracranial hypertension caused by the expansion of the tumour mass within the cranium. Moreover, patients with GBM may present with a range of neurologic deficits whose nature depends on the brain area interested by the disease (**Figure 1.1A**) (**Wen and Kesari, 2008**). Frontal lobe tumours commonly determine personality changes and mood disorders that can be mistaken for

symptoms associated to physiologic ageing process. About 20% of patients exhibit sensorimotor alterations as presenting symptom and 5% of patients present with aphasia with tumours arising in proximity of the Broca's and the Wernicke's area on the left hemisphere (**Yuile et al., 2006**). Temporal lobe tumours frequently result in epilepsy, that represent one of the main presenting symptoms (24-68% GBM) (**Breemen et al., 2009; Chaichana et al., 2009; Kerkhof et al., 2013; Wick et al., 2005**). Headache is another common presenting symptom in GBM (30% of patients) (**Yuile et al., 2006**).

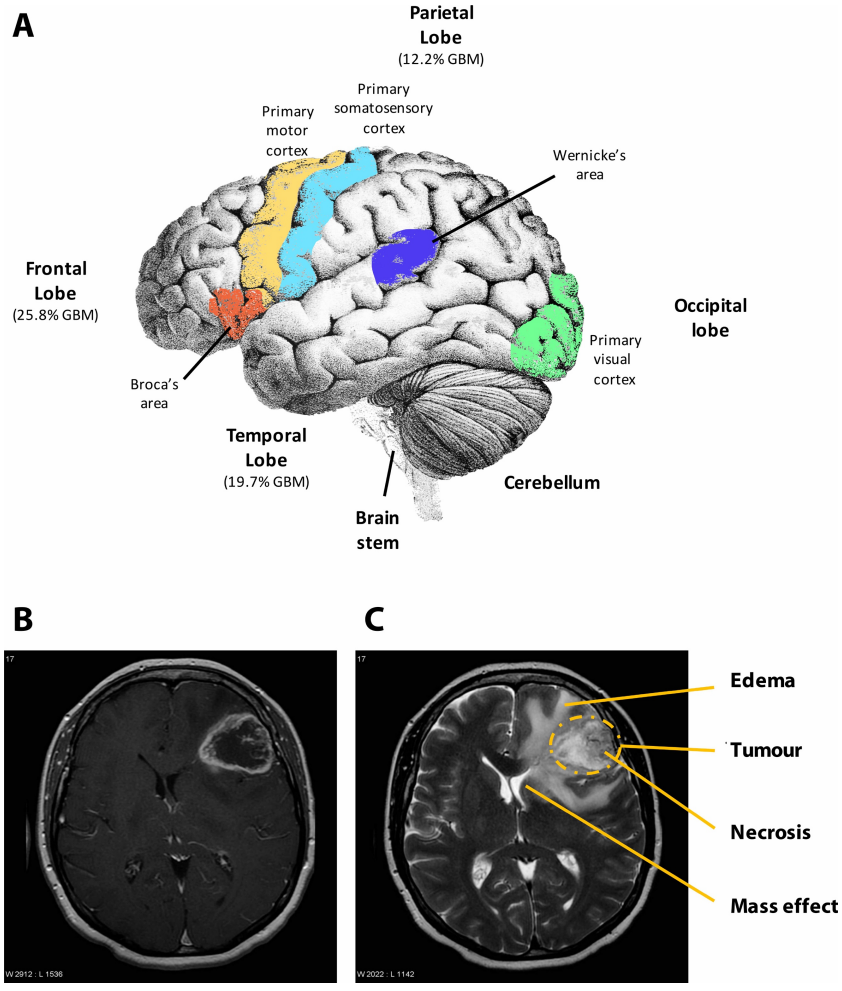

Figure 1.1. GBM localisation and diagnosis. A. Human cerebral cortex representation with frequency of GBM in the different cortical areas. Approximate localisation of eloquent areas is highlighted: (i) orange – Broca's area and (ii) violet – Wernicke's area controlling speech; (iii) yellow – primary motor cortex regulating voluntary movement; (iv) light blue – primary somatosensory cortex receiving sensory inputs from the periphery; (v) green – primary visual cortex permitting vision. Image modified from History.info website. **B**. Axial T1-C+ MRI and **C**. Axial T2W MRI showing a frontal lobe mass presenting necrosis, edema and mass effect. **B** and **C** are case courtesy of A. Prof Frank Gaillard, Radiopaedia.org, rID: 5292.

Onset of neurologic deficits is generally followed by magnetic resonance imaging (MRI) analysis showing, in the case of GBM, a mass with contrast enhancement at its margin due to blood-brain barrier disruption, central hypointensity on T2-weighted images in necrosis area, and perifocal hyperintensity on T2-weighted and fluid attenuated inversion recovery images indicative of either oedema or noncontrast-enhancing tumour (**Figure 1.1B**). Because less sensitive than MRI, computed tomography is performed only when MRI is unavailable or not possible. However, imaging scans reliability can vary and the diagnosis is confirmed only following analysis of the bioptic specimen (**Weller et al., 2014**).

Unless the tumour is multifocal or located in an "eloquent" area, i.e. areas unlikely to be resected without causing major disabilities, GBM patients are subject to surgical resection with the aim of removing most of the tumour mass. This treatment increases median overall survival from six to 12 months respect to biopsy only (**Figure 1.2A**) (**Yuile et al., 2006**). Daily radiotherapy of 60 Gy in about 30 fractions with concomitant adjuvant temozolomide (TMZ, 75 mg/m^2/day for six weeks) followed by cycles of TMZ at high-dose (150-200 mg/m^2 on days 1-5 every 28 days) prolong median OS from 12.1 to 14.6 months in patients with O^6-methylguanine-DNA methyltransferase (*MGMT*) promoter methylation compared to radiotherapy alone (**Figure 1.2B**) (**Hegi et al., 2005; Stupp et al., 2005; https://emedicine.medscape.com/**). Postoperative radiotherapy aims at reducing tumour proliferation or killing cancer cells through ionizing radiation-induced DNA damage (**Wirsching et al., 2016**) and is supposed to act synergistically with TMZ, a prodrug of the alkylating agent 5-amino-imidazole-4-carboxamide, administered orally few hours before radiotherapy. Once hydrolysed, TMZ acts by methylating O^3 site on adenines and N^7 and O^6 sites on guanines in genomic DNA causing cell cycle arrest at G2/M and eventually cell death resulting from the erroneous coupling of thymines to O^6-methylated guanine during DNA replication (**Lee, 2016**). Normally, DNA mismatch repair or base excision mechanisms are activated in order to repair methylated DNA. MGMT in particular has been shown to limit the efficacy of TMZ by transfer of the methyl group to an internal cysteine residue (**Bobola et al., 2015**). However, MGMT activity may vary widely between GBM patients and a reduced expression due to hypermethylation of its promoter region has been associated to better response to treatment with a 3.5 months increase in progression-free survival (PFS) (**Figure 1.2C**, **Bobola et al., 2015**). Despite this dismal increase in PFS and OS associated to TMZ administration, the side effects that accompanies the treatment are

quite severe, and comprise nausea and vomiting, constipation, headache, fatigue, anaemia, dyspnoea, and more rarely seizures, infection secondary to neutropenia, bleeding due to thrombocytopenia, liver disease and secondary cancers[2].

Very recently, the American food and drug administration (FDA) gave full approval on the use of bevacizumab, an anti-vascular endothelial growth factor (VEGF) recombinant antibody, in adult patients with recurrent GBM. This treatment is based on the evidence that, in order to progress and keep growing a tumour needs to sustain a high metabolic demand. The increasing nutrient supply is achieved through continuous neovascularisation, an event mainly governed by the VEGF signalling (**Batchelor et al., 2014**). Thus, the administration of antibodies anti-VEGF would impede the VEGF binding to its receptor and induce tumour starvation, limiting the tumour growth capabilities. The approval of bevacizumab is based on a still ongoing multicentre, randomised, open-label clinical phase III trial in which the addition of bevacizumab to lomustine chemotherapy[3] compared to lomustine alone was analysed. The first results of the trial indicate that the combination therapy is not effective on patients' overall survival, thus failing to meet the primary end-point of the study. However, it does prolong PFS from 1.5 to 4.2 months, therefore improving the quality of life of recurrent GBM patients (**Wick et al., 2017; https://www.gene.com/; EORTC 26101 ClinicalTrials.gov number, NCT01290939**). In Europe, bevacizumab is indicated for the treatment of different type of cancers in combination with chemotherapeutics. In 2014, the European Medicines Agency (EMA), rejected the request to change the marketing authorisation of bevacizumab for the use in newly diagnosed GBM in combination with radiotherapy and TMZ. Interestingly the rejection was based on the same result that led the FDA to approve the use of bevacizumab for recurrent GBM in the USA[4]. Currently there are 23 clinical trials ongoing in Europe evaluating the role of bevacizumab in combination with other drugs for the treatment of either newly diagnosed of recurrent glioblastoma (**https://www.clinicaltrialsregister.eu/**).

[2] http://www.merck.com

[3] Bevacizumab 10 mg/Kg every two weeks; Lomustine 90-110 mg/m2 every six weeks (cap. 160-200 mg)

[4] Source: http://www.ema.europa.eu/

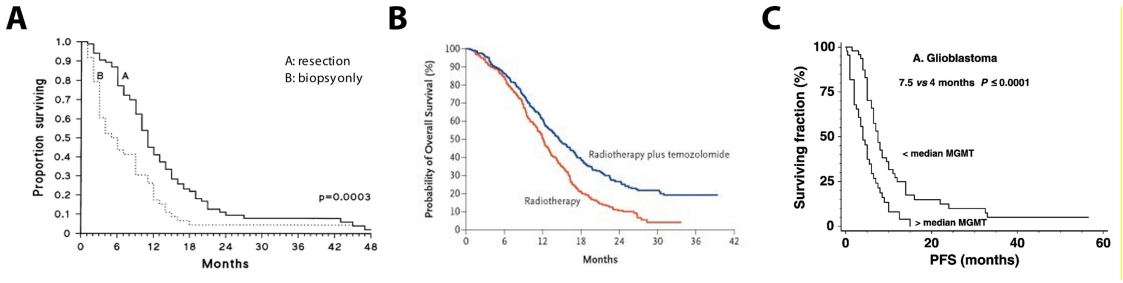

Figure 1.2. Therapeutic effect on GBM patients' overall survival. A. GBM patients survival related to degree of surgery (bulk tumour resection *versus* biopsy only) (**Yuile et al., 2006**). **B.** Kaplan-Meier curve of overall survival of GBM patients treated with radiotherapy associated to temozolomide administration *versus* radiotherapy only (**Stupp et al., 2005**). **C.** Progression free survival of GBM patients presenting different levels of MGMT activity (**Bobola et al., 2015**).

1.3 Clinical and molecular classification of glioblastoma

The vast majority of GBM is considered primary, therefore arising *de novo* within three to six months in elderly patients (mean 62 years), with only a dismal proportion (about 10%) representing an evolution from low-grade *astrocytomi* occurring in 10-15 years in younger patients (mean 45 years) (**Ohgaki et al., 2004**). Despite the different origin, primary and secondary GBM are histologically alike and molecular techniques are needed to distinguish the two subtypes. This discrimination has been proven to be prognostically meaningful by clinical analyses showing a slightly different outcome between primary and secondary GBM, with primary entities having a median OS of 4.7 months *vs*. 7.8 months in secondary diseases (**Ohgaki et al., 2004**). The first evidence of distinct genetic alterations between GBM subtypes were reported in 1996 by Kleihues and Ohgaki. Epidermal growth factor receptor (EGFR) overexpression and *tumor protein p53* (*TP53*) mutations were initially described as mutually exclusive in primary and secondary *glioblastomi* (**Watanabe et al., 1996**), suggesting not only the possibility to discriminate between the two phenotypes, but importantly, the existence of different genetic evolution pathways that may require different therapeutic treatments. Some year later, the same group reported that about 30% of primary GBM carry *TP53* mutations (**Ohgaki et al., 2004**) and therefore this marker

cannot be used as diagnostic parameter. The possibility to distinguish between the two subtypes of GBM became tangible after the identification of *Isocitrate dehydrogenase* (*IDH1/2)* gene mutations prevalently in secondary GBM (**Nobusawa et al., 2009**). *IDH1/2* mutation is one of the earliest event during gliomagenesis and persists in the progression from WHO II diffuse astrocytoma, or WHO III anaplastic astrocytoma to GBM (**Ohgaki and Kleihues, 2013**). The loss of 1p/19q in cells with *IDH1/2* mutation would then drive the low-grade glioma toward an oligodendroglial phenotype, while *astrocytomi* typically acquire *Tumor protein 53* (*TP53)* and *ATRX* mutations (**Figure 1.3**) (**Liu et al., 2012; Watanabe et al., 1996, 2001**). One consequence of the different genetic profile of primary and secondary GBM is the derivation from a different precursor cell population.

Other than patients' age distribution, the genetic differences between primary and secondary GBM also determine a divergent preferential location of the tumour. *IDH1/2* mutant GBM, as well as WHO II astrocytomi with *IDH1/2* mutations are more likely to develop in the frontal lobe and to present seizures as initial symptom (**Stockhammer et al., 2012**), while *IDH1/2* wild type GBM present widespread distribution (**Lai et al., 2011**). Similarly, *oligodendrogliomi* with 1p/19q loss form preferentially in the frontal lobe (**Laigle-Donadey et al., 2004**), further suggesting both secondary GBM and oligodendroglioma share a common origin (**Ohgaki and Kleihues, 2013**). These data suggest that primary and secondary GBM are *de facto* different tumour entities and should therefore be treated as such in order to improve patients' care.

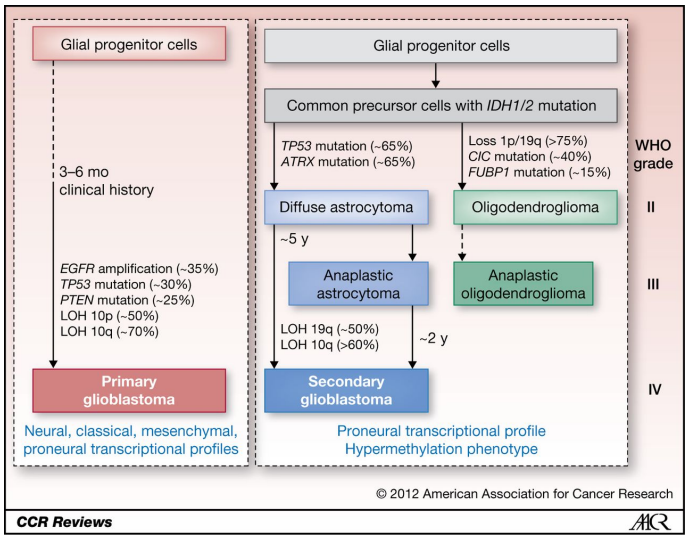

Figure 1.3. Genetic alterations leading to primary and secondary GBM. Image modified from **Ohgaki and Kleihues, 2013**.

With the aim of improving prognosis accuracy and identifying more effective treatments with a precision medicine point of view, more attention has been given to GBM molecular classification and its incorporation into routine tumour classification. The first guidelines in this direction were proposed by a delegation of the International Society of Neuropathology (ISN) in Haarlem, Netherlands, in May 2014 and then revised by the latest WHO classification of 2016. The "ISN Haarlem guidelines" indicate brain tumour diagnosis should be stratified hierarchically in layers, integrating histological classification, WHO grading, and finally molecular information (**Louis et al., 2014**). According to these guidelines, GBM is now partitioned into two main groups: the *IDH* wild type, accounting for 90% of the pathologies, and the *IDH* mutant. These are further subdivided depending on other common mutations. *IDH* wild type GBM frequently present mutations in the tumour suppressor *phosphatase and tensin homolog on chromosome 10* (*PTEN*), deletion of *cyclin-dependent kinase inhibitor 2A* and *2B* (*CDKN2A/B*), promoter mutations in the *telomerase reverse transcriptase* (*TERT*) leading to its overexpression, copy number gains on chromosome 7 and monosomy of chromosome 10 (**Aldape et al., 2015**). *TERT* promoter mutations, often associated to EGFR amplifications, are mutually exclusive with the *IDH* mutant associated ATRX mutations (**Killela et al., 2013**). Other mutations are recurrent in IDH wild type GBM, comprising *TP53*, *neurofibromatosis type 1* (*NF1*), *platelet-derived growth factor A* (*PDGFRA*), *hepatocyte growth factor* (*MET*), *cyclin-dependent kinase 4* and *6* (*CDK4* and *CDK6*) and the TP53 negative regulator *murine double minute* (*MDM2*) (**Aldape et al., 2015; Brennan et al., 2013**).

The Cancer Genome Atlas (TGCA) project also proposed a parallel molecular classification method for GBM, not based on common mutations, but on large-scale gene expression data. Integrating 200 GBM and two non-pathological brain samples, the TGCA established an 840 genes signature able to segregate GBM into four subtypes, based on the most similar neural cell type in terms of gene expression, in four main classes: *proneural*, *neural*, *classical* and *mesenchymal* (**Figure 1.4**, **Verhaak et al., 2010**).

The *classical* subtype is characterised by concomitant amplification of chromosome 7, loss of chromosome 10 and *EGFR* amplification. No mutations at the *TP53* locus, even if it is the most frequently mutated gene in GBM. Homozygous deletion of *CDKN2A* and high

expression of neural stem cell markers such as Nestin, Notch and Sonic Hedgehog family members.

The *mesenchymal* subtype present often hemizygous deletion of the 17q11.2 region harbouring *NF1* gene and a low expression level of NF1. This subtype is named after a peculiar expression of mesenchymal markers, such as *chitinase-3-like protein 1* (*CHI3L1*) and *MET* other than the astrocytic markers *CD44, MER proto-oncogene tyrosine kinase* (*MERKT*) and tumor necrosis factor (TNF) and nuclear factor kappa B (NF-κB) families' pathways that might be associated to the presence of white cells and necrosis.

The focal amplification of the 4q12 locus, containing *PDGFRA*, has been observed in all glioblastoma subtypes, though with a particular high frequency in the proneural phenotype. Consistent with a marked prevalence of *IDH* mutations, most of the secondary GBM and an overall younger age of patients are characteristics of this class. Finally, the *proneural* group shows a high expression of oligodendrocytic development genes and proneural genes, such as *doublecortin* (*DCX*), *ascheate-scute family bHLH transcription factor 1* (*ASCL1*), *transcription factor 4* (*TCF4*) and *sex determining region Y-box* (*SOX*) genes. According to the gene expression, gene ontology (GO) categories associated to this phenotype are involved in development and proliferation.

Expression of neuronal markers and a particular affinity to normal brain gene expression profile are the signature of the *neural* class of GBM, with genes mainly involved in neuron projection and synaptic function.

Despite the gene expression differences, that seem to indicate distinct tumour entities with specific driving pathways and progenitor cells, TGCA project report actually suggest the molecular subtypes of GBM behave similarly in terms of OS and macroscopic histological features. However, it is interesting to note that the response to chemotherapy may vary according to the phenotype. Verhaak and coworkers compared GBM subtype with OS in patients treated with an intensive therapy, which is now the standard treatment of concurrent chemotherapy and radiotherapy plus more than three cycles of chemotherapy, with a less intensive therapy in which the patients were treated either with a non-concurrent chemotherapy and radiotherapy or less than four cycles of chemotherapy. Only the classical and mesenchymal phenotypes resulted more sensitive to an aggressive chemotherapy, with a significant improvement in OS (**Verhaak et al., 2010**). Hence,

patients with a *neural* or *proneural* GBM, that do not experience increase in OS with the standard GBM care, might benefit from a less aggressive treatment at least in terms of side effects related to it.

Even if they are still not considered in the day to day clinical practice, the molecular subclasses of GBM are now widely used in research in the effort of identifying a more precise therapy. For instance, the concurrent use of bevacizumab in addition to the standard chemo and radiotherapy in newly diagnosed GBM was shown to prolong PFS, but not OS (**Gilbert et al., 2014; ClinicalTrials.gov number, NCT00884741**). However, a retrospective analysis suggested that a specific subgroup of patients, that are the *IDH* wild type *proneural* GBM, did benefit from bevacizumab as part of the front-line care, with an increase in OS from 12.8 to 17.1 months (**Sandmann et al., 2015**). Another study focussing on the *mesenchymal* GBM reported a significantly shorter OS associated to a high mesenchymal signature and a lower response to radiotherapy (**Bhat et al., 2013**).

However, concerns about the reliability of the TGCA molecular classification might be risen following few reports suggesting the different classes do not embody steady features representative of the whole tumour entity but might be considered pictures of unstable tumour identities or even represent an average of more subclasses present in the same tumour. In an elegant work, Patel and colleagues analysed single-cell transcriptome profile of five freshly resected GBM samples describing tumours composed of more than one molecular subtype and even single cells with a mixed phenotype (**Patel et al., 2014**). Moreover, the modulation of transcription factors has been shown to induce a switch from a molecular class to another (**Bhat et al., 2013**), suggesting a certain degree of plasticity governed GBM cell and further validation is needed before considering molecular classes as diagnostic tool.

Following the four-tier molecular classification based on transcriptome profiles, the TGCA project proposed a stratification of GBM based on DNA methylation profiles and associated gene mutations (**Brennan et al., 2013; Noushmehr et al., 2010**). Even if epigenetic marks are largely dynamic during cell differentiation or transformation, some DNA methylation pattern is retained as a sort of epigenetic memory and since they reflect the cell history, can be used for lineage classification (**Kim and Costello, 2017**). As a consequence, the molecular classification of GBM based on DNA methylation patterns is supposed to be

more reliable than transcriptome profile classification. The survival advantage in the *proneural* subclass was associated to a glioma-CpG island methylator phenotype (G-CIMP), while non-G-CIMP *proneural* and *mesenchymal* GBM showed the poorer outcome respect to the other subtypes (**Brennan et al., 2013**).

With the same goal of identifying new therapeutic approaches for GBM, Kim and colleagues proposed an alternative classification method based on micro-RNAs (miRNAs) and mRNAs expression profile (**Kim et al., 2011**). The miRNA clusterisation method identified five GBM groups resembling, and named after, all the differentiation stages of neural precursors during brain development and indirectly insinuate GBM can arise from the transformation of cells at each of these stages. Interestingly, most of the *oligoneural* GBM, that presented a lower age at diagnosis and a better prognosis respect to the other subclasses, were also classified as *proneural* using the Verhaak stratification. Also, the *radial glial* and *astrocytic* groups, that are mainly composed of the Verhaak classical and *mesenchymal* subclass respectively, showed a better response to therapy, recapitulating what already observed in the TGCA report (**Kim et al., 2011; Verhaak et al., 2010**).

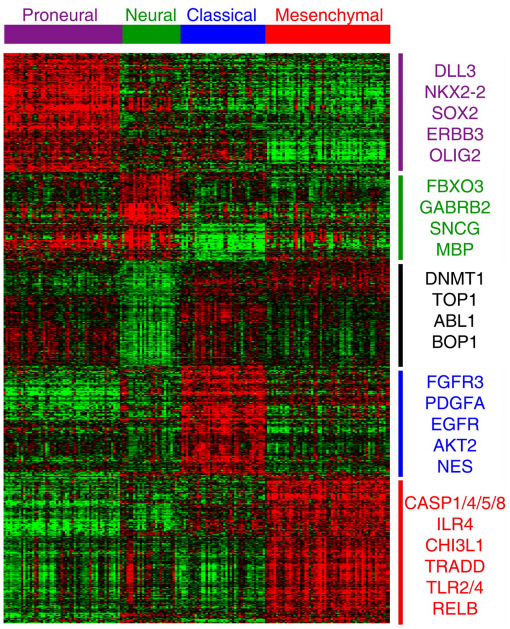

Figure 1.4. Clusterisation of GBM patients in molecular subtypes on gene expression data. Heatmap showing the predictive 840 gene list used to identify GBM molecular subtypes (**Verhaak et al., 2010**).

Chapter 2

Cancer Stem Cells of Glioblastoma

Contents

2.1 THEORIES OF TUMOUR BIOLOGY	**15**
2.2 ADULT NEUROGENESIS AND NEURAL STEM CELLS	**17**
2.3 GLIOMA STEM CELLS	**23**

2.1 Theories of tumour biology

Traditionally, a tumour is conceived as a heterogeneous cellular mass yet presenting a homogeneous proliferative ability and sharing the same genetic alterations. According to the traditional, or stochastic view of tumour biology, every cancerous cell would be able to proliferate extensively and to generate secondary tumours. The heterogeneity would derive stochastically from both intrinsic and extrinsic influences able to activate the cell potential asynchronously, and determine the proportion of tumour cells destined to proliferate while others will differentiate (**Beck and Blanpain, 2013**). However, when analysed for their tumorigenic potential, using serial xenotransplantation in animal models, not all the tumour cells are able to generate a secondary tumour. The first shake to the traditional view has been given by Bonnet and Dick, that in 1994 identified of a subpopulation of acute myeloid leukemia (AML) cells with a unique ability of regenerating the tumour. Even though they represented only 0.1% of total tumour cells, the $CD34^{+}/CD38^{-}$ AML cells were the only able to phenocopy the original tumour once transplanted in immunosuppressed mice (**Bonnet and Dick, 1997**). Interestingly, the

$CD34^+/CD38^-$ cell population corresponds to the stem cells responsible for the generation of almost the totality of the red and white cell lineages in the hematopoietic system, i.e. the one affected in acute myeloid leukemia (**Seita and Weissman, 2010**). The first cancer stem cell (CSC) population was thus identified. Starting from this evidence, the stochastic biology of tumours has been challenged by a new perspective, picturing tumours as normal tissues with an acquired ability of eluding the physiological growth regulation. A hierarchical organisation governs tissue homeostasis and assign specific roles to the different layers of cells. Grossly three types of cells can be identified in every tissue, relating self-renewal and tissue-specific functions: (i) multipotent adult stem cells (ASCs) reside at the apex of the pyramid and are responsible for the maintenance of tissue homeostasis and repair through the ability of long-term self-renewal, i.e. cell division followed by a cell fate decision with at least one daughter cell retaining the stem cell potential of the mother, and the capacity to give rise to functional and tissue specific differentiating daughter cells, (ii) committed progenitors already destined to a particular terminal cell phenotype, with a limited but burning proliferative capability and (iii) differentiated effector cells that characterise the tissue functions and physiology with no renewal capacity and constitute the great majority of the cells. The progressive acquisition of tissue-specific features and functions is therefore accompanied by the loss of renewal ability. Tightly controlled signalling pathways regulate the transition from one state to another. For instance, Repressor element 1 silencing transcription (REST) factor maintains the neural stem cells (i.e. the stem cells of the brain compartment; NSCs) in a multipotent state by promoting their self-renewal and repressing the expression of genes involved in neuronal function. During neuronal differentiation, REST levels gradually decreases, permitting the neuronal phenotype to emerge (**see chapter 3 for details**). Similarly, a tumour would be organised hierarchically, with few cancer stem cells responsible for its growth and their differentiated progeny constituting the tumour bulk (**Reya et al., 2001**). Following the original report by Bonnet and Dick, many other studies have isolated population of cells with high tumour propagating potential, from both liquid and solid tumours, such as chronic myeloid leukemia, breast cancers, colorectal carcinoma, pancreatic cancers, prostate cancers and brain cancers (**Al-Hajj et al., 2003; Collins et al., 2005; Li et al., 2007; Reya et al., 2001; Ricci-Vitiani et al., 2007; Singh et al., 2004; Sirard et al., 1996**). Even though the frequency and features of the CSCs from different tumours is variable, by comparing tumorigenic

potential of bulk versus CSCs, every study independently proved that the latter were the only able of tumour initiation. CSCs from different tumours are substantially dissimilar from each other and share more features with the ASCs of the tissue from which the tumour derive from. Signalling pathways regulating of NSCs are therefore shared with brain CSCs, in which they often transform in tumour-related circuits because of their involvement in grounding stem cells features and therefore, potentially oncogenes or tumour-suppressor. Notch pathways controls self-renewal and inhibits differentiation of NSCs, but has also been identified as regulator of brain CSC tumorigenesis (**Androutsellis-Theotokis et al., 2006; Gaiano et al., 2000; Zhu et al., 2011**). Similarly, other pathways governing self-renewal and multipotency have been investigated extensively, and considered as therapeutic targets (**Liebelt et al., 2016**). Moreover, the reduced cell cycle progression and the high expression of drug-efflux systems in common between ASCs and CSCs determines an intrinsic resistance to cytotoxic agents that represent one of the main motivation for therapeutic failure due to tumour relapses (**Clarke et al., 2006**). Decades after the first isolation, no specific markers have been described, so that CSCs are still identified functionally with a set of *in vitro* and *in vivo* assays aimed at verifying their self-renewal and differentiation ability, as well as their tumorigenic potential, with the ultimate assay being the recapitulation of the patient's tumour complexity in serial orthotopic transplantation.

2.2 Adult neurogenesis and neural stem cells

It is now established that GBM is organised hierarchically, and glioma stem cells (GSCs) are main drivers of tumorigenesis, drug resistance and tumour relapses. However, the path that took to the discovery and isolation of GSCs has been long and could not be accomplished without the description of neurogenic processes, and the subsequent/concomitant characterisation of NSCs.

The first observation of cell division in the adult rodents' brain, specifically in the subventricular zone (SVZ) lining the lateral ventricle, was reported in 1961, when autoradiography was used to detect tritiated thymidine incorporated into dividing cells' DNA, injected into mice brain (**Smart and Leblond, 1961**). Until that time, neurogenesis in

higher vertebrates was believed to be restricted to embryonic development, and inhibited in the post-natal and adult life, in order to preserve the complex integrity of the brain (**Altman, 1962; Palmer et al., 1995**). Using the same techniques, dividing cells were subsequently revealed also in the dentate gyrus of the hippocampal subgranular zone (SGZ) (**Figure 2.1A**, **Altman, 1963**). Neurogenesis is, however, a multistep process not limited to NSC proliferation, but consisting also of neuroblast migration to the final destination, differentiation and integration into neural circuits. It was therefore the detection of adult born neurons that proved adult neurogenesis to actually takes place. Altman and Das described the migration of postnatally born cells from the subventricular zone to the olfactory bulb, where they differentiate (**Figure 2.1B**, **Altman, 1969; Altman and Das, 1965**), and years later Kaplan and Hinds detected newly formed neurons in the adult dentate gyrus (**Kaplan and Hinds, 1977**). The main neurogenic areas as we know them today were therefore, discovered. Studies in birds confirmed adult neurogenesis is not a specific features of mammals, and for the first time showed that adult born neurons functionally integrates into pre-existing neural circuits and are electrophysiologically competent (**Goldman and Nottebohm, 1983; Paton and Nottebohm, 1984**). Whether adult neurogenesis was conserved in humans remained, however, an unfounded assumption until the analysis of post-mortem brain of cancer patients administered with bromodeoxyuridine, a thymidine analogue used as diagnostic, then stained with neuronal markers (**Figure 2.1C**, **Eriksson et al., 1998**). Retrospective birth dating using ^{14}C was later applied to determine cells' turnover in the adult human brain, indicating the continuous addition of about 700 new neurons per day in humans (**Spalding et al., 2013**).

Some recent evidences are now questioning whether neurogenesis actually takes place in primates' dentate gyrus, including humans, or it is lost during evolution (**Sorrels et al., 2018**). Nevertheless, the isolation of adult NSCs from many brain regions suggest these cells might cover functions other than neurogenesis (**Lie et al., 2002; Palmer et al., 1995, 1999; Shihabuddin et al., 1997; Tropepe et al., 2000; Weiss et al., 1996**). NSCs were indeed demonstrated to exert the so-called "bystander effects", releasing growth factors and neurotrophins to sustain neuronal survival, modulate immune system recruitment and reduce blood brain barrier damage following an insult (**Drago et al., 2013; Kokaia et al., 2012; Ottoboni et al., 2017**).

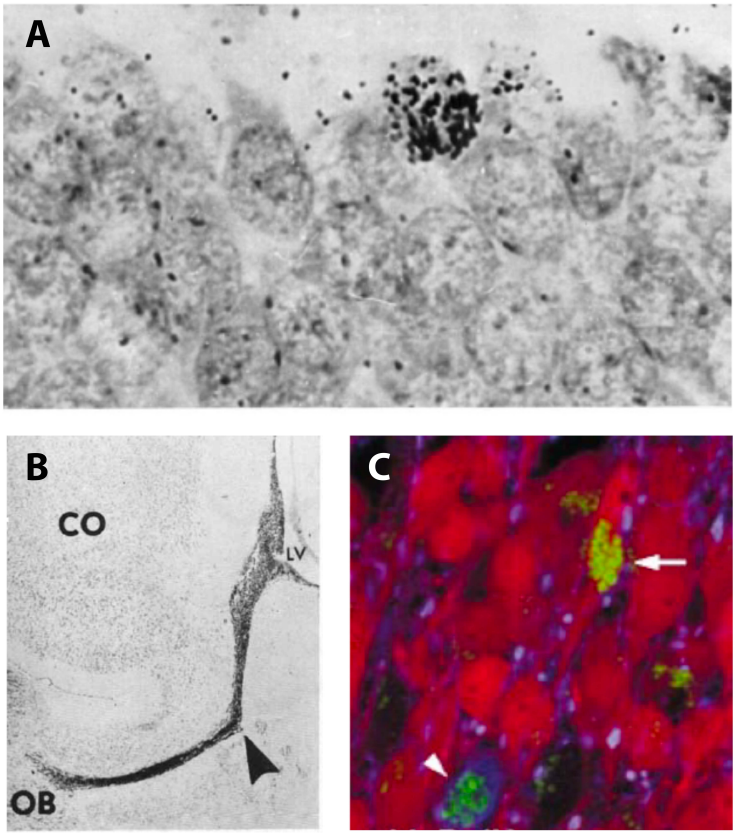

Figure 2.1. First evidences of adult neurogenesis in rodents and human brain. A. Dentate gyrus granule cells from rat hippocampus labelled with tritiated thymidine (**Altman, 1963**). **B.** Sagittal section of a 21 days old rat brain showing tritiated thymidine labelled cells in the lateral ventricle (LV) and the rostral migratory stream (arrowhead) of neuroblasts migrating towards the olfactory bulb (OB) (**Altman, 1969**). **C.** BrdU-labelled cells (green) in adult human dentate gyrus. Calbindin-expressing neurons are stained in red; GFAP positive astrocytes are stained in blue (**Eriksson et al., 1998**).

In the late 1980s pioneering studies started to set the conditions for culturing neural precursors *in vitro*. In 1988, Ron McKay's group described the use of a temperature sensitive variant of the oncogene SV40 T antigen, to control neural progenitors' differentiation. Cerebellar Nestin-positive foetal cells could be maintained as self-renewing neural progenitors at 33°C, a temperature permissive for the oncogene to be active, or pushed to differentiate into neurons or glia, by increasing the temperature to 39°C. Also, the authors noticed that differentiation could be induced by co-culturing neural progenitors with other foetal neural cells (**Frederiksen et al., 1988**). It became gradually clear that multipotency is not an intrinsic cell-autonomous feature of NSCs, but self-

renewal and differentiation are balanced through environmental signals. Immortalisation systems through oncogenes overexpression were able to provide for the low number of neural progenitors resulting from primary culture, pushing their proliferation while maintaining an immature phenotype. In these conditions however, the cell state was forced by the genetic manipulation, weakening the physiological relevance of the model. Sally Temple was the first to describe a primary oncogene-free "culture system in which cells capable of division can divide and differentiate into neurons and/or glia" (**Temple, 1989**). These cells were dissected from embryonic rat brain, mechanically dissociated, and cultured as single cells in presence of embryonic brain cells as feeder. Of the surviving cells, 19% divided during the first day in culture and about half of these kept proliferating, generating small clones with neuronal and glial morphology. Immunocytochemical staining for a neurofilament protein to identify neurons and glial-fibrillary acidic protein (GFAP) as astroglial marker were used to confirm the cell identity (**Temple, 1989**). This represented a proof of concept, that neural progenitor cells can be isolated and cultured *in vitro* without genetic transformation. In these conditions, however, the proliferative and differentiative potential of the isolated cells were limited and uncontrolled. More defined control systems needed to be developed in order to generate more stable, reproducible and tuneable NSC cultures. The hypothesis was to play with three components to find the right culture conditions: extracellular matrix components, adhesion molecules and soluble growth factors that are expressed in the developing brain or showed to have trophic effects on neural cultures (**Murphy et al., 1990**). Murphy and colleagues first reported the use of basic fibroblast-growth factor (bFGF/FGF2) to stimulate proliferation and survival of embryonic neural progenitors. Dissected neuroepithelial cells from E10 mice, cultured in presence of bFGF, formed "clusters of round cells which were not adherent and increased in size both in time up to 4-5 days and also according to the concentration of FGF" (**Murphy et al., 1990**). The same year, another growth factor was shown to have a similar effect on neural progenitors derived from E13.5-14.5 rat striatum. The exposition of neural precursors to bFGF followed by the administration of the neurotrophin nerve growth factor (NGF) was shown to specifically stimulate their self-renewal potential, with no effects on the proliferation of more differentiated cells. Furthermore, the subsequent removal of growth factors induced differentiation (**Cattaneo and McKay, 1990**). These cells, however, could

not be maintained for long time *in vitro*, appearing reminiscent of primary cultures rather than NSCs, that as such are supposed to self-renew virtually indefinetely.

Two years later, the identification of Epidermal Growth factor (EGF) and EGF receptor in the adult rodents and human brain, prompted Reynolds and Weiss in testing its effect on neural cells isolated from striatal area (including the SVZ) of 3 and 18 months mice. While most of the cells died after two days in culture, unsupported by the selected culture medium, about 1% of them adhered to the culture plate and proliferated. Few days later, the growing colonies detached, forming floating spheres of nestin immunoreactive cells. To test the potential of the cells composing the spheres, these three-dimensional structures were subsequently dissociated and plated as single cells in what will be later known as the *neurosphere assay*. New spheres were generated, in presence of EGF, with the majority of the cells expressing nestin, suggesting self-renewal ability. Importantly, the *neurosphere assay* can be reiterated serially, increasing exponentially the quantity of neural progenitors in culture. When transferred to poly-l-ornithine coated plates and left in culture for 21 days, the spheres adhered and the nestin-positive cells started to migrate out of the sphere and gradually differentiate in neurofilament-positive neurons with a round soma and thin processes, or stellate-shaped, GFAP immunoreactive astrocytes (**Reynolds and Weiss, 1992**). This represented a ground-breaking finding not only for the identifications of culture conditions for long term maintenance of neural progenitors *in vitro*, preserving their multipotency. For the first time a population of neural progenitors could be isolated from adult brains.

Following the same line, three years later, Gage and co-authors described the isolation of NSCs from adult hippocampi, SVZ, striatum and septum. Neural cells were isolated from rats older than three months and cultured in presence of bFGF, already proved to stimulate survival and proliferation of foetal hippocampal progenitors, while the adhesion was supported by coating the plastic supports with poly-l-ornithine and laminin (**Gage et al., 1995; Palmer et al., 1995; Ray et al., 1993**). Under these conditions the cells were maintained in culture for the remarkable time of one and a half years, suggesting a virtually unlimited self-renewal capacity. Although representing a mixed population of cells expressing markers of progenitors as well as of more differentiated cells, the nestin immunoreactive cells gradually became the major component, suggesting the culture

conditions are selective for the propagation of immature neural cells. The removal of bFGF from culture medium was shown to induce differentiation in both neurons and glia (**Gage et al., 1995; Palmer et al., 1995**). Another striking finding derived from the demonstration that cultured neural progenitors are able to differentiate *in vivo*, producing both neurons and astrocytes (**Gage et al., 1995**).

The culture system developed by Gage were subsequently optimised, allowing the maintenance of pure populations of NSCs *in vitro*, anyway preserving their multipotency. Conti et al. identified culture conditions to convert murine embryonic stem cells into NSCs and applied them to the isolation of NSCs directly from murine foetal CNS. Primary forebrain cells were harvested and cultured in presence of both EGF and bFGF. These cells spontaneously produced neurosphere-like floating aggregates, subsequently moved to laminin-coated wells to let them adhere. Cells outgrowing from these floating spheres presented a homogeneous bipolar morphology, expressed markers typical of neural progenitors such as nestin, paired box 6 (pax6) and SRY-box 2 (sox2) and could be serially propagated without losing multipotency. These cells were named “NS cells”. Differently from the previous protocols, no differentiated cells were found in presence of EGF and bFGF, but promptly appeared upon growth factor withdrawal or when reinjected in the mouse brain. Further evidences indicated these cells represent the resident stem cells within the neurospheres. Not only these implemented culture conditions allowed for the first time to maintain *in vitro* pure populations of NSCs, but they could also be applied for the derivation of NSCs from human foetal brain. (**Conti et al., 2005**). NS cells were successively derived with high efficiency also from adult mouse and human brain, demonstrating the Conti’s protocol is suitable for generating homogeneous NSCs from different sources (**Pollard et al., 2006; Sun et al., 2008a**).

2.3 Glioma stem cells

The very same techniques used for isolating and culturing NSCs from human foetal brain were applied by Peter Dirks' laboratory to retrospectively determine whether human brain tumours also contains CSCs, and share the hierarchical organisation already described in leukemia and breast cancer (**Al-Hajj et al., 2003; Bonnet and Dick, 1997; Lapidot et al., 1994**). In 2003, Singh and colleagues used the Reynolds and Weiss neurosphere protocol to derive and characterise glioma cells. Following the logic that took to the identification of CSCs from leukemia, Singh segregated glioma cells according to the expression of Prominin1/CD133, a transmembrane glycoprotein involved in NSC maintenance, but also expressed by endothelial and hematopoietic progenitors (**Salven et al., 2003; Yin et al., 1997**), determining that the $CD133^{+}$ brain tumour cells share overlapping features with NSCs. These cells, that were consequently termed "brain tumour stem cells" (BTSCs), can be propagated as non-adherent spheres in presence of growth factors, express the neural immature cell marker nestin and differentiate in neuronal-like and glial-like cells upon growth factors removal (**Singh et al., 2003**). To test the tumorigenic ability of BTSCs, $CD133^{+}$ and $CD133^{-}$ cells were separated from dissociated primary neurospheres and injected into immunodepressed mice. Only the $CD133^{+}$ cells were able to generate tumours. Moreover, these experimental cancers presented histological features phenocopying the cytoarchitecture and behaviour of the original human pathology. The ability to self-renew *in vivo* was also demonstrated through serial transplantation and isolation of BTSCs (**Singh et al., 2004**). Even if GBM cell lines cultured in serum are also capable of generating tumours in experimental models, these models are achieved with much less efficiency and accuracy than BTSCs (**Galli et al., 2004; Lee et al., 2006**). Despite these remarkable results, $CD133^{-}$ glioma stem cells (GSCs) were later shown to contain populations of cells with stem cell properties and tumorigenic capability, and therefore CD133 could no more be considered a cancer stem cell markers for brain tumours (**Beier et al., 2007**).

Even though effective in enriching NSCs, neurosphere condition is associated to critical problems: (i) the efficiency of NSC isolation is low, (ii) neurospheres does not represent pure populations of NSCs, rather the minority of NSCs is subject to spontaneous differentiation and cell death (**Figure 2.2A**), (iii) differentiation of NSCs cultured as neurospheres appear biased toward the astroglial lineage, (iv) the spheroid architecture

makes biochemical analyses challenging. All these issues might stem from the same three-dimensionality that characterise the neurospheres, limiting the diffusion of nutrients, oxygen and growth factors to the inner cells, and consequently affecting both survival and multipotency (**Conti et al., 2005; Woolard and Fine, 2009**). With this in mind, the protocol for isolating and culturing human adult NSCs in adhesion has been adapted for the isolation and expansion of GSCs (**Pollard et al., 2009b; Sun et al., 2008a**). As already demonstrated for NSCs, the uniform access to nutrients provided by adherent cultures suppressed spontaneous differentiation and cell death, allowing the expansion of pure population of GSCs, homogeneously expressing neural progenitor markers (**Figure 2.2A-B**). The generation of multiple cell lines from distinct subtypes of *gliomi*, indicated that specific features of the original tumour are recapitulated *in vitro*. Cell morphology, differentiation and invasive capability, in particular, were demonstrated to be cell line-specific. For instance, while most of the GSC lines mainly generate neuronal-like and astroglial-like cells when subjected to differentiation condition, a GSC line derived from a GBM with oligodendrocyte component, were found expressing markers of oligodendrocyte precursors in presence of EGF and bFGF, and mature oligodendrocyte upon differentiation. These peculiarities also emerged when the cells were tested for their tumorigenic potential. Consistently with BTSCs derived as neurospheres, the orthotopic transplantation of 100 cells in immunodeficient mice was sufficient to generate tumours phenocopying the original human disease features. This improved protocol also allowed for the isolation of GSCs with 100% efficiency, thus solving all the main issues related to neurospheres cultures (**Pollard et al., 2009a, 2009b; Reynolds and Vescovi, 2009**).

The discovery of GSCs represented a fundamental milestone in the study of GBM, opening new therapeutic options. Many studies focused on the elucidation of molecular mechanisms governing GSC tumorigenic properties and how these ultimately influence tumour behaviour. Lineage tracing experiments using mouse models have proved that a subpopulation of glioma cells with features of quiescent stem cells is responsible for tumour recurrences following temozolomide-induced initial remission (**Chen et al., 2012**). More recently, DNA barcoding has been used trace freshly dissociated cells from GBM patients upon injection in immunodeficient mice. GBM heterogeneity appears mainly driven by hierarchies of stem cells having distinct aggressiveness and treatment resistance, rather than stochastic genetic variations, and can therefore emerge as result of cell fate

decision, further supporting the CSCs theory picturing tumour growth as reminiscent of normal tissue development. While primary GBM appeared formed by many clones of cells with similar growth potential, temozolomide treatment generate a disparity in recurrent diseases, with resistant clones emerging to sustain tumour growth. This result suggests that GSCs are responsible for recurrence (**Lan et al., 2017**).

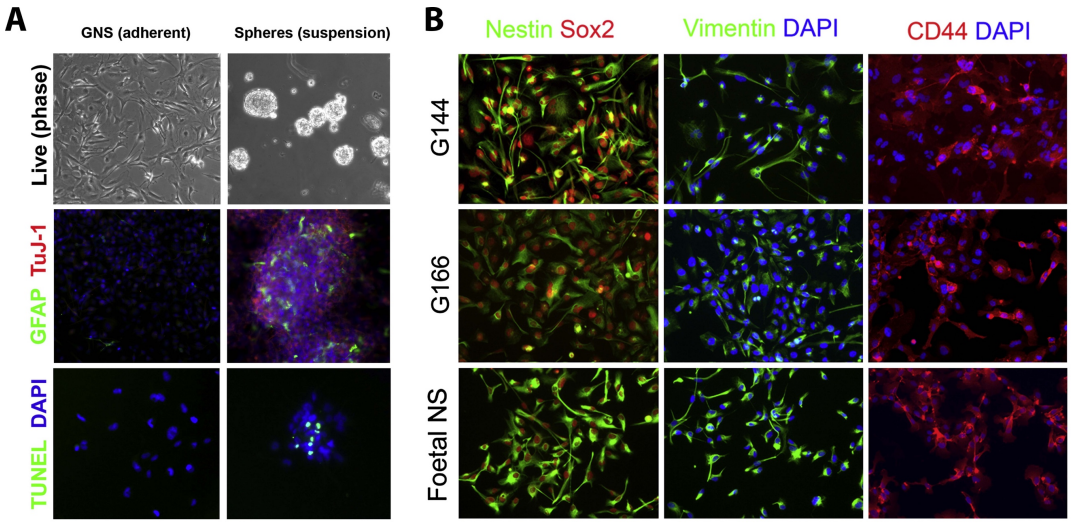

Figure 2.2. hGSCs and hNSCs cultures *in vitro*. A. Comparison of culture conditions for maintaining hGSCs *in vitro* (monolayer *versus* suspension). TuJ-1 and GFAP are used as markers of neuronal and astroglial phenotype, respectively. Tunel staining indicates apoptosis. **B.** Picture showing homogeneous expression of neural progenitor markers in both foetal-derived NS cells and hGSCs (G144 and G166) cultured on laminin substrate. Image modified from **Pollard et al., 2009b**.

Chapter 3

Repressor Element 1 Silencing Transcription Factor

Contents

3.1 DISCOVERY OF REST	**26**
3.2 MECHANISM OF ACTION OF REST	**28**
3.3 CONTROL OF REST EXPRESSION – FROM TRANSCRIPTIONAL TO POST-TRANSLATIONAL REGULATION	**32**
3.4 REST INVOLVEMENT IN STEM CELLS IDENTITY AND NEUROGENESIS	**37**
3.5 REST INVOLVEMENT IN CANCERS	**40**
3.6 REST IN GLIOBLASTOMA MULTIFORME	**41**

3.1 Discovery of REST

The Responsive Element 1/Neuron Restrictive Silencing Element (RE1/NRSE), a consensus 21 base pairs sequence, was identified in 1992 as a DNA region conferring neuronal specificity to the type II voltage-dependent sodium channel (*Scn2a*) expression in the vertebrate nervous system (**Kraner et al., 1992**). Three years later, the protein responsible for restricting *Scn2a* expression to neurons was identified and was named *Repressor Element 1 (RE1) Silencing Transcription* (REST) *factor* or *Neuron Restrictive Silencing Factor* (NRSF) (**Chong et al., 1995; Schoenherr and Anderson, 1995**). In the developing mouse embryo, REST was found expressed almost ubiquitously outside of the nervous system, and particularly in those cell types that do not express *Scn2a* (**Chong et al., 1995**). Independently, REST was detected in non-neuronal tissues and undifferentiated neural progenitors and was indicated as master negative regulator of neurogenesis following the

discovery of its ability to selectively repress neuron-specific genes through RE1 (**Schoenherr and Anderson, 1995**).

REST is a Krüppel-type zinc finger transcription factor, a family of proteins involved in several cellular processes, among which proliferation and differentiation, and for this reason, often associated to cancer development (**Tetreault et al., 2013**). After the initial studies reporting the identification of an increasing number of REST target genes involved in the regulation of neuronal processes, RE1 sequences were gradually identified also in genes not necessarily associated to neuronal function. Physiologically, REST is considered a regulator of embryonic and neural development and maturation (**Aoki, 2018; Gao et al., 2011; Kuwahara, 2013; Martin et al., 2015; Nechiporuk et al., 2016**). The combination of computational and biochemical approaches permitted the identification and classification of RE1-containing promoter regions for genes belonging to several functional categories beyond the neural/neuronal ones (**Bruce et al., 2004; Johnson et al., 2007**). Among the almost 2000 RE1 sites identified in the human genome to date, at least 40% reside close to genes expressed within the nervous system and potentially involved in neuronal function, including neurotransmitter receptors and transporters, ion channels, and vesicle trafficking and fusion, as well as genes involved in neuronal differentiation and maturation processes, e.g. axon guidance. More than 50% of the identified RE1-containing genes are not strictly regulators of neuronal activity, and are more generally associated to cell metabolism, signalling pathways, and transcription factors. Interestingly, a subset of these genes is involved in cardiac function and endocrine system development (**Bruce et al., 2004; Johnson et al., 2007**).

The canonical RE1 sequence contains two bipartite conserved sequences composed of ten base pairs divided by two nucleotides with no sequence specificity. However, by means of ChIPseq studies, Johnson and colleagues identified noncanonical RE1 sequences presenting a longer central spacer and reaching 30 base pairs (**Figure 3.1**, **Johnson et al., 2007**).

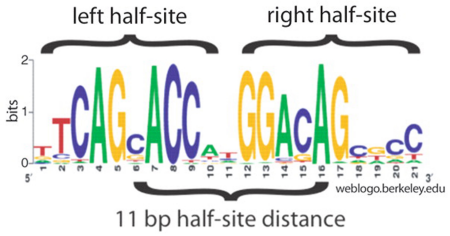

Figure 3.1. Canonical REST-binding motif (RE1, Johnson et al., 2007).

3.2 Mechanism of action of REST

To allow wrapping of the long eukaryotic genome into the nucleus, DNA interacts with histones in complexes knows as nucleosomes, that are further packed to form the chromatin. The compact and protective chromatin architecture impedes direct accessibility by regulatory complexes and the transcriptional machinery so that the expression of inaccessible genes is blocked. Local modifications of the chromatin structure are performed by chromatin-modifying enzymes to allow access to specific genes. The chromatin-modifying enzymes act through either reversible post-translational modifications of histones, to change histone-DNA interactions in order to move, disrupt or assembly nucleosomes, or DNA methylation and demethylation to regulate direct access to particular DNA sequences (**Becker and Workman, 2013; Jones et al., 2015**).

The transcriptional repression activity exerted by REST is achieved through epigenetic remodelling of the chromatin landscape into a close environment, inaccessible to non-pioneering transcription factors, i.e. transcription factors able to bind condensed chromatin. In order to mediate its function, REST orchestrates several chromatin remodelling enzymes able to remove modifications associated with active gene transcription and position marks associated to transcriptional repression in a stepwise fashion (**Ooi and Wood, 2007**). This is achieved through the particular "modular" structure of REST, in which the central eight zinc-fingers domain composes the DNA binding domain that mediates the recognition of RE1/NRSE sequences, while the C-terminal and N-terminal regions interact with two separate corepressor complexes: CoREST and mSin3a, respectively. REST functions therefore as a bridge, bringing histone deacetylases, demethylases and methylases complexes to target genes (**Figure 3.2**, **Ooi and Wood, 2007**). More in details:

1. ***CoREST complex*** is composed of histone deacetylases 1 and 2 (HDAC1/2), the SWI/SNF-related matrix-associated actin-dependent regulator of chromatin, subfamily A member 4 (SMARCA4/BRG1), lysine-specific histone demethylase 1A (KDM1A/LSD1), and the euchromatic histone-lysine N-methyltransferase 2 (EHMT2/G9a)
2. ***mSin3a complex*** comprises HDAC1/2, the retinoblastoma binding proteins 4 and 7 (RBBP4/7) and other proteins which function is still to be determined.

Once recruited to RE1 sites through its zinc-fingers domains, REST access to DNA is secured by SMARCA4/BRG1 through nucleosome repositioning (**Ooi et al., 2006**). Histone deacetylase complexes recruited by REST corepressors are then activated to remove acetyl groups from lysine residues of histone 3 and histone 4 (**Grimes et al., 2000; Huang et al., 1999; Naruse et al., 1999; Roopra et al., 2000**). In particular, deacetylation of the histone 3's lysine 9 (H3K9) promotes the KDM1A/LSD1 removal of histone 3's lysine 4 (H3K4) methylations (**Lee et al., 2005**) and EHMT2/G9a dimethylation of H3K9 itself (**Roopra et al., 2004**). Interestingly, long-term repression of REST target genes can be accomplished by stabilisation of the chromatin condensation when methylated H3K9 is bound by HP1 and recruited by adjacent nucleosomes (**Lunyak et al., 2002; Roopra et al., 2004; Wood et al., 2003**), although it is unclear how long the repression would last. In particular situations involving loss of REST, such as neuronal differentiation, RE1-containing genes repression can be maintained by CoREST and methyl-CpG-binding protein 2 (MECP2) (**Figure 3.2**, **Ballas et al., 2005; Lunyak et al., 2002; Yang et al., 2006**)**.** Two classes of REST target genes have been described according to their dependency on REST presence at their promoter. Loss of REST from RE1 triggers *Class I* genes maximal expression, while the occupancy of CoREST and MECP2 on *Class II* genes promoter secure the transcriptional repression. However, upon neuronal differentiation, membrane depolarisation determines the loss of corepressors and increased expression of the expression of *Class II* target genes (**Ballas et al., 2005**).

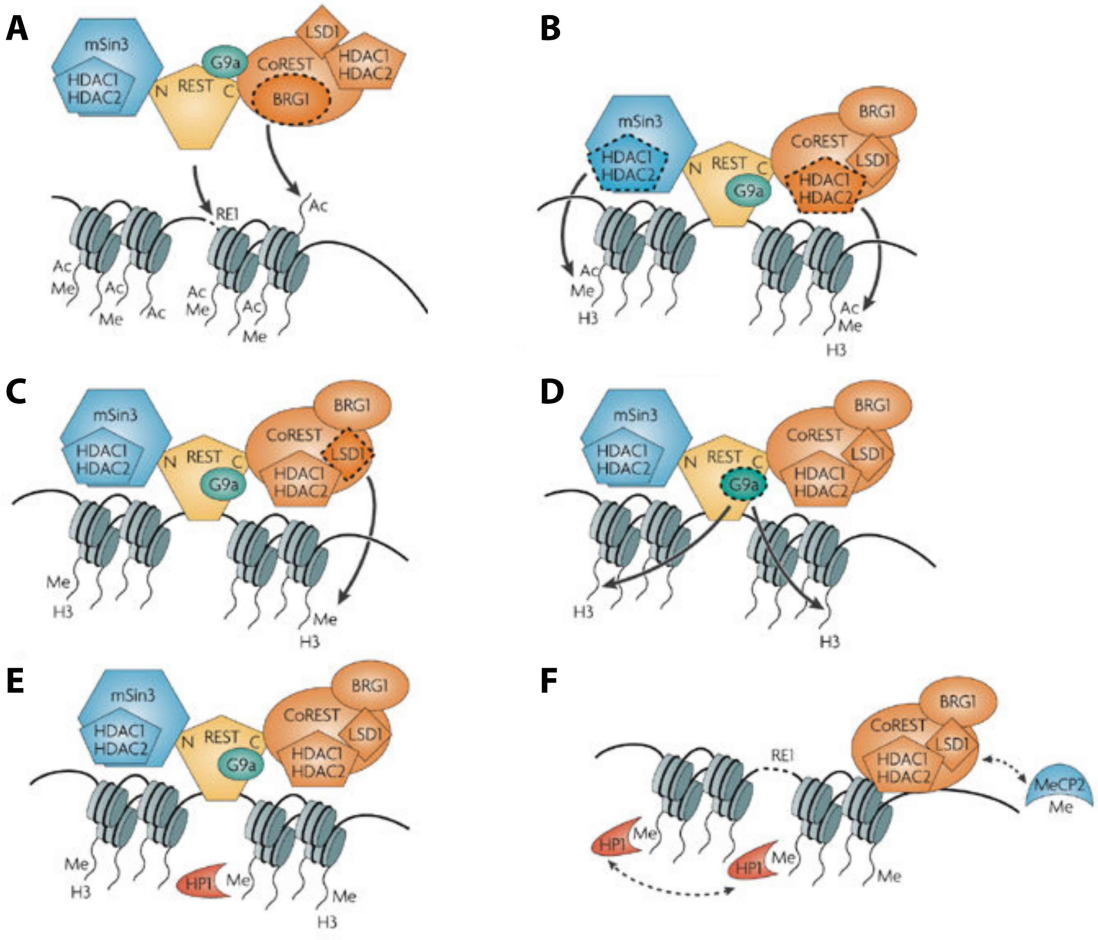

Figure 3.2 Schematic representation of REST mechanism of action. A. Recruitment of REST to RE1 sites and stabilisation of the binding to DNA through nucleosome repositioning exerted by the chromatin-remodelling enzyme BRG1. REST corepressors mSin3 and CoREST are subsequently recruited to amino and carboxy *termini* of REST. **B.** HDACs deacetylate lysine residues on histones H3 and H4. H3K9 deacetylation results in **C.** induction of LSD1 activity and **D.** H3K9 methylation by G9a, which recruit HP1 (**E**). **F.** Methylated RE1-containing genes are maintained repressed by CoREST and MeCP2 when REST is lost (i.e. during neuronal differentiation). HP1 interaction to DNA can create a compact chromatin state resulting in long-term gene silencing. Image modified from (**Ooi and Wood, 2007**).

REST repressive activity is not exerted exclusively through chromatin modification but is also mediated by direct action on the transcriptional machinery. REST has been described to mediate the activation of the RNA polymerase II small CTD phosphateses (SCPs), resulting in the inhibition of the RNA polymerase II (**Yeo et al., 2005**), and to inhibit the formation of the preinitiation complex, by direct binding on the TATA-box-binding protein (TBP, **Murai et al., 2004**).

The recruitment of different corepressors might produce the juxtaposition of specific chromatin modifications resulting in both tissue specificity of REST targets and distinct levels of gene repression (**Ballas et al., 2005; Ooi and Wood, 2007**). Trimethylation of histone 3's lysine 27 (H3K27) has been found particularly associated to the recruitment of CoREST, while most of the H3K4 trimethylation and H3K27 acetylation were mainly found in sites bound by REST-mSin3a. However, no pathway was found enriched in REST-CoREST *versus* REST-mSin3a bound genes (**Rockowitz et al., 2014**).

Although it is still unclear how corepressors are selected, as for other transcription factors (**Leung et al., 2004**), it has been proposed that the differences in RE1 sequences might have a role in the recruitment process. Three RE1 types have been classified upon comparison of REST binding in eight neural- and non-neural human cell lines: *common*, *restricted* and *unique* RE1-containing genes. *Common RE1s*, mainly corresponding to canonical RE1s, were located close to genes involved in intrinsic cellular processes and neuronal function. These RE1s are characterised by a repressive chromatin state due to H3K9 dimethylation and H3K27 trimethylation and consistently they are expressed at very low levels. Lineage- and tissue-specific processes were instead enriched in genes with *restricted* or *unique RE1s*. Interestingly, these genes were found more expressed than the ones with *common RE1s* and presented a bivalent epigenetic signature, i.e. presence of markers associated to both active and repressive chromatin state, featuring H3K9 and H3K27 acetylation, and H3K4 methylation as markers of active chromatin, as well as H3K27 trimethylation (**Bruce et al., 2009**), possibly due to a co-regulatory activity from other transcription factors or cofactors. Interestingly, the great majority of the identified binding sites were cell line specific, insinuating most of the REST activity is cell- or tissue-dependent.

The lineage specificity of REST targets was further explored by means of ChIP-sequencing and RNA-sequencing data from 15 cell lines, including self-renewing human embryonic stem cells (hESCs) and hESC-derived neurons, $CD4^+$ T cells and tumour cell lines of different origins. Only 7% of the 16.913 identified non-redundant REST binding regions, corresponding to 10.286 genes and miRNA, presented common RE1s to all the cell types considered, while 77% were shared by two or more cell lines and 16% were cell type-specific. Common REST targets exhibited lower expression levels with respect to shared and cell-specific targets (**Rockowitz et al., 2014**).

Comparative genomic analyses of REST binding also identified a certain degree of species-specificity in its activity, with ancient sites having more affinity for REST than lineage-specific RE1s (**Johnson et al., 2009**). More in detail, the comparison of REST binding sites in human *versus* murine ESCs suggested that the human-specific REST targets are more devoted to neuronal processes and involved in learning and memory and regulation of transcription, while the murine-specific REST targets were prevalently associated to signal transduction. Among the human-specific genes, in particular, several identified targets are known causal genes for several neurodegenerative diseases, suggesting that REST activity is selectively evolving as a regulator of neural functions, and that its dysfunction can lead to altered brain functions resulting in CNS disorders (**Rockowitz and Zheng, 2015**).

3.3 Control of REST expression – from transcriptional to post-translational regulation

REST gene is localised on the 4q12 chromosome (**Cowan et al., 1996**) and is composed of three main exons, highly conserved in the portion coding for the corepressors-binding and DNA-binding domains, an alternative neural-specific exon, and three non-coding alternative exons. (**Tapia-Ramrez et al., 1997; Thiel et al., 1998**). The DNA-binding domain is composed of seven zinc-fingers coded by exon IV and VI, while the zinc-finger domain associated to nuclear import is coded by exon V[5] (**Figure 3.2A**).

REST pre-mRNA is subject to alternative splicing events originating several transcripts that present different numbers of zinc-finger domains (**Figure 3.2B**). A different affinity to DNA depends on the extent of the DNA binding domain and results in a proportional gene repression activity (**Palm et al., 1999**). The neural-specific exon drives a frameshift in the coding sequence causing the formation of a truncated protein (named "sNRSF/REST4") containing only five zinc-finger domains and lacking the carboxy-terminal/CoREST binding domain, due to the premature introduction of a stop codon (**Figure 3.2B and 3.3**, **Shimojo**

[5] atlasgeneticsoncology.org

and Hersh, 2003). REST4 has been shown to act mainly as REST dominant negative by competing for RE1s and therefore promoting target de-repression (Raj et al., 2011; Tabuchi et al., 2002). The inclusion of the neural exon seems to be driven by the splicing regulator nSR100, whose expression in non-neural cells is controlled by REST itself, in a pivotal mechanism to avoid neuronal genes expression (Raj et al., 2011).

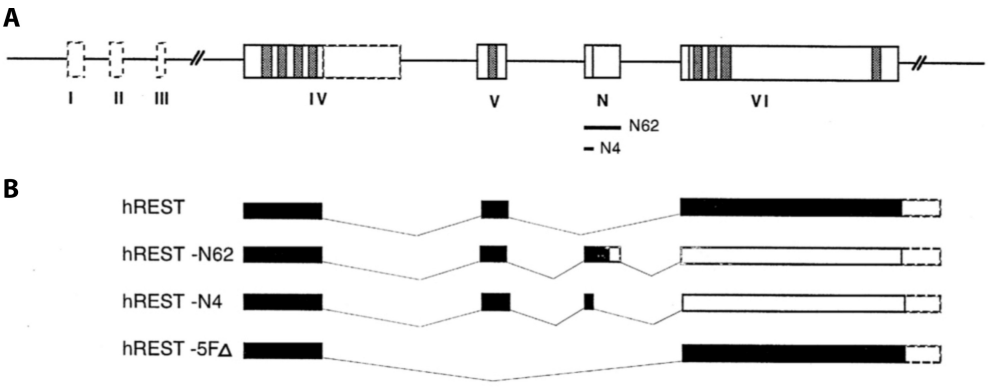

Figure 3.3. Illustration of REST gene and alternative splicing transcripts. A. Organisation of human REST gene. Exons are drawn as boxes with (i) solid outlines for coding exons and (ii) dashed outlines for untranslated exons. Introns are shown as lines. Grey bars indicate zinc-finger motifs. **B**. illustration of alternative splicing transcripts of human REST. Black boxes correspond to the open reading frame. hREST transcript result in full length REST. hREST-N62 and hREST-N4 are both translated as REST4, while in hREST-5FΔ exon V, containing a zinc-finger/NLS motif, is skipped (Palm et al., 1999).

The three alternative untranslated 5' exons (Exons I, II, and III in **Figure 3.2A**) have been associated with different promoters and transcription start sites and are characterised by GC boxes recruiting the Sp1 transcription factors to enhance REST expression. All the alternative exons have been found to drive REST expression in distinct cell types and therefore their function is still unclear, although it has been hypothesised that they might direct cell- or tissue-specific isoforms (Koenigsberger et al., 1999; Kojima et al., 2001; Palm et al., 1998).

Depending on the context, different factors are involved in the control of REST expression, both as positive or as negative regulators. REST promoter contains binding sites for Nanog and POU class 5 homeobox 1 (Oct4) that stimulate REST expression in both human and murine ESCs (Johnson et al., 2008; Loh et al., 2006). The presence of a T-cell transcription

factor (TCF) binding site in the upstream alternative exon determines the transcriptional activation of REST through canonical Wnt signalling (**Nishihara et al., 2003**), that sustains self-renewal of both embryonic, neural and cancer stem cells (**Holland et al., 2013**).

A negative regulation is exerted by the retinoic acid receptor (RAR), commonly involved in neuronal differentiation, which binds REST promoter at the level of the retinoic acid receptor element (RARE) located upstream of the transcription start site and thus represses REST expression (**Ballas et al., 2005**). Finally, the presence of RE1 sequences at REST promoter, suggests the existence of a negative feedback loop regulating REST excess (**Qureshi and Mehler, 2009**).

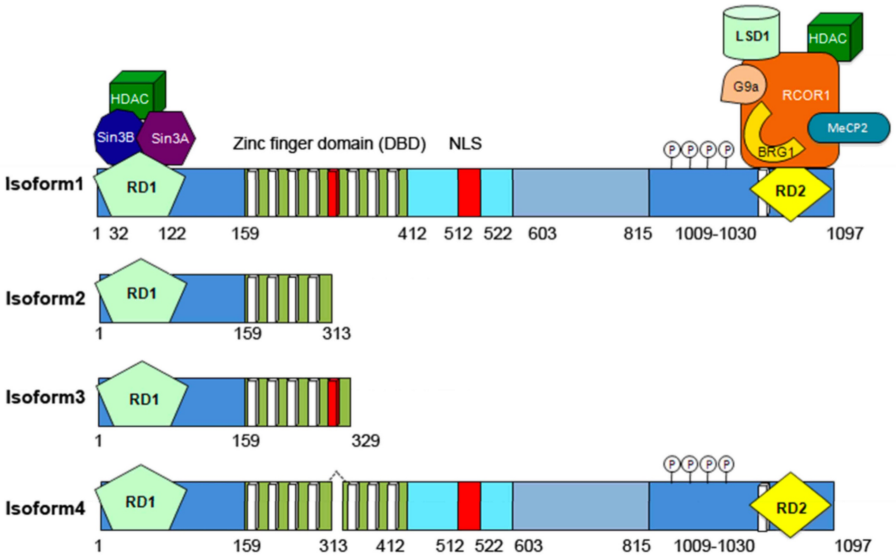

Figure 3.4. Illustration of REST protein isoforms. Isoform 1 represent full length REST protein of 1097 amino acids and 122 kDa (before post-translational modifications). Repressor domain 1 (RD1) at N-terminus is shown to bind to Sin3a/b and HDAC, while RD2 bind to CoREST complex. DNA-binding/Zinc finger domain is represented by alternate white and green bars between amino acids 159 and 412. Nuclear localisation signal (NLS) are shown in red. Isoform 2 is truncated before the NLS and localise in the cytoplasm. Isoform 3 (REST4) is also truncated, due to inclusion of a neuron-specific exon containing a stop codon. It localises in the nucleus where it has been described to inhibit REST activity by competing with RE1 sites. Isoform 4 (from hREST-5FΔ transcript), deleted selectively at the level of the fifth zinc finger containing NLS, has been described in neuroblastoma and lung cancer cell lines (**Faronato and Coulson, 2011**).

REST expression is also post-transcriptionally modulated, through specific microRNAs targeting REST mRNA. For example, miR-9, miR-124 and miR-132 are induced upon neuronal differentiation and target REST mRNA for degradation (**Conaco et al., 2006; Laneve et al., 2010; Packer et al., 2008; Wu and Xie, 2006**).

Full-length REST has a predicted molecular weight of 116 kDa. However, many reports showed a higher molecular weight when REST was tested *in vitro* and for years researchers suggested O-linked glycosylation (**Kwon et al., 2013; Lee et al., 2000, 2016; Pance et al., 2006; Shimojo et al., 1999**), as main cause of molecular weight increase, as already demonstrated for a number of other proteins (**Apweiler et al., 1999; Gross et al., 1989; Selcuk Unal et al., 2008**). REST4 was also reported to be O-glycosylated (**Lee et al., 2000**), suggesting this post-translational modification might occur on full-length REST as well. Finally, in 2013 Faronato and colleagues proved that O-glycosylations are responsible for the REST shift from 120 to 220 kDa, and that this post-translational modification is carried out at different extents in different cell types. REST is therefore translated as a 116 kDa protein and then mature into the 220 kDa O-glycosylated form that mainly localise into the nucleus (**Faronato et al., 2013**).

Nuclear localisation of REST is directed by REST/NRSF-interacting LIM domain protein (RILP), that recognises the nuclear localisation signal (NLS) in the fifth zinc-finger domain and target REST to the nucleus, where it exerts its repressive transcriptional activity (**Shimojo, 2006; Shimojo and Hersh, 2003; Shimojo et al., 2001**). The opposite mechanism is mediated by huntingtin, a ubiquitous protein subject to poly-Q expansion causative of Huntington disease. Huntingtin is able to retain REST in the cytosol of healthy neurons to inhibit its transcriptional repression on neuronal genes, among which Brain-derived neurotrophic factor (BDNF). When mutated, huntingtin lose the REST binding capacity, causing an increased nuclear localisation of REST and repression of target genes that results in neurodegeneration (**Shimojo, 2008; Zuccato et al., 2003**).

Other post-translational modifications are involved in the modulation of REST activity. An important role is played by ubiquitinases and deubiquitinases, enzymes able to transfer ubiquitin units to or from proteins in order to regulate protein turnover (**Heride et al., 2014**). Ubiquitination is carried out in a multistep fashion. The E1 ubiquitin activating enzyme transfers a ubiquitin unit to the E2 ubiquitin conjugating enzyme, and subsequently

is transferred to the E3 ubiquitin ligase. Once ubiquitin is activated through this process, the target protein is recognised by the E3 ubiquitin ligase and the ubiquitin is transferred to particular lysine residues. Such tag can target proteins to proteasome degradation. Deubiquitinases catalyse the opposite reaction, removing ubiquitin units from tagged proteins in order to balance turnover mechanisms, and avoid protein loss of function due to excessive degradation. A certain level of substrate specificity exists, so that only some proteins can be ubiquitinated or deubiquitinated by the same enzyme.

Processes of ubiquitination and deubiquitination have been shown to regulate the circadian expression of REST during cell cycle, a periodicity necessary to maintain the chromosome stability. Transcription shut down is thought to be instrumental for mitosis to properly occur and transcription factors are removed from the condensing chromosomes (**Martínez-Balbás et al., 1995**). Before mitosis onset, phosphorylated REST is ubiquitinated by the E3 ubiquitin ligase beta-transducin repeat containing E3 ubiquitin protein ligase (β-TrCP). This event, leading to proteasomal degradation, causes the derepression of the spindle assembly checkpoint associated protein MAD2, avoiding mitotic defects such as shortened mitosis, premature sister-chromatid segregation, chromosome bridges in anaphase and tetraploidy (**Guardavaccaro et al., 2008**). Following mitotic exit, non-phosphorylated REST is rapidly replenished, assisted by ubiquitin specific peptidase 15 (USP15), that support its accumulation from early G1 to late G2. USP15 localises in the cytosol and does not oppose the degradation of pre-existing nuclear REST, but it acts on newly synthesized, non-glycosylated 120 kDa REST, favouring its maintenance before glycosylation mechanisms take part (**Faronato et al., 2013**). Acting on a different binding motif than the one recognised for mitotic checkpoint regulation, the β-TrCP also facilitates REST degradation during neuronal differentiation (**Westbrook et al., 2008**). This mechanism is counterbalanced by ubiquitin specific peptidase 7 (USP7/HAUSP), able to stabilise REST and antagonise β-TrCP to maintain multipotency in neural stem cells (**Huang et al., 2011**). Interestingly, both REST ubiquitination and deubiquitination have been associated to pathological conditions. In particular, β-TrCP has been found either induced or repressed in epithelial and neural cancers, respectively, in which REST plays opposing roles (**See chapter 3.5 for details**, **Conti et al., 2012; Wagoner and Roopra, 2012; Westbrook et al., 2008**), while both USP7 and USP15 are induced in glioblastoma, likely accounting for REST overexpression (**Eichhorn et al., 2012; Yi et al., 2016**).

3.4 REST involvement in stem cells identity and neurogenesis

REST is expressed very early during development, being present already at the blastocyst stage, both in the inner cell mass, composed of pluripotent stem cells (PSCs), and in the trophoblast, that will later develop into the placenta (**Figure 3.5B**). The presence of REST in PSCs (**Figure 3.5A-B**) prompted a series of studies to address its potential involvement in the maintenance of the Oct3/4-Sox2-Nanog pluripotency core circuit. The recruitment of REST to ESC transcription factor genes, including *Nanog*, *Estrogen related receptor beta* (*Essrb)* and *Lin28*, supported the interaction with the core pluripotency circuit (**Johnson et al., 2008**). REST has also been proposed to repress microRNA-21 preventing it from targeting Sox2 to maintain self-renewal and pluripotency of murine ESCs (**Singh et al., 2008, 2015**). However, a series of studies analysing ESC lines with a reduced or null REST expression, reported that pluripotency is not affected by REST deregulation (**Buckley et al., 2009; Jørgensen and Fisher, 2010; Jørgensen et al., 2009b, 2009a; Singh et al., 2010; Yamada et al., 2010**). Rather, REST would be involved in the early phases of ESCs differentiation, in which it would repress *Nanog* to promote pluripotency exit (**Yamada et al., 2010**). Moreover, both $Rest^{+/-}$ and $Rest^{-/-}$ mice survive the blastocyst stage and show no dysfunction in gastrulation, with $Rest^{-/-}$ mice dying only at the onset of neurogenesis (E9.5-11.5) due to growth defects and abnormal brain development (**Figure 3.3D**, **Chen et al., 1998; Nechiporuk et al., 2016**). Even though REST appears dispensable for pluripotency, its molecular network is well integrated with those of Oct3/4, Sox2 and Nanog, with about 100 targets common to the four transcriptional regulators plus others shared singularly with them (**Johnson et al., 2008**).

Following gastrulation REST is ubiquitously expressed throughout the body (**Figure 3.5C**), to be finally confined out of the neuronal compartment where it controls several processes, including genomic integrity, response to hypoxia, endocrine functions, quiescence and self-renewal (**Aoki, 2018; Cavadas et al., 2016; Gao et al., 2011; Martin and Grapin-Botton, 2017; Mukherjee et al., 2016; Nechiporuk et al., 2016**). While these processes are lineage-specific, the repression of genes involved in neuronal differentiation and function is applied longitudinally to all the cell types in which REST is active. Even fully differentiated and mature neurons benefit from very small levels of REST in order to fine-tune the expression of genes controlling synaptic functions and balance their positive regulation. Upon

hyperactivation, REST expression is enhanced to repress voltage-gated Na^+ channels and restore the correct cellular homeostasis (**Jessberger et al., 2007; Palm et al., 1998; Pozzi et al., 2013**).

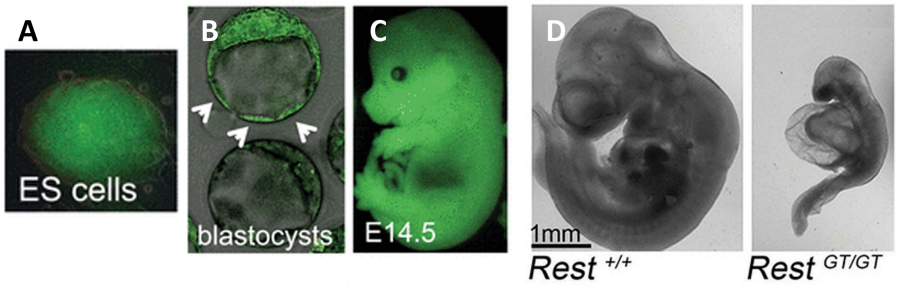

Figure 3.5. Expression of REST during development and REST KO mice. A. Rest expression visualised by GFP reporter in *Rest floxed*/+ ESCs. **B.** *Rest floxed*/+ embryo shows GFP expression in both the inner cell mass, composed of pluripotent stem cells, and the trophoectoderm at the blastocyst stage. **C.** Virtually ubiquitous REST expression in E14.5 embryo (**Aoki, 2018**). **D.** Comparison of E10.5 wild type and REST KO embryos (**Nechiporuk et al., 2016**).

During embryonic neurogenesis, REST appears to be progressively downregulated. Its expression is maximal in NSCs and declines during neuronal differentiation and maturation (**Ballas et al., 2005**). In the adults, neurogenesis is fostered by a pool of quiescent NSCs (qNSCs), that after proper stimulation is activated, becoming proliferative NSCs (aNSCs). aNSCs embark into a differentiation journey, generating first transit-amplifying progenitors (TAPs), then neuroblasts and finally exit cell cycle and start acquiring neuronal identity and functions. These main stages of neurogenesis can be identified by analysing cell morphology, proliferative capacity as well as the expression of specific markers. REST role in adult neurogenesis has been mainly enlighten in the hippocampal subgranular zone (SGZ), one of the two main neurogenic area in the adult mammalian brain. There, qNSCs have been recognised as slow-dividing, radial cells co-expressing the transcription factor Sox2 and both nestin and the glial fibrillary acidic protein (Gfap) (**Gao et al., 2011**). Following transition to TAPs, Gfap expression is lost and replaced by the proneural achaete-scute family bHLH transcription factor (Ascl1), and the proliferative marker Ki67, while the transition from late stage TAPs to neuroblasts is characterised by the induction of bHLH transcription factor neuronal differentiation 1 (NeuroD1) and the microtubule associated

protein doublecortin (Dcx) (**Gao et al., 2011; Mukherjee et al., 2016**). REST levels are maintained during the conversion from qNSCs to TAPs, to suddenly fall in neuroblasts, showing an inverse correlation with its target Ascl1 (**Ballas et al., 2005**), and appearing mutually exclusive with NeuroD1 (**Gao et al., 2011**). REST is finally restored upon loss of NeuroD1 in immature neurons (**Figure 3.6**, **Gao et al., 2011; Mukherjee et al., 2016**).

Conditional loss of Rest gene in nestin^{+} cells (NSCs and TAPs), has been shown to reduce their self-renewal and proliferative ability and trigger premature neuronal differentiation, that overtime, deplete the pool of qNSCs, thus determining the progressive loss of neurogenic capacity (**Gao et al., 2011**). More recently, integrating *in vivo* and *in vitro* models with ChIP-seq and RNA-seq techniques, Hsieh's lab explored more deeply the molecular mechanisms underlying REST requirement in the different phases of adult neurogenesis, revealing a differential transcriptional activity controlling transitions from every maturation stage. The deletion of Rest gene from qNSCs revealed a selective repression of genes involved in cell cycle and ribosome biogenesis that prevent the transition from qNSCs to TAPs. However, once the conversion in TAPs is achieved, REST transcriptional repression activity is targeted to neuronal genes, preventing neurogenesis by maintaining TAPs in a proliferative state. Still unclear is how REST differentially regulates target genes in these cell types, although this mechanism might be influenced by the presence of other transcription factors or controlled by the REST binding to different motifs: canonical RE1s in genes regulated selectively in qNSCs and a slightly altered motif on genes selectively bound in TAPs or common to the two cell types (**Mukherjee et al., 2016**).

Using a different model of REST conditional knock-out in nestin^{+} cells than the one proposed by Hsieh's lab (**Gao et al., 2011**), loss of Rest gene in NSCs has been shown to trigger a premature exit from cell cycle causing cell death due to DNA damage, highlighting a mechanism in which REST is responsible not only for properly controlling the timing of neuronal genes expression during differentiation, but also for the protection of NSCs genome in s-phase, to ensure that terminal differentiation occurs only following complete exit from the cell cycle (**Nechiporuk et al., 2016**).

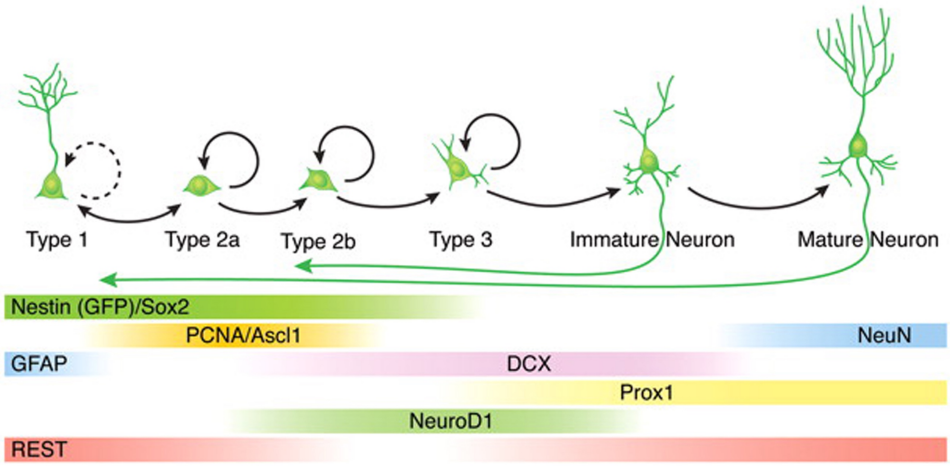

Figure 3.6. Summary of neurogenic stages, cell morphology and marker expression in the adult dentate gyrus. Type 1 cells are qNSCs characterised by the coexpression of Nestin, Sox2, GFAP, and REST. Once activated, qNSCs switch to transit amplifying progenitors, characterised by the absence of GFAP expression, a slight reduction in REST levels and the presence of the proneural transcription factor Ascl1 (type 2a, and type 2b). These markers are gradually substituted with NeuroD1 and Dcx in type 3 neuroblasts, and then Prox1 and NeuN in immature and mature dentate gyrus neurons, respectively. Note that REST expression is reduced at the neuroblasts stage, in concomitance with NeuroD1 expression, and reacquired during neuronal maturation (**Gao et al., 2011**).

3.5 REST involvement in cancers

Few years after its identification, REST started to be associated to cancer biology, first in neuroblastoma and medulloblastoma, (**Lawinger et al., 2000; Palm et al., 1999**) and then in a series of epithelial tumours, including small-cell lung cancer, prostate, breast, and colon cancers (**Coulson et al., 1999; Tawadros et al., 2005; Westbrook et al., 2005**). Currently, REST deregulation is considered an important driver of neural tumour formation and epithelial tumour aggressiveness, with many reports proposing it as prognostic marker for these types of cancer (**Coulson et al., 2000; Wagoner and Roopra, 2012; Wagoner et al., 2010**). It is interesting to note that the many and differential functions fulfilled by REST, have generated an apparently paradoxical role for REST in cancer biology. Indeed, REST has been indicated as oncogenic factor for cancers of the nervous system while being considered a tumour suppressor in epithelial neoplasia. This paradox depicting REST as either hero or villain depending on the (cellular) context can be explained however, if we

consider the complex machinery surrounding REST activity and how it regulates neurogenesis and cell cycle, as well as its more ancient role as repressor of neuronal genes. REST upregulation in neural tissues results in differentiation failure and increased self-renewal/proliferative potential of progenitor cells, determining abnormal growth. On the other hand, loss of REST induces derepression of a number of its targets, including cell survival proteins and neuronal genes in proliferating epithelial cells, giving rise to apoptotic resistant cells, with a neuroendocrine expression profile (**Coulson, 2005**).

3.6 REST in Glioblastoma Multiforme

REST was first investigated in GBM patients in 2006, when a series of genetic analyses determined that the gene is infrequently amplified in brain tumours (**Blom et al., 2006**). Three years later, the isolation and characterisation of GSCs (**see chapter II for details**), and the identification of mechanisms that regulate REST stability brought renewed attention to its possible role in GBM. The telomerase-associated protein 2 (TRF2), which acts by protecting and stabilising telomeres (**de Lange, 2005; Ning et al., 2006**), was shown to inhibit REST degradation (**Zhang et al., 2008**) and REST was for the first time detected in GSCs, inspiring the authors to hypothesise a therapeutic strategy targeting proteins important for brain tumours, yet with a limited function in post-mitotic neurons (**Zhang et al., 2009**).

In 2012, three independent laboratories confirmed that REST is highly expressed in GBM, all endorsing its oncogenic role in neural tissues and indicating it as a potential main driver of GBM aggressiveness (**Conti et al., 2012; Kamal et al., 2012; Wagoner and Roopra, 2012**). In GBM, REST immunoreactive cells represent 10-75% of the total cells, mainly representing SOX2- and nestin-positive cells found in perivascular area, region in which an enrichment of GSCs has been described (**Conti et al., 2012; Gilbertson and Rich, 2007**). These studies confirmed that GSCs express REST, and indicated its expression levels are proportional with those of other neural progenitor markers, including nestin and SOX2, thus suggesting a correlation between REST and stemness in GSCs (**Conti et al., 2012; Kamal et al., 2012**). In addition, REST protein levels in GSCs directly correlated with their tumorigenic ability, so

that those presenting high levels of REST were more tumorigenic than those expressing low levels (**Kamal et al., 2012**). Experimental manipulation of REST levels in GSCs showed that its knock-down strongly affects GSC multipotency, by reducing their self-renewal ability, sometimes to the inability to propagate the cells *in vitro*, and determined an increased proportion of cells expressing the neuronal marker Neuron-specific Class III β-Tubulin (β3-tubulin) and a reduction of those cells immunoreactive for the neural progenitor markers Nestin and Oligodendrocyte transcription factor 2 (OLIG2) (**Figure 3.7A-B**) (**Conti et al., 2012**). These experiments demonstrated that REST silencing in GSCs results in the exit from cell cycle and the transition from an immature to a more differentiated phenotype. Moreover, loss of REST in GSCs activated the apoptotic pathway, in according to what already described during neurogenesis (**Nechiporuk et al., 2016**), and reduced the cells' migratory ability. These results were confirmed *in vivo*, as REST-depleted GSCs were proved to lose their tumorigenic potential (**Figure 3.7C-D**, **Conti et al., 2012; Kamal et al., 2012**). Most interestingly, the feasibility of a therapeutic application targeting GSCs has been demonstrated by direct *in vivo* injection of lentiviral particles carrying shRNA anti-REST in established heterotopic tumours (**Conti et al., 2012**). The comparison of the expression profile of GSCs expressing high and low REST also suggested a possible implication in the regulation of cellular movement, cell-to-cell signalling, cellular growth and proliferation (**Kamal et al., 2012**).

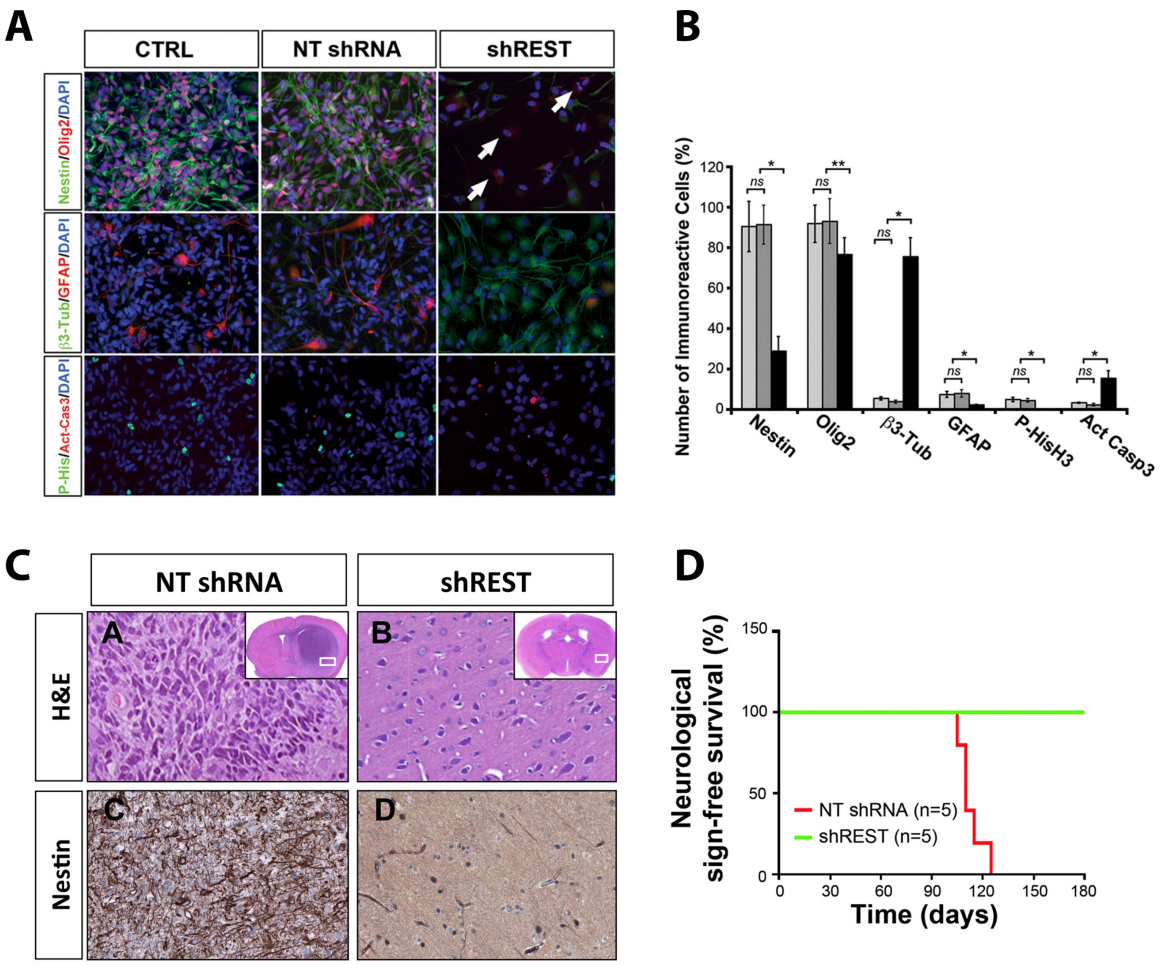

Figure 3.7. REST silencing induces neuronal-like differentiation and loss of tumorigenic properties in hGSCs. A. Expression of neural progenitors (Nestin and Olig2) and differentiation markers (β3-Tubulin and GFAP) in control and REST knock-down hGSCs (GB7 cells). P-Histone H3 and cleaved Caspase 3 were used to mark M-phase cells (actively proliferating cells) and apoptotic cells, respectively. **B**. Quantification of the cells in **A**. **C**. Coronal sections of grafted brains following injection of control and REST knock-down hGSCs. Haematoxylin & eosin (H&E) staining shows tumour formation, characterised by Nestin-immunoreactive cells. **D**. Survival curve of immunodeficient mice transplanted with either control or REST knock-down hGSCs **(Conti et al., 2012)**.

By the end of the same year, REST activity was analysed in patients and proposed as GBM prognostic marker (**Wagoner and Roopra, 2012**). A previously published REST signature, composed of 24 REST target genes and shown to have prognostic value for breast cancer patients (**Wagoner et al., 2010**), was applied to the gene expression profile of 176 brain tumours of various WHO grade and non-neoplastic brain tissues. The expression levels of the genes composing the REST signature inversely correlated with WHO tumour grade,

suggesting the existence of an association between increased transcriptional repression by REST and tumour aggressiveness.

GBM patients were then segregated in "REST-enhanced malignancies", in which the 24-REST targets were mainly downregulated respect to a non-pathological context, and "near-normal tumours", having target genes expression comparable to normal brain. As evidence of the prognostic value of the REST activity, a significant survival advantage has been associated to those GBM patients in which REST target genes expression appeared comparable to a non-neoplastic brain, while "REST-enhanced malignancies" that shows a lower REST target genes expression, had a poorer outcome (**Figure 3.8A**). REST enhanced GBM presented mainly a *classical* or *mesenchymal* expression profile, while *proneural* GBM were almost absent in patients with high REST activity (**Figure 3.8C**). In an attempt to identify a possible cause for REST overactivation in GBM, the authors analysed the copy number variation in chromosome 4q12, determining however, that the frequent focal amplifications do not localise to REST locus (**Wagoner and Roopra, 2012**).

More recently, a similar strategy has been used to develop a GBM-specific REST signature to predict GBM patients' prognosis (**Liang et al., 2016**). Differently from the previous report by Wagoner and Roopra, Liang and coauthors develop what they called "REST score" considering a set of genes generally modulated both positively and negatively in presence of REST in CNS-derived cell lines and GBM patients. Such REST score was composed of 68 genes with a positive correlation plus nine with a negative correlation to REST expression. Despite the different approach, the results obtained were consistent with those already reported. The GBM-specific REST score was able to discriminate between GBM and the adjacent normal tissue that sometimes are resected together and confirmed that a higher REST activity results in a poorer prognosis and is characteristic of *classical* and *mesenchymal* molecular subtypes of GBM. Consistently, IDH1/2 mutations, typical of *proneural* GBM and associated with a better prognosis (**see chapter 1.3 for details**) associated with a decreased REST activity. To better understand the impact of REST activity on global gene expression pattern, the REST score was correlated with transcriptomic profiles of GBM samples from the cancer genome atlas database. The gene ontology analysis of the 9533 genes significantly associated with the REST score included pathways already described to affect brain tumour aggressiveness, such as cell adhesion and

invasion, cell proliferation, protein translation, and apoptosis. To identify possible therapeutic options that take into consideration REST activity in GBM, the authors analysed a public drug sensitivity database, the Genomics of Drugs Sensitivity in Cancer (**Yang et al., 2013**), and found indication that cells expressing high levels of REST might be more sensitivity to tyrosine-kinase inhibitors, while cytotoxic drugs might be more effective in treating cells with a low REST activity (**Figure 3.8B**, **Liang et al., 2016**).

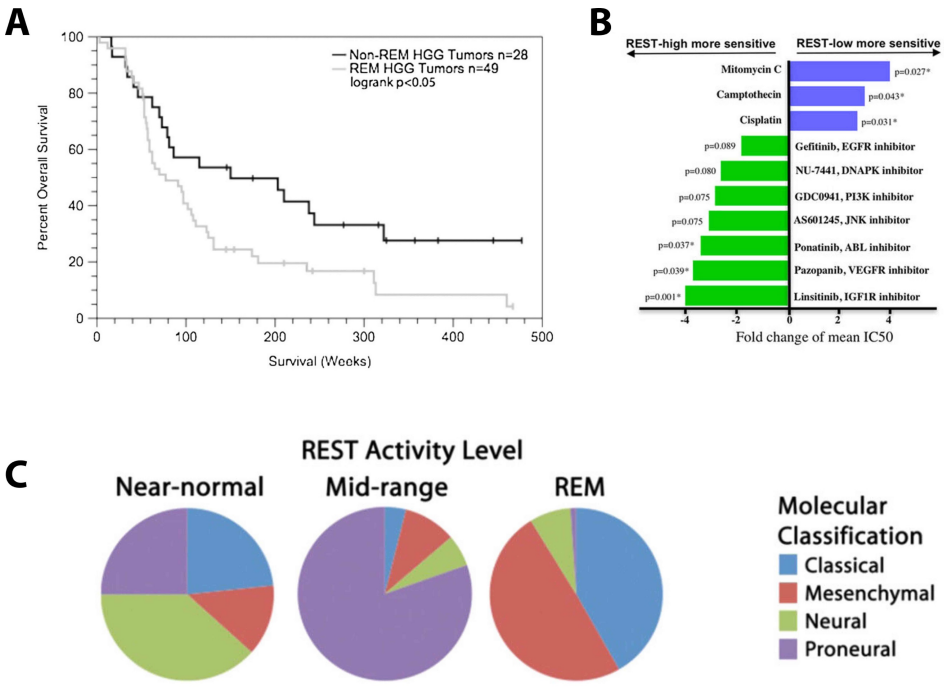

Figure 3.8. Prognostic relevance of REST activity in GBM patients. A. Kaplan-Meier survival curve of GBM patients stratified according to the expression levels of REST target genes. **B.** Bar graph showing cells sensitivity to common chemotherapeutic drugs versus protein kinase inhibitors depending on the expression levels of a GBM-specific REST signature (**Liang et al., 2016**). **C.** Molecular classification of GBM patients as in **Verhaak et al., 2010** according to the expression levels of REST target genes. REM: REST-enhanced malignancies. **A** and **C** from **Wagoner and Roopra, 2012**.

Since 2012, other reports have been published confirming the oncogenic activity of REST in GBM and focussing on the identification of REST targets and interactors able to influence tumour aggressiveness. REST has been shown to regulate proliferation and migration of non-stem GBM cells, suggesting its activity is also relevant within the more differentiated bulk tumour cells compartment. REST knock-down in these cells determine cell cycle arrest at G1, possibly mediated by the repression of cyclin D1 and cyclin E1 regulating the G1/S

transition checkpoint, while inducing genes determining migration inhibition. Interestingly, REST knock-down in GBM cell lines did not affect apoptosis (**Zhang et al., 2016**). Micro-RNA 124 is a known target of REST involved in NSC neuronal differentiation (**Conaco et al., 2006**). This relationship is maintained in GBM and GSCs, in which micro-RNA 124 affects self-renewal, apoptosis, invasive potential and tumorigenic properties *in vivo* (**Conti et al., 2012; Marisetty et al., 2017; Silber et al., 2008; Tivnan et al., 2014**). Micro-RNA 203 has also been identified as a tumour suppressor target of REST in GSCs, in which its upregulation was shown to prolong survival of mouse models of GBM, although regulating only the GSC invasiveness (**Marisetty et al., 2017**).

In the opposite direction to the established oncogenic role of REST in neural tumours, the concomitant loss of *Rest* gene in nestin^{+} neural progenitors and the *p53* tumour suppressor was described to generate brain tumours with a 66% success rate in adult mice, and among these, almost half were identified as GBM with primitive neuroectodermal tumour (PNET) features and a *proneural* expression patterns. Loss of Rest from neural progenitors never resulted in brain tumour, but it was described to trigger p53-mediated apoptosis due to DNA damage in s-phase. When *p53* is lost in combination with *Rest*, neural progenitors miss an important mechanism inducing cell death in case of DNA damage and persist, generating a tumour appearing in the adult animal. These results support the idea that REST promotes non-neuronal cell transformation, rather than initiate tumours (**Nechiporuk et al., 2016**). Primitive neuroectodermal tumours represent rare subtypes of GBM, characterised by the presence of undifferentiated cells in the cerebrum and a very poor survival (**Karsy et al., 2012**). However, the presence of IDH1/2 mutations, determining the *proneural* phenotype in GBM with a PNET component, were associated to a better prognosis than primary GBM (**Song et al., 2011**).

Overall, the increasing evidences associating REST to GBM and GSC biology, indicate the possibility of strategically influence REST functions. However, this approach must take in consideration the pivotal and widespread role of REST, preventing us from conceiving a therapy targeting REST itself that would cause substantial side effects. Nevertheless, the context-specific activities of REST are exerted through differential modulation of target genes, ultimately representing the molecular arms executing REST demands. Once identified, these target genes might be considered as selective therapeutic targets.

Results

Chapter 4

Preface

Contents

4.1 PREFACE **48**
4.1 PINDUCER SYSTEMS FOR CONTROLLED REST EXPRESSION **49**

4.1 Preface

Previous reports from our and other laboratories have identified REST as a central regulator of hGSCs fundamental properties, including their multipotency and tumorigenic competence. In particular, repression of REST in hGSCs *in vitro* results in a reduction of cell self-renewal and migratory ability, accompanied by a switch from a multipotent state to a differentiated neuronal-like state and an induction of apoptosis. These processes translated into the eradication of the hGSCs tumorigenic abilities *in vivo* (**Conti et al., 2012; Kamal et al., 2012; Zhang et al., 2016**). However, little is known about the molecular mechanisms through which REST exerts its pathological function in hGSCs. Gene expression analyses in GBM primary samples and hGSCs suggested an involvement of REST in a number of biological processes possibly accounting for its cancerous activities (**Kamal et al., 2012; Liang et al., 2016; Wagoner and Roopra, 2012**), but nevertheless none has currently identified the molecular mediators of these functions. This information will not only shed light on the role REST in hGSCs but will also provide novel exploitable targets for a therapy aimed at specifically interfere with hGSCs function(s) and ultimately reducing

GBM growth and recurrence. However, in designing a strategy intended to address this question, a significant factor that has to be acknowledged is the role of REST in other cell types. Given the similarities between hGSCs and hNSCs, part of the molecular network regulated by REST in hGSCs is likely shared with their non-pathological counterparts. As a consequence, considering these molecules as target of a therapy might reasonably result in undesired side effects.

4.1 pINDUCER systems for controlled REST expression

In order to identify the molecular network regulated by REST specifically in hGSCs, we generated human GSC and NSC lines in which REST expression can be manipulated inducibly. We took advantage of a series of single vector Tet-on systems for modifying REST expression in an inducible way already described in **Meerbrey et al., 2011,** and we use them for generating hGSC and hNSC lines in which REST can be either silenced or overexpressed following administration of doxycycline into the culture medium. In order to identify the best vector, we tested two systems to mediate REST knock-down (**Figure 5.1A-B**) and two for REST overexpression (**Figure 5.1C-D**) along with their relative Scrambled shRNA or empty vector controls (not shown). These lentiviral constructs are composed of:

i. a constitutive region where the ubiquitin promoter (Ubc) drives a stable expression of a reverse tetracycline transactivator (rtTA)
ii. a reporter gene for infection (enhanced green fluorescent protein, eGFP) or an antibiotic resistance cassette (puromycin resistance, Puro, or neomycin resistance, Neo)
iii. an inducible region where tetracycline responsive element (TRE) controls the expression of either an anti-REST shRNA (along with a turbo-red fluorescent protein-tRFP as marker of induction) or REST cDNA sequence.

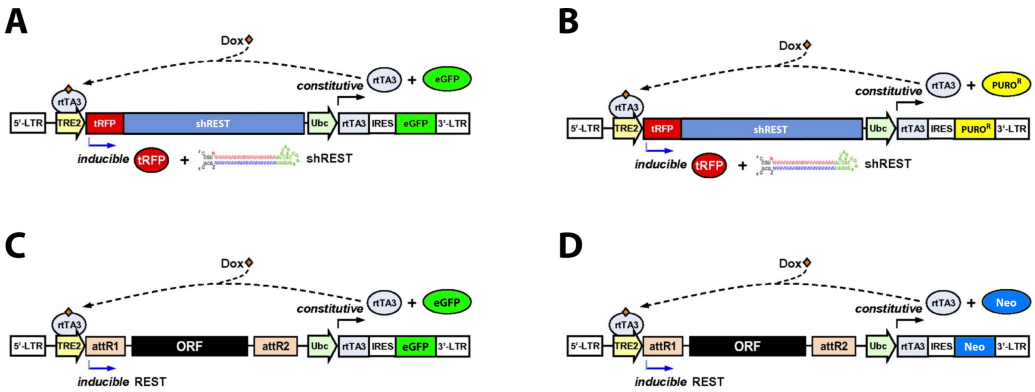

Figure 4.1. Tet-on systems for modulating REST expression used in the study. Schemes of the lentiviral vectors exploited to modulate REST expression inducibly. **A-B**. anti-REST shRNA expressing vectors pIND11shREST (**A**) and pIND10shREST (**B**). **C-D**. REST overexpressing vectors pIND22hREST (**C**) and pIND20hREST (**D**). Control Scrambled-expressing shRNA or empty vectors (not shown) are named pIND11, pIND10, pIND22 and pIND20.

Chapter 5

Generation and Characterisation of hGSCs and hNSCs Systems for Inducible Silencing of REST

Contents

5.1 GENERATION OF REST INDUCIBLE KNOCK-DOWN HUMAN GLIOMA STEM CELL LINES	**51**
5.2 GENERATION OF REST INDUCIBLE KNOCK-DOWN HUMAN NEURAL STEM CELLS	**63**
5.3 EFFECT OF REST LOSS OF FUNCTION ON HGSCS AND HNSCS PROPERTIES	**65**

5.1 Generation of REST inducible knock-down human Glioma Stem Cell lines

As parental hGSCs, we chose the GB7 cell line previously generated in our laboratory. These cells have been shown to be multipotent and highly tumorigenic, with their GSC properties being strongly affected following REST knock-down (**Conti et al., 2012**).

To quickly test the functionality of the pINDUCER system, we performed a pilot experiment in which hGSCs cells were infected with lentiviral particles carrying either pINDUCER11-shREST or pINDUCER11 (control shRNA-Scrambled, shSCRMBL) vectors (**Figure 4.1A**). Two days after infection, fluorescence imaging revealed the presence of $eGFP^+$ cells in both pIND11 (55% $eGFP^+$ cells/total cells) and pIND11shREST (87% $eGFP^+$ cells/total cells) hGSC cultures, indicating the effective expression of the constitutive region of the constructs (**Figure 5.1A, upper section**). At this stage, cultures were treated with 300 ng/ml doxycycline for 48 hours. Administration of doxycycline into the culture media resulted in

the expression of the tRFP reporter, with signal being visible already after 24 hours (**Figure 5.1A, lower section**). After 48 hours of doxycycline induction, cultures were lysed and processed for RNA extraction. We then performed a quantitative reverse transcription-polymerase chain reaction (qRT-PCR) to evaluate REST modulation in the cultures. Control hGSCs infected with pIND11 showed no variation in REST transcript levels following doxycycline treatment, while the expression of the shRNA anti-REST (shREST) in the pIND11shREST hGSCs resulted in a 40% reduction of REST mRNA (0.58 ± 0.08 folds with respect to untreated pIND11shREST hGSCs, **Figure 5.1B**). Expression analysis of known REST targets revealed an induction of synaptosome associated protein 25 (SNAP25, 5.78 ± 0.75 folds) and brain-derived neurotrophic factor (BDNF, 1.53 ± 0.03 folds), suggesting a de-repression of REST-modulated genes (**Figure 5.1C**). These results indicate that a reduction of REST mRNA levels occurs in doxycycline-treated pIND11shREST hGSCs and that doxycycline treatment does not affect REST levels in control pIND11 hGSCs. Furthermore, the de-repression of some of the REST target genes in doxycycline-treated pIND11shREST hGSCs represents a functional evidence of a reduced REST activity as consequence of its downregulation.

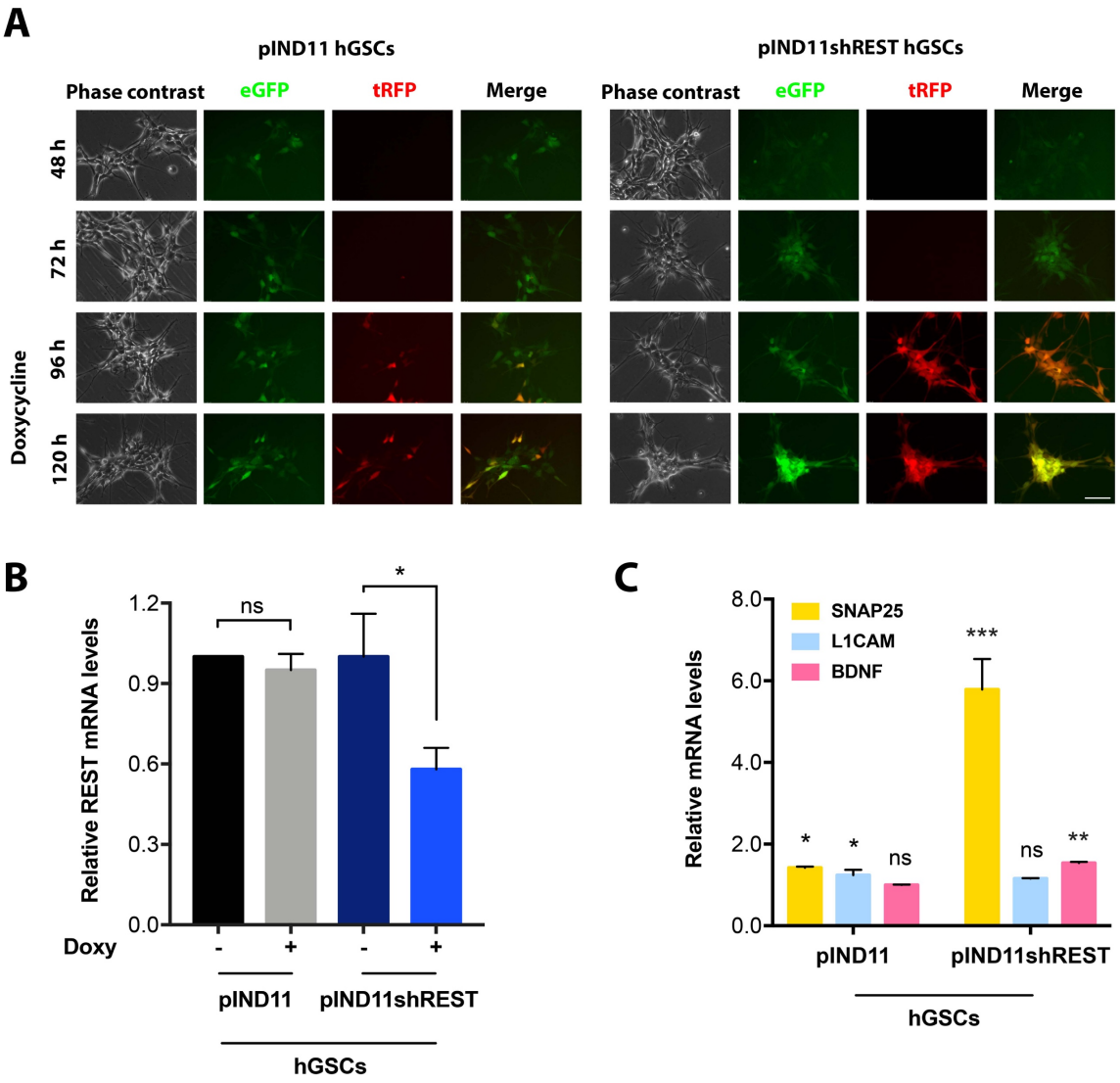

Figure 5.1. Pilot experiment: infection of hGSCs cells with pIND11 and pIND11shREST and qRT-PCR analysis. A. Representative pictures of hGSCs infected with either pIND11 or pIND11shREST; 72h after infection, cultures were treated with 300 ng/ml doxycycline for 48 hours. eGFP expression indicates infected cells, tRFP expression indicates activation of the Tet-on system. Indicated time is from infection. Scale bar: 100 µm. **B**. qRT-PCR assay for REST expression. **C**. qRT-PCR assay for REST target genes expression. qRT-PCR quantifications have been normalised on untreated cells. Results are expressed as mean ± standard deviation and statistical significance inferred using unpaired t-test.
ns: non-statistically significant; *: $p < 0.05$; **: $p < 0.01$; ***: $p < 0.001$.

The concentration of doxycycline tested in the first experiment was the highest used in the original report where the pINDUCER systems has been described (**Meerbrey et al., 2011**). Doxycycline concentration influences the levels of shRNA induced, resulting in different extent of RNA interference and may be affected by (i) the cell type considered and by (ii)

how expressed are the genomic regions where the lentiviral constructs are integrated. In order to define the optimal doxycycline dose for obtaining the highest induction of the Tet-on system in our cells without affecting their normal behaviour, we decided to perform a dose-response experiment in which the cells were treated with different concentration of doxycycline (from 25 to 500 ng/ml) for 48 hours and their RNA analysed to quantify the modulation of the levels of REST and its target genes (**Figure 5.2**). Morphological analyses of the cultures revealed no evident changes, suggesting the absence of unspecific doxycycline-induced effects, even at the highest concentration used (**Figure 5.2A**). Interestingly, we found that tRFP expression was dependent on the concentration of doxycycline as we could observe a proportional increase in both the number of $tRFP^+$ cells as well as the intensity of the fluorescent signal depending on the concentration of doxycycline (**Figure 5.2A**). These results suggest a dose-dependent expression of the inducible region of the pINDUCER system that may result in different levels of REST silencing. We performed a qRT-PCR assay in order to evaluate whether REST knock-down is also dependent on the concentration of doxycycline in the medium. As shown in **figure 5.2B**, pIND11 hGSCs reported a small, not significant, variation in REST mRNA levels between different doxycycline doses and anyway not proportional to the concentration of doxycycline. *Vice versa*, the pIND11shREST hGSCs treated with increasing doses of doxycycline exhibited a dose-response silencing of REST, reaching a maximum of 40% repression (0.60 ± 0.04 folds with respect to untreated pIND11shREST hGSCs) with the highest concentration of doxycycline considered (**Figure 5.2B**). The dose-response effect was also observed in the de-repression of REST target genes, proportional to the concentration of doxycycline used (**Figure 5.2C**). These results highlight one more time the specificity of the pINDUCER11shREST system in the downregulation of REST, but also show that REST expression is tunable depending on the experimental variation of the culture conditions (i.e. doxycycline dose). Since none of the concentration of doxycycline tested affected pIND11 hGSCs behaviour, we chose 500 ng/ml as optimal concentration for obtaining the maximum level of REST knock-down in our next experiments.

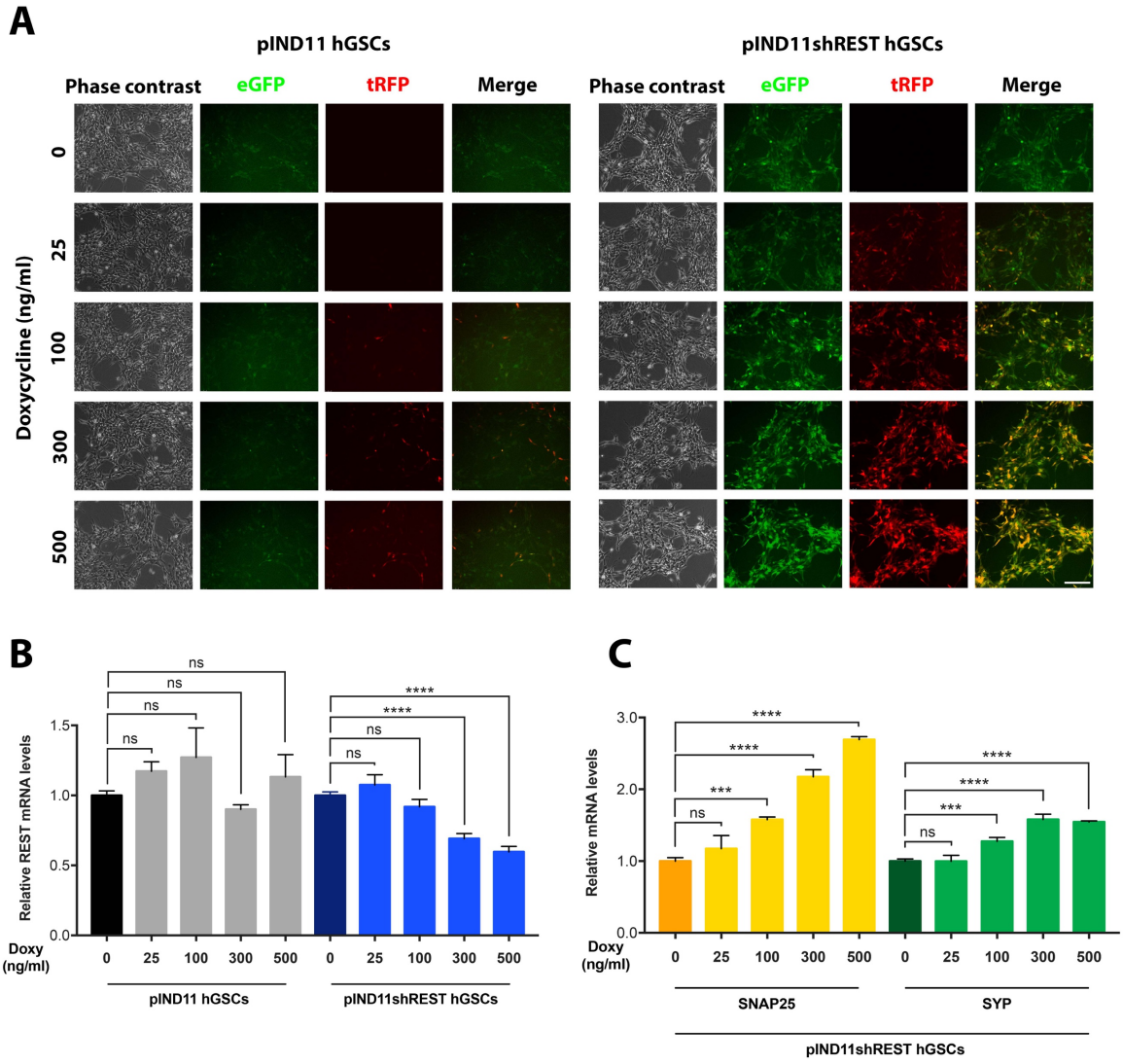

Figure 5.2. Doxycycline dose selection in pIND11 GSCs and pIND11shREST hGSCs. A. Representative pictures of pIND11 hGSCs and pIND11shREST hGSCs treated with different doses of doxycycline for 48 hours. eGFP expression indicates infected cells, tRFP expression indicates activation of the Tet-on system. Scale bar: 200 µm. **B**. qRT-PCR assay for REST expression. **C**. qRT-PCR assay for REST target genes expression. qRT-PCR quantifications have been normalised on untreated cells. Results are expressed as mean ± standard deviation and statistical significance inferred using one-way analysis of variance with a Dunnett's post-hoc test.
ns: non-statistically significant; ***: $p < 0.001$; ****: $p < 0.0001$.

Another parameter influencing shRNA expression in Tet-on systems is the timing of induction of the transgene. In order to verify whether we can enhance the degree of REST knock-down in pIND11shREST hGSCs by playing with the timing of treatment, we performed a time course experiment in which the cells were treated with the same concentration of doxycycline (500 ng/ml) for different time, and we analysed the relative

mRNAs amount of REST and SNAP25 as representative of REST-target modulation at different time points (**Figure 5.3**). During the five days of experiment, we could observe the pIND11 hGSCs growing at an apparent normal rate, indicating a prolonged exposure to doxycycline did not hamper cell cycle (**Figure 5.3A**). Also, looking at the intensification of the tRFP signal over time, the activation of the Tet-on system appeared to increase progressively. However, the shREST-mediated REST knock-down did not follow the same kinetics, as the lowest level of REST transcript was observed at 24 hours of treatment (0.58 ± 0.01 folds with respect to no doxy treated pIND11shREST hGSCs) and then gradually rose with time (**Figure 5.3B**). This result suggests that the increased tRFP-derived fluorescence observed over time is due to an accumulation of the fluorescent protein leading to an increased signal rather than a time-dependent induction of the TRE-regulated transgenes. Despite of this apparent defect in maintaining reduced REST levels, the prolonged de-repression of SNAP25 during the course of the experiment (**Figure 5.3C,** fold changes with respect to no doxy treated pIND11shREST hGSCs: 2.16 ± 0.32 at 24 hours, 2.54 ± 0.10 at 48 hours, 2.33 ± 0.17 at 72 hours, and 2.84 ± 0.36 at 96 hours) suggests that REST protein remained downregulated opening to the possibility to assess long-term effects of REST loss of function using this system.

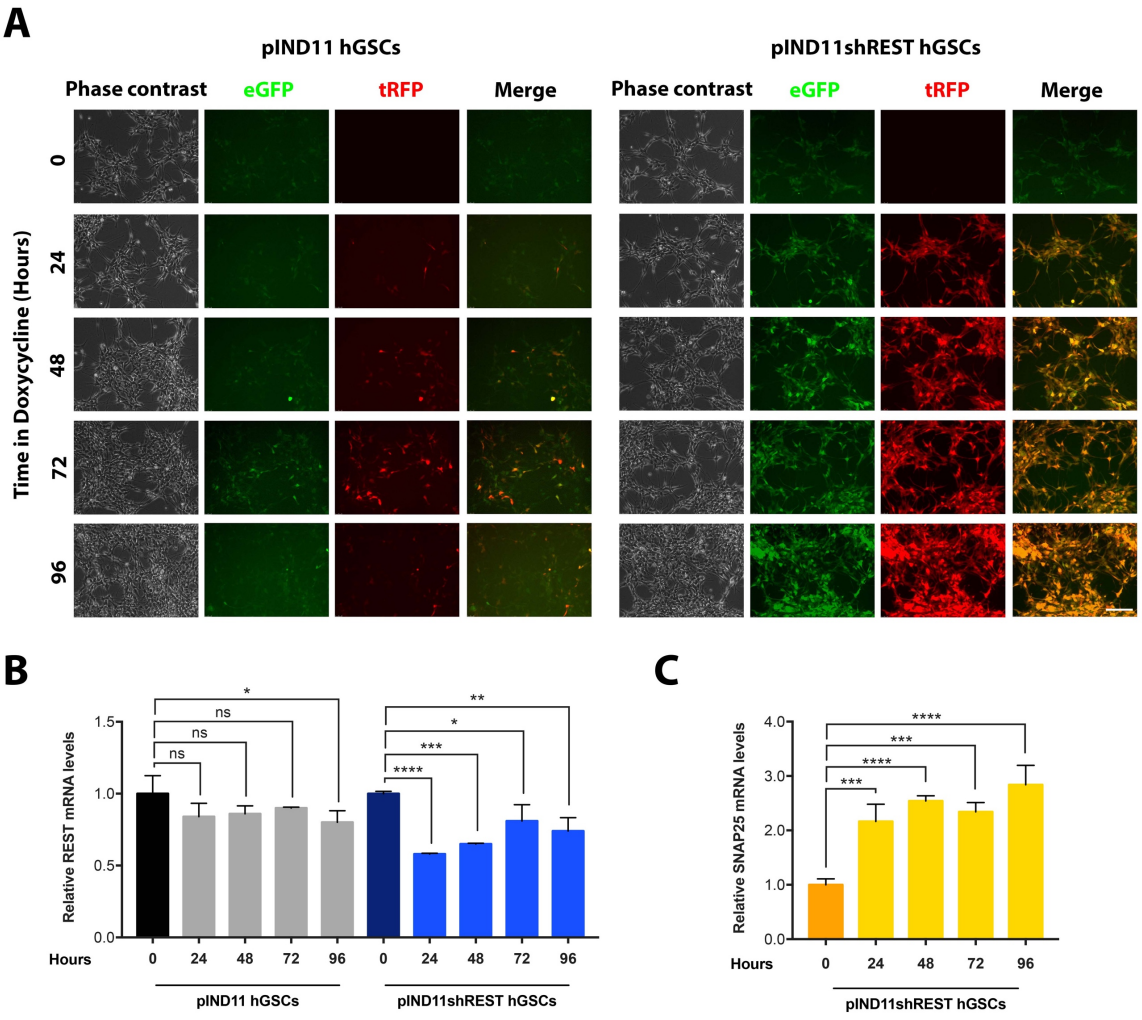

Figure 5.3. Time course induction of pIND11 hGSCs and pIND11shREST hGSCs. A. Representative pictures of pIND11 hGSCs and pIND11shREST hGSCs treated with 500 ng/ml doxycycline for up to 96 hours. eGFP expression indicates infected cells, tRFP expression indicates activation of the Tet-on system. Scale bar: 200 µm. **B**. qRT-PCR assay for REST expression. **C**. qRT-PCR assay for the REST target gene SNAP25 expression. qRT-PCR quantifications have been normalised on untreated cells. Results are expressed as mean ± standard deviation and statistical significance inferred using one-way analysis of variance with a Dunnett's post-hoc test.
ns: non-statistically significant; *: $p < 0.05$; **: $p < 0.01$; ***: $p < 0.001$; ****: $p < 0.0001$.

Overall, the pIND11shREST system is effective in selectively silencing REST in an inducible way. However, we noticed a certain degree of variability in eGFP expression within both pIND11 hGSCs and pIND11shREST hGSCs populations. This is due to the heterogeneous extents of transgene expression and may reflect a variable ability of knocking REST down from cell to cell. As shown in **figure 5.4B-C**, the analysis carried out at the flow cytometer revealed the presence of populations of $eGFP^+$ cells presenting different intensity of the

fluorescent signal, thus confirming our previous qualitative observations. To select the cells expressing high transgene levels, we decided to sort cells basing on the eGFP expression levels, using a fluorescence activated cell sorting (FACS), in order to isolate subpopulations with low, medium or high eGFP signal. Given the general low intensity of the eGFP signal of pIND11 hGSCs, in this case we collected cells with medium-to-high eGFP signal, discarding those with a negative-to-low eGFP signal, obtaining 94.30% of medium-high eGFP^{+} cells (**Figure 5.4B**). Since the eGFP signal of the pIND11shREST hGSCs was one order of magnitude greater than pIND11 hGSCs, with the aim of generating cells with a different power of REST silencing, we decided to collect two populations of eGFP-expressing hGSCs, the one with a medium and the one with a high eGFP intensity, obtaining 95.90% and 80.20% purity, respectively (**Figure 5.4C**).

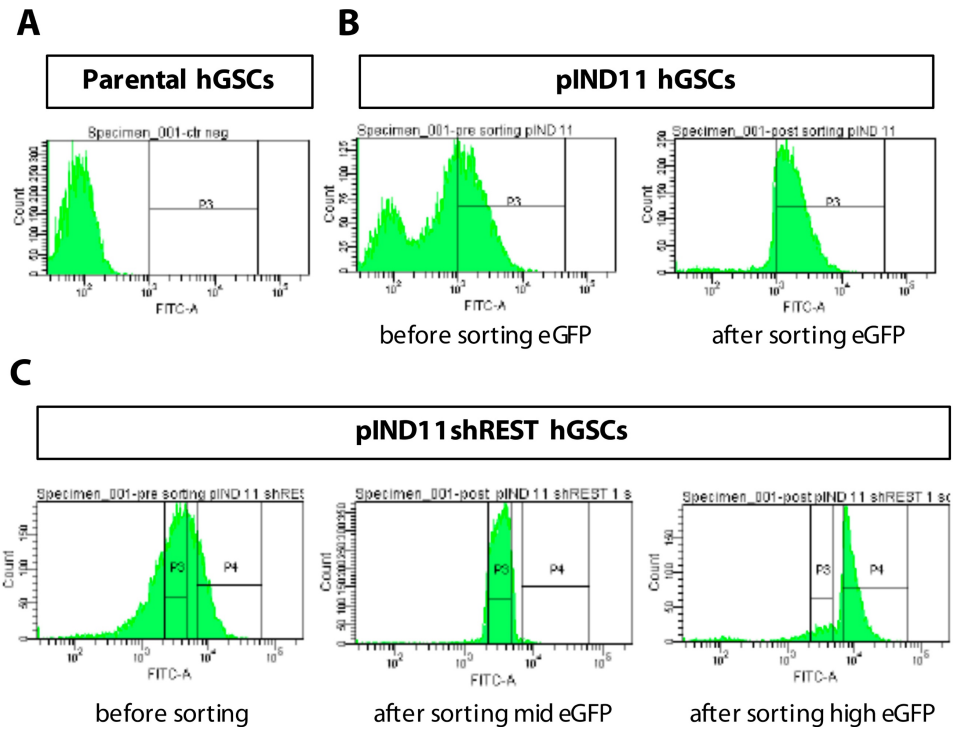

Figure 5.4. FACS-Sorting of pIND11 GSCs and pIND11shRESThGSCs. A. eGFP expression of parental-non-infected hGSCs used to select the sorting gate (P3). **B**. eGFP expression of pIND11 hGSCs before and after sorting. **C**. eGFP expression of pIND11shREST hGSCs before and after sorting.

To verify whether the sorted high eGFP pIND11shREST hGSCs exhibited higher REST knock-down ability than the unsorted ones, we performed a time course experiment of induction and verified the relative amount of REST mRNA and protein in the different populations (**Figure 5.5**). Since the previous time course indicated the maximum knock-down at 24-48 hours of induction, we decided to focus on these short time points. Live cell imaging showed a more homogeneous eGFP signal between cells, along with a general increase in its intensity with respect to unsorted cells, confirming the results obtained from the flow cytometry analysis post-sorting (**Figure 5.5A**). The qRT-PCR analysis showed that sorted high $eGFP^+$ pIND11shREST hGSCs not only retained the REST knock-down ability, but as expected, their silencing efficiency is improved as REST mRNA was reduced to 0.52 ± 0.06 folds at 24 hours and 0.64 ± 0.09 folds at 48 hours of treatment with doxycycline. We therefore gained about 10% increase in REST knock-down (**Figure 5.3B and 5.5B**), accompanied by about 2-fold increase in de-repression of SNAP25 mRNA with respect to unsorted cells (**Figure 5.3C and 5.5C**). Finally, Western blot assay showed that REST knock-down resulted, at protein level, in a 20% reduction at 24 hours (0.83 folds) and to 70% at 48 hours (0.34 folds) (**Figure 5.5D**).

Overall, the pINDUCER11shREST system appears effective in reducing REST expression in hGSCs in an inducible way. In addition, either by using different concentration of doxycycline or considering different time points, it is possible to tune REST knock-down to different extents. However, a significant question mark remains because of the heterogeneous intensity of the eGFP fluorescence within shREST and control cell populations, even after the selection through cell sorting. This variability possibly reflects an instability of the system, that may eventually result in a drift from the known REST modulation as time goes by.

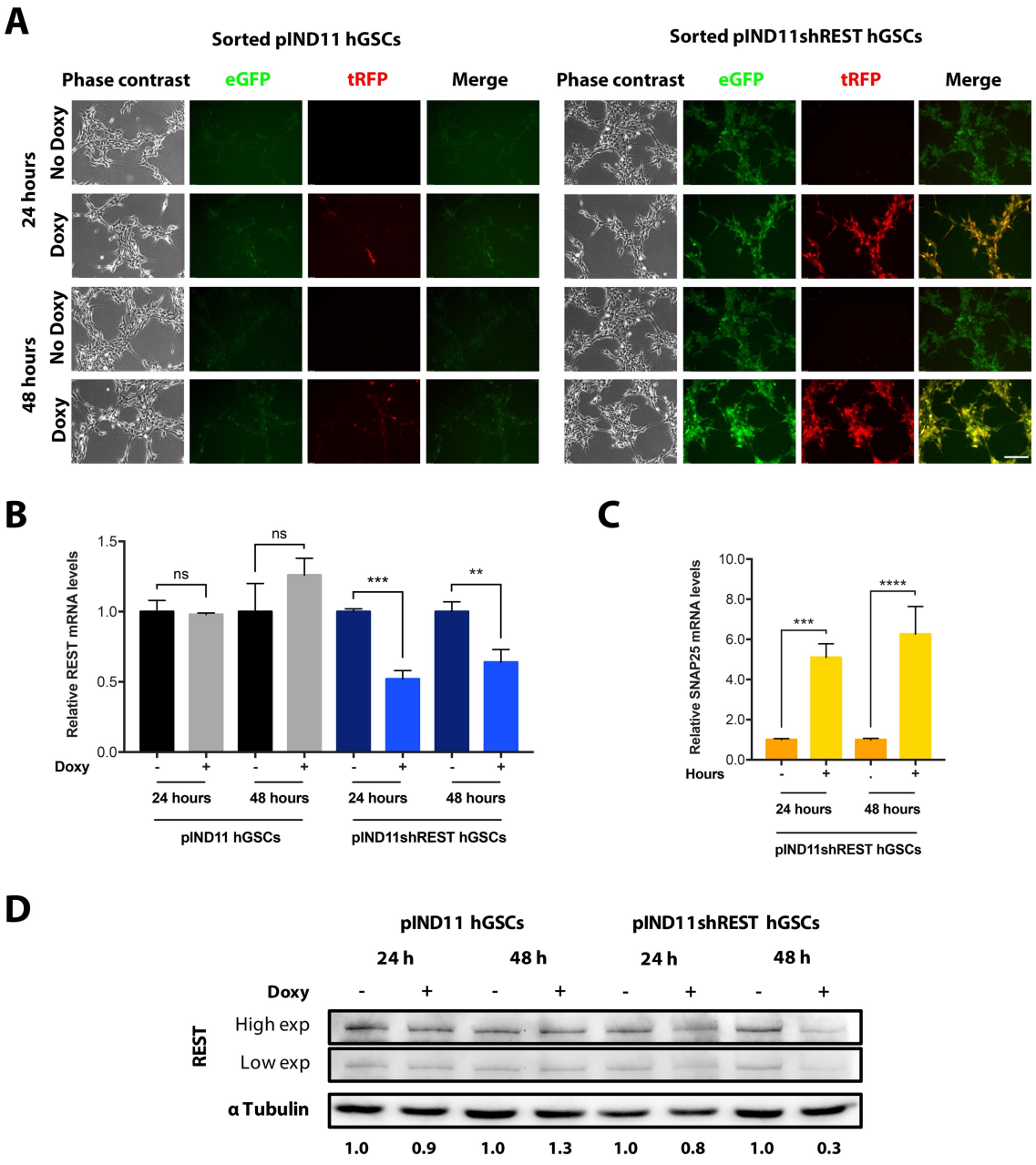

Figure 5.5. Time course induction of FACS-sorted pIND11 hGSCs and pIND11shREST hGSCs. A. Representative pictures of FACS-sorted pIND11 hGSCs and pIND11shREST hGSCs treated with 500 ng/ml doxycycline for 48 hours. eGFP expression indicates infected cells, tRFP expression indicates activation of the Tet-on system. Scale bar: 200 µm. **B**. qRT-PCR assay for REST expression. **C**. qRT-PCR assay for the REST target gene SNAP25 expression. **D**. Representative picture of western blot analysis for REST and relative densitometric quantification. qRT-PCR and immunoblotting quantifications have been normalised on untreated cells at the corresponding time point. Results are expressed as mean ± standard deviation and statistical significance inferred using t-test.
ns: non-statistically significant; **: $p < 0.01$; ***: $p < 0.001$; ****: $p < 0.0001$.

In order to select the best pINDUCER system for knocking REST down, we tested also the pINDUCER10shREST system. This system differs from pINDUCER11shREST since the eGFP cassette is replaced by a puromycin resistance cassette, thus providing the possibility to select the transduced cells (**Figure 4.1B**). Infection of the parental hGSCs and puromycin selection led to the generation of control pIND10 and pIND10shREST hGSCs. To verify whether the pIND10shREST hGSCs represent a valuable alternative to pIND11shREST hGSCs in interfering with REST expression, we performed an induction experiment in which the cultures were exposed to doxycycline for 48 hours and the expression of REST and its target gene SNAP25 were analysed. As already observed in pIND11shREST hGSCs, real-time fluorescent imaging inspection of pIND10shREST hGSCs showed a strong expression of the tRFP reporter of induction starting already 24 hours following the addiction of doxycycline (**Figure 5.6A**). Real-time PCR analysis revealed that levels of REST transcript in pIND10shREST hGSCs decremented to 0.58 ± 0.04 folds at 48 hours of doxycycline induction. At protein level, we measured a 91% decrease in REST expression (0.09 folds) that caused a de-repression of SNAP25 and synaptophysin (SYP) transcripts by 6.53 ± 0.26 and 1.74 ± 0.08 folds, respectively. Short-hairpin SCRMBL-expressing pIND10 hGSCs showed no significant changes in both REST and its targets expression (**Figure 5.6B-D** and data not shown).

Given the stronger activity of REST silencing showed by pINDUCER10shREST with respect to pINDUCER11shREST system, in terms of both timing and degree, we elected pIND10shREST hGSCs as optimal model for REST silencing.

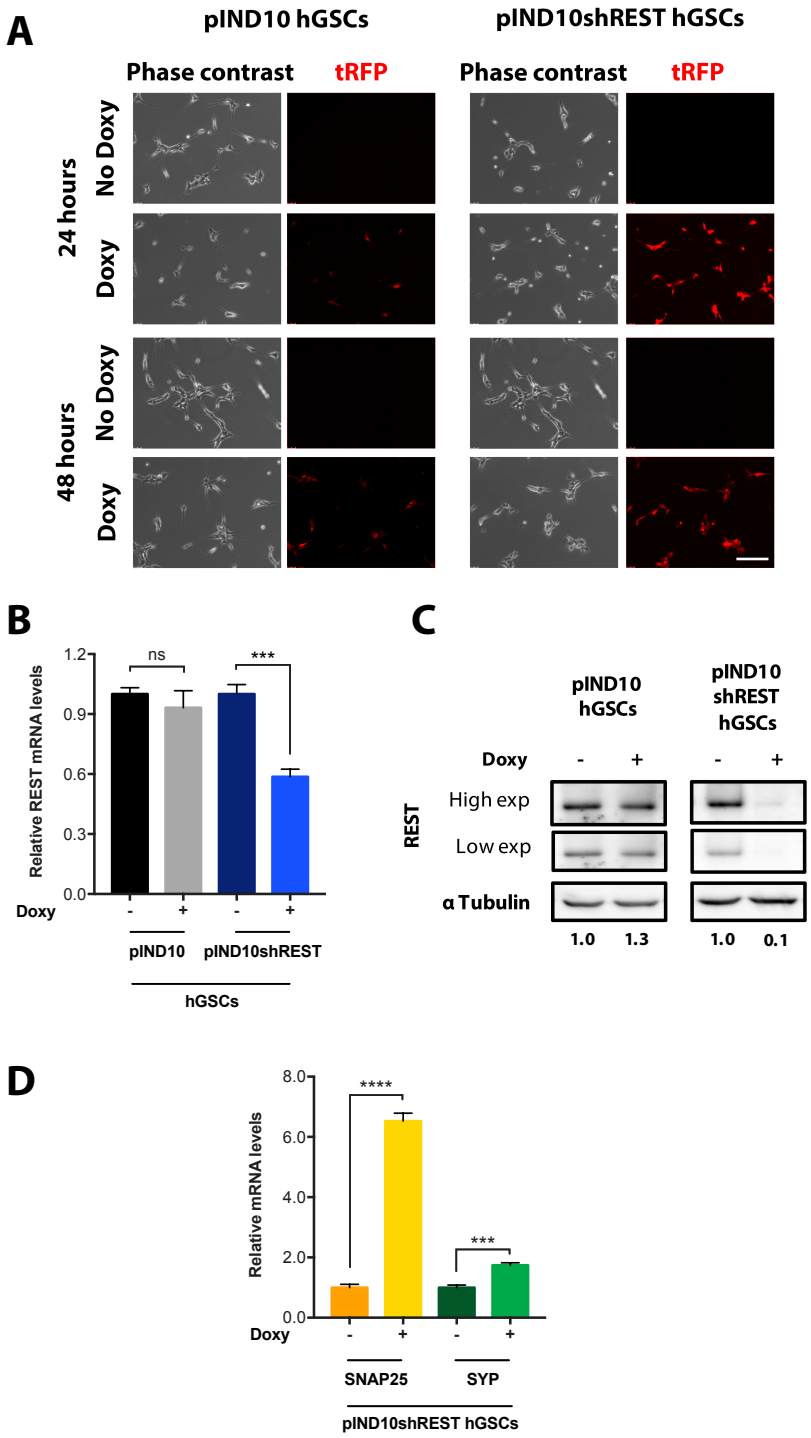

Figure 5.6. Time course induction of pIND10 hGSCs and pIND10shREST hGSCs. A. Representative pictures of pIND10 hGSCs and pIND10shREST hGSCs treated with 500 ng/ml doxycycline for 48 hours. tRFP expression indicates activation of the Tet-on system. Scale bar: 200 µm. **B**. qRT-PCR assay for REST expression after 48h induction. **C**. Representative picture of western blot analysis for REST and relative densitometric quantification. **D**. qRT-PCR assay for selected REST target genes expression at 48h. qRT-PCR and immunoblotting quantifications have been normalised on untreated cells at the corresponding time point. Results are expressed as mean ± standard deviation and statistical significance inferred using t-test.
ns: non-statistically significant; ***: $p < 0.001$; ****: $p < 0.0001$.

5.2 Generation of REST inducible knock-down human Neural Stem Cells

As non-malignant hNSCs exploited to develop the REST inducible system, we chose AF22 cells, originally described in **Falk et al., 2012**. These cells have been obtained from normal human induced pluripotent stem cells (iPSCs) and show features that make them ideal as parental cells to be engineered, as they are:

i. Homogeneously composed of self-renewing human Neural Stem cells
ii. Fast dividing
iii. Stable at genomic level
iv. Highly neurogenic
v. Easily amenable to genetic manipulation by viral-gene delivery

AF22 cells were infected with either pINDUCER10 or pINDUCER10shREST lentiviral particles to generate the non-tumour cell line to be compared with hGSCs. Once selected using puromycin, the pIND10shREST hNSCs were assayed in a time course experiment to verify whether we can efficiently achieve REST silencing as previously shown for hGSCs. Similar to what we previously observed with the REST KD hGSCs, the addition of doxycycline to the culture media induced the expression of the tRFP protein already after 24 hours, suggesting the proper activation of the TRE regulated elements. This was not accompanied by evident effects on growth and morphology of the cells as shown in **figure 5.7A**. Immunoblot assay showed a 67% decrease of REST protein levels (0.33 folds) occurring in pIND10shREST hNSCs after 48 hours of doxycycline treatment (**Figure 5.7B**). No significant reduction in REST protein levels was found upon induction of control pIND10 hNSCs. Quantitative RT-PCR analysis of REST transcript levels in pIND10shREST hNSCs, showed a silencing to 0.34 ± 0.04 and 0.80 ± 0.04 folds at 24 and 48 hours, respectively (**Figure 5.7C**). Interestingly, although REST mRNA silencing appears to be very minor after two days of doxycycline induction, western blot results indicated that REST silencing at protein level remains quite consistent (**Figure 5.7B**). Quantitative RT-PCR analysis of SNAP25 transcript levels showed a derepression of this gene to 2.00 ± 0.12 folds only after 48 hours of doxycycline treatment (**Figure 5.7D**) thus confirming a reduced REST activity at this stage in pIND10shREST hNSCs. The use of the pINDUCER10shREST system in hNSCs allows a kinetics of REST silencing similar to the one observed in REST KD performed in hGSCs.

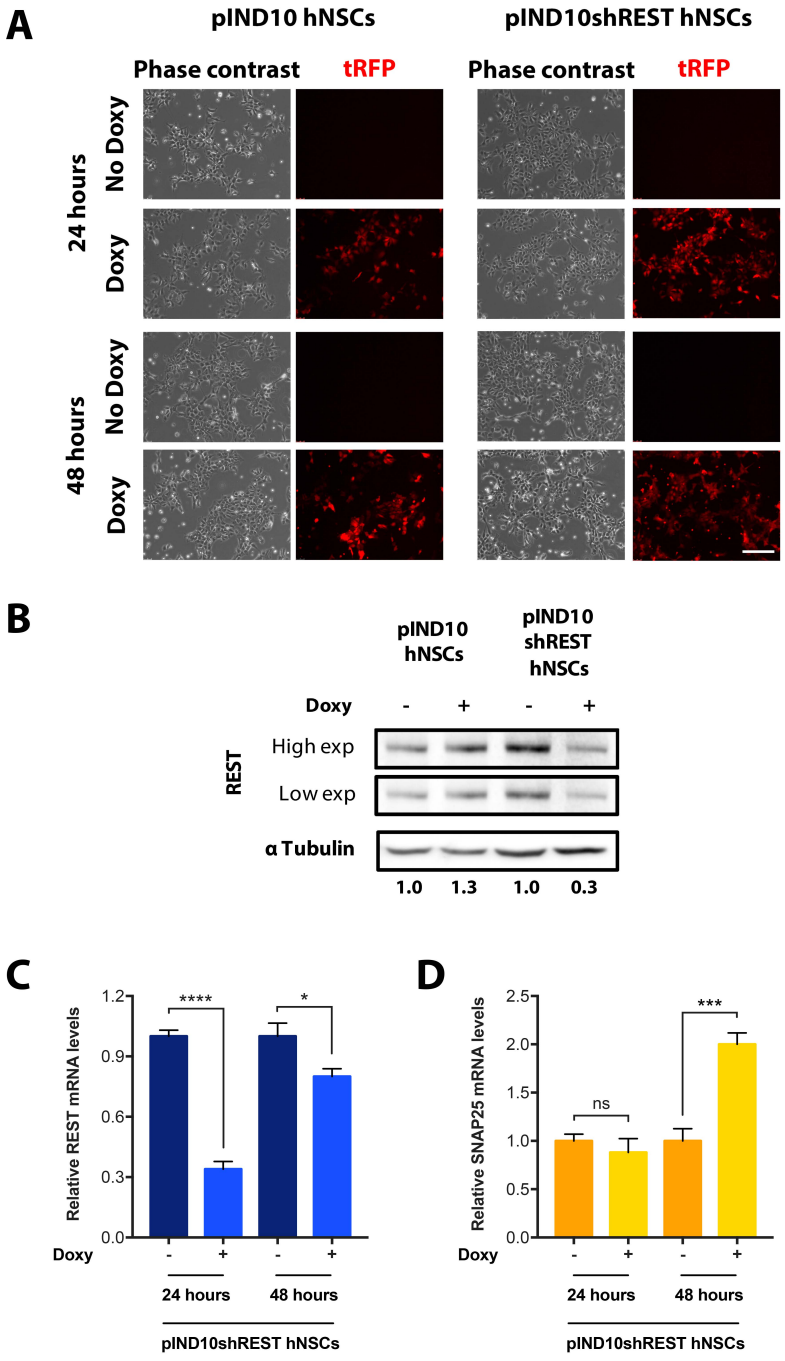

Figure 5.7. Time course induction of pIND10 hNSCs and pIND10shREST hNSCs. A. Representative pictures of pIND10 hNSCs and pIND10shREST hNSCs treated with 500 ng/ml doxycycline for up to 48 hours. tRFP expression indicates activation of the Tet-on system (induced cells). Scale bar: 200 µm. **B**. Representative picture of western blot analysis for REST and relative densitometric quantification. **C**. qRT-PCR assay for REST expression. **D**. qRT-PCR assay for the REST target gene (SNAP25) expression. qRT-PCR and immunoblotting quantifications have been normalised on untreated cells at the corresponding time point. Results are expressed as mean ± standard deviation and statistical significance inferred using t-test.
ns: non-statistically significant; *: $p < 0.05$; ***: $p < 0.001$; ****: $p < 0.0001$.

5.3 Effect of REST loss of function on hGSCs and hNSCs properties

Once established the REST inducible knock-down hNSCs and hGSCs lines and set up the conditions to obtain an optimal downregulation of REST in short time, we compared the differential functional effects resulting from REST silencing in hGSCs and hNSCs.

REST has been characterised as modulator of many cellular activities and in both hNSCs and hGSCs has been associated to the regulation of cell proliferation, differentiation and apoptosis (**See chapter 3.4 and 3.6 for details**). The evaluation of these parameters is important to verify whether our systems behave accordingly with what already described in literature and to validate them for subsequent gene expression analyses.

For the direct comparison studies, we have included the following cell lines:

i. CTRL hGSCs (corresponding to pIND10 hGSCs)
ii. REST KD hGSCs (corresponding to pIND10shREST hGSCs)
iii. CTRL hNSCs (corresponding to pIND10 hNSCs)
iv. REST KD hNSCs (corresponding to pIND10shREST hNSCs)

Silencing of REST affects hGSCs and hNSCs cell growth

As initial analysis, we performed a cell proliferation assay by means of the 3-(4,5-Dimethylthiazol-2-yl)-2,5-Diphenyltetrazolium Bromide (MTT) assay. In line with other reports, REST KD cells cultured in presence of doxycycline showed a significant reduction in cell proliferation starting from 48 hours *in vitro* (**Figure 5.8A-B**). On the other hand, CTRL hNSCs and hGSCs did not shown any modification in cell proliferation following induction, indicating that the expression of non-targeting shRNAs does not alter cell growth (data not shown). To note, in some systems tetracycline and its analogues have been reported to target mitochondrial activity affecting cell metabolism and viability (**Chatzispyrou et al., 2015**). However, the fact that, CTRL cells with or without doxycycline performed similarly suggests mitochondrial function is not affected by the treatment.

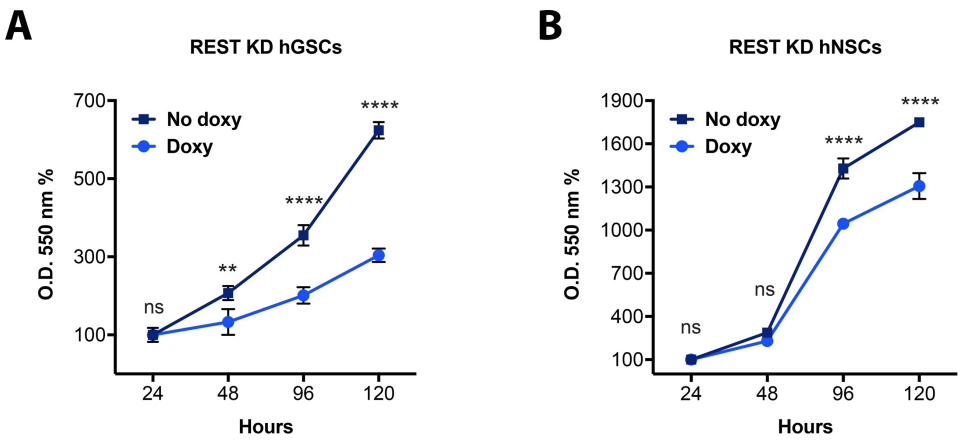

Figure 5.8. REST knock-down affects proliferative ability of both hGSCs and hNSCs. A. Growth assay on hGSCs REST KD treated with or without 500 ng/ml doxycycline. **B**. Growth assay on hNSCs REST KD treated with or without 500 ng/ml doxycycline. Results are expressed as % of O.D. 550 nm measured at 24 hours ± standard deviation and statistical significance inferred using two-way analysis of variance with a Sidak's post-hoc test.
ns: non-statistically significant; **: $p < 0.01$; ****: $p < 0.0001$.

Silencing of REST induces neuronal differentiation of hGSCs and hNSCs

Loss of REST function has been shown to affect hNSCs and hGSCs behaviour in terms of induction of neuronal differentiation and loss of multipotency. In order to investigate whether such phenotype occurs in our hNSCs and hGSCs lines, we tested whether REST knock-down can be maintained for long time *in vitro*. We initially analysed REST expression by means of immunocytochemistry in long-term induced (ten days) REST KD hNSCs and hGSCs. CTRL hNSCs and hGSCs did not shown any significant effect on REST immunoreactive signal, both in term of intensity and localization, further proving that non-targeting shRNAs do not alter cell properties/behaviour (data not shown). On the contrary, we observed a remarkable downregulation in the intensity of REST immunoreactivity following doxycycline treatment in both REST KD hNSCs and hGSCs, thus indicating that REST repression can be long-term maintained (**Figure 5.9**).

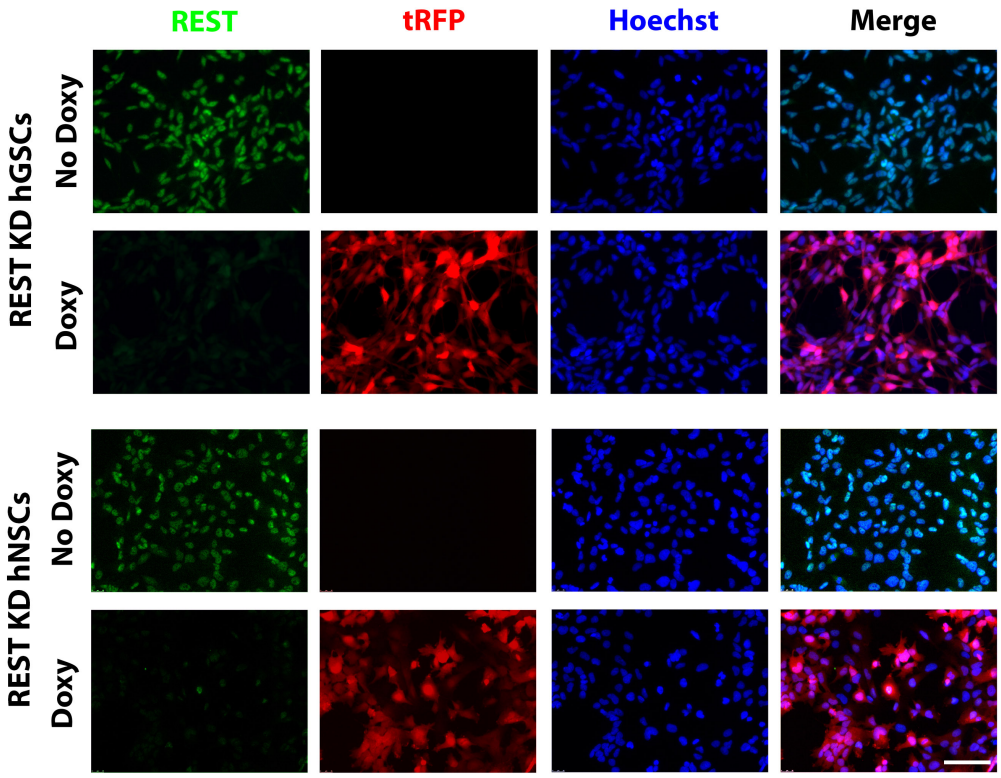

Figure 5.9. REST knock-down can be long term maintained in both REST KD hGSCs and hNSCs. Immunofluorescence for REST expression. Representative pictures of REST KD hGSCs (upper panels) and REST KD hNSCs (lower panels) treated with 500 ng/ml doxycycline for ten days. tRFP expression indicates activation of the Tet-on system (induced cells). Scale bar: 100 µm.

We then proceeded by examining the effects of REST silencing in self-renewal medium, i.e. a condition conceived for minimizing cell differentiation, on the expression of a set of markers associated to multipotent or differentiated cell states (**Figure 5.10 and 5.11**). Sox2 and Nestin are considered hallmark of multipotent neural progenitors, normally repressed upon differentiation to mature brain cells. Neuron-specific Class III β-Tubulin (β3-Tubulin) and glial fibrillary acidic protein (GFAP) are markers of neuronal and astrocytic differentiation, respectively, generally not expressed by hNSCs and hGSCs cultured in self-renewal conditions (**Falk et al., 2012; Pollard et al., 2009b**). Untreated hNSCs and hGSCs presented a very strong immunoreactivity for Nestin, that did not significantly change upon REST knock-down (data not shown). Conversely, REST silencing strongly affected Sox2 expression in hGSCs, as demonstrated by the loss of Sox2 immunoreactive signal in the doxycycline-treated cells (**Figure 5.10A-B**, 43.27 ± 4.97% doxy *versus* 89.94 ± 0.99% no doxy). Interestingly, REST knock-down in hNSCs led to only a slight, non-statistically

significant reduction in the number of $Sox2^+$ cells (**Figure 5.10A and C**, 60.40 ± 3.15% doxy *versus* 74.46 ± 5.55% no doxy). This result suggests that a prolonged repression of REST impairs hGSCs multipotency, even though it is not enough for the cells to completely differentiate, as shown by the maintenance of Nestin expression. The trend of hNSCs to lose Sox2 immunoreactivity following silencing of REST, indicates a similar yet smaller sensitivity to REST loss, with respect to the behaviour observed in hGSCs. In the same conditions, analysis of expression of differentiation markers pointed out an increased presence of β3-tubulin immunoreactive cells in both doxycycline-treated REST KD hNSCs (27.29 ± 1.21% doxy *versus* 9.87 ± 2.27% no doxy) and REST KD hGSCs (60.46 ± 5.16% doxy *versus* 3.6 ± 0.6% no doxy) (**Figure 5.11A-C**), supporting the effects of REST knock-down in eliciting exit from a multipotent state and acquisition of a neuronal character. Interestingly, we also found that the number of GFAP immunoreactive cells increased in doxycycline-treated REST KD hNSCs (25.96 ± 13.31% *versus* 10.30 ± 7.78% no doxy) and REST KD hGSCs (22.19 ± 2.20% *versus* 13.40 ± 4.88% no doxy), tough not to a statistically significant level (**Figure 5.11D-F).** These results are in line with previous reports of REST as a transcriptional repressor of neuronal genes and major gatekeeper of neuronal differentiation.

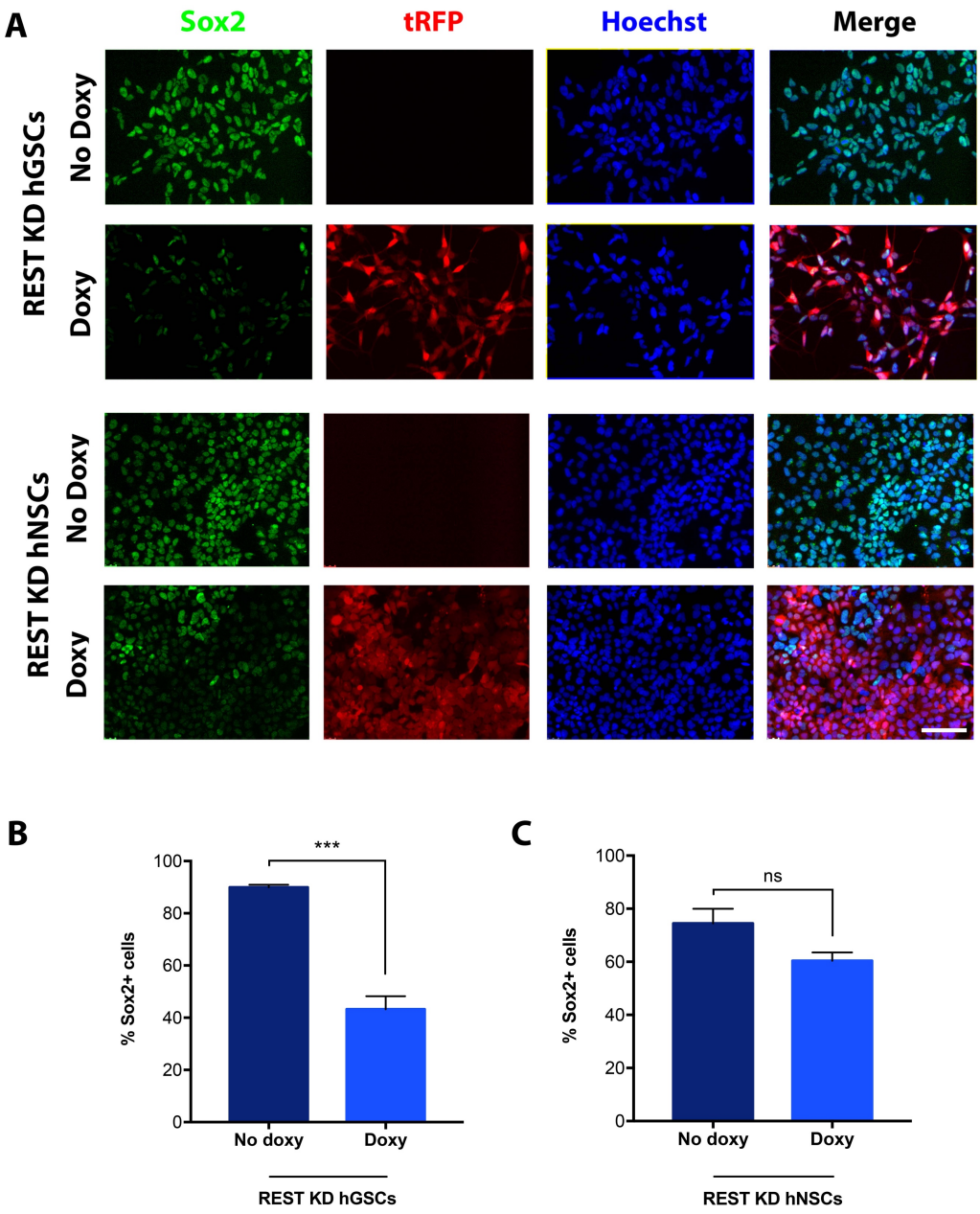

Figure 5.10. REST knock-down reduces Sox2 expression in hGSCs but not in hNSCs. A. Representative pictures of Sox2 Immunofluorescence assay performed in REST KD (upper panels) hGSCs and REST KD hNSCs (lower panels) treated with 500 ng/ml doxycycline for ten days. tRFP expression indicates activation of the Tet-on system. Scale bar: 100 µm. **B**. Quantification of $Sox2^{+}$ cells in REST KD hGSC cultures. **C**. Quantification of $Sox2^{+}$ cells in REST KD hNSC cultures. Quantification is normalised on untreated cells and expressed as % of immunoreactive cells on total number of cells. Results are expressed as mean ± standard deviation and statistical significance inferred using t-test.

ns: non-statistically significant; ***: $p < 0.001$.

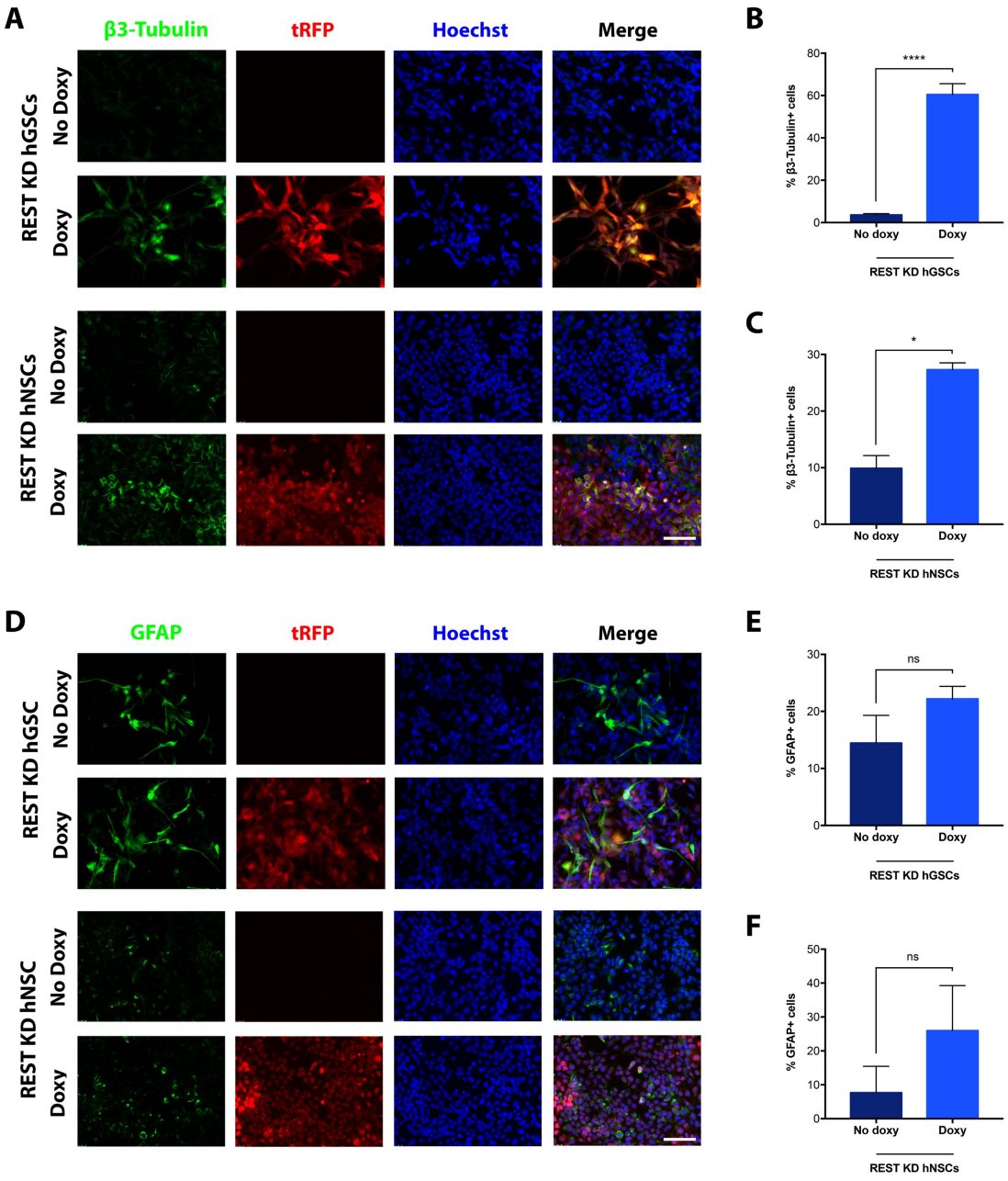

Figure 5.11. REST knock-down induces neuronal differentiation in both hGSCs and hNSCs. A. Representative pictures of immunofluorescence for β3-tubulin expression on REST KD hGSCs (upper panels) and REST KD hNSCs (lower panels) treated with 500 ng/ml doxycycline for ten days. tRFP expression indicates activation of the Tet-on system. Scale bar: 100 µm. **B**. Quantification of β3-tubulin$^+$ cells in REST KD cultures hGSCs. **C**. Quantification of β3-tubulin$^+$ cells in REST KD hNSC cultures. **D**. Representative pictures of immunofluorescence for GFAP expression on REST KD hGSCs (upper panels) and REST KD hNSCs (lower panels) treated with 500 ng/ml doxycycline for ten days. tRFP expression indicates activation of the Tet-on system. Scale bar: 100 µm. **E**. Quantification of GFAP$^+$ cells in REST KD hGSC cultures. **F**. Quantification of GFAP$^+$ cells in REST KD hNSC cultures. Quantification is normalised on untreated cells and expressed as % of immunoreactive cells on total number of cells. Results are expressed as mean ± standard deviation and statistical significance inferred using t-test.

ns: non-statistically significant; *: $p < 0.05$; ****: $p < 0.0001$.

Silencing of REST induces hGSCs but not hNSCs apoptosis

Finally, we analysed the occurrence of apoptosis in the cultures by means of cleaved caspase 3 expression in REST KD hNSC and hGSC cultures treated with or without doxycycline for ten days. Immunofluorescence analysis highlighted an increased number of cleaved caspase 3 immunoreactive hGSCs following REST knock-down (**Figure 5.12A-B** 246.97 ± 45.40% doxy *versus* 100.00 ± 28.76% no doxy), while no significant effect was present in hNSCs REST KD (**Figure 5.12A and C** 116.56 ± 59.95% doxy *versus* 100.00 ± 33.55% no doxy), suggesting hGSCs survival depends on REST levels.

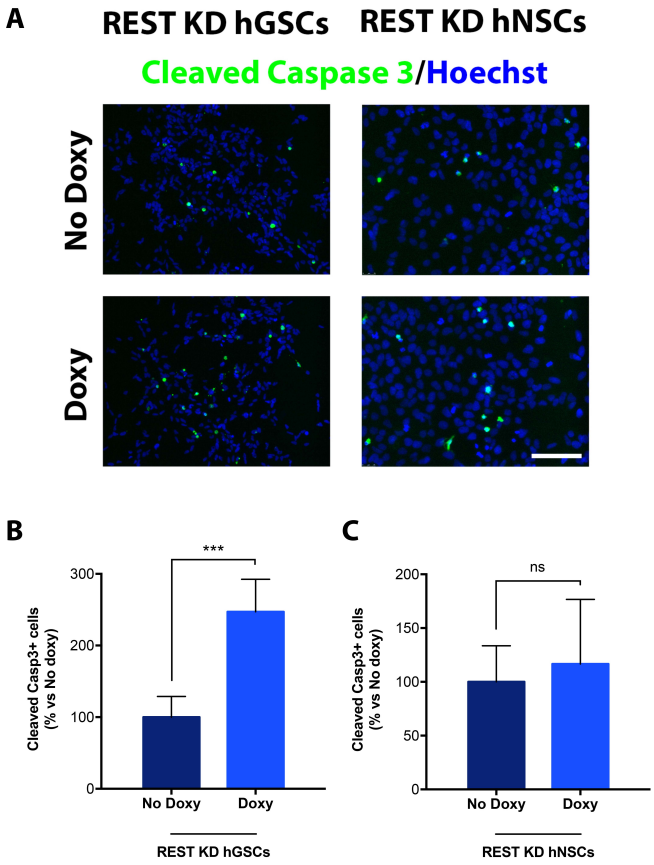

Figure 5.12. REST knock-down induces apoptosis in hGSCs but not in hNSCs. A. Representative pictures of immunofluorescence assay for cleaved caspase 3 performed on REST KD hGSCs (left panels) and REST KD hNSCs (right panels) treated with 500 ng/ml doxycycline for ten days. Scale bar: 100 µm. **B**. Quantification of cleaved caspase 3^+ cells in REST KD hGSC cultures. **C**. Quantification of cleaved caspase 3^+ cells in REST KD hNSC cultures. Quantification is normalised on untreated cells and expressed as % of immunoreactive cells on total number of cells. Results are expressed as mean ± standard deviation and statistical significance inferred using t-test.
ns: non-statistically significant; ***: $p < 0.001$.

Chapter 6

Generation and Characterisation of hGSC and hNSC Systems for Inducible Overexpression of REST

Contents

6.1 GENERATION OF REST INDUCIBLE OVEREXPRESSION HUMAN GLIOMA STEM CELL LINES	**72**
6.2 GENERATION OF REST INDUCIBLE OVEREXPRESSION HUMAN NEURAL STEM CELLS	**79**
6.3 EFFECT OF REST GAIN OF FUNCTION ON HGSCS AND HNSCS PROPERTIES	**81**

6.1 Generation of REST inducible overexpression human Glioma Stem Cell lines

To identify the optimal system for overexpressing REST, we infected hGSC cultures with lentiviral particles carrying either pINDUCER20hREST vector or the relative control vector pINDUCER20 (**Figure 4.1D**). Infected cultures were then selected by means of treatment with the neomycin analogue G418. Once selected, we tested the performance of the cultures in terms of REST overexpression levels. To this end, an initial pilot experiment was performed inducing cells with the conditions previously described for REST KD lines. Effective induction was assessed by analysing the relative REST mRNA levels and a selection of REST target genes. Quantitative RT-PCR assay showed a high and specific induction of REST transcript levels only upon addition of doxycycline in pIND20hREST hGSCs (**Figure 6.1A**, fold change with respect to no doxy treated pIND20hREST hGSCs: 25.66 ± 2.01). Control pIND20 hGSC cultures did not exhibit significant changes in REST transcript levels,

thus indicating the specificity of the system and no effects of doxycycline treatment *per se* in altering REST transcription (**Figure 6.1A**). Contrary to what observed when REST was silenced, the overexpression of REST did not cause any modulation of SNAP25 mRNA levels. However, both VGF and TUBB3 were significantly repressed in REST overexpressing cells, suggesting an increased REST activity possibly due to the its induction at protein level (**Figure 6.1B**). This result suggests that the pIND20hREST hGSCs are amenable for inducing REST overexpression upon doxycycline exposure. Also, based on these results, we chose VGF as optimal target gene to evaluate REST activity in the future experiments as among the target genes considered, its expression appeared more suitable to monitor REST upregulation.

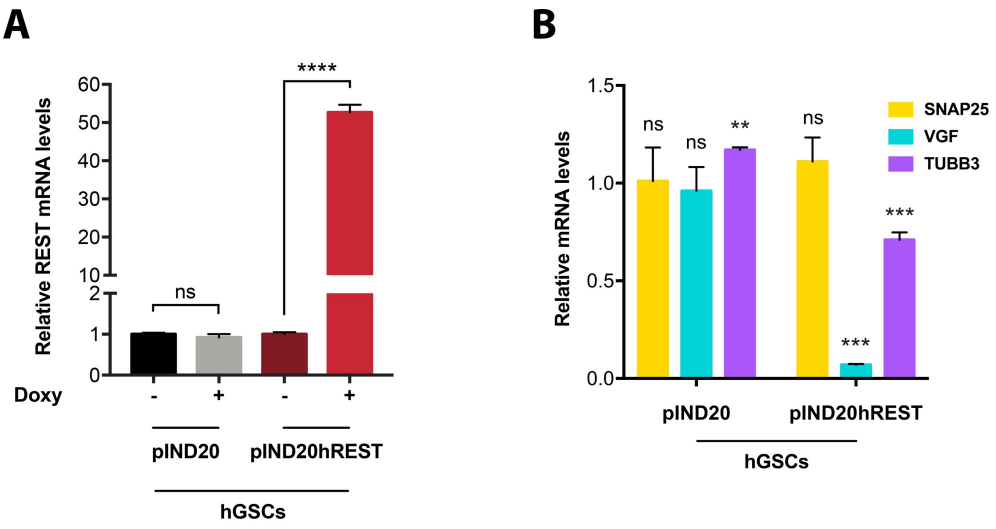

Figure 6.1. Pilot experiment: infection of hGSCs cells with pIND20 and pIND20shREST and qRT-PCR for 48 hours. A. qRT-PCR assay for REST expression in pIND20 hGSCs and pIND20hREST hGSCs treated with or without 500 ng/ml doxycycline for 48 hours. **B**. qRT-PCR assay for REST target genes expression on doxy treated pIND20 hGSCs and pIND20hREST hGSCs normalised on no doxy treated cells. qRT-PCR quantifications have been normalised on untreated cells. Results are expressed as mean ± standard deviation and statistical significance inferred using t-test.
ns: non-statistically significant; **: $p < 0.01$; ***: $p < 0.001$; ****: $p < 0.0001$.

In order to determine the best condition to overexpress REST, we performed a time course experiment of induction. Since the excess of REST is usually managed by the cell via ubiquitination and proteasome degradation (**Guardavaccaro et al., 2008; Huang et al.,**

2011; Singh et al., 2011; Westbrook et al., 2008), we treated the cells with the proteasome inhibitor MG-132, in order to maximize the amount of REST following induction. Upon doxycycline treatment, pIND20hREST hGSCs exhibited an apparent light reduction in proliferation without anyway showing any appreciable morphological change during the course of the experiment (**Figure 6.2A**). As observed in the pilot experiment, REST was successfully and highly overexpressed selectively in the induced pIND20hREST hGSCs, while pIND20 hGSCs did not show any modulation in REST levels (**Figure 6.2B**). Overexpression started at 24 hours of induction and lasted for the 72 hours of doxycycline treatment, though showing a progressive reduction with time (Fold change with respect to no doxy treated pIND20hREST hGSCs: 54.56 ± 1.81 at 24 hours, 40.37 ± 1.61 at 48 hours, and 33.21 ± 1.69 folds at 72 hours) likely due to the activation of intrinsic cells' mechanisms to control REST levels. Concurrently, we observed an increased repression of VGF transcripts levels (**Figure 6.2C**, fold change with respect to no doxy treated pIND20hREST hGSCs: 0.07 ± 0.00 at 24 hours, 0.07 ± 0.01 at 48 hours, and 0.10 ± 0.01 at 72 hours). The induction of REST transcripts resulted in a consistent overexpression also at protein level with a 24.38 folds increase at 24 hours, 14.61 folds at 48, and 6.00 folds at 72 hours (**Figure 6.2D**). As expected, the proteasome inhibitor MG-132 was able to counteract the degradation of REST, increasing the doxycycline-induced overexpression by six folds at 48 hours (85.48 folds) and two folds at 72 hours (11.94 folds) of induction. Little variation in REST protein was observed also in the control pIND20 hGSCs, especially when treated with MG-132, however with a lower degree than pIND20hREST cultures (**Figure 6.2D**). This is attributable to a reduced degradation of the endogenous REST because of the inhibition of the proteasome activity by MG-132.

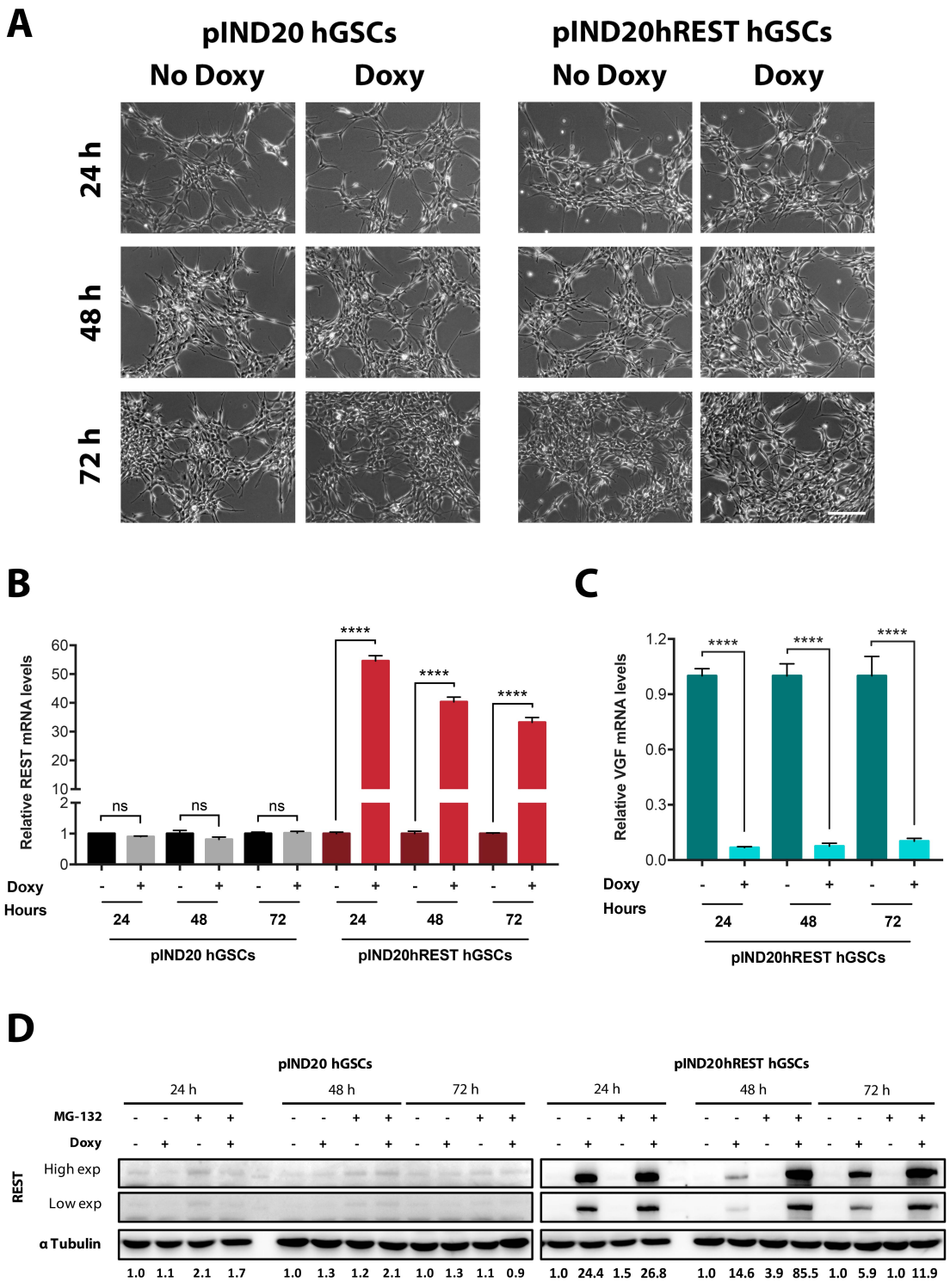

Figure 6.2. Time course induction of pIND20 hGSCs and pIND20shREST hGSCs. A. Representative pictures of pIND20 hGSCs and pIND20hREST hGSCs treated with 500 ng/ml doxycycline for up to 72 hours. Scale bar: 200 µm. **B**. qRT-PCR assay for REST expression. **C**. qRT-PCR assay for the REST target gene VGF expression. **D**. Representative picture of western blot analysis for REST and relative densitometric quantification. qRT-PCR and immunoblotting quantifications have been normalised on untreated cells at the corresponding time point. Results are expressed as mean ± standard deviation and statistical significance inferred using t-test.
ns: non-statistically significant; ****: $p < 0.0001$.

In parallel with pIND20hREST hGSCs, in order to select the best system for REST overexpression we generated also pIND22hREST hGSCs and the relative control pIND22 hGSC line. This system differs from pINDUCER20hREST since the Neomycin resistance cassette is replaced by an eGFP cassette, thus allowing live recognition of transduced cells (**Figure 4.1C**). Following infection with lentiviral particles carrying either pIND22hREST vector or the relative control vector pIND22, the cells grew apparently normally with no evident changes in morphology. However, eGFP signal was barely visible in both cell lines at the fluorescent microscope (data not shown). Investigation of the percentage of infected cells by FACS analysis reported that only 2.6% of the pIND22 hGSCs and 12.8% of the pIND22hREST hGSCs were $eGFP^+$ (**Figure 6.3B-C before sorting**), thus confirming our qualitative observations. To increase the number of infected cells in the two populations, we selected $eGFP^+$ cells by means of cell sorting. In this way, we managed to increase the fraction of infected cells in the pIND22hREST hGSCs population to 72.4% (**Figure 6.3D**). Unfortunately, we could not perform a post-sorting analysis of the pIND22 hGSCs as the cells were too few to be tested immediately. To compare the efficacy of the pIND22hREST hGSCs with the previously characterised pIND20hREST hGSCs in inducing REST expression, we treated the cultures with doxycycline for 48 hours and analysed the expression of REST and its target gene VGF (**Figure 6.4**). Despite cell sorting selection, live cell imaging showed a very minor percentage of $eGFP^+$ cells (**Figure 6.4A**). Nonetheless, following doxycycline treatment, we observed a 24.18 ± 1.65 folds and 27.06 ± 4.49 folds increase in pIND22hREST hGSCs at 24 and 48 hours, respectively (**Figure 6.4B**). No effects on REST mRNA levels were visible in doxycycline-treated pIND22 hGSCs (**Figure 6.4B**). Importantly, the observed raising in REST transcript levels resulted in an increased repression of the REST target gene VGF (**Figure 6.4C**, fold change with respect to non-induced pIND22hREST hGSCs: 0.39 ± 0.02 at 24 hours, and 0.25 ± 0.03 at 48 hours), indicative of a higher REST transcriptional repression activity. Also, following doxycycline treatment, REST protein levels were found increased exclusively in pIND22hREST hGSC line (**Figure 6.4D**, fold change with respect to non-induced pIND22hREST hGSCs: 2.73 at 24 hours and 8.32 at 48), though at a lesser extent than in pIND20hREST hGSCs, even when MG-132 was added to the cultures.

Based on these results, we selected the pIND20hREST hGSC line as the optimal system to study the effects of REST overexpression.

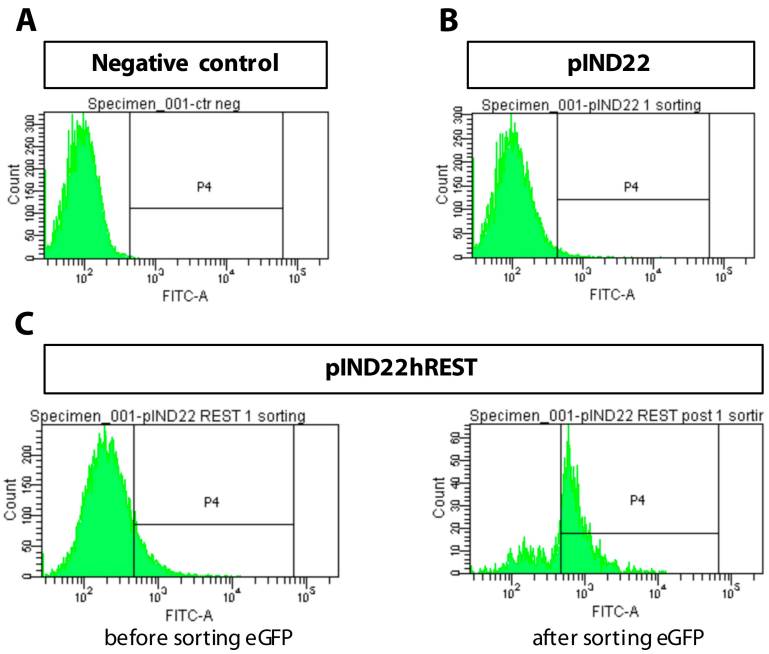

Figure 6.3. FACS-Sorting of eGFP^{+} pIND22 and pIND22hREST hGSCs. A. eGFP expression of parental non-infected hGSCs used to select the sorting gate (P4). **B**. eGFP expression of pIND22 hGSCs before and after sorting. **C**. eGFP expression of pIND22hREST hGSCs before and after sorting.

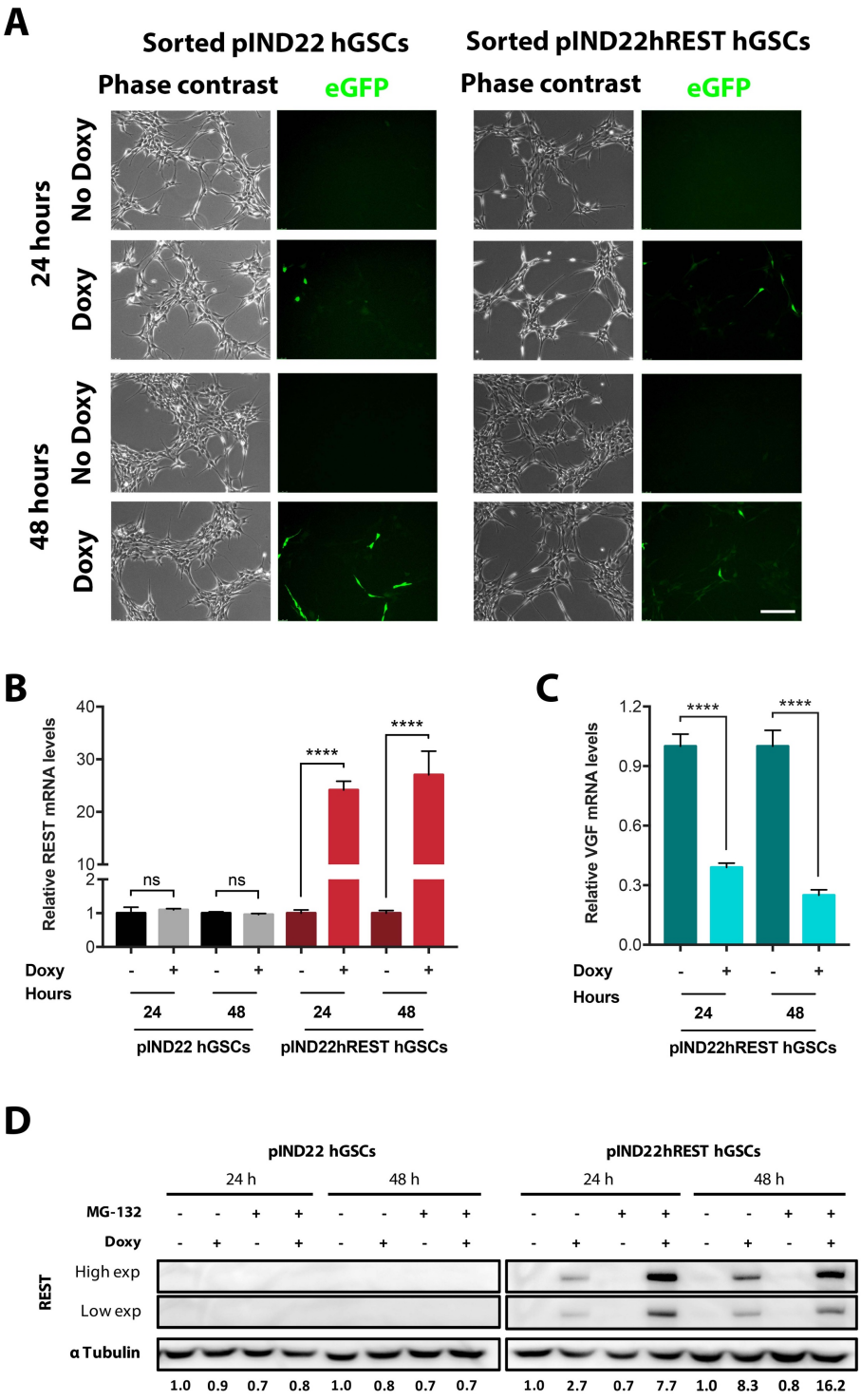

Figure 6.4. Time course induction of pIND22 hGSCs and pIND22hREST hGSCs. A. Representative pictures of pIND22 hGSCs and pIND22hREST hGSCs treated with 500 ng/ml doxycycline for up to 48 hours. Scale bar: 200 µm. **B**. qRT-PCR assay for REST expression. **C**. qRT-PCR assay for the REST target gene VGF expression. **D**. Representative picture of western blot analysis for REST and relative densitometric quantification. qRT-PCR and immunoblotting quantifications have been normalised on untreated cells at the corresponding time point. Results are expressed as mean ± standard deviation and statistical significance inferred using t-test.
ns: non-statistically significant; ****: $p < 0.0001$.

6.2 Generation of REST inducible overexpression human Neural Stem Cells

Once generated the REST OE hGSCs and defined the condition for REST overexpression, we transduced hNSCs with lentiviral particles carrying pIND20hREST or control pIND20 vectors and selected with G418 to generate pIND20hREST and pIND20 hNSC lines. These cell lines will be used to compare the differential effects of REST overexpression in hNSCs *versus* hGSCs. We therefore evaluated the responsiveness of the cultures by treating cells with doxycycline for 24 hours and assaying by qRT-PCR the expression levels of REST and a selection of REST target genes (**Figure 6.5**). Interestingly, REST-overexpressing hNSCs showed a reduction of cell proliferation similar to what previously observed in pIND20hREST hGSCs (data not shown), though they also presented evident signs of cell detachment with respect to untreated pIND20hREST hNSCs and pIND20 hNSCs, possibly due to the repression of many adhesion molecules known to be controlled by REST (**Figure 6.5A,** **Sun et al., 2005, 2008; Johnson et al., 2006; Otto et al., 2007**). Cultures of pIND20hREST hNSC showed a marked increase of REST mRNA (**Figure 6.5B**, fold change with respect to no doxy pIND20hREST hNSCs: 149.11 ± 22.03) associated with the repression of REST target genes expression (**Figure 6.5C**, fold change with respect to no doxy pIND20hREST hNSCs, VGF: 0.44 ± 0.11 folds, BDNF: 0.70 ± 0.04 folds, and SYP: 0.53 ± 0.06 folds). Importantly, doxycycline-treated control pIND20 hNSC cultures did not exhibit significant effects both on the transcript levels of REST (**Figure 6.5B**) and on its target genes (not shown). Western bot analysis showed that doxycycline treatment resulted in a 31.47 folds increment in REST protein levels in pIND20hREST hNSC cultures while no significant effects are visible on control pIND20 hNSCs (**Figure 6.5D**).

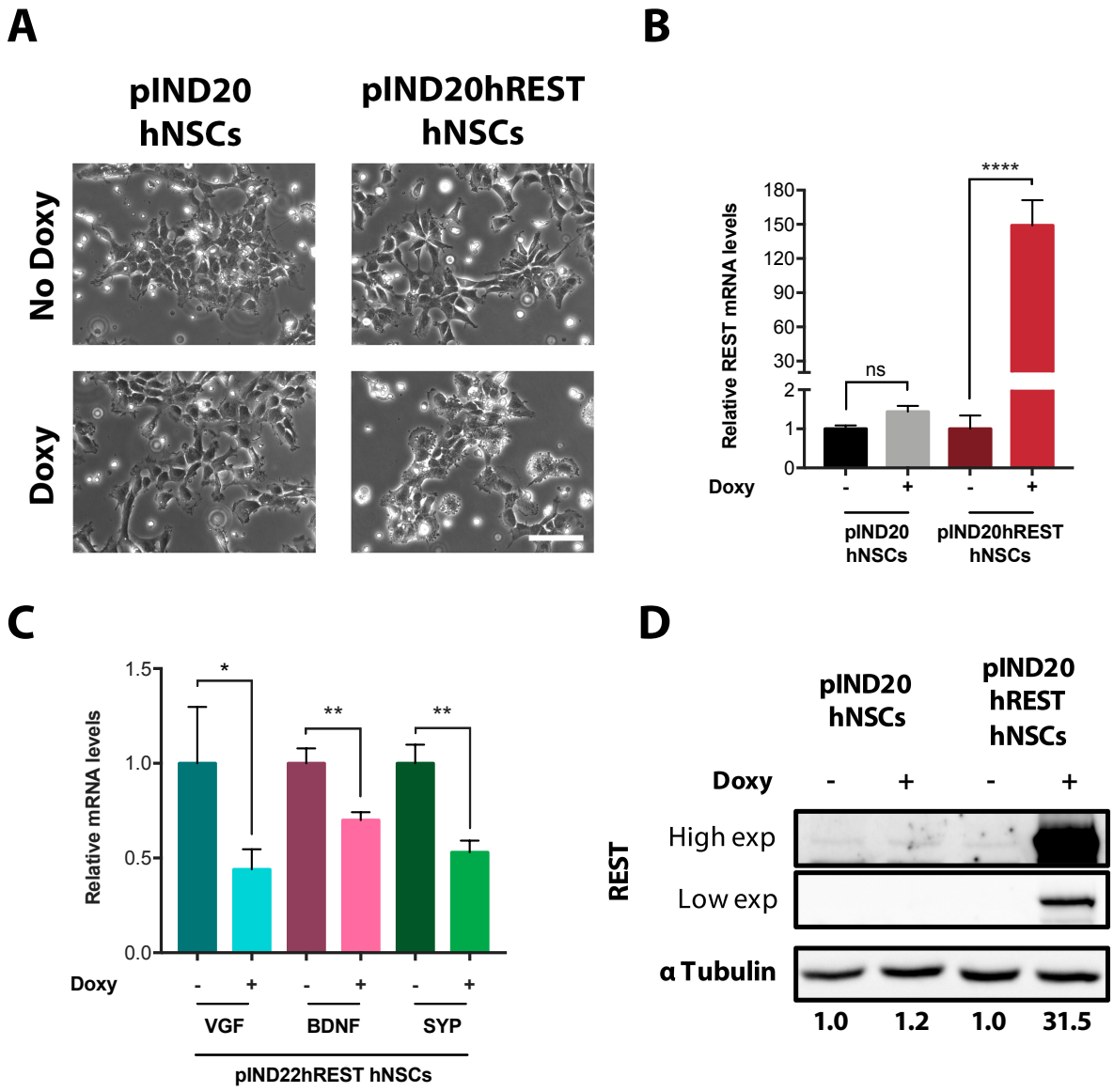

Figure 6.5. Induction of pIND20 hNSCs and pIND20shREST hNSCs. A. Representative pictures of pIND20 hNSCs and pIND20hREST hNSCs treated with 500 ng/ml doxycycline for 24 hours. Scale bar: 100 µm. **B**. qRT-PCR assay for REST expression. **C**. qRT-PCR assay for selected REST target genes expression. **D**. Representative picture of western blot analysis for REST and relative densitometric quantification. qRT-PCR and immunoblotting quantifications have been normalised on untreated cells at the corresponding time point. Results are expressed as mean ± standard deviation and statistical significance inferred using t-test.

ns: non-statistically significant; *: $p < 0.05$; **: $p < 0.01$; ****: $p < 0.0001$.

6.3 Effect of REST gain of function on hGSCs and hNSCs properties

Having established the REST overexpressing hGSC and hNSC lines and defined the experimental conditions for effective REST induction, we investigated the REST-mediated functional effects on cell proliferation, multipotency and apoptosis. Since REST is generally highly active in neural progenitors and GSCs, few REST-overexpression studies have been reported in these types of cells.

For the direct comparison studies have included the following cell lines:

i. CTRL OE hGSCs (corresponding to pIND20 hGSCs)
ii. REST OE hGSCs (corresponding to pIND20hREST hGSCs)
iii. CTRL OE hNSCs (corresponding to pIND20 hNSCs)
iv. REST OE hNSCs (corresponding to pIND20hREST hNSCs)

REST overexpression affects hGSCs and hNSCs cell growth

Cell growth evaluated by means of the MTT assay following doxycycline treatment showed a reduction in cell proliferation both in REST OE hGSCs and hNSCs (**Figure 6.6A-B**). REST OE hGSCs demonstrated a 24,7% reduction of cell number at 96 hours and 45,3% reduction at 120 hours, while REST OE hNSCs presented a 64,1% and 65,2% reduction of cell number at 96 hours and 120 hours respectively. On the other hand, CTRL OE hGSCs and hNSCs did not show any alteration in cell proliferation (data not shown), underlying once again that the concentration of doxycycline used for activating the Tet-on system is non-toxic and did not alters cell growth.

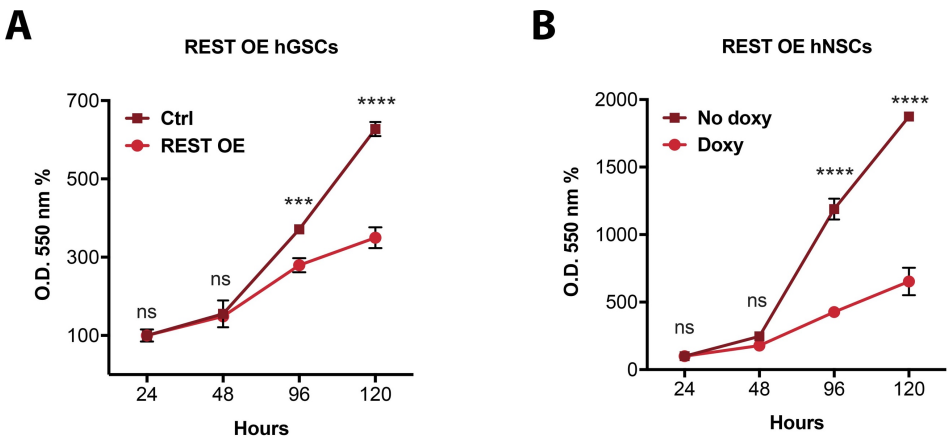

Figure 6.6. REST overexpression affects proliferative ability of both hGSCs and hNSCs. A. Growth assay on REST OE hGSCs treated with or without 500 ng/ml doxycycline. **B**. Growth assay on REST OE hNSCs treated with or without 500 ng/ml doxycycline. Results are expressed as % of O.D. 550 nm measured at 24 hours ± standard deviation and statistical significance inferred using two-way analysis of variance with a Sidak's post-hoc test.
ns: non-statistically significant; ***: $p < 0.001$; ****: $p < 0.0001$.

REST overexpression induces quiescence in hGSCs and hNSCs

The reduction in cell proliferation that we observed following REST silencing was attributable to a gradual acquisition of a neuronal phenotype accompanied by cell cycle exit. To test whether the reduced growth exhibited following overexpression of REST may be due to the same pro-differentiative effect or to other mechanisms, we cultured REST OE hGSCs and hNSCs in presence of doxycycline. We initially analysed REST expression by means of immunocytochemistry in long-term induced (ten days) CTRL and REST OE hGSCs and hNSCs. We found that REST immunoreactivity increased dramatically in both doxycycline-treated REST OE hGSC and hNSC cells (**Figure 6.7**). Analysis of NSC markers, Sox2 showed no differences in the number of $Sox2^+$ cells between hNSCs and hGSCs overexpressing REST and non-induced cells (not shown). Nonetheless, an evident increase in the intensity of Sox2 immunoreactive signal in doxycycline-treated REST OE hGSCs and hNSCs was visible (**Figure 6.8**). Also, we found that while the number of $Nestin^+$ cells was not affected, with nearly all of the cells in culture being positive for this marker (**Figure 6.9B and E**, 96.54 ± 1.01% doxy *versus* 98.78 ± 1.08% no doxy treated REST OE hGSCs; 95.56 ± 6.29% doxy *versus* 95.87 ± 5.35% no doxy treated REST OE hNSCs), a marked increase in

GFAP$^+$ cells occurred (fold of increase of GFAP$^+$ hNSCs: 5.42; fold of increase of GFAP$^+$ hGSCs: 6.98) in REST-overexpressing hGSCs and hNSCs (**Figure 6.9C and F**). Interestingly, the gain in GFAP expression determined an increased number of Nestin and GFAP co-expressing cells (**Figure 6.9D and G**, fold of increase of Nestin$^+$/GFAP$^+$ hNSCs: 5.18; fold of increase of Nestin$^+$/GFAP$^+$ hGSCs: 9.11). On the whole, these results indicate that following REST overexpression in hNSCs and hGSCs, most of the cells in culture exhibit reduced cell growth and co-expression of Nestin, GFAP and Sox2.

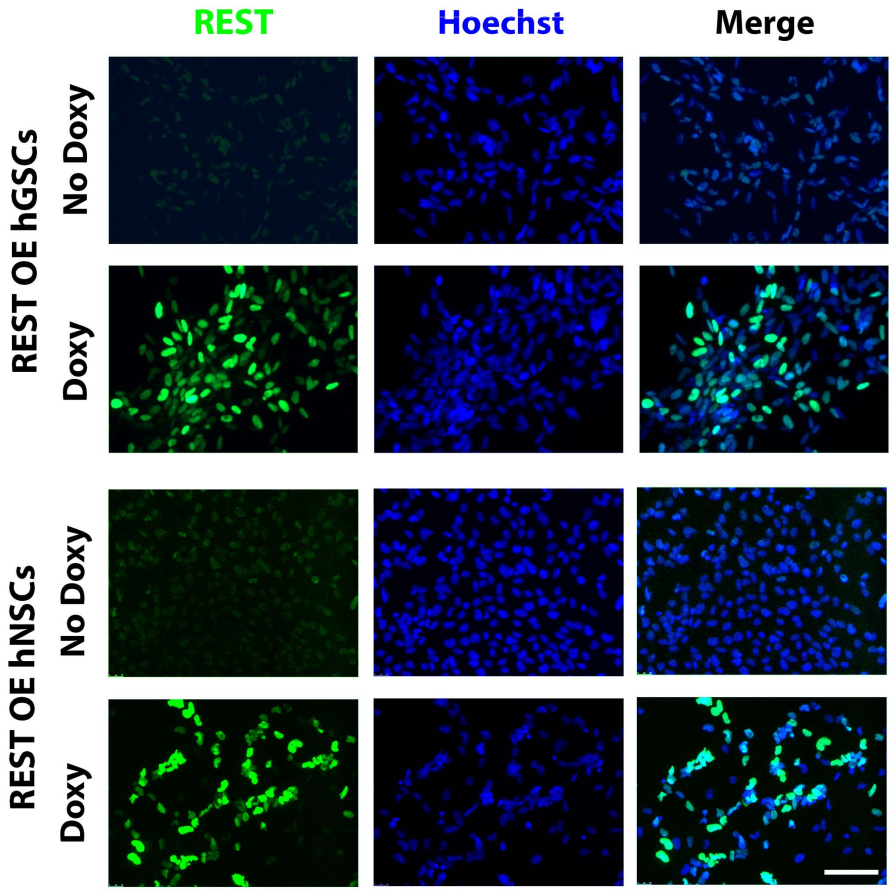

Figure 6.7. REST overexpression can be long term maintained in both REST OE hGSCs and hNSCs. Representative pictures of immunofluorescence for REST expression performed on REST OE hGSCs (upper panels) and REST OE hNSCs (lower panels) treated with 500 ng/ml doxycycline for ten days. Scale bar: 100 µm.

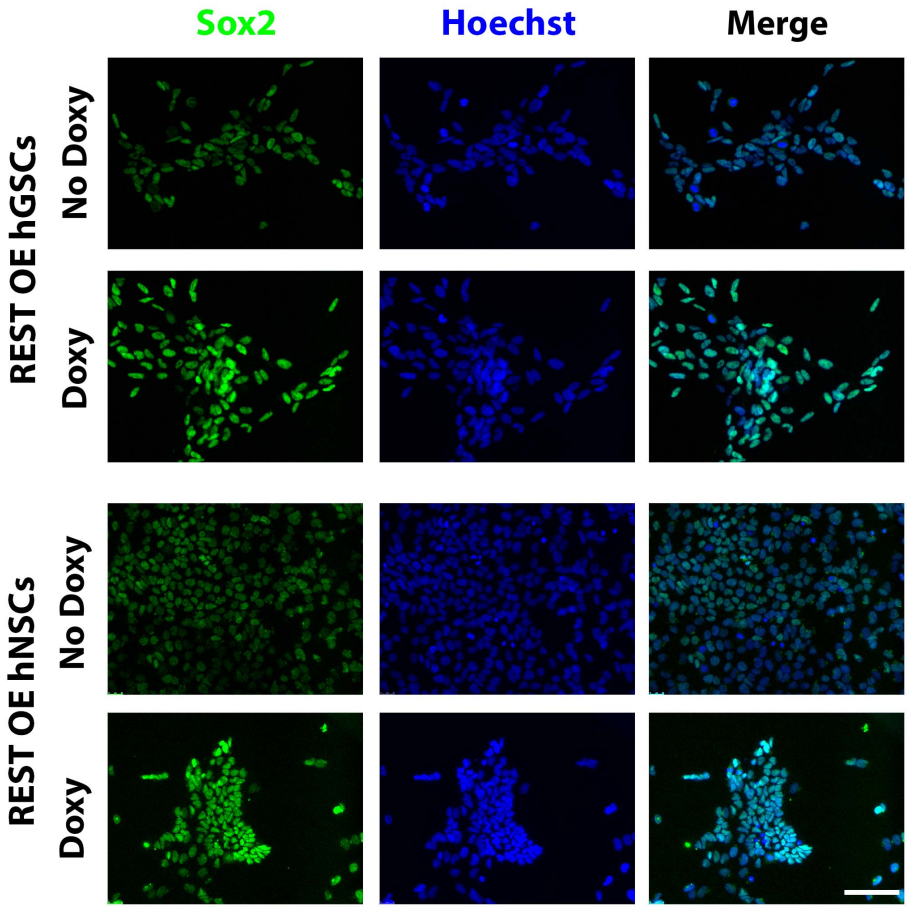

Figure 6.8. REST overexpression induces Sox2 expression in hGSCs and hNSCs. Representative pictures of immunofluorescence for Sox2 expression performed on REST OE hGSCs (upper panels) and REST OE hNSCs (lower panels) treated with 500 ng/ml doxycycline for ten days.
Scale bar: 100 µm.

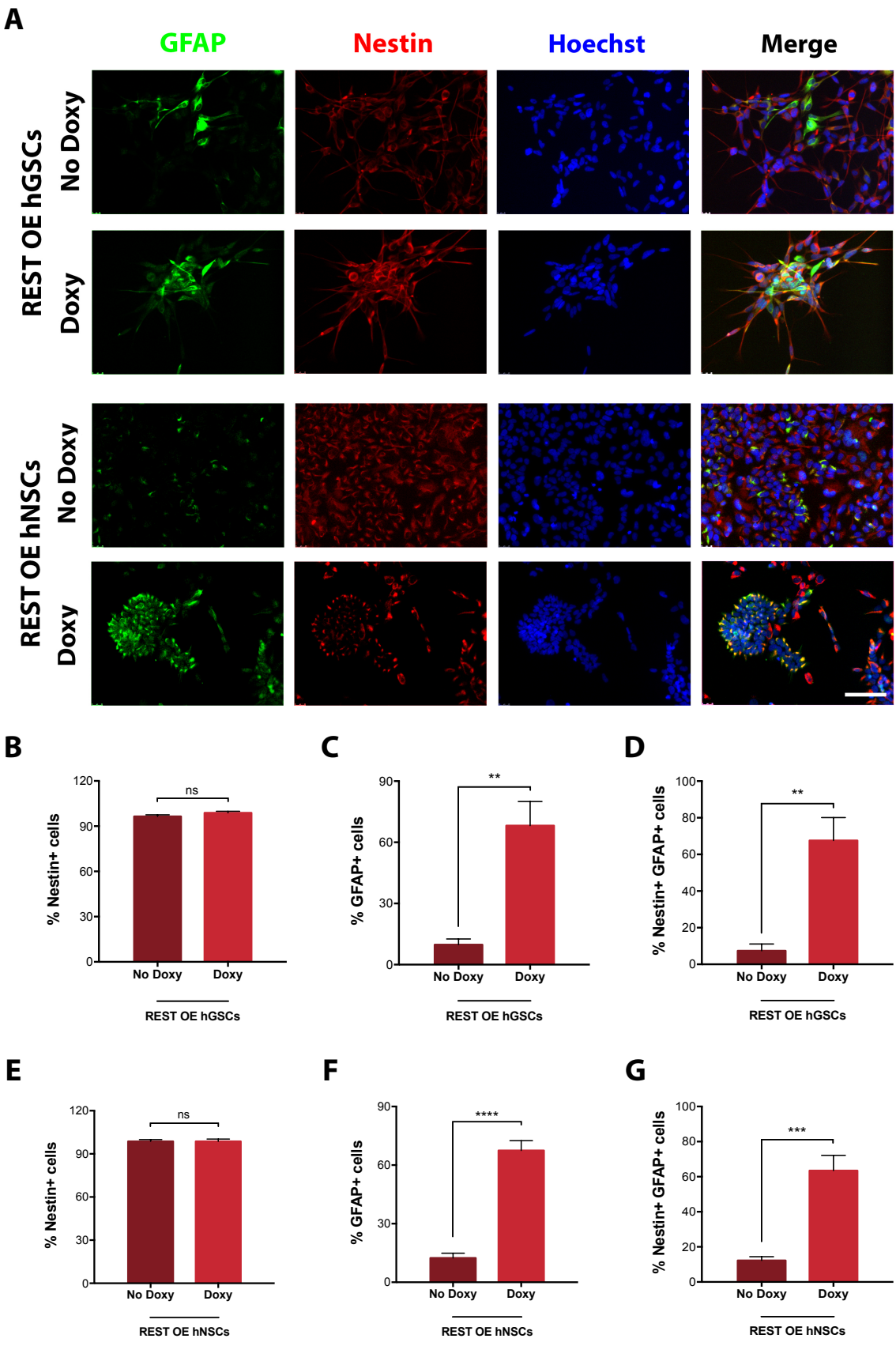
A
GFAP
Nestin
Hoechst
Merge
REST OE hGSCs
No Doxy
Doxy
REST OE hNSCs
No Doxy
Doxy
B
% Nestin+ cells
ns
No Doxy
Doxy
REST OE hGSCs
C
% GFAP+ cells
**
No Doxy
Doxy
REST OE hGSCs
D
% Nestin+ GFAP+ cells
**
No Doxy
Doxy
REST OE hGSCs
E
% Nestin+ cells
ns
No Doxy
Doxy
REST OE hNSCs
F
% GFAP+ cells
****
No Doxy
Doxy
REST OE hNSCs
G
% Nestin+ GFAP+ cells
***
No Doxy
Doxy
REST OE hNSCs

Figure 6.9. REST overexpression induces quiescent neural stem cells markers in both hGSCs and hNSCs. A. Representative pictures of immunofluorescence for Nestin and GFAP expression performed on REST OE hGSCs (upper panels) and REST OE hNSCs (lower panels) treated with 500 ng/ml doxycycline for ten days. Scale bar: 100 µm. **B**. Quantification of $Nestin^+$ cells in REST OE hGSC cultures. **C**. Quantification of $GFAP^+$ cells (%) in REST OE hGSC cultures. **D**. Quantification of $Nestin^+/GFAP^+$ cells in REST OE hGSCs. **E**. Quantification of $Nestin^+$ cells in REST OE hNSC cultures. **F**. Quantification of $GFAP^+$ cells in REST OE hNSC. **G**. Quantification of $Nestin^+/GFAP^+$ cells in REST OE hNSC cultures. Quantification is normalised on untreated cells and expressed as % of immunoreactive cells on total number of cells. Results are expressed as mean ± standard deviation and statistical significance inferred using t-test.
ns: non-statistically significant; **: $p < 0.01$; ***: $p < 0.001$; ****: $p < 0.0001$.

REST overexpression does not impact hGSCs and hNSCs viability

We analysed the occurrence of apoptosis in the cultures by means of cleaved caspase 3 expression in REST OE hNSC and hGSC cultures treated with or without doxycycline for ten days. No significant differences in the percentage of cleaved caspase 3^+ cells were found between untreated and doxycycline treated hGSCs and hNSCs REST OE (hGSCs: 153.81 ± 75.69% doxy *versus* 100.00 ± 36.19% no doxy; hNSCs: 109.92 ± 17.07% doxy *versus* 100.00 ± 28.26% no doxy) (**Figure 7.10A-C**), suggesting that programmed cell death does not contribute to the reduced number of cells measured in REST overexpressing cultures.

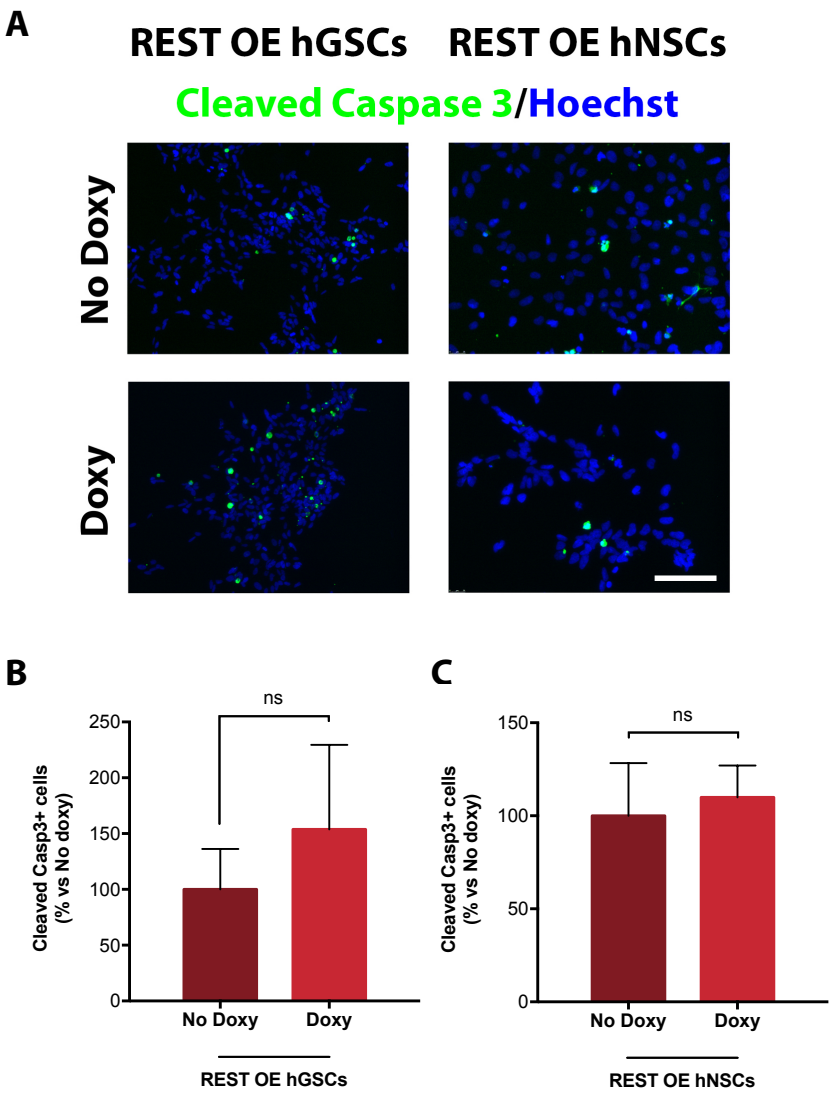

Figure 6.10. REST overexpression does not influence apoptosis in hGSCs or hNSCs. A. Representative pictures of immunofluorescence for cleaved caspase 3 expression performed on REST OE hGSCs (left panels) and REST OE hNSCs (right panels) treated with 500 ng/ml doxycycline for ten days. Scale bar: 100 µm. **B**. Quantification of cleaved caspase 3^+ cells in REST OE hGSCs. **C**. Quantification of cleaved caspase 3^+ cells in REST OE hNSCs. Quantification is normalised on untreated cells and expressed as % of immunoreactive cells on total number of cells. Results are expressed as mean ± standard deviation and statistical significance inferred using t-test.
ns: non-statistically significant.

Chapter 7

Gene Expression Analysis of REST Modulated hGSCs and hNSCs

Contents

7.1 COMPARING REST MODULATED HGSCS TO HNSCS REVEALS HGSCS SPECIFIC EFFECT OF REST 88
7.2 REST CONTROLS NEURAL MULTIPOTENCY THROUGH MODULATION OF NEURONAL DIFFERENTIATION, PROLIFERATION AND CELL METABOLISM 93
7.3 HGSC-SPECIFIC REST-REGULATED GENES REGULATES NEURONAL DIFFERENTIATION, PROLIFERATION AND CELL METABOLISM 101
7.4 REPRESSION OF HGSC-SPECIFIC REST REGULATED GENES IS ASSOCIATED TO POORER PROGNOSIS 105

7.1 Comparing REST modulated hGSCs to hNSCs reveals hGSCs specific effect of REST

To identify molecular networks differentially governed by REST in hGSCs *versus* hNSCs, we took advantage of microarray technology using the novel Affymentrix Clariom D platform for the interrogation of more than 540.000 transcripts. These include well annotated genes, non-coding RNAs and splice variants, although in the context of this PhD thesis work we focused our attention exclusively on coding RNAs.

To study gene expression modifications specifically driven by REST activity in hGSCs and hNSCs, we decided to include the samples listed in **Table 7.1**, aiming at comparing the list of differentially expressed genes in REST overexpressing hGSCs or hNSCs, with the ones obtained from REST silenced cells (**Table 7.2, comparisons 4 and 8**). These gene lists were

produced intersecting gene expression data from doxycycline treated REST KD and REST OE hGSCs and hNSCs with the corresponding untreated control cells (**Table 7.2, comparisons 2, 3, 6, and 7**). Finally, tumour and non-pathological REST-specific targets were identified intersecting the differentially expressed genes in REST-modulated hGSCs with those whose expression changes in REST-modulated hNSCs (**Table 7.2, comparison 9**). Moreover, since REST modulation was achieved through Tet-on systems, we included parental hGSCs and hNSCs treated with or without doxycycline, in order to identify those differentially-modulated genes whose expression is driven by the presence of doxycycline (**Table 7.2, comparisons 1 and 5**).

Sample ID	Sample name
i	hGSCs
ii	hGSCs + doxycycline
iii	REST KD hGSCs + doxycycline (referred as REST KD hGSCs)
iv	REST OE hGSCs
v	REST OE hGSCs + doxycycline (referred as REST OE hGSCs)
vi	hNSCs no doxy
vii	hNSCs + doxycycline
viii	REST KD hNSCs + doxycycline (referred as REST KD hNSCs)
ix	REST OE hNSCs
x	REST OE hNSCs + doxycycline (referred as REST OE hNSCs)

Table 7.1. List of samples included in the gene expression analysis.

Comparison ID	Comparison	Result
1	ii versus i	Effect of doxycycline on hGSCs
2	iii versus i	Effect of REST knock-down on hGSCs
3	v versus iv	Effect of REST overexpression on hGSCs
4	3 versus 2	Effect of REST on hGSCs
5	x versus ix	Effect of doxycycline on hNSCs
6	viii versus vi	Effect of REST knock-down on hNSCs
7	vii versus vi	Effect of REST overexpression on hNSCs
8	7 versus 8	Effect of REST in hNSCs
9	8 versus 4	Cell type specific effect of REST

Table 7.2. List of comparisons considered for identifying differentially expressed genes upon REST modulation.

Our aim was to achieve the strongest modulation of REST in short time points in order to be able to observe potential direct effects of REST transcriptional activity and limit indirect gene expression modulation by other factors downstream of REST. Based on the characterisation of REST modulation in hGSCs and hNSCs (**chapter 4 and 5**), we chose to treat the cells using 500 ng/ml of doxycycline, which we demonstrated to produce a specific and strong activation of the Tet-on system in our experimental settings (**Figure 5.2B-C**), without anyway affecting cells' survival and growth. REST OE hGSCs and hNSCs were treated for 24 hours, the earliest time points to achieve REST protein overexpression following doxycycline treatment (**Figure 6.2D and 6.5D**), accompanied by an increased repression of REST target genes (**Figure 6.2C and 6.5C**). Effective REST silencing appeared slower than overexpression, probably because it is achieved through a more complex mechanism with doxycycline driving the transcription of shRNAs anti-REST that are subsequently processed by intracellular machinery to mediate the degradation of the endogenous REST mRNA and protein. For this reason, we treated the REST KD hGSCs and hNSCs for 48 hours to obtain REST protein downregulation (**Figure 5.6C and 5.7B**) and REST target genes derepression (**Figure 5.6D and 5.7D**).

RNAs from the samples listed in **table 7.1** were retro-transcribed and hybridised on microarray chips, passing the quality control tests for sample's reliability, and the data were processed in bioinformatics analyses. Unsupervised analysis was performed using hierarchical clustering analysis with Ward.2 method and Euclidian distance using probes with variance more than 90%. This analysis highlighted a clear difference between hGSCs and hNSCs experimental groups at the transcriptome level. Indeed, the analysis produced a segregation into two major clusters, composed selectively by either hGSCs or hNSCs, independently from REST modulation (**Figure 7.1**). Within the two macro-groups, the second layer of clustering is composed according to the level of REST expression, with REST-overexpressing cells clustering separately from REST-silencing cells and separately from untreated/parental samples.

Differentially expressed transcripts in doxycycline treated *versus* control were selected with a false discovery rate (FDR) < 0.05. Using this criterion, we obtained 550 (among which 532 downregulated) and 150 (among which 145 downregulated) differentially expressed coding transcripts in REST overexpressing hGSCs and hNSCs *versus* control cells,

respectively (**Appendix A and C**). We selected 406 differentially expressed coding genes (among which 368 upregulated) in doxycycline treated REST KD hGSCs *versus* control cells (**Appendix B**). Surprisingly, only 9 coding transcripts (all of them upregulated) resulted differentially expressed in REST KD hNSCs *versus* control cells (**Appendix D**). This result was unexpected given our previous molecular and phenotypic characterisation of the cells and the literature data, suggesting REST downregulation deeply impact hNSCs biology. Moreover, before sending RNA samples for microarray analysis we tested *REST* and REST target genes modulation by qRT-PCR obtaining results comparable to the ones presented in **figure 5.7C and D** (data not shown). Comparison of parental untreated cells *versus* parental cells cultured in presence of doxycycline identified differentially expressed transcripts whose regulation is affected by doxycycline treatment. These genes were subsequently subtracted by the list derived from the comparison of REST OE or REST KD hGSCs and hNSCs with the respective untreated cell lines. Among the 466 genes (201 coding genes) modulated by doxycycline in hGSCs, none was shared with either induced REST KD or REST OE hGSCs. Similarly, none of the 801 transcripts (451 coding genes) differentially regulated by the treatment in parental hNSCs was shared with either REST OE or REST KD hNSCs.

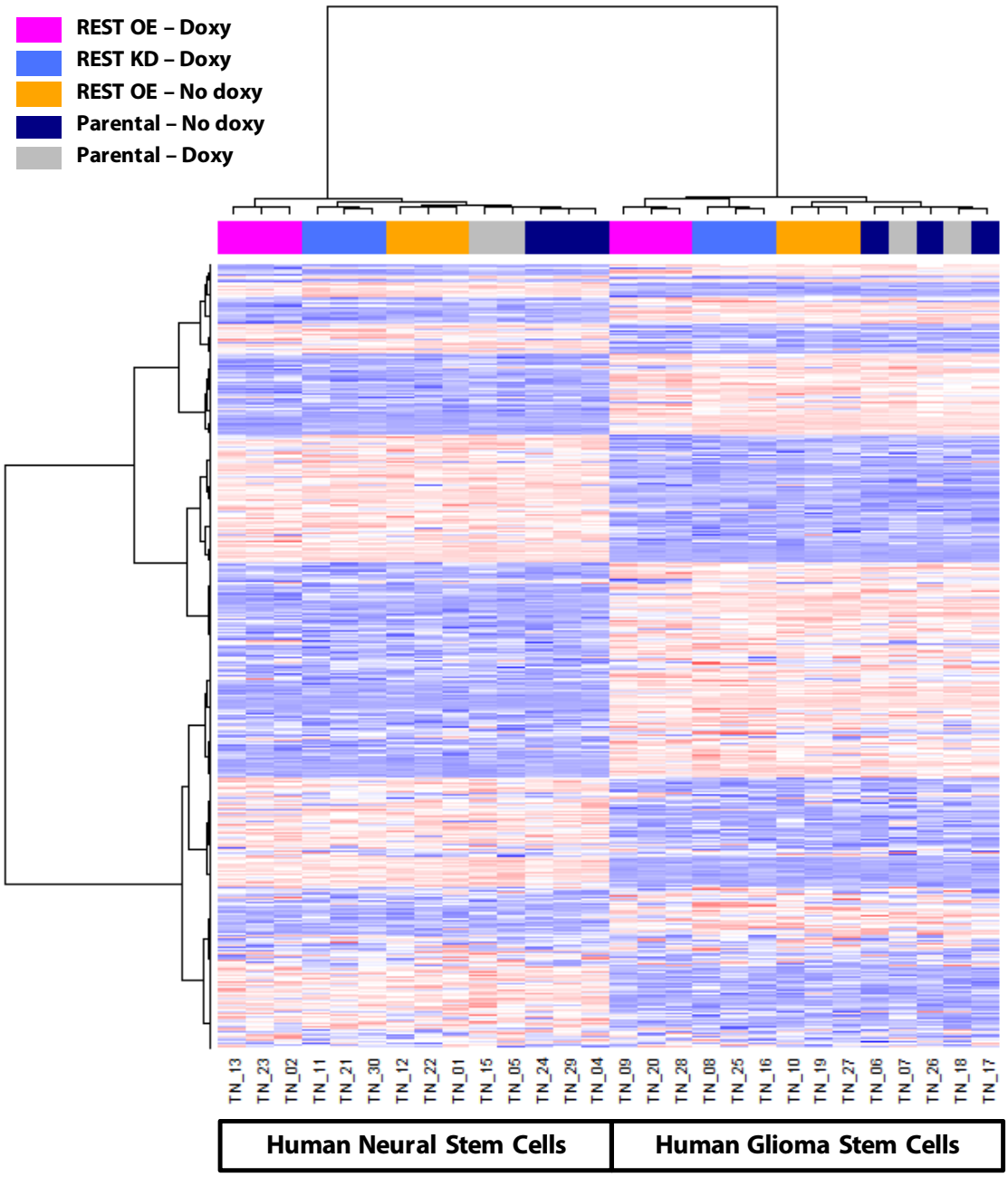

Figure 7.1. Microarray analysis of REST-modulated hGSCs and hNSCs. Hierarchical clustering of parental hGSCs and hNSCs treated with or without doxycycline for 48 hours, REST KD hGSCs and hNSCs treated with doxycycline for 48 hours, and REST OE hGSCs and hNSCs treated with or without doxycycline for 24 hours.

7.2 REST controls neural multipotency through modulation of neuronal differentiation, proliferation and cell metabolism

Aiming at identifying the main pathways deregulated upon REST modulation, we performed a gene set enrichment analysis (GSEA) considering all the gene set with $p < 0.001$ enriched in doxycycline-treated REST KD and REST OE hGSCs and REST OE hNSCs. According to the previously identified role of REST in embryonic and neural development, most of the gene ontology (GO) terms were attributable to neural development and morphogenesis, neural cell projection, membrane potential and synaptic transmission, and embryonic development processes (**Figure 7.2-7.4**). Among all of the pathways controlling the stem cell behaviour, Wnt was the single over-represented in REST OE hGSCs and hNSCs (**Figure 7.2 and 7.4**). Interestingly, both hGSCs and hNSCs network are enriched in processes related to cell metabolism and oxidative stress (**Figure 7.2-7.4 and 7.5**), suggesting a potential implication of REST in these two mechanisms not currently associated to its function. Unfortunately, the little dimension of the REST KD hNSCs dataset prevented us from performing any computational prediction on biological processes modulated by REST silencing in hNSCs. The literature screenings we performed on the REST KD hNSCs dataset suggested these genes are associated to neuronal maturation (CRABP2, SLITRK1, UNC5C, UNC13A), NSCs self-renewal (ID2 and EGR1), cell metabolism (ASS1, CRABP2, and ID2), and neural diseases such as Alzheimer's, amyotrophic lateral sclerosis/frontotemporal dementia and Tourette syndrome (PLAU, SLITRK1, UNC13A) (**Shaheen et al., n.d.; Budhu and Noy, 2002; Aruga and Mikoshiba, 2003; Abelson et al., 2005; Riemenschneider et al., 2006; Chaerkady et al., 2009; Alagappan et al., 2013; Park et al., 2013; Diekstra et al., 2014; Shao et al., 2017; Lipstein et al., 2017, http://www.uniprot.org, and http://www.ebi.ac.uk/GOA**).

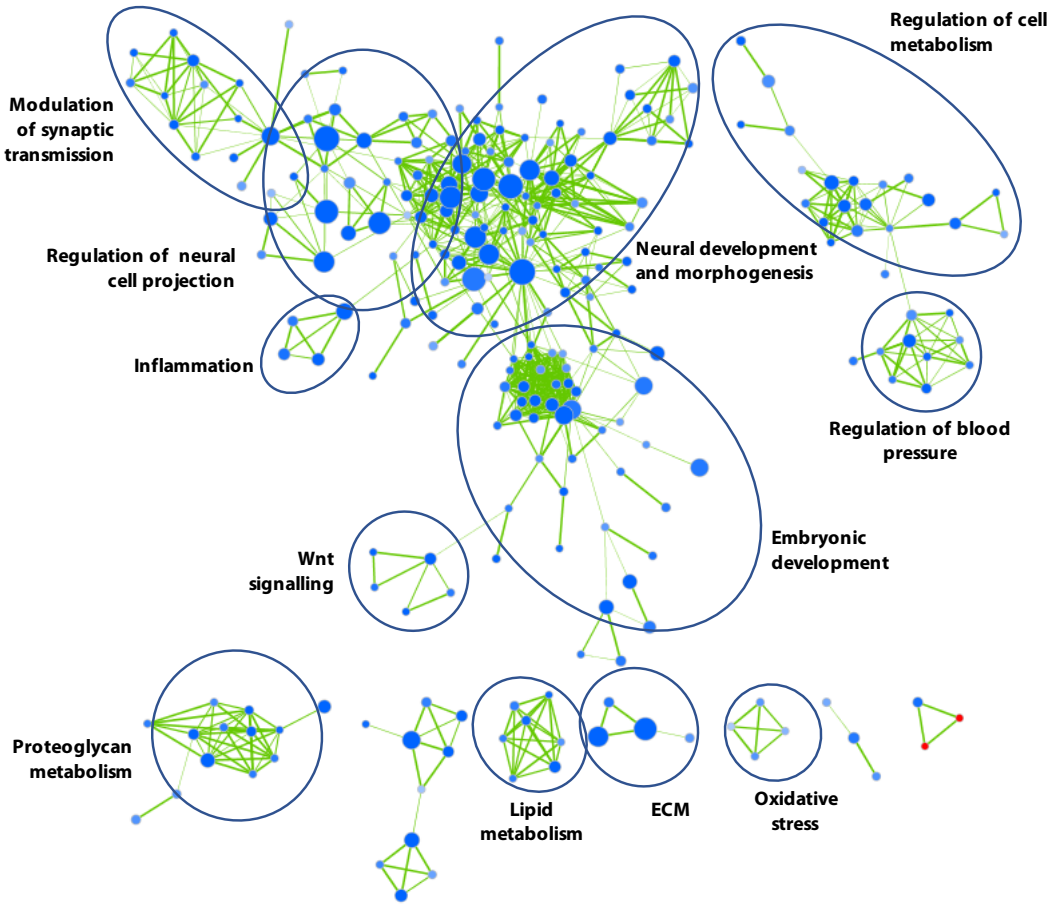

Figure 7.2. Enrichment maps of REST-overexpressing hGSCs. Networks of c5 Gene Ontology from Gene Set Enrichment Analysis derived including gene set with size > 15 and FDR cut-off < 0.25 and p-value < 0.05. Dataset: REST OE hGSCs treated with doxycycline *versus* untreated cells.

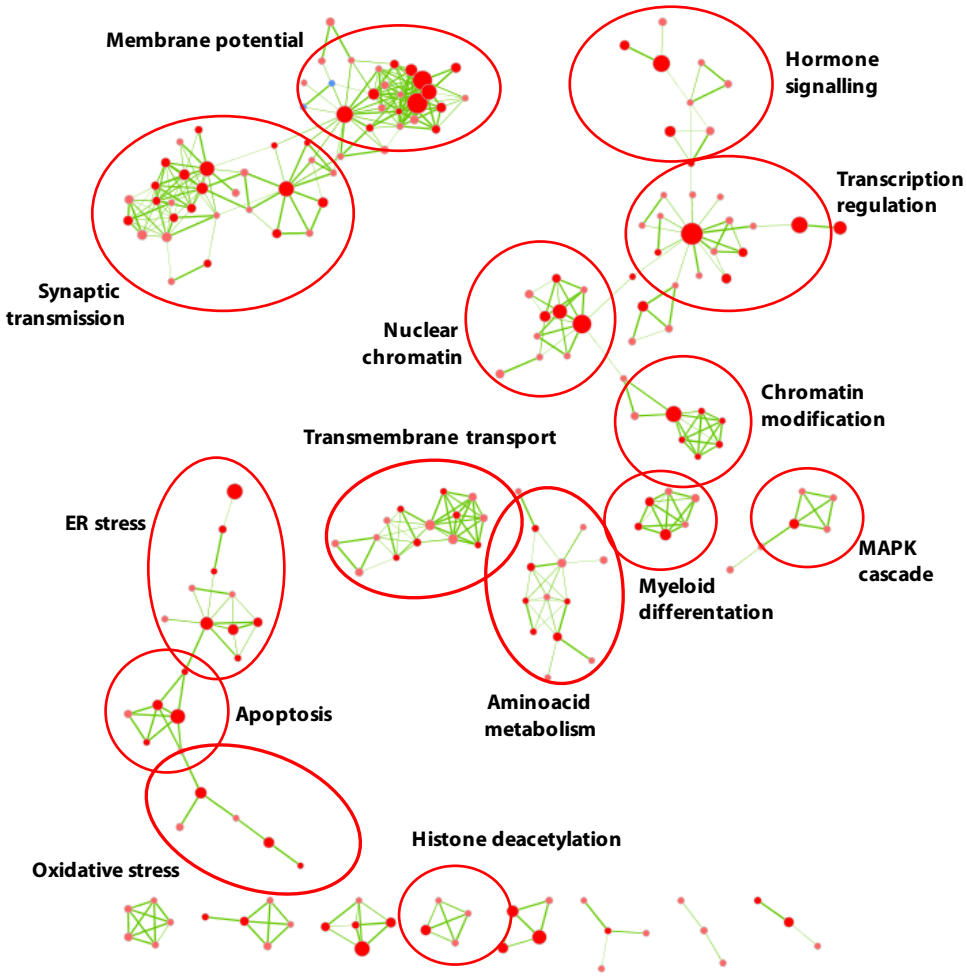

Figure 7.3. Enrichment maps of REST knock-down hGSCs. Networks of c5 Gene Ontology from Gene Set Enrichment Analysis derived including gene set with size > 15 and FDR cut-off < 0.25 and p-value < 0.05. Dataset: REST KD hGSCs treated with doxycycline *versus* untreated cells.

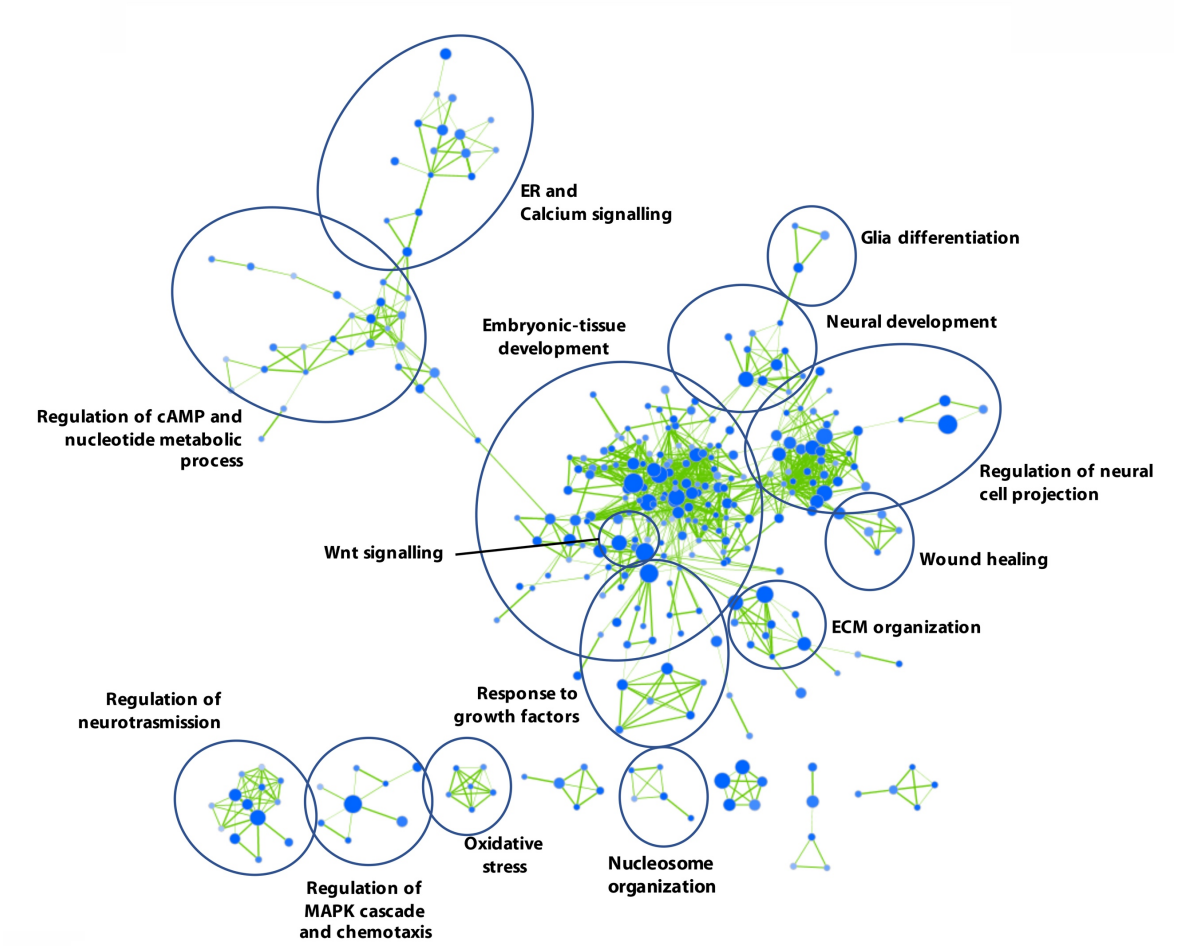

Figure 7.4. Enrichment maps of REST-overexpressing hNSCs. Networks of c5 Gene Ontology from Gene Set Enrichment Analysis derived including gene set with size > 15 and FDR cut-off < 0.25 and p-value < 0.05. Dataset: REST OE hNSCs treated with doxycycline *versus* untreated cells.

We then analysed gene ontology processes in REST OE hGSCs and hNSCs and REST KD hGSCs and divided them according to the direction of gene deregulation upon modulation of REST (**Figure 7.5**). Respect to GSEA, this analysis better highlighted the different role REST covers in hGSCs and hNSCs, as well as the changes in gene expression happening soon after overexpression and silencing of REST in hGSCs. For instance, the most significantly deregulated process in REST OE hNSCs is *R-HAS-112315: Transmission across Chemical Synapses*, that also represent also the only neuronal-related process in hNSCs, while the most affected process in REST OE hGSCs is *GO:0007156: homophilic cell adhesion via plasma membrane adhesion molecules*, that is followed by a series of processes associated to nervous system development and neuron maturation (**Figure 7.5B and C**). Regulation of cell-matrix adhesion (GO:0007160) also appears among the processes regulated by gene downregulated upon silencing of REST in hGSCs (**Figure 7.5A**). REST has already been described to regulate both cell-cell interaction and cell-matrix adhesion molecules during ESCs conversion to NSCs and neuronal differentiation (**Johnson et al., 2006; Otto et al., 2007; Sun et al., 2005, 2008b**), and our phenotypic characterisation of REST modulated hGSCs and hNSCs identified modifications in cell-cell interaction manifested by cells growing closer to each other in both doxycycline-treated REST OE hGSCs and hNSCs respect to untreated cultures. However, it is interesting to note that only hGSCs showed an enrichment of such processes. Genes associated to circadian rhythm and lipid-steroid metabolisms/gluconeogenesis/PPARα signalling, functions described to influence cell differentiation, were enriched in hGSCs in which REST levels were modulated (**Figure 7.5**). Based on these premises, we decided to look for the specific transcripts associated to cell metabolism and circadian rhythm and modulated in REST OE and REST KD hGSCs. We were able to identify genes that play roles in different cell metabolism branches, including amino acid-, cholesterol-, fatty acids-, glucidic-, nucleotides-, nitrogen- metabolism, autophagy and oxidative phosphorylation, as well as transcription factors master regulators of energetic metabolism and mitochondrial biogenesis (e.g. NR1D1 and PPARGC1A). Interestingly, almost the totality of the identified genes appeared downregulated following REST overexpression, suggesting the establishment of a general shutdown of cell metabolism and rhythmic processes at different levels (**Figure 7.6A**). *Vice versa*, REST KD hGSCs showed a general upregulation of the same pathways (**Figure 7.6B**).

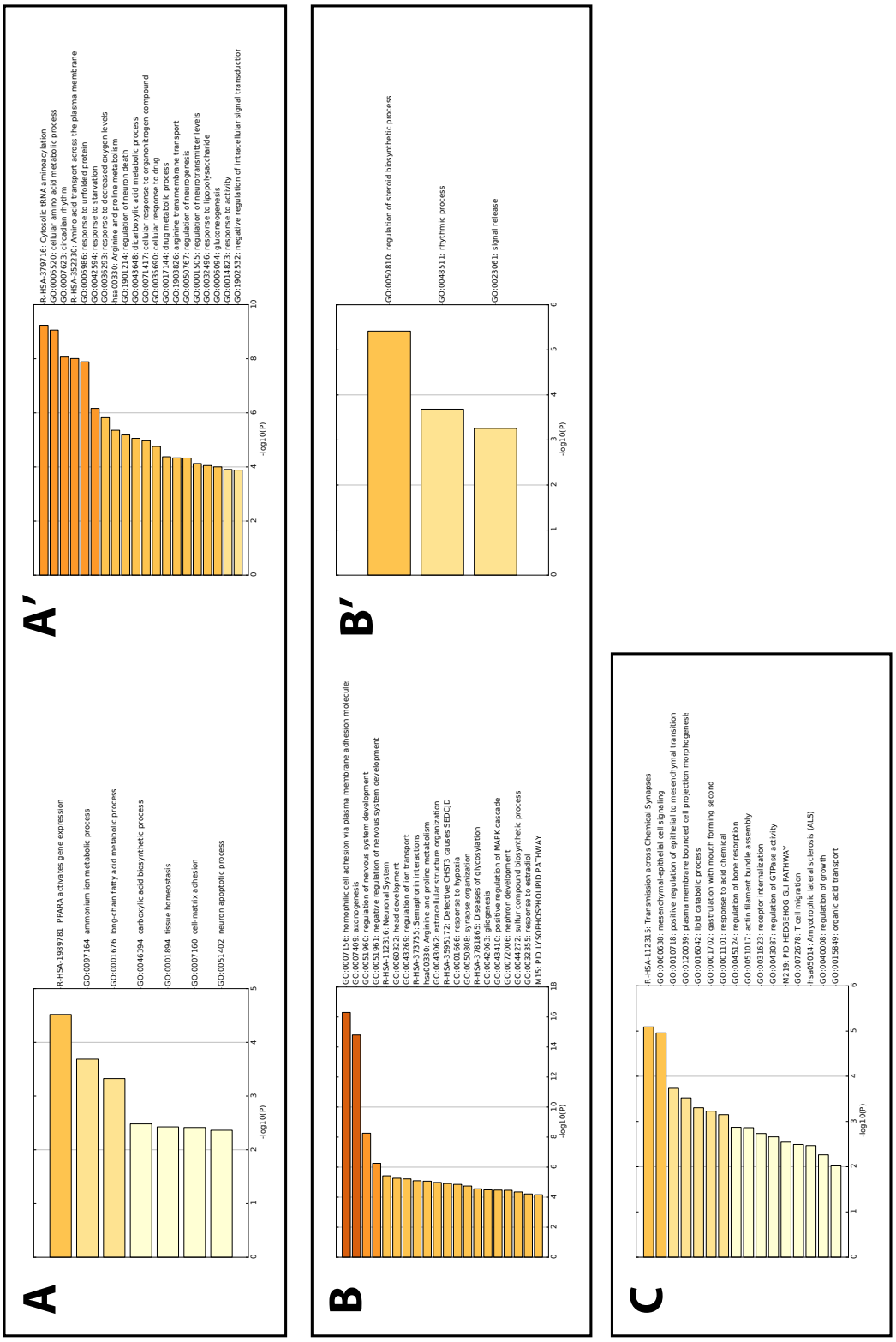

Figure 7.5. Gene ontology analysis of REST-modulated transcripts. A. GO from genes downregulated upon silencing of REST in hGSCs. **A'**. GO from genes upregulated upon silencing of REST in hGSCs. **B.** GO from genes downregulated upon overexpression of REST in hGSCs. **B'**. GO from genes upregulated upon overexpression of REST in hGSCs. **C**. GO from genes downregulated upon overexpression of REST in hNSCs.

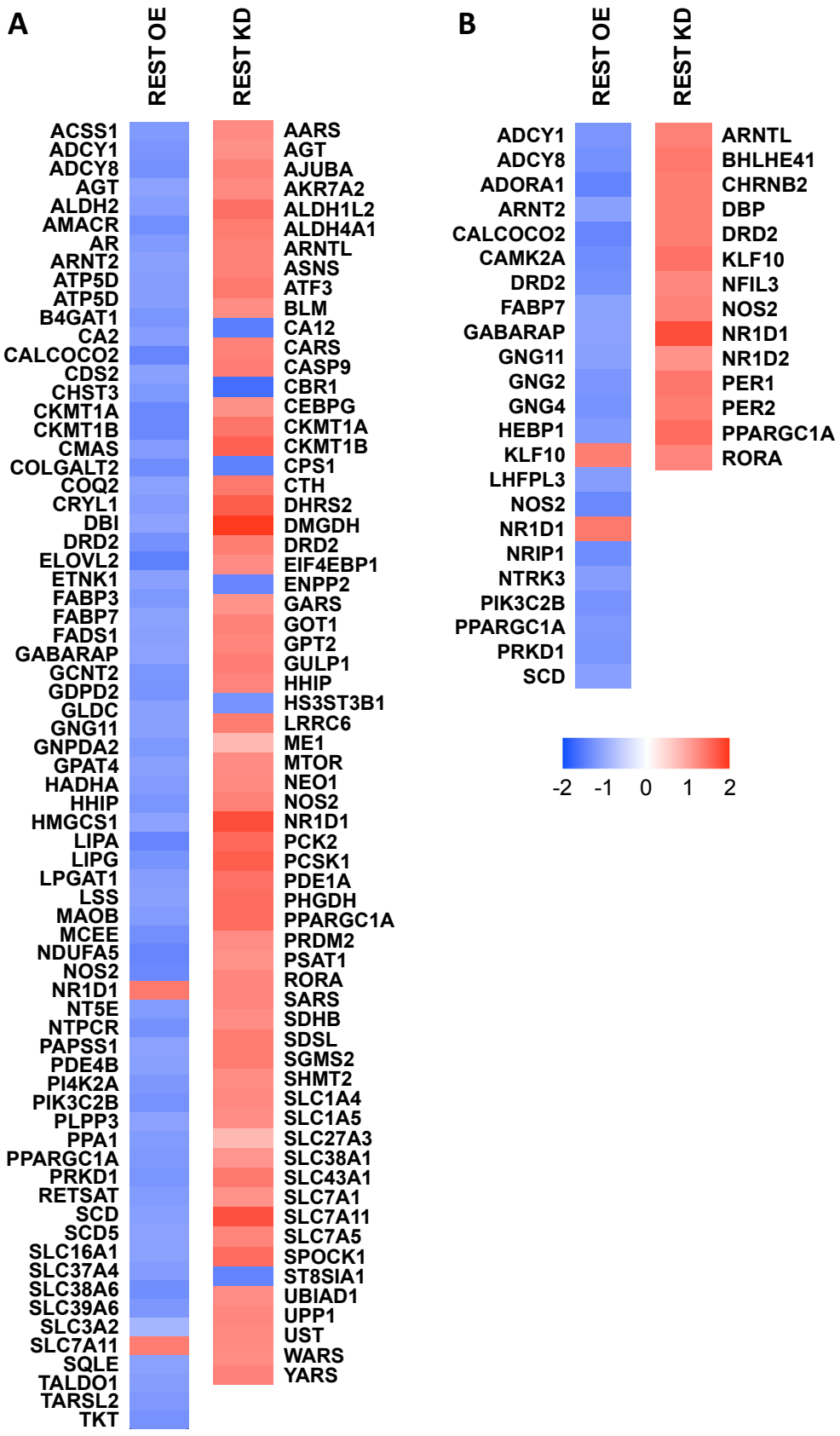

Figure 7.6. REST regulates pathways associated to the induction of a quiescence state in hGSCs. **A**. Genes associated to cell metabolism in REST KD and REST OE hGSCs. **B**. Genes associated to circadian rhythm in REST KD and REST OE hGSCs. Fold change is expressed as log2.

To better investigate REST potential roles in these process, we took advantage of Integrated System for Motif Activity Response Analysis (ISMARA) to look for key transcription factors (TFs) predicted to have a differential activity in REST OE hGSCs. We crossed this list of TFs with the gene set associated to the transition from quiescent to activated NSCs identified in **Shin et al., 2015**. This analysis produced a set of 13 TFs that might be responsible for the (i) induction of quiescence following REST overexpression as for (ii) the neuronal-like differentiation observed upon REST knock-down in hGSCs (**Table 7.5 left**). Next, we screened among differentially expressed transcripts in REST OE hGSCs for the presence of additional quiescent NSCs-associated genes. Interestingly, our analysis showed a downregulation of Ascl1, as well as SHh signalling activation and modulation of lipid/steroid metabolism, all events already reported to lead to the acquisition of a quiescent state in NSCs (**Table 7.3 right**).

Motif	Target genes' expression in REST OE GSCs vs. no doxy
ATF4/CREB2	upregulated
EOMES/TBR2	upregulated
GRHL1	upregulated
HES1	upregulated
KLF15	upregulated
ZBTB4	upregulated
INSM1	downregulated
IRF3	downregulated
NFIA	downregulated
NR2E1/TLX	downregulated
SOX11	downregulated
SOX9	downregulated
TCF7L2/TCF4	downregulated

Symbol	Description	REST OE (Fold change vs No Doxy)
ASCL1	achaete-scute family bHLH transcription factor 1	-1,32
PTCH1	patched 1	-1,15
HHIP	hedgehog interacting protein	-1,24
NR1D1	nuclear receptor subfamily 1 group D member 1	1,35
FABP7	fatty acid binding protein 7	-1,08
SCD	stearoyl-CoA desaturase	-1,14
SQLE	squalene epoxidase	-1,11
HMGCS1	3-hydroxy-3-methylglutaryl-CoA synthase 1	-1,09

Table 7.3. List of transcription factors (left table) and genes (right table) modulated in REST-overexpressing hGSCs showing association to a quiescent NSCs state and the relative modulation *versus* no doxy treated REST OE hGSCs.

To verify whether hGSCs acquire features of quiescent NSCs following overexpression of REST, other than the co-expression of Nestin and GFAP, we treated hGSCs REST OE and REST KD cells with doxycycline for ten days and counted the number of Ascl1 and Ki67 immunoreactive cells. As shown in **figure 7.7A**, REST overexpression resulted in a reduction

of Ascl1^{+} and Ki67^{+} cells (Ascl1: 58.58 ± 20.60% doxy *versus* 100.00 ± 9.95% no doxy; Ki67: 86.16 ± 4.90% doxy *versus* 100.00 ± 4.55% no doxy), indicative of an increased quiescent state. Interestingly, also REST KD hGSCs showed a reduction in Ki67 immunoreactive cells, although not accompanied by Ascl1 modulation (**Figure 7.7B**, Ascl1: 115.27 ± 5.99% doxy *versus* 100.00 ± 30.55% no doxy; Ki67: 77.88 ± 5.70% doxy *versus* 100.00 ± 6.08% no doxy), suggesting cell cycle exit.

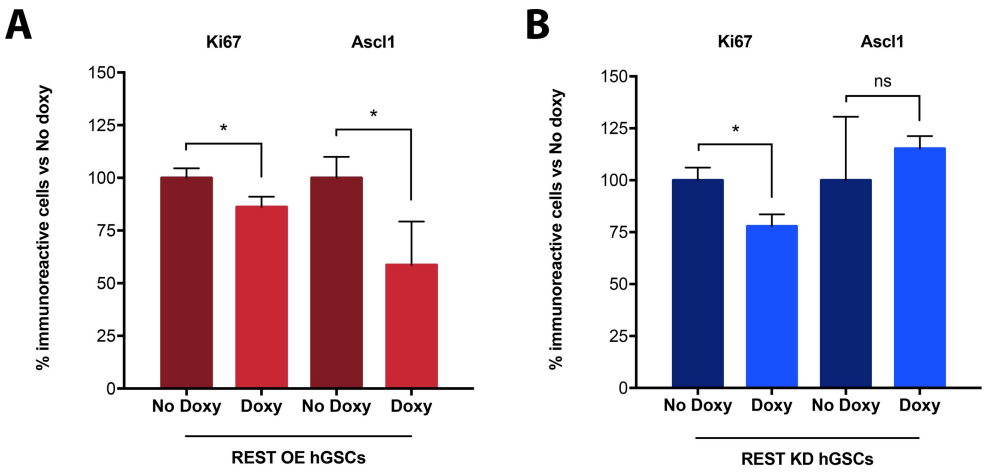

Figure 7.7. REST overexpression induces a quiescent neural stem cell-associated phenotype. A. Quantification of Ki67^{+} and Ascl1^{+} cells in REST OE hGSCs. **B**. Quantification of Ki67^{+} and Ascl1^{+} cells in REST KD hGSCs. Quantification is normalised on untreated cells and expressed as % of immunoreactive cells on total number of cells. Results are expressed as mean ± standard deviation and statistical significance inferred using t-test.
ns: non-statistically significant. *: $p < 0.05$

7.3 hGSC-specific REST-regulated genes regulates neuronal differentiation, proliferation and cell metabolism

In order to identify the molecular network specifically regulated by REST in hGSCs, we selected the differentially-regulated genes that are both repressed in REST OE cells and upregulated in REST KD cells as potential direct REST targets, and we crossed the list derived from hGSCs with the one derived from hNSCs (**Figure 7.8 and comparison 9 in table 7.2**). Unexpectedly, none of the REST targets in the hNSCs list is shared with hGSCs,

suggesting that even though the two cell types present very similar features and some of these are regulated by REST, the different cell landscape might deeply influence REST activity. To confirm that identified REST-regulated hGSC-specific genes might effectively represent direct REST targets, we screened for the presence of RE1 motifs in their promoter region, considering 1000 bps to and from the gene's transcription start site (FDR < 0.1, **table 7.4**). Interestingly, only six of the 16 identified genes presented REST binding sites in their promoters, suggesting they are potential direct targets of REST. These are genes involved in neuronal differentiation and function (ELAVL4 and ANKS1B), associated with hGSCs proliferation (DRD2), and with cell metabolism (CKMT1A/B andPPARGC1A).

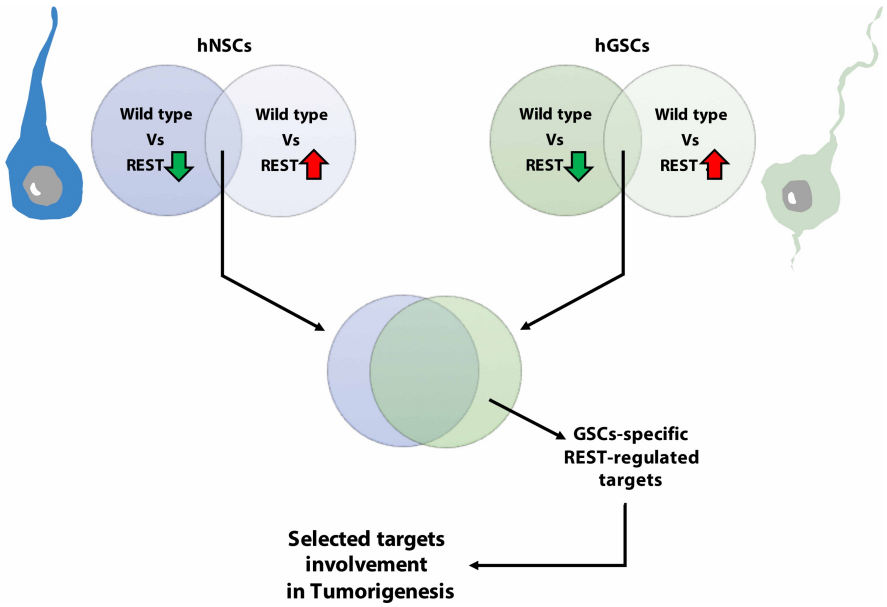

Figure 7.8. Experimental strategy for identifying REST-regulated in hGSC-specific molecular circuitries and targets.

Investigating the hGSC-specific REST-regulated genes for the presence of common transcription factor binding sites, we found 13 out of 16 genes potentially regulated by NeuroD (**table 7.4**), a REST target, basic helix loop helix transcription factor, known to instructs cells for neuronal differentiation and involved in pancreatic development (**Johnson et al., 2007; Kemp et al., 2003a**).

Symbol	Description	REST KD Fold change	REST OE Fold change	RE1 motif	NeuroD motif
ANKS1B	ankyrin repeat and sterile alpha motif domain containing 1B	2,96	-2,05	yes	yes
CKMT1A	creatine kinase, mitochondrial 1A	8,19	-3,92	yes	yes
CKMT1B	creatine kinase, mitochondrial 1B	8,41	-2,41	yes	yes
DRD2	dopamine receptor D2	6,63	-4,59	yes	yes
ELAVL4	ELAV like RNA binding protein 4	10,94	-3,23	yes	yes
PPARGC1A	PPARG coactivator 1 alpha	9,12	-3,17	yes	no
AGT	angiotensinogen	3,88	-3,02	no	yes
CADPS2	calcium dependent secretion activator 2	4,61	-2,4	no	no
CAMKV	CaM kinase like vesicle associated	2,6	-2,35	no	yes
CNRIP1	cannabinoid receptor interacting protein 1	3,25	-2,9	no	yes
DUSP15	dual specificity phosphatase 15	3,61	-2,37	no	yes
GABBR2	gamma-aminobutyric acid type B receptor subunit 2	2,64	-2,97	no	yes
HHIP	hedgehog interacting protein	3,69	-3,41	no	no
NFASC	neurofascin	2,73	-5,63	no	yes
NOS2	nitric oxide synthase 2	2,93	-4,31	no	yes
PDGFRA	platelet derived growth factor receptor alpha	3,57	-2,72	no	yes

Table 7.4. List of hGSC-specific REST-regulated coding transcripts.

To validate the modulation and the tumour-specificity of the REST-regulated hGSC-specific genes identified by our bioinformatics analysis, we produced biological replicates of the samples used for the microarray analyses and performed a qRT-PCR assay comparing REST-modulated hGSCs and hNSCs (**Figure 7.9 and table 7.5**). Of the analysed genes, DRD2, HHIP, NOS2, GABBR2, PPARGC1A, AGT, NFASC, ANKS1B, CADPS2, CAMKV, CNRIP1, and DUSP15 were confirmed as hGSC-specific and regulated according to the expression of REST. Indeed, they were found more repressed following REST overexpression and de-repressed after REST knock-down. Also, the transcriptional regulation of these genes did not appear to be REST-dependent in hNSCs (i.e. NOS2, CAMKV, and DUSP15) or their expression showed modifications not in accordance with REST activity. For instance, DRD2 and NFASC appeared upregulated and HHIP, ANKS1B, and CADPS2 downregulated in both in REST KD and in REST OE hNSCs; AGT was upregulated in REST OE hNSCs, while REST silencing did not produce any effect on its expression; PPARGC1A and CNRIP1 were downregulated in REST OE hNSCs, with no modulation occurred following REST knock-down; GABBR2 was upregulated in REST KD hNSCs and did not changed in REST OE hNSCs. The remaining four

genes were either REST-dependent (CKMT1A/B) or independent (ELAVL4 and PDGFRA) in both hGSCs and hNSCs (**Table 7.5**).

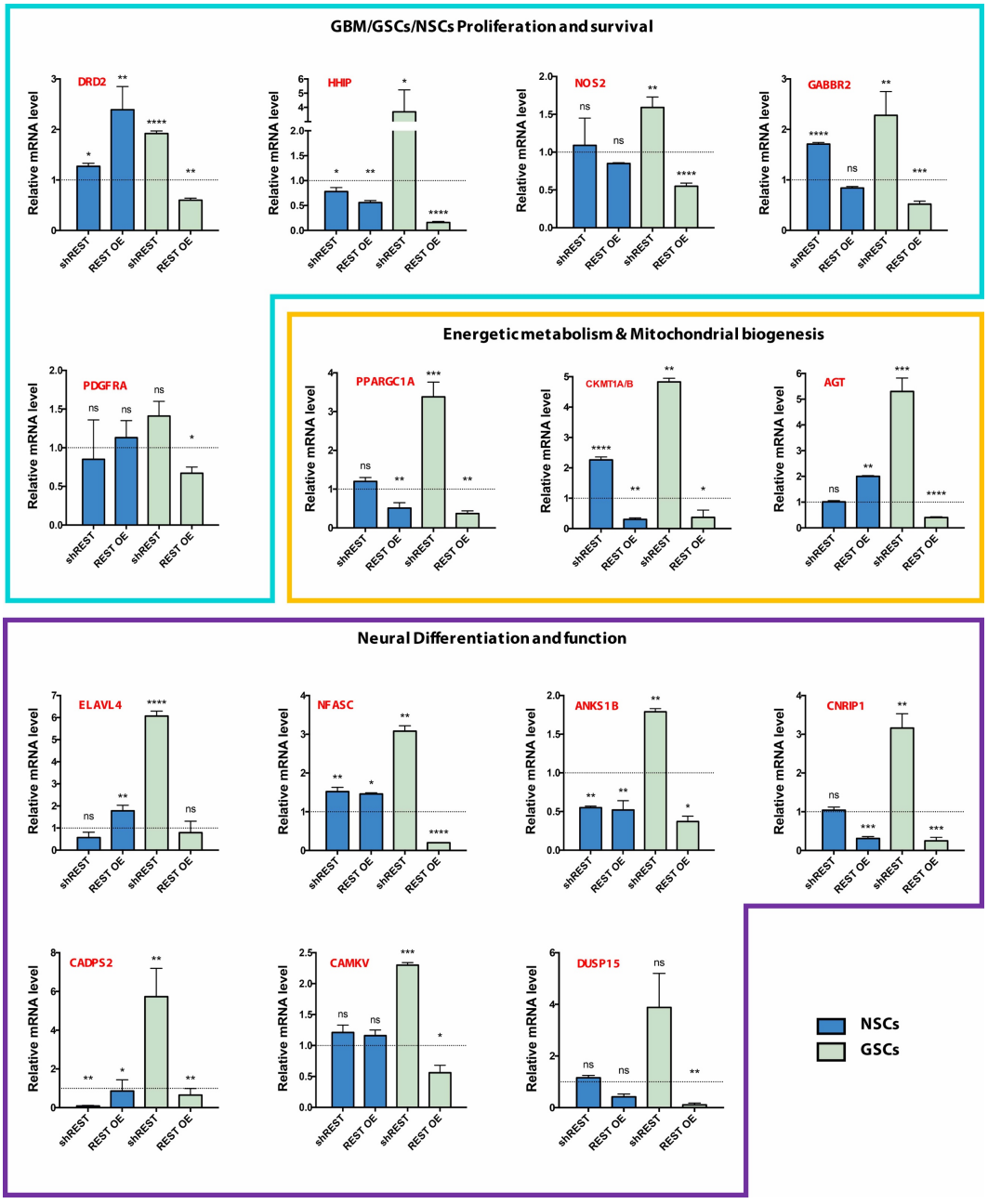

Figure 7.9. Validation of hGSC-specific REST-regulated genes identified by microarray analysis. qRT-PCR assays for the hGSC-specific REST target genes expression. REST KD hGSCs and hNSCs were treated with or without 500 ng/ml for 48 hours, while REST OE hGSCs and hNSCs were treated with or without 500 ng/ml for 24 hours before lysis for RNA extraction. qRT-PCR quantifications have been normalised on untreated cells (not shown). Results are expressed as mean ± standard deviation and statistical significance inferred using t-test.
ns: non-statistically significant; *: $p < 0.05$; **: $p < 0.01$; ***: $p < 0.001$; ****: $p < 0.0001$.

gene	hNSCs		hGSCs	
	shREST	REST OE	shREST	REST OE
AGT	1.01 ± 0.05	2.00 ± 0.03	5.3 ± 0.52	0.4 ± 0.03
ANKS1B	0.55 ± 0.02	0.52 ± 0.12	1.79 ± 0.04	0.37 ± 0.07
CADPS2	0.09 ± 0.03	0.86 ± 0.58	5.73 ± 1.46	0.65 ± 0.34
CAMKV	1.21 ± 0.12	1.16 ± 0.09	2.3 ± 0.04	0.56 ± 0.12
CKMT1A/B	2.26 ± 0.04	0.3 ± 0.05	4.83 ± 0.12	0.37 ± 0.24
CNRIP1	1.04 ± 0.08	0.31 ± 0.05	3.16 ± 0.37	0.25 ± 0.09
DRD2	1.27 ± 0.06	2.39 ± 0.46	1.92 ± 0.05	0.6 ± 0.04
DUSP15	1.16 ± 0.09	0.42 ± 0.11	3.88 ± 1.32	0.11 ± 0.07
ELAVL4	0.57 ± 0.24	1.78 ± 0.25	6.07 ± 0.22	0.79 ± 0.52
GABBR2	1.71 ± 0.03	0.84 ± 0.03	2.28 ± 0.47	0.52 ± 0.06
HHIP	0.78 ± 0.08	0.56 ± 0.04	3.69 ± 1.54	0.16 ± 0.02
NFASC	1.52 ± 0.11	1.46 ± 0.03	3.08 ± 0.14	0.2 ± 0.00
NOS2	1.09 ± 0.36	0.85 ± 0.01	1.59 ± 0.14	0.55 ± 0.04
PDGFRA	0.85 ± 0.51	1.13 ± 0.22	1.41 ± 0.19	0.67 ± 0.08
PPARGC1A	1.2 ± 0.10	0.51 ± 0.14	3.38 ± 0.38	0.37 ± 0.07

Table 7.5. Quantitative RT-PCR data from validation of hGSC-specific REST-regulated genes. Data are shown as fold change ± standard deviation.

7.4 Repression of hGSC-specific REST regulated genes is associated to poorer prognosis

Considering REST-regulated hGSC-specific genes identified in the previous section (**Table 7.4**) we generated the hGSCs REST score and integrated this signature with clinical information from GBM patients, in order to evaluate the prognostic potential of the genes modulated by REST in hGSCs. In particular, we considered the TGCA cohort of GBM patients which included data on overall survival (OS) and progression-free survival (PFS) from 519 GBM patients, 171 of which classified for tumour molecular subtypes (**McLendon et al., 2008**), and the "Sun" cohort, comprising 176 patients clustered per WHO tumour grade plus normal individuals (**Sun et al., 2006**).

An inverse correlation was enlightened between the REST expression and the REST score in both the TGCA (**Figure 7.10A,** $r = -0.46$ e $p < 0.0001$) and the "Sun" (**Figure 7.10E**, $r = -0.75$ e $p < 0.0001$) cohorts of patients, indicating that a higher REST expression causes a repression of the hGSC REST score genes in glioma patients and *vice versa*. These results

suggest that even if the patients' RNA were sampled from whole gliomi specimens, without distinguishing between hGSCs and non stem-like glioma cell populations, the REST score is suitable for analyses performed on glioma tumours *in toto*. Considering the TGCA cohort of patients, we found the stratification of both the patients' OS and PFS not significantly altered according to the hGSC REST score (**Figure 7.10B-C**). However, both the *classical* and *mesenchymal* GBM molecular subtypes resulted associated to a lower hGSC REST score and therefore exhibiting a higher REST activity. On the other hand, the *proneural* subtype GBM showed an intermediate hGSC REST score between the four subclasses. Finally, the *neural* GBM subtype presented the higher hGSC REST score (**Figure 7.10D**).

Next, we integrated the hGSC REST score with the expression profile of *gliomi* of different WHO grades. This classification is based on the integration between molecular and clinical aspects of *gliomi* in order to establish prognosis and predict disease progression over time. A WHO grade I glioma is generally well circumscribed and curable by surgical resection, while a WHO grade IV glioma (GBM) is a fast growing, treatment resistance entity with a very poor prognosis (**See chapter 1.1 for details**). The hGSC REST score here established inversely correlated with glioma WHO grade, with a higher score, due to a lower REST activity, associated to non-neoplastic brain, and a progressively lower score as the tumour grade increases (**Figure 7.10F-G**), suggesting that the REST transcriptional activity is directly proportional to glioma aggressiveness.

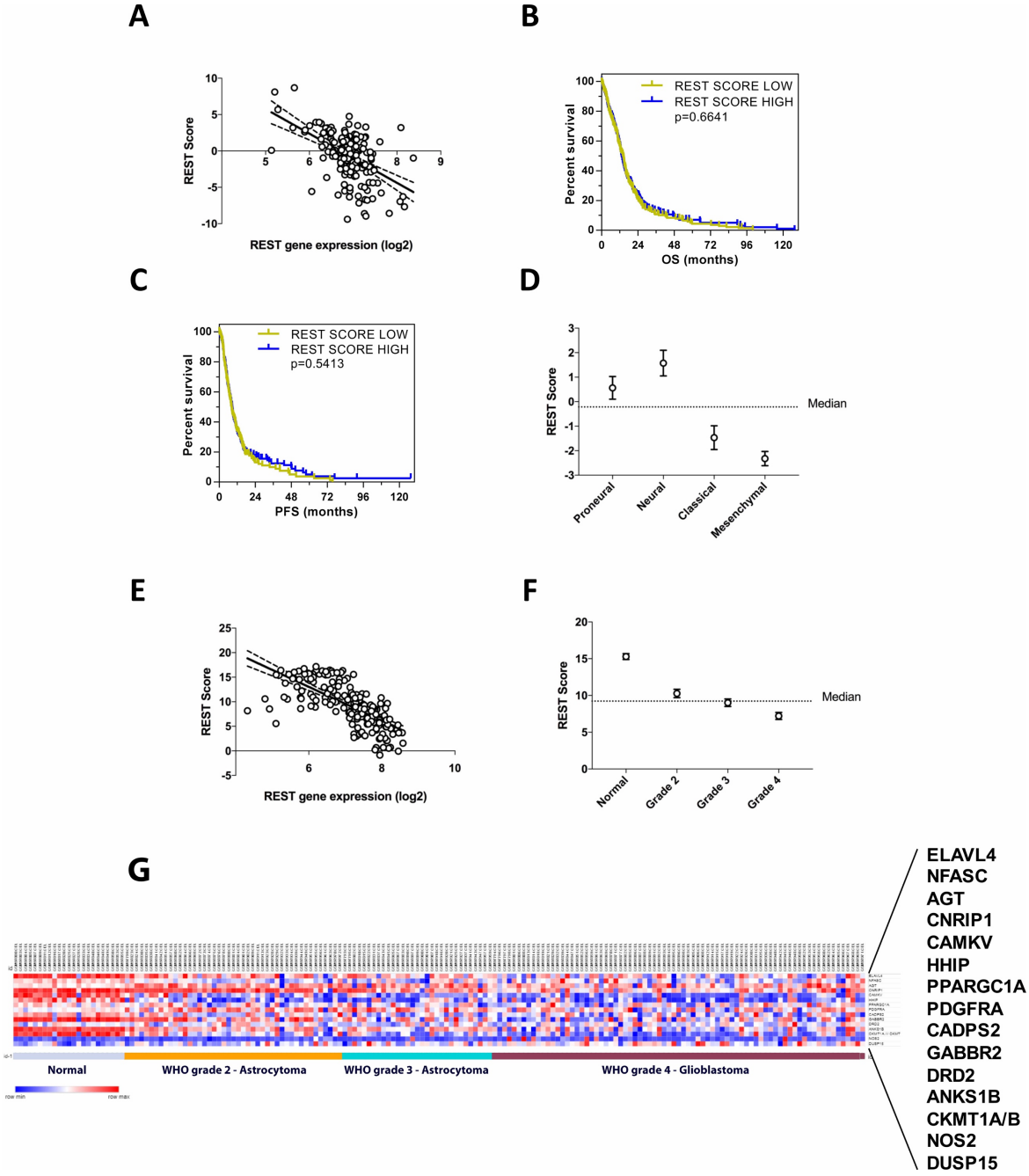

Figure 7.10. Prognostic potential of the hGSC REST score. A. Correlation between REST gene expression and the hGSC REST score in the TCGA cohort, r = -0.46 and p < 0.0001. **B**. Correlation between the hGSC REST score and OS of GBM patients from the TCGA cohort. **C**. Correlation between the hGSC REST score and PFS of GBM patients from the TCGA cohort. **D**. Correlation between the hGSC REST score and the GBM molecular subclasses from the TCGA cohort. **E**. Correlation between REST gene expression and the hGSC REST score in the "Sun" cohort, r = - 0.75 e p < 0.0001. **F**. Correlation between the hGSC REST score and the WHO *gliomi* tumour grade from the "Sun" cohort. **G**. Heat map showing correlation between the hGSC REST score and the WHO *gliomi* tumour grade from the "Sun" cohort.

Conclusions

Chapter 8

Discussion

Contents

8.1 hGSCs targeted therapy	**109**
8.2 REST controls differentiation and quiescence of both hGSCs and hNSCs	**110**
8.3 REST orchestrates multiple processes to regulate quiescence in hGSCs	**113**
8.4 hGSC-specific REST targets regulate multipotency and have prognostic relevance	**116**
8.5 Future perspectives and Concluding remarks	**121**

8.1 hGSCs targeted therapy

The identification of cancer stem cells (CSCs) residing in GBM represented an important step toward our comprehension of tumour biology and the design of novel and rational therapeutic options. As in non-pathological tissues, in which pools of stem cells control homeostasis through their ability to differentiate into effector cells that contribute to tissue function, the hierarchical vision of tumour biology would envision GBM as stratified in cells possessing increasing levels of maturation, with the most differentiated ones representing the tumour bulk, and few slow-cycling CSCs as main driver of tumour growth, chemoresistance, and relapses.

Understanding the biology of GSCs is the key to disclose new and effective targeted approaches. To this aim, the starting point has often been the macroscopic similarity between CSCs and non-tumour adult stem cells (ASCs). Both cell types are characterised by self-renewal and differentiation abilities as well as the expression of common markers and

signalling pathways regulating their behaviour. The CSC peculiarities manifest more explicitly when they are orthotopically xenotransplanted in experimental animal models: while ASCs differentiate into tissue derivatives and integrate with the resident cells (e.g. forming functional neural circuits in the case of neural tissues-derived stem cells), the genetic aberrations acquired during cancer development establish tumorigenic features in CSCs that also determine a deviant differentiation, resulting in the formation of a cancerous mass resembling the tumour of origin. Even if quite alike, cancer and adult stem cells must therefore show subtle differences in molecular mechanisms regulating their behaviour.

Communal ASCs and CSCs signalling pathways are involved in controlling cells' multipotency, through transcription factors/master regulators of proliferation, survival, and differentiation. Even though these pathways share the same mediators and therefore produce similar effects in both normal and cancerous stem cells, in depth investigations in tumour contexts often revealed their oncogenic-dark side. In this regard, REST has been shown to maintain NSCs multipotency by repressing neuronal genes expression, activating self-renewal and survival mechanisms (**Mukherjee et al., 2016; Nechiporuk et al., 2016**), and analogous effects have been described in GSCs, although it has been also shown to promotes tumorigenesis (**Conti et al., 2012; Kamal et al., 2012**).

8.2 REST controls differentiation and quiescence markers expression in both hGSCs and hNSCs

In line with the previously demonstrated anti-neurogenic effects exerted by REST in both hGSCs and hNSCs, we found that REST long-term silencing results in loss of multipotency and the acquisition of a neuronal (-like) phenotype (**Figure 5.9 – 5.11**). These effects are supported by the progressive reduction both in cell growth and Sox2 immunoreactivity, accompanied by the upregulation of β3-Tubulin. Although commonly used to identify neural and glioma cells states, these markers have also been involved in GBM biology and linked to REST expression. For instance, Sox2 has been shown to play essential roles in the

maintenance of multipotency in neural progenitors and hGSCs (**Basu-Roy et al., 2015; Favaro et al., 2014; Mao et al., 2015; Pevny and Nicolis, 2010**) and its levels were shown to correlate to those of REST in hGSCs (**Kamal et al., 2012**). Also, importantly to GBM patients' survival, a lower Sox2 expression is generally associated to a better prognosis (**Ben-Porath et al., 2008; Sathyan et al., 2015**). On the contrary, β3-tubulin expression marks neuronal cells and inversely correlates with REST. Similarly, hGSCs do not normally express β3-tubulin when maintained in self-renewal, but some of them might upregulate it when induced to differentiate, suggesting it is dispensable for tumorigenic processes in GBM (**Pollard et al., 2009b**). A number of studies on GBM however reported β3-tubulin abnormally upregulated, coexpressed with Nestin and GFAP, and proposed it as pharmacological target (**Katsetos et al., 2011**). Moreover, β3-tubulin in other tumours has been shown to play major role in chemoresistance and cellular adaptation to oxidative stress (**Cicchillitti et al., 2008; De Donato et al., 2012; Gan et al., 2007**). It is therefore possible, that although not contributing to tumour growth, β3-tubulin does sustain survival of differentiated tumour cells.

We also confirmed that loss of REST causes a reduction in self-renewing ability of both hGSCs and hNSCs (**Figure 5.8**), an event required for NSCs to acquire a neuronal phenotype. These results indicate that despite the culture conditions were selected for suppressing differentiation and maintaining hGSCs and hNSCs in a self-renewing and multipotent state, loss of REST function induces a neuronal-like differentiation. This might be associated to the loss of hGSCs tumorigenic competence, in line with previous reports from our laboratory and others (**Conti et al., 2012; Kamal et al., 2012; Marisetty et al., 2017; Zhang et al., 2016**). Interestingly, by analysing the number of cleaved caspase 3^+ cells upon REST knock-down, we found induction of apoptosis in hGSCs, while we did not observe the same effect in hNSCs (**Figure 5.12**). Caspase 3 represents the meeting point between the apoptotic intrinsic and extrinsic pathways, and it is considered a general marker of programmed cell death. This result might correlate with the observations by **Nechiporuk et al., 2016**, reporting REST to protect neural progenitors from DNA damage until they are ready for neurogenesis. Since in our model, only the deprivation of REST from hGSCs results in apoptosis, we could speculate that that the chromosomal abnormalities already present in tumour cells make them more prone to cell death.

Overall, the phenotype emerged from REST knock-down in hGSCs and hNSCs confirmed the previously described roles of REST on proliferation, differentiation and apoptosis. Interestingly, the comparison between the two cell types revealed a palpable difference in sensitivity to REST deprivation, as hGSCs showed a stronger phenotype following REST knock-down in all of the analyses considered. One possible explanation is that the different origin of the cells (tumour *versus* non-tumour derivation) reflects a different network of genes regulated by REST, eventually leading to divergent activities. Variation in biological processes in which REST is involved in and the tolerance of the cells to changes in its levels/activity might be at the base of the observed differential activity.

The overexpression of REST in hGSCs and hNSCs caused a reduction in cell proliferation, similarly to REST KD conditions (**Figure 6.6**), although not accompanied by cell death (**Figure 6.10**). This aspect might suggest that the cells are either differentiating or exiting cell cycle. Upon long-term REST overexpression, we found an increased Sox2 immunoreactivity, indicating that the cells maintained a multipotent and tumorigenic phenotype (**Figure 6.8**). This condition was also characterised by an increased number of cells exhibiting the coexpression of GFAP and Nestin, that typically mark quiescent adult NSCs. In GBM, besides being used as differentiation marker, GFAP role is largely unclear. It has been proposed to be downregulated due to promoter methylation and that its expression negatively correlates with GBM histological malignancy (**Hara et al., 1991; Restrepo et al., 2011**). However, GFAP appears expressed in a subset of Sox2 and Nestin-expressing GBM cells exhibiting increased tumorigenic ability *in vivo* with respect to $GFAP^-/Sox2^-$ cells (**Hägerstrand et al., 2011**). hGSCs express variable levels of GFAP depending on the GBM they derive from and potentially on the cell progenitor originating GBM (**Pollard et al., 2009b**). *In vivo*, NSCs expressing high levels of REST have been reported to exit cell cycle and acquire a quiescent-like state, characterised by the co-presence of Nestin, Sox2 and GFAP (**See chapter 3.4 for details**, **Gao et al., 2011; Mukherjee et al., 2016**). We can thus speculate that increased activity of REST in hGSCs and hNSCs do not hamper the multipotency maintenance yet might push these cells towards quiescence *status*.

8.3 REST orchestrates multiple processes to regulate quiescence in hGSCs

In order to identify the main differences in REST activity in hGSCs *versus* hNSCs, we have performed a gene ontology analysis on REST modulated cells. Our results showed that, even though very few genes are communal between hGSCs and hNSCs, most of the biological processes regulated in these cells are shared. Indeed, we found REST to be involved mainly in brain development, neuronal activity and neural differentiation processes in both hGSCs and hNSCs (**Figure 7.2-7.5**). This is in line with previous description of REST transcriptional networks (**See chapter 3.4 for details**). Noteworthy, in both hGSCs and hNSCs we found a deregulation of one of the main pathways controlling NSCs biology: the Wnt signalling (**Figure 7.2 and 7.4**). In particular, induction of Wnt has been shown to dramatically increase proliferation and differentiation of adult NSCs through induction of the proneural genes Ngn2 and NeuroD1 (**Jang et al., 2013; Kuwabara et al., 2009; Lie et al., 2005**). Wnt appears therefore to stimulate adult NSCs exit from quiescence and neuronal differentiation in a process mediated at least in part by the repression of REST through the Wnt-target miR-20 (**Cui et al., 2016**). Nonetheless, the link between REST and Wnt has not been explored in a brain tumour context.

Our gene ontology analysis on REST-modulated cells also highlighted a previously undescribed regulation of cell metabolism in both hGSCs and hNSCs (**Figure 7.2-7.4**). Indeed, along with terms associated to neuronal differentiation and function that are present in both REST OE and REST KD hGSCs, genes regulating lipid and steroid metabolism, cell adhesion and migration, and response to hypoxia were found deregulated in REST OE hGSCs (**Figure 7.5B-B'**), while REST knock-down in hGSCs causes deregulation of genes involved in cell death, cell-matrix interaction, gluconeogenesis, PPARα signalling and circadian rhythms (**Figure 7.5A-A'**). A number of genes associated to circadian rhythm have been reported to be expressed by $Nestin^{+}/GFAP^{+}$ NSCs in the murine SVZ, where they regulate neuronal differentiation processes (**Kimiwada et al., 2009**). Among them, NR1D1 controls proliferation of SGZ resident NSCs and regulates the expression of FABP7, a NSCs marker associated to fatty acids uptake (**Schnell et al., 2014**). In GBM cells, both NR1D1 and FABP7 were shown to regulate cell proliferation and migration (**De Rosa et al., 2012; Schnell et al., 2014**). NR1D1 was also shown to inhibit *de novo* lipogenesis and autophagy resulting in a delayed GBM growth *in vivo* (**Sulli et al., 2018**). Finally, **Kamal et al., 2012**

identified lipid metabolism among the processes potentially regulated by REST in hGSCs, although they did not explore further this relationship. Moreover, the REST target miR-124 is able to directly repress the circadian regulator Clock, leading to impairments in GBM cells' proliferative and migratory ability (**Li et al., 2013**). Since cell metabolism and circadian rhythm are deeply interconnected, and both have been shown to influence NSC quiescence (**Fitzsimons et al., 2016; Kim et al., 2014**), we screened for genes associated to these processes. Interestingly almost the totality of the cell metabolism- and circadian rhythms-associated genes that we have identified resulted to be downregulated in REST OE hGSCs and upregulated in REST KD hGSCs (**Figure 7.6**), suggesting that REST modulation is deeply interconnected with cellular metabolic processes. Alteration of cell metabolism might work in concert with other REST-regulated processes in inducing the phenotypical modifications observed in REST modulated-hGSCs. The overexpression of REST determines the acquisition of characters typical of quiescent NSCs (**Figure from 6.6 to 6.10**), accompanied by reduction of energetic demand, and therefore the metabolic genes are repressed. On the other hand, REST silencing appears to induce cell differentiation (**Figure from 6.8 to 6.12**), involving substantial changes in cell metabolism that are manifested by induction of genes belonging to several metabolic pathways.

In our analyses, REST-overexpressing hGSCs were indeed characterised by a deregulation of transcription factors previously reported to regulate the transition from quiescent to activated NSCs (**Table 7.5 right,** **Shin et al., 2015**). These transcription factors were shown to regulate processes that in GBM or hNSCs include protein translation and cell cycle (**ATF4/CREB2**), multipotency and differentiation (**KLF15, NR2E1/TLX, INSM1, NFIA, SOX9**), expression of quiescent NSCs markers (**NR2E1/TLX**), and are part of, or interact with, other signalling pathways involved in NSCs quiescence, among which BMP, Wnt, Ascl1 (**NR2E1/TLX, HES1, TCF7L2**/**TCF4**) (**Elmi et al., 2010; Imayoshi et al., 2013; Li et al., 2012; Liang et al., 2014; Liu et al., 2016; Negrini et al., 2013; Ohtsuka et al., 2011; Qin et al., 2014; Qu et al., 2010; Rozpedek et al., 2016; Sasai et al., 1992; Urbán and Guillemot, 2014; Zhu et al., 2014**). Their combinatorial modulation by REST might therefore cause the acquisition of a quiescent state.

In REST OE hGSCs, we also identified genes belonging to pathways reported to influence quiescence in NSCs (**Table 7.5 right**), specifically:

- **ASCL1** is a direct target of REST reported to play a crucial role in the induction of quiescence exit in Nestin^{+}/GFAP^{+} NSCs. Ascl1 induction in quiescent NSCs has been shown to switch them into proliferative (activated) NSCs (**Andersen et al., 2014; Ballas et al., 2005; Gao et al., 2011**).
- Sonic Hedgehog pathway effectors: Patched1 (**PTCH1**) and hedgehog interacting protein (**HHIP**) are two inhibitors of the SHh signalling, which long term activation determine an increase in the fraction of quiescent NSCs causing a decreased neurogenesis (**Daynac et al., 2016**).
- Lipid and cholesterol metabolism: The inhibition of fatty acids metabolism due to an increased activity of **NR1D1** in NSCs has been shown to result in a repression of stearoyl-CoA desaturase (**SCD**) and **FABP7** expression. These, together with a reduced sterol availability (due to repression of **HMGCS1** and **SQLE**) determine a reduced NSCs proliferation and neurogenesis (**Giachino et al., 2014; Knobloch et al., 2012; Saito et al., 2009; Schnell et al., 2014; Sulli et al., 2018**).

Overall, the deregulation of quiescent-associated pathways identified in REST-modulated hGSCs point towards a REST-controlled process leading to reduction of neuronal-like differentiation and maintenance of hGSCs multipotency, while inducing a reduced cell cycle activity. These biological functions, along with the repression of protein translation and the cells' energetic metabolism are typical of dormant NSCs. To verify our interpretation of *in silico* analyses, we tested the expression of Ascl1 and Ki67 in REST modulated hGSCs (**Figure 7.7**). Despite the cells have been cultured in self-renewal medium, both REST knock-down and REST overexpressing hGSCs showed an increase in number of cells that have exit cell cycle, suggesting they are either differentiating or have acquired a quiescent state. However, only REST OE hGSCs cells presented a reduced immunoreactivity for Ascl1, in line with the Ascl1 role in inducing NSCs exit from quiescence and induction of differentiation (**Andersen et al., 2014; Urbán et al., 2016**).

8.4 hGSC-specific REST targets regulate multipotency and have prognostic relevance

Regardless of the reported similarities with NSCs, GSCs also present tumorigenic features that are strongly influenced by REST levels, leading to the conclusion that REST facilitates gliomagenesis and may therefore represent a potential target for GBM care. However, unless suitable for local applications, the use of anti-REST drugs might harbour substantial side effects due to activity in undesired cell types. Antagonising REST activity in the brain would potentially reduce GBM growth, as already demonstrated in pre-clinical studies using animal models (**Conti et al., 2012; Kamal et al., 2012; Marisetty et al., 2017**), yet also affect the NSC compartment behaviour. A strategy to deal with these off-target effects is represented by directly targeting disease-specific effectors of multipotency-associated pathways. To this aim, gene expression approaches allows for the identification of differentially expressed transcripts in multiple cell types.

Our transcriptomic analysis was designed to identify selective hGSCs REST targets that are not shared with hNSCs. Focussing only on coding transcripts, we were able to identify 16 REST-dependent genes, uniquely altered in hGSCs and not in hNSCs (**Table 7.6**). The hGSC-specific REST-regulated genes are involved in processes deeply influenced by REST levels, such as neural differentiation (*ELAVL4, CNRIP1, DUSP15*), as well as hNSCs and hGSCs proliferation (*DRD2, HHIP, NOS2, GABBR2, CNRIP1, PDGFRA*), but are also implicated in mitochondrial activity and cell metabolism (*PPARGC1A, CKMT1A/B, AGT*) (**Aguado et al., 2007a, 2007b; Akamatsu et al., 2005; Bronicki and Jasmin, 2013; Chen et al., 2014; Eyler et al., 2011; Jornayvaz and Shulman, 2010; Juillerat-Jeanneret et al., 2004; Li et al., 2017; Lowe et al., 2013; Schmidt et al., 2012; Smith et al., 2015; Yan et al., 2013; Zhang et al., 2013**). We were surprised to find genes involved in cell metabolism since this kind of process has never been associated to REST, although extensively reported to impact NSC stemness through regulation of the availability of substrates for powering the cells (**Knobloch and Jessberger, 2017**). For instance, fatty acids were proposed to be used by NSCs, both as building blocks for membrane, and as energetic source alternative to glucose. NSCs greatly rely on glycolysis, *de novo* lipogenesis and fatty acids oxidation for supporting their energetic demand for expansion, and their differentiation is allowed upon switching

from glycolytic to oxidative metabolism (**Candelario et al., 2013; Knobloch et al., 2012; Lange et al., 2016; Stoll et al., 2015; Xie et al., 2016**). Indeed, the inhibition of mitochondrial metabolism in NSCs determines the induction glycolytic processes to support cell survival, but also leads to abnormal cell proliferation and the acquisition of tumorigenic properties (**Bartesaghi et al., 2015**). In tumours however, it is still debated whether CSCs mainly rely on glycolysis or oxidative phosphorylation and cases of metabolic switch have been described (**Peiris-Pagès et al., 2016**).

Interestingly, only six of the hGSC-specific REST-regulated genes identified in our study have a RE1 motifs in the promoter region, suggesting they are potential direct targets of REST. These include:

i. ELAV-like RNA binding protein 4 (*ELAVL4*/HuD), a known regulator of neuronal genes-associated mRNAs stability, therefore favouring neuronal differentiation. A reduced ELAVL4 activity has been reported to determine an increased proportion of slow dividing NSCs in the adult SVZ (**Akamatsu et al., 2005; Bronicki and Jasmin, 2013**).

ii. Dopamine receptor D2 (*DRD2*), a G-protein coupled receptor already validated as target of REST in murine cells (**Sun et al., 2005**) that mediates the tumorigenic potential of PRRX1 in hGSCs (PRRX1 fold-change in REST OE hGSCs: -2.73, **Li et al., 2017**). In GBM, it is upregulated specifically in respect to surrounding normal brain tissue, in which it would stimulates EGFR signalling by inhibiting Rap1-GTP. The combined inhibition of dopamine receptors and EGFR signalling was also found to promote survival in experimental animal models of GBM (**Li et al., 2014**).

iii. Peroxisome proliferator-activated receptor gamma, coactivator 1 alpha (*PPARGC1A*) encoding for PGC1α, a master regulator of mitochondrial biogenesis and a transcriptional coactivator of PPARs signalling that regulates energetic metabolism (**Jornayvaz and Shulman, 2010**).

iv. Creatine kinases mitochondrial 1A/B (*CKMT1*/uMtCK), neuronal-specific isoforms of creatine kinase involved in the cells' energetic metabolism by shuttling the high energy phosphate derived from oxidative phosphorylation to the cytosol (**Lowe et al., 2013**). CKMT1s have been described as oncogenic in breast carcinoma, a neoplasia derived from epithelial cells in which REST acts as an oncosuppressor

(**Qian et al., 2012; Wagoner et al., 2010**).

v. Ankyrin repeat and sterile alpha motif domain containing 1B (*ANKS1B*/AIDA1), a brain enriched protein involved in several neural disorders for its ability to modulate glutamatergic transmission at the post synaptic densities and to consequently regulate neuronal gene expression. ANKS1B is a known interactor of amyloid beta precursor protein, but it has also been shown to regulate endothelial cells permeability and EphA signalling to control cell motility and axon outgrowth (**Ghersi et al., 2004; Herberich et al., 2015; Shin et al., 2007; Tindi et al., 2015**).

Further experiments would be necessary to clarify why these potential direct targets of REST are differentially regulated in hGSCs *versus* hNSCs. Many factors could influence target selectivity of REST transcriptional repression in distinct cell types, such as the availability of different cofactors, the interplay with other transcription factors regulating the expression of RE1-containing genes, as well as the chromatin landscape. Our validation by qRT-PCR confirmed that, among the RE1-containing genes, *DRD2*, *PPARGC1A*, and *ANKS1B* are selectively regulated by REST in hGSCs in a canonical fashion, i.e. derepressed in REST KD cells and repressed in REST OE cells. For instance, *PPARGC1A* is effectively repressed by REST in hGSCs and hNSCs, but it is de-repressed only in REST KD hGSCs, while its expression does not change in REST KD hNSCs. One possibility is that *PPARGC1A* represents a *Class II* target as proposed by **Ballas et al., 2005**, so that even upon downregulation of REST, the repression is maintained by its cofactors. Also, other transcriptional repressors might preserve the levels of *PPARGC1A* in REST OE hNSCs. *ANKS1B* appears repressed both in REST KD and REST OE hNSCs, suggesting that even if high levels of REST are likely to control *ANKS1B* expression, other transcription factors de-repressed in REST KD hNSCs might exert an indirect repression of the gene. Finally, *DRD2* appears upregulated in both REST KD and REST OE hNSCs. Interestingly, in a previous report that identified DRD2 as direct target of REST in murine cells, RE1 sites were found to be occupied by REST in ESCs and hippocampal tissue, but not in NSCs (**Sun et al., 2005**). Also, even if REST was present at the promoter level, hippocampal cells showed a strong upregulation of DRD2. Unfortunately, it is still unclear how REST is able to select between different RE1 sites, as well as how REST bound genes are sometimes found induced.

Even if most of the hGSC-specific REST-regulated genes do not show any RE1 site proximal

to the transcription start site, almost the totality of them could be indirectly regulated by REST through its target NeuroD (**Table 6.6**, **Gao et al., 2011; Kemp et al., 2003b; Lunyak and Rosenfeld, 2005; Martin et al., 2015; Schoenherr and Anderson, 1995**). A similar kinetic might be maintained in GBM cells, in which treatment with the mTOR inhibitor rapamycin has been shown to induce NeuroD expression in parallel with the inhibition of cell migration and Nestin expression (**Ferrucci et al., 2017**), similarly to what happens upon REST knock-down. It would be interesting to experimentally verify whether NeuroD binds to the predicted responsive elements of these genes.

Interestingly, the list of hGSCs REST targets also includes platelet-derived growth factor receptor A (PDGFRA), which gene has already been confirmed as target of REST in murine cells (with a RE1 site located at 40 kb from 5', **Sun et al., 2005**), and is frequently amplified in GBM, particularly associated to GBM presenting oligodendroglial features (**Dai et al., 2001; Joensuu et al., 2005; Smith et al., 2000; Suzuki et al., 2004; Uhrbom et al., 1998; Wagoner and Roopra, 2012**). Also, PDGFRA has been proposed to mark a subpopulation of $GFAP^-$ adult neural precursors and to be required for oligodendrogenesis. These cells were able to generate a glioma-like hyperplasia in response to PDGF infusions (**Chojnacki et al., 2011**). It is possible that REST repression of *PDGFRA* in our hGSCs entails mechanisms of control of multipotency, inhibiting the acquisition of oligodendroglial features to promote a quiescent-like $GFAP^+$ state.

Among the identified hGSC-specific REST-regulated genes, the neural transmitter regulator CADPS2 and the sonic hedgehog inhibitor HHIP do not present any REST or NeuroD binding elements (**Chang et al., 2016; Cisternas et al., 2003; Sadakata et al., 2012; Yan et al., 2013**), although we cannot exclude the presence of distant silencers, i.e. DNA sequences regulating genes' transcription although residing very far away from the regulated gene, through which REST might regulate CADPS2 and HHIP expression.

The hGSCs REST score we generated using the hGSC-specific REST-regulated genes showed an inverse correlation with REST expression in GBM patients, indicative of an increased transcriptional repression in presence of REST (**Figure 7.10A and E**). Even if the hGSCs REST score has been obtained from the analysis of a minor subpopulation of cells in the tumour bulk, i.e. the hGSCs, these genes behave similarly in gene expression experiments performed on *gliomi* as a whole, suggesting the signature we identified might be applied in

clinical analyses on tumour specimens. The hGSCs REST score has been tested for its prognostic potential in two independent cohorts of patients (**Figure 7.10**). REST showed an inverse correlation with the *gliomi* WHO grade, exhibiting a lower activity (high hGSCs REST score) in healthy individuals and a progressively higher activity from WHO grade 2 to 4 (**Figure 7.10F**), suggesting that REST transcriptional repression is generally lower in non-pathological human brain and increases gradually according to glioma aggressiveness. We also compared the hGSCs REST score with GBM molecular subtypes. The four GBM subtypes were established by analysing the transcriptional profiles of GBM samples, and correlate with patients' survival and therapeutic response. In particular, the *proneural* class of GBM, which presents a high hGSCs REST score, is characterised by the overexpression of both PDGFRA (one of the genes composing the hGSCs REST score) and the proneural gene Ascl1 (repressed in REST OE hGSCs), and recognised as the less aggressive subtype, with patients experiencing a longer survival than the ones belonging to *neural*, *classical* or *mesenchymal* GBM subtypes (**Brennan et al., 2013**). Conversely, a lower hGSCs REST score is associated to the *classical* and *mesenchymal* molecular subtypes of GBM (**Figure 7.10D**), that represent the most aggressive phenotypes (**Sidaway, 2017; Wang et al., 2017**). These results suggest that even though the hGSCs REST score does not directly impact patients' OS and PFS within the GBM group (**Figure 7.10B and C**), the association with molecular phenotypes of GBM featuring distinct clinical course determines an indirect relationship between our hGSCs REST signature and patients' survival. These results are in line with previously derived REST signatures from GBM specimens and human cell lines, that showed a correlation with glioma WHO grade, with high grade malignancies presenting higher REST activity than low grade tumours (**Wagoner and Roopra, 2012**), as well as an overall higher REST activity in the *classical* and *mesenchymal* subtypes, an intermediate REST activity in the *proneural* subtype and a lower REST activity in the *neural* subtype (**Liang et al., 2016; Wagoner and Roopra, 2012**). Differently from our hGSCs REST score however, the previously published REST signatures were also shown to correlate with patients' OS. This might be due to the distinct derivation of the biological samples in our study.

This is the first time that a REST signature is derived from hGSCs and shown to have potential prognostic relevance. Also, given the patients' gene expression data were derived from GBM specimens without discerning between tumour cell subpopulations, this result implies that the hGSC-specific REST-regulated genes might also influence non stem-like

GBM cells functions. If this will be proven to be true, then a pharmacological therapy aimed at the hGSC-specific REST-regulated genes will results in targeting both the hGSCs and the differentiated GBM cells, affecting the tumours at multiple levels.

8.5 Future perspectives and Concluding remarks

Basal levels of REST have been shown to sustain multipotency and self-renewal, while blocking differentiation both in hGSCs and hNSCs. Thus, manipulating REST levels can lead to substantial alterations in these events. Indeed, silencing of REST stimulates neuronal (-like) differentiation both in hGSCs and hNSCs, while increased REST levels results in preservation of multipotency in these cell types, and has been shown to induce a quiescent status in adult murine NSCs. Our results suggest that REST ability to drive quiescence might also be maintained in hGSCs. Acting as a molecular switch between three cell states (quiescent, proliferative, and differentiated), REST levels need to be precisely fine-tuned to sustain self-renewal and a deviation from this level might induce opposed cell fates. Our bioinformatics analyses suggest that REST activity is exerted through regulation of multiple processes, including cell proliferation, neuronal differentiation, and cell metabolism, cooperating to properly achieve cell transition from one state to another.

The conservation of REST-regulated mechanisms in hGSCs might profoundly influence GBM behaviour. An induced quiescent state would result in a delayed tumour growth, however not correlated to a less malignant phenotype. This delayed disease progression would likely be accompanied by increased resistance to chemo and radiotherapies, so that the tumour would be characterised by a slower, yet relentless growth. Since quiescence is a reversible condition, it implies that dormant hGSCs can potentially be activated to fast proliferative hGSCs and re-establish the rapid tumour growth typical of GBM. According to our data, this process would be partially governed by a set of genes whose transcription in hGSCs is dependent on REST levels. A therapeutic loss of function approach for REST would initiate the transition of quiescent to activated hGSCs, and then to differentiated-like cells, thus resulting in either apoptosis for premature activation of the differentiation programme or

increased sensitivity to common chemotherapeutics. Our analyses have identified a set of hGSCs-selective REST-targets potentially regulating cell proliferation, differentiation, and metabolism that might be considered for a therapeutic approach to REST-mediated tumorigenesis in order to minimise potential side effects emerging from a direct targeting of REST.

Our results raise a number of question that need to be addressed to better understand the differential role exerted by REST in hGSCs respect to hNSCs and to validate the hGSC-specific REST-regulated genes before a clinical approach is ventured. For instance:

Does REST actually regulate cell metabolism in hNSCs and hGSCs? A set of biochemical analyses on cell metabolism should be performed to identify whether the transcriptomic modifications observed *in silico* reflects biological variation in cell metabolism and behaviour.

Does REST truly induce quiescence in hGSCs? To this aim, a deeper investigation of REST OE hGSCs is required to clarify cell cycle variations, as well as whether the phenotype is reversible and involves multipotency preservation.

What are the consequences of hGSCs quiescence in GBM? Importantly, are quiescent hGSCs tumorigenic and chemoresistant? These questions could be addressed by a set of *in vitro* and *in vivo* experiments aimed at verifying REST OE hGSCs survival/tumour growth upon treatment with chemotherapeutic drugs.

Are the hGSC-specific REST-regulated genes direct target of REST? To this aim we should extend our bioinformatic approach in order to increase our predictive power of RE1 sites and widen it to atypical RE1s potentially involved in regulating hGSC-specific REST-regulated genes expression. Chromatin immunoprecipitation (ChIP) should then validate the actual binding of REST to hGSC-specific REST-regulated genes in hGSCs.

How does REST choses different targets in hGSCs and hNSCs? Differential binding of a particular transcription factor in different cell types might be influenced by motif variations at REST binding sites, and expression of REST cofactors. ChIP-sequencing could be exploited to identify alternative REST binding sites, as well as cofactors enrichment at the hGSC-specific REST-regulated genes *loci*.

Do the hGSC-specific REST-regulated genes actually impact hGSCs tumorigenic abilities and GBM clinical course? This point should be addressed with gain and loss of function approaches for the modulation of every hGSC-specific REST-regulated gene in hGSCs followed by phenotypical analyses on cells' behaviour *in vitro* and tumorigenic competence *in vivo*. These set of experiments will clarify whether the hGSC-specific REST-regulated genes are actual therapeutic targets for GBM.

Further studies are required to test our model. However, our results highlight that the REST-dependent regulation of hGSCs multipotency is established by modulating multiple processes in order to reach a tight control of quiescence, proliferation and differentiation, ultimately influencing GBM aggressiveness.

Methods

Chapter 9

Methods

Contents

9.1 CELL CULTURES	**125**
9.2 PRODUCTION OF LENTIVIRAL PARTICLES CARRYING PINDUCER SYSTEMS	**127**
9.3 FLOW CYTOMETRY AND CELL SORTING	**127**
9.4 REAL-TIME QUANTITATIVE POLYMERASE CHAIN REACTION	**128**
9.5 IMMUNOBLOTTING	**128**
9.6 IMMUNOSTAINING	**129**
9.7 CELL PROLIFERATION ASSAY	**129**
9.8 MICROARRAY AND GENE EXPRESSION ANALYSES	**130**
9.9 STATISTICS	**132**
9.10 LIST OF PRIMERS	**133**
9.11 LIST OF ANTIBODIES	**134**

9.1 Cell cultures

GB7 cells, in this manuscript named hGSCs, were derived in by Professor Luciano Conti (Centre for Integrative Biology, University of Trento, Trento, Italy) and characterised in **Conti et al., 2012**. hGSCs were routinely passaged every 3-5 days at a density of 5-15 x 10^3 cells/cm^2 on laminin-coated plastic culture vessels prepared with 3 µg/ml Laminin (Thermo Fisher Scientific) diluted in self-renewal medium and incubated at 37 °C, 5% CO_2 for 3-5 hours. For hGSCs passaging, the culture medium was collected and the cells incubated for 1 minute with StemPro Accutase (Thermo Fisher Scientific). Single cells suspension was then diluted in conditioned medium and spun down at 260g for 3 minutes before being

resuspended in fresh medium and plated onto the coated vessels. hGSCs self-renewal medium is composed of Euromed-N medium (Euroclone), N2 Supplement (1%, Thermo Fisher Scientific), B27 Supplement (2%, Thermo Fisher Scientific), EGF (20 ng/ml, Peprotech), bFGF (20 ng/ml, Peprotech), Glutamax (2mM, Thermo Fisher Scientific), and Pen/Strep (100X).

AF22 cells (**Falk et al., 2012**) were kindly donated by Professor Austin Smith (Cambridge Stem Cell Institute, University of Cambridge, UK), in this manuscript called hNSCs, were routinely passaged every 2-3 days at a density of 25-35 x 10^3 cells/cm^2 on laminin-coated plastic culture vessels prepared as above. For hNSCs passaging, the culture medium was collected and the cells incubated for 30-60 seconds with StemPro Accutase (Thermo Fisher Scientific). Single cells were then diluted in conditioned medium and spun down at 260g for 3 minutes before being resuspended in fresh medium and plated onto the coated vessels. hNSCs self-renewal medium is composed of DMEM/F-12 (Thermo Fisher Scientific), N2 Supplement (1%, Thermo Fisher Scientific), B27 Supplement (0.1%, Thermo Fisher Scientific), EGF (10 ng/ml, Peprotech), bFGF (10 ng/ml, Peprotech, Cod. 100-18b), Glutamax (2mM, Thermo Fisher Scientific), and Pen/Strep (100X).

Unless stated differently, doxycycline treatment was performed by addition of 500 ng/ml doxycycline to the culture medium, and medium was renewed every day. No doxy indicates untreated cells.

For the generation of the hGSCs and hNSCs pINDUCER cell lines, 1/12 of the concentrated lentiviral particles was used to infect either 5 x 10^3 hGSCs/cm^2 or 20 x 10^3 hNSCs/cm^2. After 8 hours, the medium was completely renewed and 72 hours post infection the cells were treated as follows for positively select the transduced cells, until non-infected control cells died completely:

- 1.0 µg/ml puromycin (Thermos Fisher Scientific) for hGSCs pINDUCER10 and hGSCs pINDUCER10shREST
- 300 µg/ml G418 (Thermos Fisher Scientific) for hGSCs pINDUCER20 and hGSCs pINDUCER20hREST
- 0.3 µg/ml puromycin (Thermos Fisher Scientific) for hNSCs pINDUCER10 and hNSCs pINDUCER10shREST

– 200 µg/ml G418 (Thermos Fisher Scientific) for hNSCs pINDUCER20 and hNSCs pINDUCER20hREST

9.2 Production of lentiviral particles carrying pINDUCER systems

The day before transfection 60 x 10^3 cells/cm^2 human embryonic kidney 293T cells/cm^2 were seeded in DMEM (Thermo Fisher Scientific) containing 10% foetal bovine serum (FBS, Thermo Fisher Scientific) and left undisturbed overnight. The next morning the cells were transfected using the $CaPO_4$ method with 20 µg of each pINDUCER vectors (**Meerbrey et al., 2011**) (kindly donated by Dr. Thomas Westbrook, Department of Molecular and Human Genetics, Baylor College of Medicine, Houston, TX, USA), 15 µg of psPAX2 vector (kindly donated by Professor M. Pizzato, Centre for Integrative Biology, University of Trento, Italy), and 5 µg of VSV-G. Two days from the transfection, the supernatant was collected and concentrated using the Lenti-X concentrator reagent (Clontech) following manufacturer recommendations.

9.3 Flow cytometry and cell sorting

Flow cytometry and FACS sorting experiments were performed in collaboration with Dr. Isabella Pesce of the CIBIO Cell Analysis and Separation Core Facility (CASCF). EGFP+ fluorescent pIND11 hGSCs, pIND11shREST hGSCs, pIND22 hGSCs, and pIND22hREST hGSCs were isolated using a FACS Aria II (Becton Dickinson) in the purity precision mode with a nozzle of 100 µm and at the appropriate sort rate (e.g. below 80 cells per second). A negative control of non-fluorescent cells (**Figure 5A and 17A**) was used to determine the background fluorescence such that less than 1% of non-fluorescent cells were included in the sort gate. The purity of sorted cells was examined immediately after sorting with a FACS Canto A (Becton Dickinson).

9.4 Real-time quantitative polymerase chain reaction

Cells were lysed using the TriFast reagent (Euroclone) and the RNA extracted following the common Tri procedure as in **Chomczynski and Mackey, 1995**.

RNA retro-transcription was performed using the iScript cDNA Synthesis kit (Biorad) following manufacturer recommendations with 500 ng RNA per sample.

The real-time quantitative polymerase chain reaction (qRT-PCR) was carried out using the SSO Advanced Universal SyBR Green Supermix kit (Biorad) and the Biorad CFX96 touch thermocycler. The reaction mix contained 7.5 µl of SSO Advanced Universal SyBR Green Supermix, 2 µl of 2 µM primers forward + reverse suspension, 1.5 µl nuclease-free water and 5 ng of 1.25 ng/µl RNA. Thermocycler was set as follows: 95°C for 3 minutes followed by 40 cycles of (I) 95°C for 10 seconds and (II) 60°C for 30 seconds with detection. Samples were normalised using ACTB as reference gene.

9.5 Immunoblotting

Cells were lysed using the SDS sample buffer prepared as follow: 62.5 mM Tris-HCl pH 6.8, 2% SDS, 10% Glycerol, 50 mM DTT. Samples were boiled for 5 minutes at 95°C before loading into a 7% polyacrylamide gel run at 100 Volts constant. Following electrophoresis, proteins were transferred to a PVDF membrane (Biorad) using a wet blot apparatus at 100 Volts constant. Proteins were treated with 0.4% paraformaldehyde in phosphate buffered saline solution for 30 minutes at room temperature as suggested in **Lee and Kamitani, 2011**, before incubation with the primary antibodies overnight at 4°C in agitation and secondary antibodies for 2 hours at room temperature. Luminescent signal was detected using the Clarity ECL reagents (Biorad) in a dark chamber Uvitec Alliance (Uvitec) and the manufacturer software to acquire and analyse the data. Buffer composition: running buffer

is 25 mM Tris Base, 192 mM Glycine and 0.1% SDS; transfer buffer is 25 mM Tris Base, 190 mM Glycine, 20% methanol; blocking solution is 10% milk in 20 mM Tris Base pH7.5, 150 mM NaCl, 0.1% Tween 20; antibodies were diluted in 5% milk in 20 mM Tris Base pH7.5, 150 mM NaCl, 0.1% Tween 20.

9.6 Immunostaining

Cells were fixed with 4% paraformaldehyde for 15 minutes at room temperature, then permeabilised with permeabilisation buffer for 15 minutes at room temperature and blocked with blocking buffer for 2 hours, before incubating them with the primary antibodies diluted in antibody solution over night at 4°C. After three washes with phosphate buffered saline solution, cells were incubated with the appropriate AlexaFluor 488 and AlexaFluor-596 secondary antibodies (Molecular Probes) at 1:500 dilution for 2 hours. Nuclei were counterstained using Hoechst 33258 before imaging with a Leica DMIL or a Zeiss Axio Observer Z1 inverted epifluorescent microscopes.

Buffers composition: permeabilisation buffer is composed of 0.5% Triton X-100 diluted in phosphate buffered saline; blocking buffer contains 5% FBS/0.3% Triton X-100 in phosphate buffered saline; antibody solution is made of 3% FBS/0.2% Triton X-100 in phosphate buffered saline. For quantifying immunopositive cells for the indicated antigen the number of fluorescent cells per picture was normalised on the number of cells, evaluated using nuclei staining.

9.7 Cell proliferation assay

3-(4,5-Dimethylthiazol-2-yl)-2,5-Diphenyltetrazolium Bromide (MTT) assay was performed to test cell proliferation. hGSCs REST KD, hGSCs REST OE, hNSCs REST KD and hNSCs REST OE were seeded on laminin-coated culture vessels at a density of 10 x 10^3 cells/cm^2 and 2.5 x 10^3 cells/cm^2 respectively and left undisturbed overnight. The next day, the cells were

treated with 500 ng/ml doxycycline and the MTT assay was performed by incubating the cells with 1.5 mg/ml MTT for 90 minutes and resuspension of the precipitated formazan salt in isopropanol at 24, 48, 96, and 120 hours following induction of the Tet-on systems. Absorbance was read at 550 nm using the Infinite 200 Pro (Tecan) plate reader.

9.8 Microarray and gene expression analyses

Microarray and bioinformatics analyses were performed in collaboration with Prof. Giuseppe Basso, Dr. Silvia Bresolin and Dr. Luca Persano of the Laboratory of Onco-Hematology, Dept. of Women's and Children's Health, University of Padova, Padova, Italy.

For microarray experiments, biological triplicates of hNSCs/hGSCs REST OE and hNSCs/hGSCs REST KD were treated for 24 and 48 hours respectively with 500 ng/ml doxycycline. RNA was extracted according to the common Tri procedure and analysed using Eukaryote Total RNA Nano 2100 bioanalyzer (Agilent) for their quality. RNA with a RIN > 9.5 were considered for the experiments. In vitro transcription, hybridization and biotin labelling were performed according to Human Clariom D Assay (Thermofisher, Waltham, MA, USA). CEL files were generated using Expression Console Suite Software and normalized with RMA (www.r-projects.org) and Transcriptome Analysis Console Software (TAC v.4.0.0.25). Unsupervised analysis was performed using hierarchical clustering analysis with Ward.2 method and Euclidian distance using probes with variance more than 90%. All transcription clusters (TC) were divided and analysed separately based on their mapping in coding or non-coding genes. Differentially expressed genes were identified using Significance Analysis of Microarray algorithm coded in the samr R package (**Tusher et al., 2001**). In SAM, we estimated the percentage of false positive predictions (i.e., False Discovery Rate, FDR) with 100 permutations. TC with FDR<0.05 were considered significant.

For coding regions, Gene Set Enrichment Analysis (GSEA) was performed using GSEAv2.0 with TC ranked by signal-to-noise ratio and statistical significance determined by 1000 permutations (**Subramanian et al., 2005**). Gene sets permutations (< 7 replicates in each class) were used to enable direct comparisons between REST OE or REST KD doxycycline

induction and REST OE or REST KD without doxycycline induction in both hGSC and hNSCs. Minimum gene set size was set to 15. For GSEA an FDR cutoff < 0.25 was used. MgSigDataBase derived from c5 Gene Ontology dataset were selected to obtain the enrichment gene sets. Enrichment map was generated using Enrichment Map Cytoscape v3.5.1 plug-in (**Merico et al., 2010**). Only gene sets with p-value ≤ 0.05, derived from c5 Gene Ontology MSigDB GSEA were used to build the network. To generate the gene sets relationship, we used Overlap Coefficient parameters (Overlap Coefficient = [size of (A intersect B)] / [size of (minimum(A , B))], where A and B are two gene sets). Redundant gene sets with common biological function were grouped in cluster and manually labelled with Gene Ontology terms.

Selected GO terms were performed according to Metascape tool (http://metascape.org) on differentially significant TC (**Tripathi et al., 2015**). Enriched terms (GO/KEGG terms, canonical pathways, hall mark gene sets), hypergeometric p-value and enrichment factors were calculated and used for filtering. Colour code indicate the grade of significance of terms.

Common genes resulted up-regulated in REST KD cells and down-regulated in REST OE cells after doxycycline induction were considered as potential target genes of REST and used to generate the REST score. We evaluate the prognostic potential of this score in two different cohorts of GBM patients: cohort 1 (TCGA cohort, **McLendon et al., 2008**), and cohort 2 (Sun cohort, **Sun et al., 2006**). The log2 expression values for each sample in each dataset were centred to zero mean. The sum of the mean-centred log2 expression values of the REST target genes was used as the REST Score for each subject of both cohorts. REST Score were applied among different GBM molecular subtypes in cohort 1 and among different glioma grades in cohort 2. In the graphs, median of REST Score of whole samples was indicated. Graphs were generated with Graph Pad Prism 6.07 (GraphPad, La Jolla, CA). REST target genes were used to clusterise patients of cohort 2 with a hierarchical clustering analysis and to generate level plot of patients of cohort 2. For both cohorts Spearman correlation was used to assess the correlation between the calculated REST Score of each patient and its relative REST gene expression value.

To computationally predicted regulatory sites for transcription factors (TFs) and micro-RNAs (miRNAs) in doxy vs no doxy in both hNSCs and hGSCs we used ISMARA analysis

according to default parameters (**Balwierz et al., 2014**). For each motif inferred activities across the input samples, predicted genome-wide targets, enriched pathways and functional classes of genes, and direct interactions between regulators were reported.
The prediction of transcription factor binding sites on the hGSC-specific REST regulated genes was performed using MotifMap system according to default parameters (**Daily et al., 2011; Xie et al., 2009**). Transcription factor binding sites with a FDR < 0.1 were considered statistically significant and included in our analysis.

9.9 Statistics

For all experiments, data are expressed as mean ± standard deviation. Data distribution was assessed for normality using the Shapiro-Wilk test. To determine statistical significance, we used the unpaired t-test or, for multiple comparisons, a one-way analysis of variance followed by a Dunnett's post-hoc test or a two-way analysis of variance followed by a Sidak's post-hoc test. A P value of less than 0.05 was considered statistically significant. Statistical analysis was performed using Prism7 (GraphPad Software, La Jolla, CA).

9.10 List of primers

Gene	Primer sequence	Product lenght (bp)
AGT	F- TGGACAGCACCCTGGCTTTCAA	111
	R- ACACTGAGGTGCTGTTGTCCAC	
ACTINB	F- GACAGGATGCAGAAGGAGATTACTG	72
	R- CTCAGGAGGAGCAATGATCTTGAT	
BDNF	F- TAACGGCGGCAGACAAAAAGA	101
	R- GAAGTATTGCTTCAGTTGGCCT	
CKMT1A/B	F- AGTGAACGACGGAGGCTGTATC	237
	R- CTGATCTAGCGTCCAACCAGTG	
CNRIP1	F- CGGTCTTTTACAAGGTGGACGG	154
	R- AGTTCCAGTGGGACAAGCACAC	
DRD2	F- CAATACGCGCTACAGCTCCAAG	130
	R- GGCAATGATGCACTCGTTCTGG	
ELAVL4	F- CCCAGAAGGAACTGGAGCAACT	145
	R- CCTTTGATGGCTTCTTCTGCCTC	
GABBR2	F- GTTGCTCAAGCACTACCAGTGG	105
	R- TCCTCGCCATACAGAACTCCAG	
HHIP	F- GCCATTCAGTAATGGTCCTTTGG	141
	R- TGCCACTGCTTTGTCACAGGAC	
L1CAM	F- CCCGACCGATGAAAGATGAG	208
	R- TCCTTCTTGCCACTGTACTG	
NOS2	F- GCTCTACACCTCCAATGTGACC	136
	R- CTGCCGAGATTTGAGCCTCATG	
PLP2	F- CGCACTCGAAAGGGAATCCT	198
	R- GAAGAAATCACTCCAGGGCCA	
PPARGC1A	F- ACCAAACCCACAGAGAACAG	124
	R- GGGTCAGAGGAAGAGATAAAGTTG	
REST	F- ACTTTGTCCTTACTCAAGTTCTCA	132
	R- GCATGGCGGGTTACTTCATGTT	
SNAP25	F- TAC ACA GAA TCG CCA GAT CG	103
	ACC ACT TCC CAG CAT CTT TG	
SYP	F- TCGGCTTTGTGAAGGTGCTGCA	115
	R- TCACTCTCGGTCTTGTTGGCAC	
TUBB3	F- TCAGCGTCTACTACAACGAGGC	120
	R- GCCTGAAGAGATGTCCAAAGGC	
VGF	F- ACACGCTGACCCGAGTGAATCT	137
	R- CATACGCGCCTGGAATTGAGAG	

9.11 List of antibodies

Antigen/Name	Company	Code	Dilution for immunoblotting	Dilution for Immunostaining
Ascl-1	Santa Cruz	sc-390794		1:100
β3-Tubulin	Promega	G712A		1:1000
Cleaved Caspase 3	Cell Signaling	9661s		1:500
GFAP	DAKO	Z0334		1:1000
Ki67	ABCAM	ab15580		1:1000
Nestin	RD System	MAB1259		1:300
REST	Millipore	07-579	1:1000	1:300
Sox2	Millipore	AB5603		1:1000
α-Tubulin	Santa Cruz	sc-53646	1:1000	
Anti Mouse IgG AlexaFluor 488	Molecular Probes	A11001		1:500
Anti Mouse IgG AlexaFluor 568	Molecular Probes	A11004		1:500
Anti Rabbit IgG AlexaFluor 488	Molecular Probes	A11008		1:500
Anti Rabbit IgG AlexaFluor 568	Molecular Probes	A11011		1:500
Immun-Star goat anti-mouse (GAM)-HRP	Biorad	1705047	1:2000	
Immun-Star goat anti-rabbit (GAM)-HRP	Biorad	1705046	1:2000	

Appendix

Lists of Differentially Expressed Coding Genes

A. List of coding genes differentially expressed in doxycycline-treated REST OE hGSCs *versus* untreated cells.

Probe	Gene	FC (log2)
TC0900010262.hg.1	gleytoyby	1,9974
TC0900009335.hg.1	fleewarby; rawswey	1,9589
TC1600008917.hg.1	neereyby	1,8702
TC1200008280.hg.1	vawjyby	1,8123
TC1300006438.hg.1	BNIP3P7	1,6927
TC2100006544.hg.1	AJ239321.3	1,6662
TC0400007609.hg.1	REST	1,5706
TC0900009334.hg.1	moyswey	1,5173
TC1500010723.hg.1	CHAC1	1,4037
TC1700010604.hg.1	NR1D1	1,3455
TC0100011463.hg.1	SYT14	1,3161
TC1300007491.hg.1	KLF5	1,3146
TC0400011920.hg.1	SLC7A11	1,3064
TC0800011334.hg.1	KLF10	1,2953
TC0700011930.hg.1	shukar	1,2912
TC0500008785.hg.1	EGR1	1,2758
TC0500012177.hg.1	fawstoyby	1,2501
TC1100007884.hg.1	SLC3A2	1,1331
TC1200008683.hg.1	CHST11	0,9346
TC0500007738.hg.1	MAP1B	0,9334
TC1300008497.hg.1	UBL3	0,9256
TC0100018273.hg.1	ATP1A1	0,9255
TC1800007680.hg.1	CNDP2	0,9237
TC0600009332.hg.1	FABP7	0,9232
TC1700007360.hg.1	TMEM97	0,9225
TCOX00007558.hg.1	NLGN3	0,9209
TC0700010728.hg.1	HERPUD2	0,9204
TC0200011171.hg.1	SH3BP4	0,9180
TC0500010635.hg.1	HMGCS1	0,9168
TC1200007895.hg.1	OS9	0,9167
TC0100018443.hg.1	PLPP3	0,9159
TC0700012636.hg.1	PODXL	0,9145
TC0800010002.hg.1	DUSP4	0,9145
TCOX00008521.hg.1	SLC9A6	0,9135
TC1600011398.hg.1	MMP2	0,9134
TC1700012344.hg.1	GABARAP	0,9129
TC0200009065.hg.1	DBI	0,9129
TC1800008285.hg.1	NPC1	0,9122
TC0600010572.hg.1	TUBB2B	0,9122
TC2200007505.hg.1	SEPT3	0,9122
TC0100015819.hg.1	S100A10	0,9120
TC0100018565.hg.1	AGT	0,9113
TC0100006931.hg.1	PDPN	0,9109
TC1200009071.hg.1	PEBP1	0,9108
TC0400011538.hg.1	PAPSS1	0,9108
TC0400011180.hg.1	SCD5	0,9106
TC0200010443.hg.1	CFLAR	0,9082
TC1100011157.hg.1	PPP1R14B	0,9077
TC0200010801.hg.1	ROCD1	0,9077

Probe	Gene	FC (log2)
TC0600014283.hg.1	NUDT3	0,9075
TC2000009469.hg.1	ZFP64	0,9049
TC1200007832.hg.1	NABP2	0,9048
TC0500011260.hg.1	SERINC5	0,9046
TC1900010855.hg.1	CADM4	0,9033
TC1400010317.hg.1	CKB	0,9029
TC0600009262.hg.1	SLC35F1	0,9029
TC0400011202.hg.1	COQ2	0,9024
TC1100011010.hg.1	PRPF19	0,9023
TC0700011710.hg.1	SLC25A40	0,9022
TC0200010545.hg.1	NRP2	0,9011
TC1000009844.hg.1	SEPHS1	0,9010
TCOX00007267.hg.1	MAGED1	0,9008
TC0900008684.hg.1	GPR21; RABGAP1	0,9007
TC0600013528.hg.1	LATS1	0,9002
TC0100013182.hg.1	CAMK2N1	0,9001
TC0500008890.hg.1	PCDHGC3; PCDHGA12; I	0,9001
TC0700010760.hg.1	ELMO1	0,8992
TC0800010936.hg.1	PMP2	0,8991
TC0100015310.hg.1	SLC16A1	0,8988
TC0800008783.hg.1	SQLE	0,8988
TC0100018479.hg.1	NOTCH2NL	0,8986
TC0600009019.hg.1	SOBP	0,8984
TC0400009322.hg.1	GALNT7	0,8982
TC2100008477.hg.1	S100B	0,8982
TC1500007980.hg.1	CHRNA5	0,8974
TC2000009317.hg.1	SULF2	0,8973
TC0600009808.hg.1	PCMT1	0,8967
TC2200009142.hg.1	MLC1	0,8963
TC0900009489.hg.1	GLDC	0,8960
TC0100010806.hg.1	XPR1	0,8954
TC1100007285.hg.1	FIX1	0,8953
TC0900011035.hg.1	TMEM246	0,8950
TC1100011050.hg.1	FADS1; MIR1908	0,8941
TC0100010543.hg.1	ATP1B1	0,8939
TC0600010132.hg.1	wusmoyby	0,8934
TC0300013684.hg.1	TFRC	0,8929
TC1100012041.hg.1	lawmaw	0,8927
TC0200016767.hg.1	MREG	0,8927
TC1200007070.hg.1	ETNK1	0,8916
TC0700010604.hg.1	CPVL	0,8916
TC0100010609.hg.1	DNM3	0,8911
TC0800011252.hg.1	noyuya	0,8910
TC0700008360.hg.1	CASD1	0,8909
TC0100016021.hg.1	MRPL24	0,8906
TC0800007419.hg.1	GPAT4	0,8903
TC2100008462.hg.1	LSS	0,8902
TC2000008023.hg.1	SLCO4A1	0,8902
TC1500008245.hg.1	ABHD2	0,8901

Probe	Gene	FC (log2)
TC0700006715.hg.1	PHF14	0,8893
TC2000006601.hg.1	CDS2	0,8891
TC0300008412.hg.1	GAP43	0,8874
TC1500008038.hg.1	ARNT2; MIR5572	0,8872
TC1400009784.hg.1	VIPAS39	0,8868
TC0100008625.hg.1	PDE4B	0,8867
TC0700006906.hg.1	KLHL7	0,8855
TC0400009892.hg.1	CRMP1	0,8852
TC0700008351.hg.1	GNG11	0,8849
TC0100007334.hg.1	LYPLA2	0,8842
TC0800006566.hg.1	AGPAT5	0,8839
TC0200016586.hg.1	HSPE1-MOB4	0,8835
TC0100010301.hg.1	VANGL2	0,8832
TC0400008450.hg.1	ANK2	0,8829
TC0500011775.hg.1	SEMA6A	0,8823
TC0200016585.hg.1	MOB4	0,8821
TC0800010918.hg.1	ZNF704	0,8819
TC0400010991.hg.1	barskyby	0,8818
TC1400009524.hg.1	ZFP36L1	0,8814
TC0500011725.hg.1	MCC	0,8808
TC0700011603.hg.1	MAGI2	0,8807
TC0600010565.hg.1	TUBB2A	0,8807
TC1700011234.hg.1	CUEDC1	0,8800
TC1000008643.hg.1	SCD	0,8797
TC0500007607.hg.1	NLN	0,8792
TC0100015483.hg.1	NOTCH2	0,8789
TC0100018511.hg.1	C1orf61	0,8786
TCOX00011279.hg.1	TSPAN7	0,8785
TC0900007085.hg.1	TESK1; MIR4667	0,8778
TC1000009387.hg.1	PPP2R2D	0,8774
TC1300006601.hg.1	SPATA13; C1QTNF9	0,8774
TC0300007645.hg.1	PTPRG	0,8772
TC0500008086.hg.1	NR2F1	0,8769
TC0400012796.hg.1	PDGFRA	0,8769
TC0200007446.hg.1	PRKCE	0,8768
TC1700010209.hg.1	TLCD1	0,8765
TC0900009957.hg.1	HINT2	0,8765
TC0400011721.hg.1	MAD2L1	0,8758
TC1600011560.hg.1	MTSS1L	0,8758
TC0400010077.hg.1	RAB28	0,8755
TC1100007030.hg.1	NAV2	0,8755
TC2000007457.hg.1	PKIG	0,8755
TC0400010989.hg.1	ADAMTS3	0,8754
TC1700008995.hg.1	SEPT9	0,8753
TC1200008688.hg.1	tachaw	0,8753
TCOX00010506.hg.1	AMMECR1	0,8746
TC0400008972.hg.1	DCLK2	0,8745
TC0600010131.hg.1	derfleeby	0,8743
TC1500009355.hg.1	SHC4	0,8734

Probe	Gene	FC (log2)
TC1500010350.hg.1	NTRK3	0,8732
TC1300007104.hg.1	LRCH1	0,8725
TC0100010612.hg.1	gokerbo	0,8724
TC0800010275.hg.1	PLAT	0,8723
TC0500010043.hg.1	SEMA5A	0,8721
TC2000008721.hg.1	APMAP	0,8716
TC1400007610.hg.1	shuvy	0,8715
TC0500010628.hg.1	ANXA2R	0,8712
TC0300012073.hg.1	LSAMP	0,8707
TC0100016597.hg.1	STX6	0,8705
TC0500013384.hg.1	PPP2R2B	0,8700
TC0200008908.hg.1	noypubo	0,8697
TC0500007972.hg.1	VCAN	0,8692
TC0300009147.hg.1	RNF13	0,8692
TC0900010886.hg.1	PTCH1	0,8681
TC1100006487.hg.1	TALDO1	0,8675
TC0700008677.hg.1	LHFPL3	0,8673
TC0100013545.hg.1	SDC3	0,8673
TC2200009328.hg.1	HPS4	0,8671
TC1900006520.hg.1	ATP5D	0,8670
TC0100017500.hg.1	TMEM63A	0,8666
TC1400007554.hg.1	SLC39A9	0,8663
TC0800011646.hg.1	HAS2	0,8659
TC0200008464.hg.1	KCNIP3	0,8656
TC0300006465.hg.1	LRRN1	0,8653
TC2000009363.hg.1	slorsabu	0,8651
TC2000009809.hg.1	KCNQ2	0,8651
TC0100010556.hg.1	MRPS10P1	0,8651
TC0400008091.hg.1	SPP1	0,8650
TC0100017223.hg.1	LPGAT1	0,8646
TC0300008467.hg.1	ARHGAP31	0,8643
TC0200011503.hg.1	PXDN	0,8642
TC1100012270.hg.1	fawglybu	0,8636
TC0100013730.hg.1	GRIK3	0,8634
TC1600010557.hg.1	RP11-744D14.1	0,8630
TC0100014315.hg.1	derperbu	0,8629
TC0400009038.hg.1	KIAA0922	0,8625
TC0400011650.hg.1	ARSJ	0,8617
TC0100010188.hg.1	BCAN	0,8617
TC0900010375.hg.1	keeveyby	0,8616
TC1100008881.hg.1	ARHGAP42	0,8614
TC0400010519.hg.1	APBB2	0,8608
TC0200013638.hg.1	LONRF2	0,8607
TC1200012707.hg.1	ALDH2	0,8607
TC0800008126.hg.1	CA2	0,8596
TC1100012229.hg.1	KDELC2	0,8590
TC1400008486.hg.1	CRIP2	0,8590
TC1200008698.hg.1	speyglerby	0,8589
TC1400008229.hg.1	MEG3; MIR770	0,8585

Probe	Gene	FC (log2)
TC2000007760.hg.1	TSHZ2	0,8580
TC1500007677.hg.1	CORO2B	0,8577
TC1100012269.hg.1	ARHGAP20	0,8573
TC0400011182.hg.1	natore	0,8573
TC0500008356.hg.1	KCNN2	0,8571
TC1200011657.hg.1	ANKS1B	0,8564
TC2100007968.hg.1	C21orf62	0,8559
TC2000010022.hg.1	ZNFX1	0,8558
TC0600013604.hg.1	RGS17	0,8540
TC0900007429.hg.1	peetoybu	0,8540
TC1000007698.hg.1	CISD1	0,8533
TC0100017748.hg.1	SIPA1L2	0,8533
TC1100012509.hg.1	SLC37A4	0,8530
TC0400012990.hg.1	DDX60L	0,8529
TC0600008261.hg.1	LOC730101	0,8529
TC0200006788.hg.1	DDX1	0,8526
TC1300009796.hg.1	sheyserby	0,8524
TC1000012579.hg.1	SLIT1; ARHGAP19-SLIT1	0,8521
TC0600010707.hg.1	NRN1	0,8513
TC1700012347.hg.1	GPS2	0,8511
TC1100008409.hg.1	PPME1	0,8510
TC0100014988.hg.1	F3	0,8508
TC0600009831.hg.1	PPP1R14C	0,8507
TC0300009713.hg.1	EPHB3	0,8502
TC0800007114.hg.1	SCARA3	0,8502
TC0200014204.hg.1	HS6ST1	0,8492
TC1300008922.hg.1	EBPL	0,8491
TC1200009192.hg.1	BCL7A	0,8487
TC1200008848.hg.1	TCTN1	0,8485
TC1500008043.hg.1	ABHD17C	0,8485
TC1200010397.hg.1	CPNE8	0,8482
TC1400009766.hg.1	IRF2BPL	0,8479
TC1700008868.hg.1	TMEM104	0,8478
TC0X00009707.hg.1	MAGED4; MAGED4B; SI	0,8478
TC1200007061.hg.1	CMAS	0,8476
TC1200010185.hg.1	ITPR2	0,8475
TC1000009152.hg.1	HTRA1	0,8470
TC1300008253.hg.1	CRYL1	0,8468
TC0200012030.hg.1	HADHA	0,8467
TC0400009110.hg.1	GRIA2	0,8465
TC0800007995.hg.1	CRISPLD1	0,8460
TC0700009082.hg.1	SMO	0,8457
TC1000010725.hg.1	CCDC6	0,8457
TC1000010914.hg.1	PPA1	0,8456
TC0X00009486.hg.1	MAOB	0,8453
TC0100010795.hg.1	choylobu	0,8447
TC1400010729.hg.1	DTD2	0,8441
TC0600008697.hg.1	NT5E	0,8440
TC1700007170.hg.1	MAPK7	0,8434

Probe	Gene	FC (log2)
TC1100012906.hg.1	IGSF9B	0,8434
TC0300009353.hg.1	PPM1L	0,8425
TC0600012713.hg.1	PREP	0,8423
TC2100006951.hg.1	OLIG1	0,8418
TC0X00010933.hg.1	ARHGEF6	0,8417
TC1700007634.hg.1	ZNHIT3	0,8415
TC0700008897.hg.1	LSM8	0,8415
TC0200013261.hg.1	RETSAT	0,8414
TC1100012528.hg.1	THY1	0,8412
TC0100009364.hg.1	CSF1	0,8400
TC1200012385.hg.1	RP11-955H22.2	0,8389
TC1800009034.hg.1	FAM69C	0,8388
TC0700009778.hg.1	warsharby	0,8387
TC0900011192.hg.1	LPAR1	0,8385
TC1800009255.hg.1	mykey	0,8385
TC0100006932.hg.1	symeybu	0,8383
TC0400011750.hg.1	TRPC3	0,8382
TC0600012887.hg.1	leygloyby	0,8379
TC0100007845.hg.1	MANEAL	0,8370
TC2000008267.hg.1	RASSF2	0,8361
TC0100016155.hg.1	USF1	0,8357
TC2000008722.hg.1	ACSS1	0,8354
TC0700009782.hg.1	zasmawbu	0,8350
TC2000009180.hg.1	OSER1	0,8350
TC0700012444.hg.1	CADPS2	0,8345
TC0700010501.hg.1	DFNA5	0,8339
TC1700007520.hg.1	CDK5R1	0,8335
TC0X00007493.hg.1	AR	0,8334
TC0200015350.hg.1	RFTN2	0,8333
TC0900011565.hg.1	ANGPTL2	0,8331
TC2000009997.hg.1	DUSP15	0,8326
TC1200009981.hg.1	HEBP1	0,8321
TC0700010504.hg.1	OSBPL3	0,8316
TC0600006659.hg.1	BPHL	0,8314
TC1100012352.hg.1	TMPRSS5	0,8305
TC0100012899.hg.1	RNU5E-4P	0,8304
TC0100017066.hg.1	KLHDC8A	0,8297
TC1100007301.hg.1	PRR5L	0,8295
TC1300009012.hg.1	THSD1	0,8291
TC1500010672.hg.1	TARSL2	0,8291
TC1600008627.hg.1	HSBP1	0,8288
TC0300013877.hg.1	EPHB1	0,8288
TC0500013296.hg.1	C1QTNF3-AMACR	0,8286
TC0400010242.hg.1	PPARGC1A	0,8279
TC1200009157.hg.1	P2RX7	0,8276
TC0100017145.hg.1	PLXNA2	0,8275
TC0600014357.hg.1	LRP11	0,8273
TC0200016430.hg.1	MORN2	0,8269
TC0400012641.hg.1	PDLIM3	0,8263

Probe	Gene	FC (log2)
TC0200011898.hg.1	SDC1	0,8261
TC0500012388.hg.1	DPYSL3	0,8258
TC2000009579.hg.1	BMP7	0,8253
TC0700012637.hg.1	seykee	0,8253
TC0700008361.hg.1	peekar	0,8251
TC0100008978.hg.1	LRRC8B	0,8251
TC1600008005.hg.1	ADGRG1	0,8249
TC1700007429.hg.1	ANKRD13B	0,8249
TC0700009779.hg.1	cheyko	0,8245
TC0800009771.hg.1	ratimu	0,8241
TC1400009080.hg.1	vaslee	0,8236
TC0900009905.hg.1	CNTFR	0,8231
TC0400010580.hg.1	GNPDA2	0,8229
TC0100013561.hg.1	FABP3	0,8228
TC1900011844.hg.1	MFSD12	0,8228
TC0700006908.hg.1	AK3P3	0,8224
TC1100012520.hg.1	MCAM; MIR6756	0,8224
TC0200011219.hg.1	ACKR3	0,8223
TC1000007976.hg.1	CHST3	0,8222
TC0800010631.hg.1	TTPA	0,8221
TC0900008516.hg.1	C9orf91	0,8219
TC0400009330.hg.1	SAP30	0,8219
TC0900010200.hg.1	LOC102724238; LOC554	0,8217
TC0500009346.hg.1	WWC1	0,8207
TC0200015865.hg.1	SCG2	0,8206
TC0X00008125.hg.1	PAK3	0,8191
TC0100013998.hg.1	HECTD3	0,8176
TC0500012189.hg.1	LRRTM2	0,8171
TC1000012490.hg.1	PI4K2A	0,8169
TC0300011084.hg.1	CAMKV	0,8168
TC1700008677.hg.1	CACNG4	0,8167
TC0X00007274.hg.1	MAGED4B; MAGED4; SI	0,8160
TC0900007115.hg.1	GLIPR2	0,8159
TC0800012309.hg.1	C8orf46	0,8152
TC1800008474.hg.1	SLC39A6	0,8145
TC0100016121.hg.1	KCNJ10	0,8136
TC0900008804.hg.1	ZNF79	0,8135
TC1100013229.hg.1	FXYD6; FXYD6-FXYD2; F	0,8135
TC1400010756.hg.1	GPR135	0,8131
TC2000007973.hg.1	CDH4	0,8130
TC0X00006816.hg.1	PDK3	0,8128
TC1400007259.hg.1	PELI2	0,8126
TC1400007154.hg.1	GNG2	0,8124
TC0100010571.hg.1	PRRX1	0,8118
TC1800007753.hg.1	sloyflo	0,8117
TC1700008440.hg.1	PPM1E	0,8116
TC0800009793.hg.1	SLC18A1	0,8112
TC0200010726.hg.1	TMEM169	0,8107
TC1100011762.hg.1	blarmoy	0,8103

Probe	Gene	FC (log2)
TC0700007426.hg.1	ADCY1	0,8100
TC0700009770.hg.1	DPP6	0,8097
TC0700009089.hg.1	STRIP2	0,8097
TC1100012905.hg.1	MIR4697HG; MIR4697	0,8096
TC0100008243.hg.1	ELAVL4	0,8092
TC0200007047.hg.1	DPYSL5	0,8089
TC2000007772.hg.1	fawro	0,8088
TC1400010757.hg.1	L3HYPDH	0,8073
TC0900010975.hg.1	GABBR2	0,8068
TC2000009768.hg.1	SLCO4A1-AS1	0,8063
TC1400008816.hg.1	PRKD1	0,8063
TC1100006760.hg.1	PPFIBP2	0,8058
TC0300012074.hg.1	geebarbu	0,8057
TC0400008892.hg.1	HHIP	0,8046
TC0400012437.hg.1	SCRG1	0,8043
TC0100011665.hg.1	MARC1	0,8043
TC1000008733.hg.1	MFSD13A	0,8038
TC0300013793.hg.1	TMEM43	0,8034
TC0600009350.hg.1	RNF217	0,8027
TC0600006918.hg.1	GCNT2	0,8025
TC0200007028.hg.1	GAREM2	0,8023
TC1000010722.hg.1	SLC16A9	0,8023
TC0300013461.hg.1	MASP1	0,8018
TC0200007029.hg.1	titamo	0,8015
TC1000008645.hg.1	skawfoy	0,8009
TC1800007446.hg.1	SEC11C	0,8005
TC0900009776.hg.1	MOB3B	0,8001
TC1500008247.hg.1	noswy	0,7990
TC1100011285.hg.1	B4GAT1	0,7989
TC0X00011332.hg.1	PLXNB3	0,7985
TC0200016496.hg.1	CNNM3	0,7985
TC0600011507.hg.1	PSMB8	0,7979
TC0500006676.hg.1	MIR4458; MIR4458HG	0,7976
TC0700012761.hg.1	ZC3HAV1	0,7975
TC1200009307.hg.1	TMEM132B	0,7969
TC1400009175.hg.1	NID2	0,7966
TC0X00006791.hg.1	PTCHD1	0,7965
TC0800008324.hg.1	MATN2	0,7964
TC0100015286.hg.1	jyleybo	0,7964
TC0300008355.hg.1	BOC	0,7944
TC1100011789.hg.1	FAM181B	0,7944
TC1500009505.hg.1	PRTG	0,7944
TC0900007221.hg.1	LOC102724238; LOC554	0,7944
TC0300010282.hg.1	TIMP4	0,7942
TC0X00007539.hg.1	GDPD2	0,7936
TC1400009732.hg.1	C14orf1	0,7927
TC0900009574.hg.1	RP11-408A13.2	0,7923
TC1100006516.hg.1	BRSK2	0,7922
TC0100015288.hg.1	KCND3	0,7922

Probe	Gene	FC (log2)
TC0200015893.hg.1	DOCK10	0,7921
TC0500007368.hg.1	ITGA2	0,7919
TC1700012337.hg.1	P2RX5	0,7910
TC1400006551.hg.1	ARHGEF40	0,7896
TC0X00010032.hg.1	CITED1	0,7895
TC0X00011159.hg.1	HAUS7; TREX2	0,7895
TC0100018445.hg.1	DAB1	0,7895
TC1700007192.hg.1	bawverbu	0,7895
TC0300013831.hg.1	SEMA3B; MIR6872	0,7895
TC0200016774.hg.1	ABCB6	0,7894
TC1800007298.hg.1	LIPG	0,7893
TC1700011236.hg.1	showee	0,7888
TC0600009333.hg.1	SMPDL3A	0,7886
TC2200008844.hg.1	snaree	0,7884
TC0100017834.hg.1	GNG4	0,7883
TC0800008474.hg.1	BAALC	0,7882
TC1600008021.hg.1	MMP15	0,7878
TC1100009598.hg.1	kleemaby	0,7868
TC0900010135.hg.1	RP11-157L3.3	0,7865
TC2200009252.hg.1	SEC14L2	0,7863
TC0100012010.hg.1	SLC35F3	0,7862
TC1200007899.hg.1	MARCH9	0,7861
TC0700009781.hg.1	shako	0,7861
TC0300012066.hg.1	AC069063.1	0,7860
TC0400011429.hg.1	DDIT4L	0,7856
TC1200008920.hg.1	OAS3	0,7850
TC0200009994.hg.1	CDCA7	0,7849
TC0900009145.hg.1	OLFM1	0,7843
TC0200010919.hg.1	kymeebo	0,7836
TC0100017029.hg.1	PIK3C2B	0,7824
TC0300011200.hg.1	TKT	0,7822
TC1500008757.hg.1	ATP10A	0,7818
TC1500007545.hg.1	SNX1	0,7811
TC0100017833.hg.1	MTCO3P46	0,7802
TC0200015764.hg.1	CNPPD1	0,7801
TC0100016983.hg.1	CHI3L1	0,7797
TC1500007238.hg.1	TMOD2	0,7792
TC0400007799.hg.1	SLC4A4	0,7785
TC1100006911.hg.1	SPON1	0,7784
TC1200012855.hg.1	VSIG10	0,7783
TC0200011268.hg.1	RAMP1	0,7782
TC0400010775.hg.1	HOPX	0,7771
TC0400007803.hg.1	nokime	0,7765
TC0X00007713.hg.1	LPAR4	0,7760
TC0900007797.hg.1	sporlaw	0,7750
TC1100012350.hg.1	DRD2	0,7745
TC1300009781.hg.1	COL4A1	0,7742
TC1600010202.hg.1	NDUFA5P11	0,7732
TC0800011844.hg.1	ADCY8	0,7730

Probe	Gene	FC (log2)
TC0100011999.hg.1	NTPCR	0,7728
TC1800009252.hg.1	GALR1	0,7728
TC0100018461.hg.1	AKNAD1	0,7725
TC0100011527.hg.1	NENF	0,7721
TC0100014486.hg.1	LOC101927139; RP11-3	0,7713
TC0X00008032.hg.1	RPL18AP14	0,7686
TC0100014904.hg.1	HFM1	0,7677
TC0900011970.hg.1	QSOX2	0,7676
TC2200008251.hg.1	CTA-221G9.10	0,7675
TC1900011842.hg.1	DIRAS1	0,7653
TC0200013019.hg.1	MCEE	0,7648
TC0X00010670.hg.1	TMEM255A	0,7636
TC1100008969.hg.1	ELMOD1	0,7633
TC0100017388.hg.1	swoyzybo	0,7632
TC0100011211.hg.1	GPR37L1	0,7624
TC1200012111.hg.1	TAOK3	0,7623
TC0200010112.hg.1	RBM45	0,7615
TC0500013297.hg.1	AMACR	0,7593
TC0600008956.hg.1	swuglerby	0,7577
TC1400010616.hg.1	SLC38A6	0,7565
TC0700009389.hg.1	NDUFB10P2	0,7562
TC1200008650.hg.1	ASCL1	0,7559
TC1200011225.hg.1	BEST3	0,7555
TC0500009400.hg.1	KCNIP1	0,7539
TC0700006690.hg.1	NXPH1	0,7530
TC0100016344.hg.1	veybar	0,7525
TC1500007008.hg.1	TYRO3	0,7520
TC0100013692.hg.1	KIAA0319L	0,7516
TC0500012463.hg.1	CAMK2A	0,7509
TC0100016664.hg.1	COLGALT2	0,7508
TC2000008031.hg.1	COL9A3	0,7490
TC1100007037.hg.1	neemee	0,7489
TC0X00007661.hg.1	RP11-130N24.2	0,7488
TC1300010037.hg.1	KIAA0226L	0,7474
TC0800011105.hg.1	TRIQK	0,7462
TC1100012308.hg.1	CRYAB	0,7456
TC0700006562.hg.1	LFNG; MIR4648	0,7449
TC0900011423.hg.1	TTLL11	0,7446
TC2100008545.hg.1	NRIP1	0,7445
TC0400009376.hg.1	WDR17	0,7444
TC1500008511.hg.1	LRRC28	0,7444
TC1200007594.hg.1	ASIC1	0,7443
TC1500007922.hg.1	blyzoybu	0,7423
TC1700012338.hg.1	P2RX5-TAX1BP3	0,7410
TC0100006934.hg.1	klaleebo	0,7388
TC0700007105.hg.1	ADCYAP1R1	0,7386
TC0500010046.hg.1	ryskuby	0,7384
TC0600014328.hg.1	OSTM1	0,7370
TC1700008768.hg.1	KCNJ16	0,7364

Probe	Gene	FC (log2)
TC0900009774.hg.1	LINC00032	0,7347
TC1200008942.hg.1	PLBD2	0,7327
TC0200010854.hg.1	TMEM198	0,7311
TC1200008731.hg.1	RFX4	0,7306
TC0100016504.hg.1	rorjawbu	0,7303
TC1100012919.hg.1	THYN1	0,7287
TC1500007062.hg.1	CKMT1B; CKMT1A	0,7266
TC1700012376.hg.1	NOS2	0,7257
TC0400007868.hg.1	PARM1	0,7255
TC1000009104.hg.1	PLPP4	0,7251
TC0600013535.hg.1	klawjee	0,7240
TC0300014031.hg.1	CCDC80; LINC01279	0,7229
TC1500007067.hg.1	CKMT1A	0,7225
TC0500010049.hg.1	saskuby	0,7215
TC2200006945.hg.1	SEZ6L	0,7192
TC0500012464.hg.1	feeswubu	0,7190
TC2000009823.hg.1	STMN3	0,7174
TC1700012178.hg.1	WSCD1	0,7157
TC1700008175.hg.1	CALCOCO2	0,7112
TC1500010136.hg.1	ACSBG1	0,7112
TC0900011501.hg.1	NR6A1	0,7100
TC0400011486.hg.1	CXXC4	0,7092
TC0700013612.hg.1	NDUFA5	0,7078
TC1000012577.hg.1	LIPA	0,7064
TC0300010989.hg.1	CSPG5	0,7060
TC0300012358.hg.1	lerdabo	0,7046
TC1900011867.hg.1	TMEM205	0,7041
TC0X00010107.hg.1	ZDHHC15	0,7038
TC1400007120.hg.1	ATL1	0,7028
TC1200012708.hg.1	OAS1	0,7022
TC0300008558.hg.1	DTX3L	0,7017
TC1100012890.hg.1	blawmaby	0,7013
TC0200007155.hg.1	EHD3	0,7010
TC1100012698.hg.1	HEPACAM	0,7005
TC1100012893.hg.1	nermor	0,7001
TC0200008907.hg.1	skyder	0,6989
TC0100011245.hg.1	ADORA1	0,6975
TC0X00009685.hg.1	klabor	0,6929
TC0100012149.hg.1	FMN2; ADH5P3	0,6920
TC1200012561.hg.1	ZNF891	0,6887
TC0100011316.hg.1	NFASC	0,6862
TC0100008588.hg.1	EFCAB7; DLEU2L	0,6853
TC1500010601.hg.1	teypoy	0,6846
TC0600010802.hg.1	ELOVL2	0,6820
TC0400010243.hg.1	jarsmerby	0,6753
TC0800007526.hg.1	NDUFA5P12	0,6753
TC0100007862.hg.1	plopybu	0,6691
TC0300009301.hg.1	PTX3	0,6643
TC0700012036.hg.1	VGF	0,6614

Probe	Gene	FC (log2)
TC0300012191.hg.1	PARP9	0,6583
TC0200012933.hg.1	CNRIP1	0,6531
TC1400009770.hg.1	ZDHHC22	0,6499
TC1200011385.hg.1	LIN7A	0,6474
TC1200010132.hg.1	kerchaw	0,6425
TC1200006905.hg.1	FAM234B	0,6375
TC0600014110.hg.1	PSMB9	0,6287
TC1200008176.hg.1	LGR5	0,6234
TC1200008733.hg.1	najeeby	0,6212
TC1700011261.hg.1	SEPT4	0,6047
TC2000006676.hg.1	LAMP5	0,5913

B. List of coding genes differentially expressed in doxycycline-treated REST KD hGSCs *versus* untreated cells.

Probe	Gene	FC (log2)
TC0900009335.hg.1	fleewarby; rawswey	2,8431
TC1600008917.hg.1	neereyby	2,3190
TC0Y00007291.hg.1	warbo	2,0106
TC1500010723.hg.1	CHAC1	2,0058
TC0Y00007289.hg.1	rarsybo	1,9641
TC0100006905.hg.1	C1orf158	1,9422
TC0Y00007303.hg.1	sharbo	1,9298
TC0Y00007308.hg.1	blerbo	1,9298
TC0900009334.hg.1	moyswey	1,9217
TC1500008772.hg.1	GABRB3	1,9164
TC2000006444.hg.1	TRIB3	1,9004
TC0500013332.hg.1	DMGDH	1,8979
TC0300013275.hg.1	PEX5L	1,8841
TC0Y00007307.hg.1	korbo	1,8649
TC0Y00007301.hg.1	shabo	1,8649
TC0Y00007297.hg.1	snubar	1,8649
TC0Y00007296.hg.1	sorbo	1,8649
TC0Y00007288.hg.1	wubo	1,8649
TC0Y00007305.hg.1	merbo	1,8441
TC0Y00007292.hg.1	tybo	1,8409
TC0Y00007298.hg.1	skybor	1,8338
TC0Y00007290.hg.1	vubo	1,8282
TC0Y00007285.hg.1	zeybu	1,8267
TC0300011485.hg.1	FOXP1	1,8053
TC0Y00007309.hg.1	blabo	1,8045
TC0Y00007304.hg.1	pabo	1,7826
TC0Y00007302.hg.1	pleybo	1,7826
TC0Y00007300.hg.1	shorbo	1,7826
TC0Y00007295.hg.1	sybo	1,7826
TC0800008263.hg.1	ESRP1	1,7802
TC0900010006.hg.1	veesarby	1,7786
TC0Y00007299.hg.1	skeybo	1,7741
TC0Y00007287.hg.1	zobo	1,7741
TC0Y00007294.hg.1	tobo	1,7676
TC1700010604.hg.1	NR1D1	1,7328
TC0400009566.hg.1	tusweebu	1,7081
TC0200014819.hg.1	SCN9A	1,6977
TC0400011920.hg.1	SLC7A11	1,6945
TC1200007881.hg.1	INHBE	1,6691
TC0500009344.hg.1	pawsteeby	1,6612
TC1400008034.hg.1	UNC79	1,6548
TC0100008648.hg.1	IL23R	1,6472
TC0X00010583.hg.1	porgar	1,6422
TC1200008726.hg.1	TCP11L2	1,6406
TC1500010042.hg.1	CYP1A1	1,6216
TC0100016678.hg.1	FAM129A	1,6192
TC0900007380.hg.1	jorskobu	1,6101
TC1900011057.hg.1	PLA2G4C	1,6011

Probe	Gene	FC (log2)
TC0100015864.hg.1	S100A6	1,5996
TC2000006627.hg.1	CHGB	1,5979
TC1400006697.hg.1	DHRS2	1,5940
TC0100009727.hg.1	sparma	1,5919
TC1200007871.hg.1	smaplerby	1,5879
TC1100007826.hg.1	BEST1	1,5866
TC0500011513.hg.1	PCSK1	1,5796
TC0100008243.hg.1	ELAVL4	1,5763
TC0200012933.hg.1	CNRIP1	1,5712
TC0200009539.hg.1	ARHGAP15	1,5575
TC1500007062.hg.1	CKMT1B; CKMT1A	1,5560
TC0Y00006474.hg.1	CD99P1; NCRNA00103	1,5541
TC0800007992.hg.1	MIR2052	1,5477
TC1300008644.hg.1	POSTN	1,5393
TC0100010387.hg.1	DDR2	1,5373
TC0900010221.hg.1	zarskubu	1,5267
TC0900006655.hg.1	LURAP1L	1,5240
TC0X00010473.hg.1	TSC22D3	1,5128
TC1700010997.hg.1	HOXB9	1,5069
TC0X00006476.hg.1	CD99P1	1,5029
TC1900011882.hg.1	ZNF442	1,4980
TC1700007993.hg.1	RUNDC3A	1,4940
TC0300013879.hg.1	IL2RB	1,4935
TC1900007045.hg.1	ZNF441	1,4877
TC1200010968.hg.1	DDIT3	1,4869
TC2000006688.hg.1	SNAP25	1,4854
TC0800008478.hg.1	FZD6	1,4807
TC1400006715.hg.1	PCK2	1,4784
TC0500011648.hg.1	EFNA5	1,4745
TC0200014775.hg.1	KCNH7	1,4647
TC0100009621.hg.1	PHGDH	1,4640
TC0500012138.hg.1	SPOCK1	1,4621
TC0100009837.hg.1	PDE4DIP	1,4545
TC0200016464.hg.1	APLF	1,4527
TC1700007585.hg.1	SLFN5	1,4517
TC1000008535.hg.1	ZNF518A	1,4485
TC1900007001.hg.1	C19orf38	1,4482
TC0400009705.hg.1	peysperby	1,4459
TC0400010242.hg.1	PPARGC1A	1,4458
TC0500009488.hg.1	CREBRF	1,4429
TC0800009404.hg.1	geegeyby	1,4411
TC1900010334.hg.1	TSHZ3	1,4405
TC1400009329.hg.1	RTN1	1,4380
TC1100010440.hg.1	MPPED2	1,4373
TC0500008966.hg.1	gluja	1,4342
TC1500008777.hg.1	skoter	1,4321
TC0900011120.hg.1	KLF4	1,4317
TC0100015684.hg.1	fleygee	1,4312

Probe	Gene	FC (log2)
TC1200011770.hg.1	ALDH1L2	1,4311
TC0100016822.hg.1	KCNT2	1,4268
TC1000007990.hg.1	DDIT4	1,4223
TC0400008106.hg.1	HERC5	1,4190
TC1900011770.hg.1	C5AR1	1,4190
TC0200015128.hg.1	PDE1A	1,4149
TC0800007372.hg.1	ADAM5	1,4115
TC1700006622.hg.1	kergler	1,4092
TC0100007552.hg.1	SESN2	1,4077
TC0700012798.hg.1	KDM7A	1,4040
TC1900008362.hg.1	IGFL1P1	1,4038
TC0800011334.hg.1	KLF10	1,4037
TC0100014769.hg.1	MCOLN3	1,4030
TC1500010725.hg.1	CAPN3	1,4026
TC0500007000.hg.1	LINC01021	1,3990
TC0700012444.hg.1	CADPS2	1,3981
TC0500009103.hg.1	IRGM	1,3924
TC0800010330.hg.1	ASNSP1	1,3899
TC1200009565.hg.1	dablar	1,3828
TC0900012240.hg.1	AQP7P2	1,3820
TC0100017844.hg.1	NID1	1,3806
TC0100012793.hg.1	wormabo	1,3794
TC1500007067.hg.1	CKMT1A	1,3774
TC1100012230.hg.1	EXPH5	1,3763
TC1700007864.hg.1	TTC25	1,3747
TC1700011558.hg.1	SLC16A6	1,3720
TC0600012372.hg.1	LCA5	1,3682
TC2200009303.hg.1	MAPK8IP2	1,3650
TC2000008250.hg.1	swoyror	1,3640
TC1700012353.hg.1	PER1; MIR6883	1,3599
TC0800007269.hg.1	UNC5D	1,3587
TC1200010182.hg.1	BHLHE41	1,3562
TC0100006865.hg.1	AGTRAP	1,3561
TC0100017849.hg.1	ERO1B	1,3521
TC0X00010837.hg.1	MBNL3	1,3511
TC1100009682.hg.1	stertobo	1,3506
TC0100008697.hg.1	CTH	1,3503
TC0100011533.hg.1	ATF3	1,3464
TC0800007335.hg.1	LETM2	1,3451
TC1100011754.hg.1	TENM4	1,3421
TC1200007010.hg.1	PLEKHA5	1,3418
TC1100010893.hg.1	SLC43A1	1,3413
TC0100006864.hg.1	DRAXIN	1,3356
TC0200015307.hg.1	DNAH7	1,3352
TC2200008370.hg.1	XBP1	1,3326
TC0600011234.hg.1	HIST1H4L	1,3297
TC1200011567.hg.1	TMCC3; MIR7844	1,3292
TC1300007491.hg.1	KLF5	1,3290

Probe	Gene	FC (log2)
TC1900008489.hg.1	FGF21	1,3261
TC0100006934.hg.1	klaleebo	1,3260
TC0200016224.hg.1	PER2	1,3247
TC0500008785.hg.1	EGR1	1,3242
TC1200008949.hg.1	SDSL	1,3214
TC0800011861.hg.1	LRRC6	1,3205
TC0200016720.hg.1	RNF149	1,3194
TC0X00010369.hg.1	ARMCX2	1,3194
TC0100015286.hg.1	jylevbo	1,3189
TC1700010560.hg.1	PLXDC1	1,3186
TC0100018417.hg.1	ALDH4A1	1,3154
TC0900010608.hg.1	suploybu	1,3144
TC0400008345.hg.1	SGMS2	1,3138
TC0500007337.hg.1	PARP8	1,3129
TC0300007454.hg.1	PARP3	1,3101
TC0300006985.hg.1	CCR4	1,3085
TC0200015645.hg.1	ABCA12	1,3074
TC0700013424.hg.1	GS1-259H13.2; TCONS_l2_	1,3057
TC0X00008235.hg.1	LONRF3	1,3056
TC1000007361.hg.1	RP11-96F8.1	1,3055
TC2000007448.hg.1	GDAP1L1	1,3053
TC0100012792.hg.1	plerlarbu	1,3026
TC0800011064.hg.1	CALB1	1,3026
TC0300013734.hg.1	storkawbo	1,3015
TC0200010236.hg.1	GULP1	1,3014
TC0100013000.hg.1	CASP9	1,3002
TC0200016074.hg.1	NGEF	1,2996
TC0100006881.hg.1	TNFRSF1B; MIR4632; MIR	1,2969
TC0100010085.hg.1	CHRNB2	1,2963
TC1900009729.hg.1	ZNF563	1,2953
TC1100012350.hg.1	DRD2	1,2947
TC1900011084.hg.1	DBP	1,2936
TC1900009984.hg.1	UNC13A	1,2925
TC0700013442.hg.1	LSMEM1	1,2924
TC1900007043.hg.1	ZNF833P	1,2916
TC1300008492.hg.1	kleyspar	1,2908
TC0100006862.hg.1	FBXO6	1,2890
TC0100015685.hg.1	LOC653513	1,2879
TC1100010946.hg.1	LPXN	1,2878
TC2000007213.hg.1	MMP24	1,2865
TC0600009821.hg.1	ULBP1	1,2852
TC0100008517.hg.1	NFIA	1,2841
TC0100013018.hg.1	ZBTB17	1,2807
TC0400011279.hg.1	ABCG2	1,2805
TC0700008182.hg.1	kleysmeebu	1,2798
TC0500010169.hg.1	ANKH	1,2794
TC1700012376.hg.1	NOS2	1,2792
TC0400012769.hg.1	BST1	1,2786

Probe	Gene	FC (log2)
TC1100007884.hg.1	SLC3A2	1,2786
TC1000011585.hg.1	GOT1	1,2777
TC0100006861.hg.1	FBXO44	1,2765
TC1100006899.hg.1	ARNTL	1,2764
TC0600013431.hg.1	PLAGL1; HYMAI	1,2763
TC0700013527.hg.1	SKAP2	1,2749
TC0100017851.hg.1	korlawbo	1,2743
TC1900007127.hg.1	IER2	1,2732
TC0700011876.hg.1	ASNS	1,2728
TC1900007061.hg.1	ZNF844	1,2718
TC0100008620.hg.1	DNAJC6	1,2717
TC0100010526.hg.1	TBX19	1,2686
TC1100011761.hg.1	zorgleebu	1,2652
TC0600008622.hg.1	SH3BGRL2	1,2650
TC0700008918.hg.1	KCND2	1,2625
TC1100009824.hg.1	CARS	1,2621
TC0100018280.hg.1	FAM231D; LINC00869	1,2621
TC0500011448.hg.1	ARRDC3	1,2621
TC0800008848.hg.1	PVT1; MIR1204	1,2620
TC0500012177.hg.1	fawstoyby	1,2598
TC0100006977.hg.1	TMEM51	1,2587
TC0100013629.hg.1	YARS	1,2584
TC0100013075.hg.1	ferpabu	1,2582
TC2000009997.hg.1	DUSP15	1,2566
TC1000009725.hg.1	SFMBT2	1,2564
TC1400010715.hg.1	AJUBA	1,2543
TC1500007237.hg.1	SCG3	1,2535
TC0100006859.hg.1	gorreybo	1,2520
TC0900007669.hg.1	speeplorbu	1,2506
TC1500010244.hg.1	AP3B2	1,2488
TC1200011474.hg.1	ATP2B1	1,2459
TC0100013038.hg.1	FBXO42	1,2456
TC0100006991.hg.1	RSC1A1; DDI2	1,2451
TC1700010975.hg.1	smawrer	1,2448
TC0900008497.hg.1	ZNF618	1,2448
TC0600014350.hg.1	TXLNB	1,2409
TC1500010869.hg.1	CCPG1; MIR628	1,2408
TC0200011837.hg.1	FAM49A	1,2404
TC1600011186.hg.1	SLC7A5	1,2402
TC1100008149.hg.1	wostuby	1,2396
TC0400010785.hg.1	IGFBP7	1,2388
TC0X00010326.hg.1	PCDH19	1,2362
TC0900010219.hg.1	AQP7P1	1,2361
TC0100015805.hg.1	CELF3	1,2353
TC0800008299.hg.1	SDC2	1,2346
TC0400007928.hg.1	FRAS1	1,2344
TC0100017828.hg.1	B3GALNT2	1,2343
TC0100009344.hg.1	SARS	1,2342

Probe	Gene	FC (log2)
TC1600007982.hg.1	HERPUD1	1,2334
TC0400008892.hg.1	HHIP	1,2328
TC0100012901.hg.1	KIAA2013	1,2280
TC1500009641.hg.1	RORA	1,2279
TC1200008918.hg.1	RPH3A	1,2269
TC1200011657.hg.1	ANKS1B	1,2263
TC0400007489.hg.1	RP11-241F15.10	1,2258
TC1600007723.hg.1	GPT2	1,2247
TC1100012775.hg.1	ETS1	1,2236
TC0100014502.hg.1	WDR78	1,2234
TC1700010811.hg.1	HDAC5	1,2233
TC0500012870.hg.1	STC2	1,2224
TC0100018475.hg.1	LINC01138	1,2199
TC0300011084.hg.1	CAMKV	1,2185
TC0700007477.hg.1	UPP1	1,2170
TC0100012099.hg.1	ACTN2	1,2149
TC0100007035.hg.1	lolerbo	1,2146
TC1900011673.hg.1	CCDC130	1,2132
TC1900009137.hg.1	CBARP	1,2128
TC1800007014.hg.1	DSG2	1,2093
TC1700007677.hg.1	DUSP14	1,2081
TC0900010769.hg.1	NFIL3	1,2079
TC1900011880.hg.1	ZNF44	1,2055
TC0700013428.hg.1	PILRB; STAG3L5P; PVRIG2	1,2046
TC0100017957.hg.1	PLD5	1,2039
TC0100013072.hg.1	ATP13A2	1,2037
TC0100006884.hg.1	VPS13D	1,2034
TC1400010261.hg.1	MOK	1,2021
TC0600013361.hg.1	CITED2	1,2018
TC0200007821.hg.1	SLC1A4	1,1975
TC0100013049.hg.1	NBPF1	1,1974
TC1100008904.hg.1	YAP1	1,1956
TC1700008082.hg.1	MAPT	1,1954
TC0700013429.hg.1	PILRA	1,1952
TC0100017836.hg.1	LYST	1,1938
TC0900010975.hg.1	GABBR2	1,1930
TC0600009364.hg.1	NCOA7	1,1929
TC1100007429.hg.1	MAPK8IP1	1,1927
TC0100012849.hg.1	CASZ1	1,1926
TC0100007038.hg.1	NECAP2	1,1920
TC0700013050.hg.1	KCNH2	1,1919
TC0100006875.hg.1	MFN2	1,1906
TC0400012796.hg.1	PDGFRA	1,1905
TC0100007034.hg.1	sneebaw	1,1903
TC1600009952.hg.1	YPEL3	1,1895
TC0100018166.hg.1	CLCN6	1,1888
TC1900008496.hg.1	PPP1R15A	1,1874
TC1500007814.hg.1	NEO1	1,1866

Probe	Gene	FC (log2)
TC0600009783.hg.1	UST	1,1866
TC0600011136.hg.1	HIST1H2BG	1,1862
TC2000006571.hg.1	SMOX	1,1843
TC1900009511.hg.1	TIMM44	1,1840
TC0100011316.hg.1	NFASC	1,1837
TC0100012895.hg.1	MTHFR	1,1827
TC0100013131.hg.1	AKR7A2	1,1802
TC0100013758.hg.1	INPP5B	1,1777
TC0700008181.hg.1	GNAI1	1,1729
TC0700012971.hg.1	ZNF425	1,1729
TC0100007033.hg.1	zawrobu	1,1727
TC0400010663.hg.1	RP11-241F15.1	1,1726
TC1600010752.hg.1	AARS	1,1726
TC0X00007310.hg.1	TSPYL2	1,1715
TC1600009088.hg.1	PKD1; MIR6511B2; MIR65	1,1710
TC0100017793.hg.1	IRF2BP2	1,1706
TC0100006994.hg.1	PLEKHM2	1,1692
TC0100012872.hg.1	MTOR	1,1683
TC1200006787.hg.1	GABARAPL1	1,1668
TC0100009654.hg.1	glozerbo	1,1636
TC0400010656.hg.1	RP11-1281K21.1	1,1636
TC0500009521.hg.1	CPEB4	1,1635
TC0800007316.hg.1	EIF4EBP1	1,1628
TC0100007160.hg.1	MRTO4	1,1622
TC0500009706.hg.1	SQSTM1	1,1617
TC0200010219.hg.1	FAM171B	1,1595
TC1200007866.hg.1	SHMT2	1,1592
TC1200012238.hg.1	ZCCHC8	1,1587
TC0900007418.hg.1	LOC100133920	1,1582
TC1400010195.hg.1	WARS	1,1573
TC1500008470.hg.1	ARRDC4	1,1566
TC2100007543.hg.1	bP-21264C1.1	1,1562
TC1500008328.hg.1	BLM	1,1558
TC1900009076.hg.1	PLPP2	1,1547
TC0100006937.hg.1	PRDM2	1,1524
TC0100013073.hg.1	SDHB	1,1501
TC1600011488.hg.1	MIR6511A3; MIR6511A4	1,1482
TC0100006852.hg.1	UBIAD1	1,1481
TC1900011004.hg.1	SLC1A5	1,1479
TC1000011904.hg.1	ABLIM1	1,1476
TC0700008494.hg.1	BUD31	1,1469
TC0100007162.hg.1	PQLC2	1,1467
TC0700008747.hg.1	HBP1	1,1461
TC0100013713.hg.1	STK40	1,1461
TC0300012449.hg.1	CPNE4	1,1432
TC0100012870.hg.1	EXOSC10	1,1418
TC0100012889.hg.1	MAD2L2	1,1415
TC1100011611.hg.1	PGM2L1	1,1415

Probe	Gene	FC (log2)
TC0100009900.hg.1	CIART	1,1386
TC1900007777.hg.1	CEBPG	1,1346
TC0800009868.hg.1	TNFRSF10B	1,1330
TC0900010395.hg.1	HSPB1P1	1,1324
TC0500008941.hg.1	ARHGAP26	1,1317
TC0100013481.hg.1	SNORA44; SNORA61; SNC	1,1307
TC1200009239.hg.1	KMT5A	1,1297
TC0100013087.hg.1	RCC2	1,1295
TC0100007006.hg.1	SPEN	1,1262
TC0100013126.hg.1	EMC1	1,1255
TC0100018565.hg.1	AGT	1,1250
TC0100013123.hg.1	UBR4	1,1229
TC0100006989.hg.1	DNAJC16	1,1223
TC0200008071.hg.1	MTHFD2	1,1211
TC0900007667.hg.1	PSAT1	1,1196
TC0700009734.hg.1	RP11-208G20.2	1,1183
TC0700007795.hg.1	CCT6P3	1,1178
TC1200012650.hg.1	MARS; MIR6758	1,1177
TC0300006847.hg.1	NR1D2	1,1165
TC0100018568.hg.1	ARID4B	1,1151
TC0800011312.hg.1	RRM2B	1,1129
TC1300008487.hg.1	SLC7A1	1,1124
TC1100010688.hg.1	PHF21A	1,1100
TC0900010789.hg.1	IARS	1,1078
TC1600009524.hg.1	NPIPA5	1,1052
TC0700007098.hg.1	GARS	1,1043
TC0600007285.hg.1	HIST1H2AE	1,1002
TC0100012869.hg.1	SRM	1,1002
TC0100018507.hg.1	ARHGEF2	1,1002
TC0300012918.hg.1	CCNL1	1,0973
TC1200008002.hg.1	XPOT	1,0902
TC1200010516.hg.1	SLC38A1	1,0775
TC1800006650.hg.1	RAB31	0,8892
TC0700009145.hg.1	MEST	0,8778
TC0600011960.hg.1	TNFRSF21	0,8306
TC0600013186.hg.1	CTGF	0,8168
TC0300011597.hg.1	ZNF717	0,7994
TC0500009141.hg.1	GRIA1	0,7905
TC1700006946.hg.1	HS3ST3B1	0,7892
TC0X00007222.hg.1	PLP2	0,7891
TC1000010070.hg.1	PRTFDC1	0,7692
TC0700008809.hg.1	LRRN3	0,7548
TC0600012434.hg.1	ME1	0,7387
TC0100018299.hg.1	SLC27A3	0,7310
TC1900010117.hg.1	feytawbu	0,7299
TC1100009078.hg.1	TTC12	0,7296
TC0900009581.hg.1	FREM1	0,7261
TC0700011658.hg.1	SEMA3E	0,7253

Probe	Gene	FC (log2)
TC0400006439.hg.1	blarfley	0,7195
TC0100011621.hg.1	TGFB2; TGFB2-OT1	0,7148
TC0800011620.hg.1	ENPP2	0,7040
TC0X00008017.hg.1	PLP1	0,7031
TC0400006437.hg.1	ZNF718	0,6978
TC0X00008316.hg.1	GRIA3	0,6971
TC1200012775.hg.1	ST8SIA1	0,6970
TC0200010658.hg.1	CPS1	0,6877
TC0400006718.hg.1	SORCS2	0,6874
TC0X00011248.hg.1	TMLHE	0,6851
TC0900010056.hg.1	ANKRD18A; FAM95C	0,6847
TC0900009912.hg.1	SIGMAR1	0,6823
TC0500008632.hg.1	SLC22A5	0,6704
TC0X00008871.hg.1	RP13-228J13.5	0,6696
TC1100010792.hg.1	FOLH1	0,6676
TC1500009709.hg.1	CA12	0,6673
TC1200008224.hg.1	GLIPR1	0,6669
TC0X00011247.hg.1	moho	0,6603
TC0400008725.hg.1	PCDH10	0,6600
TC0400012903.hg.1	PROM1	0,6485
TC1700009888.hg.1	CENPV	0,6432
TC2100007032.hg.1	CBR1	0,6042

C. List of coding genes differentially expressed in doxycycline-treated REST KD hNSCs *versus* untreated cells

Probe	Gene	FC (log2)
TC1200008280.hg.1	vawjyby	1,7320
TC0900009326.hg.1	sherwarby	1,5998
TC0400007609.hg.1	REST	1,5862
TC0X00007222.hg.1	PLP2	1,5556
TC0100011463.hg.1	SYT14	1,4935
TC0400011744.hg.1	ANXA5	0,9010
TC1000010725.hg.1	CCDC6	0,8935
TC0800007051.hg.1	NEFM	0,8926
TC1100012262.hg.1	RDX	0,8925
TC0300013684.hg.1	TFRC	0,8864
TC1100012303.hg.1	PPP2R1B	0,8847
TC0800006566.hg.1	AGPAT5	0,8844
TC0200007047.hg.1	DPYSL5	0,8836
TC0100006931.hg.1	PDPN	0,8823
TC2000009809.hg.1	KCNQ2	0,8819
TC0600009262.hg.1	SLC35F1	0,8819
TC0200010236.hg.1	GULP1	0,8819
TC1400009732.hg.1	C14orf1	0,8793
TC0900100052.hg.1	IGFBPL1	0,8775
TC0100007334.hg.1	LYPLA2	0,8758
TC0400010465.hg.1	UGDH	0,8723
TC0100011721.hg.1	CAPN2	0,8719
TC0800007316.hg.1	EIF4EBP1	0,8702
TC1800008474.hg.1	SLC39A6	0,8686
TC1200007832.hg.1	NABP2	0,8644
TC0600009808.hg.1	PCMT1	0,8618
TC1600010557.hg.1	RP11-744D14.1	0,8609
TC1500008360.hg.1	SLCO3A1	0,8589
TC0100009364.hg.1	CSF1	0,8587
TC0300011200.hg.1	TKT	0,8578
TC2000008721.hg.1	APMAP	0,8552
TC0200009065.hg.1	DBI	0,8523
TC1800007298.hg.1	LIPG	0,8506
TC1500007545.hg.1	SNX1	0,8498
TC0300011247.hg.1	WNT5A	0,8482
TC0900009905.hg.1	CNTFR	0,8471
TC0200006788.hg.1	DDX1	0,8470
TC0500009161.hg.1	SAP30L	0,8452
TC0600012713.hg.1	PREP	0,8442
TC0400009892.hg.1	CRMP1	0,8438
TC1700009850.hg.1	PMP22	0,8421
TC0200013616.hg.1	AFF3	0,8420
TC0700010989.hg.1	TNS3	0,8416
TC0700008351.hg.1	GNG11	0,8409
TC0200012030.hg.1	HADHA	0,8408
TC1100012229.hg.1	KDELC2	0,8400
TC0500009141.hg.1	GRIA1	0,8391

Probe	Gene	FC (log2)
TC0100017834.hg.1	GNG4	0,8366
TC0300014031.hg.1	CCDC80; LINC01279	0,8365
TC0600009263.hg.1	beevybo	0,8364
TC1400007154.hg.1	GNG2	0,8359
TC1600010809.hg.1	TXNL4B	0,8357
TC1400010729.hg.1	DTD2	0,8349
TC0500010043.hg.1	SEMA5A	0,8348
TC0200006795.hg.1	MYCN	0,8341
TC1100012509.hg.1	SLC37A4	0,8337
TC1000012577.hg.1	LIPA	0,8322
TC0900008949.hg.1	NCS1	0,8313
TC1700012347.hg.1	GPS2	0,8305
TC0400009330.hg.1	SAP30	0,8300
TC0100009241.hg.1	S1PR1	0,8295
TC0600009332.hg.1	FABP7	0,8280
TC1000008478.hg.1	CYP26A1	0,8245
TC0600012544.hg.1	RRAGD	0,8239
TC0500006665.hg.1	ADCY2	0,8238
TC0700012233.hg.1	sehura	0,8206
TC0300012082.hg.1	plobabo	0,8203
TC0900009489.hg.1	GLDC	0,8203
TC0300013793.hg.1	TMEM43	0,8201
TC1900006520.hg.1	ATP5D	0,8197
TC0900011603.hg.1	ENG	0,8182
TC0100013561.hg.1	FABP3	0,8181
TC0200011886.hg.1	WDR35	0,8176
TC0700010504.hg.1	OSBPL3	0,8160
TC0200015764.hg.1	CNPPD1	0,8160
TC0700009606.hg.1	ZNF282	0,8156
TC1200007037.hg.1	PDE3A	0,8132
TC0900008314.hg.1	FSD1L	0,8128
TC1500008511.hg.1	LRRC28	0,8078
TC1300006979.hg.1	RGCC	0,8077
TC2000006791.hg.1	PCSK2	0,8069
TC0200009994.hg.1	CDCA7	0,8065
TC0800011713.hg.1	MTSS1	0,8055
TC1200009981.hg.1	HEBP1	0,8053
TC0600014328.hg.1	OSTM1	0,8047
TC1700008440.hg.1	PPM1E	0,8047
TC0300010989.hg.1	CSPG5	0,7990
TC0100013692.hg.1	KIAA0319L	0,7983
TC1200008275.hg.1	SYT1	0,7979
TC1700008677.hg.1	CACNG4	0,7956
TC1000008733.hg.1	MFSD13A	0,7955
TC0100014904.hg.1	HFM1	0,7938
TC0800011611.hg.1	TNFRSF11B	0,7935
TC0200011219.hg.1	ACKR3	0,7930

Probe	Gene	FC (log2)
TC1300007104.hg.1	LRCH1	0,7889
TC1000010722.hg.1	SLC16A9	0,7872
TC0900011423.hg.1	TTLL11	0,7867
TC0700013612.hg.1	NDUFA5	0,7865
TC1100011285.hg.1	B4GAT1	0,7861
TC0200007029.hg.1	titamo	0,7856
TC1800007446.hg.1	SEC11C	0,7838
TC1000009857.hg.1	snareeby	0,7837
TC0800009905.hg.1	NEFL	0,7825
TC0100011999.hg.1	NTPCR	0,7823
TC0500007494.hg.1	RAB3C	0,7779
TC1200007630.hg.1	LETMD1	0,7779
TC1700012229.hg.1	RHBDL3	0,7774
TC1500009830.hg.1	LCTL	0,7764
TC1100012919.hg.1	THYN1	0,7762
TC0700013027.hg.1	RARRES2	0,7759
TC0100016664.hg.1	COLGALT2	0,7741
TC0100014960.hg.1	temira	0,7733
TC0500009346.hg.1	WWC1	0,7720
TC0800008474.hg.1	BAALC	0,7718
TC1200008942.hg.1	PLBD2	0,7706
TC0600013535.hg.1	klawjee	0,7636
TC0X00006816.hg.1	PDK3	0,7620
TC0500010651.hg.1	FGF10	0,7607
TC0200007155.hg.1	EHD3	0,7580
TC0X00011159.hg.1	HAUS7; TREX2	0,7575
TC1700008175.hg.1	CALCOCO2	0,7560
TC0200010112.hg.1	RBM45	0,7556
TC0100012149.hg.1	FMN2; ADH5P3	0,7538
TC0300013932.hg.1	SRGAP3	0,7526
TC0400012474.hg.1	ferborbo	0,7498
TC0800007136.hg.1	skaworby	0,7493
TC0100013999.hg.1	ZSWIM5	0,7457
TC0600010802.hg.1	ELOVL2	0,7430
TC1900007766.hg.1	LRP3	0,7337
TC0700012761.hg.1	ZC3HAV1	0,7291
TC0100014326.hg.1	slormubo	0,7271
TC0100018445.hg.1	DAB1	0,7259
TC0900007752.hg.1	NTRK2	0,7230
TC1100008969.hg.1	ELMOD1	0,7167
TC1500007067.hg.1	CKMT1A	0,7133
TC0700008240.hg.1	GRM3	0,7124
TC0100009442.hg.1	WNT2B	0,7075
TC2000009823.hg.1	STMN3	0,7055
TC0400009376.hg.1	WDR17	0,7008
TC1200006905.hg.1	FAM234B	0,6995
TC1900011867.hg.1	TMEM205	0,6937

Probe	Gene	FC (log2)
TC0600010804.hg.1	terroyby	0,6916
TC0900008694.hg.1	CRB2	0,6586
TC1400008263.hg.1	SNORD113	0,6431
TC0300012087.hg.1	zoybarbu	0,6347
TC1200011385.hg.1	LIN7A	0,6292
TC1400009151.hg.1	TRIM9	0,6223
TC0100009897.hg.1	CA14	0,6159
TC0200012933.hg.1	CNRIP1	0,6111
TC0500008869.hg.1	VTRNA1-3	0,6045

D. List of coding genes differentially expressed in doxycycline-treated REST KD hNSCs *versus* untreated cells.

Probe	Gene	FC (log2)
TC1900009984.hg.1	UNC13A	1,5571
TC1300009376.hg.1	SLITRK1	1,4081
TC0900008953.hg.1	ASS1	1,3294
TC0200006627.hg.1	ID2	1,2944
TC0100016018.hg.1	CRABP2	1,2804
TC1000008054.hg.1	PLAU	1,2779
TC0500008785.hg.1	EGR1	1,2763
TC0400011359.hg.1	UNC5C	1,2382
TCOX00008785.hg.1	BGN	1,1872

List of Abbreviations

AGT	Angiotensinogen
AML	Acute myeloid leukemia
ANKS1B	Ankyrin repeat and sterile alpha motif domain containing 1B
ASCL1	Ascheate-scute family bHLH transcription factor 1
ASCs	Adult Stem Cells
ASS1	Argininosuccinate synthase 1
ATF4/CREB2	Activating transcription factor 4
ATRX	ATRX, chromatin remodeler
BDNF	Brain-Derived Neurotrophic factor
bFGF	Basic fibroblast-growth factor
BMP	Bone morphogenetic protein
bps	Base pairs
BTSCs	Brain Tumour Stem Cells
CADPS2	Calcium dependent secretion activator 2
CAMKV	CaM kinase like vesicle associated
CaPO4	Calcium phosphate
CDK	Cyclin-Dependent Kinase
CDKN2	Cyclin-Dependent Kinase Inhibitor 2
CHI3L1	Chitinase-3-Like protein 1
ChIP	Chromatin immunoprecipitation
CKMT1A/B	Creatine kinase, mitochondrial 1A/B
CNRIP1	Cannabinoid receptor interacting protein 1
CNS	Central Nervous System
CoREST	REST corepressor 1
CRABP2	Cellular retinoic acid binding protein 2
CSCs	Cancer Stem Cells
DCX	Doublecortin
Doxy	Doxycycline
DRD2	Dopamine receptor D2

DUSP15	Dual specificity phosphatase 15
EGF	Epidermal Growth factor
eGFP	Enhanced Green Fluorescent Protein
EGFR	Epidermal Growth Factor Receptor
EGR1	Early growth response 1
EHMT2/G9a	Euchromatic histone-lysine N-methyltransferase 2
ELAVL4	ELAV like RNA binding protein 4
EMA	European Medicines Agency
EphA	Ephrin A
ESCs	Embryonic stem cells
ESSRB	Estrogen related receptor, beta
FABP7	Fatty acid binding protein 7
FACS	Fluorescence activated cell sorting
FDA	Food and Drug Administration
FDR	False discovery rate
G-CIMP	Glioma-CpG island methylator phenotype
GABBR2	Gamma-aminobutyric acid type B receptor subunit 2
GBM	Glioblastoma Multiforme
GFAP	Glial-fibrillary acidic protein
GO	Gene Ontology
GSCs	Glioma Stem Cells
GSEA	Gene Set Enrichment Analysis
H&E	Haematoxylin & Eosin
H3K27	Histone 3's lysine 27
H3K4	Histone 3's lysine 4
H3K9	Histone 3's lysine 9
HDAC	Histone deacetylases
HES1	Hes family bHLH transcription factor 1
HHIP	Hedgehog interacting protein
HMGCS1	3-hydroxy-3-methylglutaryl-CoA synthase 1
ID2	Inhibitor of DNA binding 2
IDH	Isocitrate dehydrogenase
INSM1	INSM transcriptional repressor 1
iPSCs	Induced Pluripotent Stem Cells
ISMARA	Integrated System for Motif Activity Response Analysis
ISN	International Society of Neuropathology
KD	Knock-down
kDa	Kilo Dalton
KDM1A/LSD1	Lysine-specific histone demethylase 1A
ki67	Marker of proliferation Ki-67
KLF15	Kruppel-like factor 15

LIN28	Lin-28 homolog A
LV	Lateral ventricle
MAD2	Mitotic spindle assembly checkpoint protein MAD2
MDM2	Murine Double Minute
MECP2	Methyl-CpG-binding protein 2
MERKT	MER proto-oncogene tyrosine kinase
MET	Hepatocyte growth factor
MGMT	O^6-methylguanine-DNA methyltransferase
miRNAs	Micro-RNAs
MRI	Magnetic Resonance Imaging
mSin3a	SIN3 transcription regulator family member A
MTT	3-(4,5-Dimethylthiazol-2-yl)-2,5-Diphenyltetrazolium Bromide
NANOG	Nanog homeobox
NeuroD1	Neuronal differentiation 1
NF-κB	Nuclear Factor Kappa B
NF1	Neurofibromatosis type 1
NFASC	Neurofascin
NFIA	Nuclear factor I A
NGF	Nerve growth factor
NLS	Nuclear localisation signal
NOS2	Nitric oxide synthase 2, inducible
NR1D1	Nuclear receptor subfamily 1 group D member 1
NR2E1/TLX	Nuclear receptor subfamily 2 group E member 1
ns	Non-statistically significant
NSCs	Neural Stem Cells
OB	Olfactory bulb
OCT4	POU class 5 homeobox 1
OE	Overexpression
OLIG2	Oligodendrocyte transcription factor 2
OS	Overall Survival
PAX6	Paired box 6
PDGFRA	Platelet-Derived Growth Factor A
PDGFRA	Platelet derived growth factor receptor alpha
PFS	Progression-Free Survival
PLAU	Plasminogen activator, urokinase
PNET	Primitive neuroectodermal tumour
PPARGC1A	Peroxisome proliferative activated receptor, gamma, coactivator 1 alpha
PRRX1	Paired related homeobox 1
PSCs	Pluripotent Stem Cells
PTCH1	Patched1
PTEN	Phosphatase and Tensin Homolog on Chromosome 10

PURO	Puromycin resistance
Rap1-GTP	RAP1A, member of RAS oncogene family
RAR	Retinoic acid receptor
RARE	Retinoic acid receptor element
RBBPs	Retinoblastoma binding proteins
RD1	Repressor domain 1
RE1/NRSE	Responsive Element 1/Neuron Restrictive Silencing Element
REST/NRSF	RE1-Silencing Transcription Factor/Neuron Restrictive Silencing Factor
RILP	REST/NRSF-interacting LIM domain protein
rtTA	Reverse tetracycline transactivator
SCD	Stearoyl-CoA desaturase
Scn2a	Type II voltage-dependent sodium channel
SCPs	RNA polymerase II small CTD phosphateses
SGZ	Subgranular zone
SHh	Sonic hedgehog
shREST	Short-hairpin RNA anti-REST
shRNA	Short-hairpin RNA
shSCRMBL	Short-hairpin RNA Scrambled
SLITRK1	SLIT and NTRK like family member 1
SMARCA4/BRG1	SWI/SNF-related matrix-associated actin-dependent regulator of chromatin, subfamily A member 4
SNAP25	Synaptosome associated protein 25
SOX	Sex determining region Y-box
SOX2	SRY (sex determining region Y)-box 2
SOX9	SRY (sex determining region Y)-box 9
SQLE	Squalene epoxidase
SVZ	Subventricular zone
SYP	Synaptophysin
TAPs	Transit amplifying progenitors
TBP	TATA-box-binding protein
TCF	T-cell transcription factor
TCF4	transcription factor 4
TCF7L2/TCF4	Transcription factor 7 like 2
TERT	Telomerase Reverse Transcriptase
TFs	Transcription factors
TGCA	The Cancer Genome Atlas
TMZ	Temozolomide
TNF	Tumor Necrosis Factor
TP53	Tumor Protein p53
TRE	Tetracycline responsive element
TRF2	Telomerase-associated protein 2
tRFP	Turbo-red fluorescent protein

Ubc	Ubiquitin promoter
UNC13A	Unc-13 homolog A
UNC5C	Unc-5 netrin receptor C
USP15	Ubiquitin specific peptidase 15
USP7	Ubiquitin specific peptidase 7
VEGF	Vascular Endothelial Growth Factor
WHO	World Health Organisation
Wnt	wingless integrated
β-TrCP	Beta-transducin repeat containing E3 ubiquitin protein ligase
β3-tubulin	Neuron-specific Class III β-Tubulin

Bibliography

Abelson, J.F., Kwan, K.Y., O'Roak, B.J., Baek, D.Y., Stillman, A.A., Morgan, T.M., Mathews, C.A., Pauls, D.L., Rasin, M.-R., Gunel, M., et al. (2005). Sequence Variants in SLITRK1 Are Associated with Tourette's Syndrome. Science (80-.). *310*, 317–320.

Aguado, T., Carracedo, A., Julien, B., Velasco, G., Milman, G., Mechoulam, R., Alvarez, L., Guzmán, M., and Galve-Roperh, I. (2007a). Cannabinoids Induce Glioma Stem-like Cell Differentiation and Inhibit Gliomagenesis. J. Biol. Chem. *282*, 6854–6862.

Aguado, T., Romero, E., Monory, K., Palazuelos, J., Sendtner, M., Marsicano, G., Lutz, B., Guzmán, M., and Galve-Roperh, I. (2007b). The CB_1 Cannabinoid Receptor Mediates Excitotoxicity-induced Neural Progenitor Proliferation and Neurogenesis. J. Biol. Chem. *282*, 23892–23898.

Akamatsu, W., Fujihara, H., Mitsuhashi, T., Yano, M., Shibata, S., Hayakawa, Y., Okano, H.J., Sakakibara, S.-I., Takano, H., Takano, T., et al. (2005). The RNA-binding protein HuD regulates neuronal cell identity and maturation. Proc. Natl. Acad. Sci. U. S. A. *102*, 4625–4630.

Al-Hajj, M., Wicha, M.S., Benito-Hernandez, A., Morrison, S.J., and Clarke, M.F. (2003). Prospective identification of tumorigenic breast cancer cells. Proc. Natl. Acad. Sci. U. S. A. *100*, 3983–3988.

Alagappan, D., Balan, M., Jiang, Y., Cohen, R.B., Kotenko, S. V., and Levison, S.W. (2013). Egr-1 is a Critical Regulator of EGF-Receptor-Mediated Expansion of Subventricular Zone Neural Stem Cells and Progenitors During Recovery from Hypoxia–Hypoglycemia. ASN Neuro *5*, AN20120032.

Aldape, K., Zadeh, G., Mansouri, S., Reifenberger, G., and von Deimling, A. (2015). Glioblastoma: pathology, molecular mechanisms and markers. Acta Neuropathol. *129*, 829–848.

Altman, J. (1962). Are new neurons formed in the brains of adult mammals? Science *135*, 1127–1128.

Altman, J. (1963). Autoradiographic investigation of cell proliferation in the brains of rats and cats. Anat. Rec. *145*, 573–591.

Altman, J. (1969). Autoradiographic and histological studies of postnatal neurogenesis. IV. Cell proliferation and migration in the anterior forebrain, with special reference to persisting neurogenesis in the olfactory bulb. J. Comp. Neurol. *137*, 433–457.

Altman, J., and Das, G.D. (1965). Post-natal origin of microneurones in the rat brain. Nature *207*, 953–956.

Andersen, J., Urbán, N., Achimastou, A., Ito, A., Simic, M., Ullom, K., Martynoga, B., Lebel, M., Göritz, C., Frisén, J., et al. (2014). A transcriptional mechanism integrating inputs from extracellular signals to activate hippocampal stem cells. Neuron *83*, 1085–1097.

Androutsellis-Theotokis, A., Leker, R.R., Soldner, F., Hoeppner, D.J., Ravin, R., Poser, S.W., Rueger, M.A., Bae, S.-K., Kittappa, R., and McKay, R.D.G. (2006). Notch signalling regulates stem cell numbers in vitro and in vivo. Nature *442*, 823–826.

Aoki, H. (2018). Novel Rest functions revealed by conditional gene ablation. Med. Mol. Morphol.

Apweiler, R., Hermjakob, H., and Sharon, N. (1999). On the frequency of protein glycosylation, as deduced from analysis of the SWISS-PROT database. Biochim. Biophys. Acta *1473*, 4–8.

Aruga, J., and Mikoshiba, K. (2003). Identification and characterization of Slitrk, a novel neuronal transmembrane protein family controlling neurite outgrowth. Mol. Cell. Neurosci. *24*, 117–129.

Ballas, N., Grunseich, C., Lu, D.D., Speh, J.C., and Mandel, G. (2005). REST and its corepressors mediate plasticity of neuronal gene chromatin throughout neurogenesis. Cell *121*, 645–657.

Balwierz, P.J., Pachkov, M., Arnold, P., Gruber, A.J., Zavolan, M., and van Nimwegen, E. (2014). ISMARA: automated modeling of genomic signals as a democracy of regulatory motifs. Genome Res. *24*, 869–884.

Bartesaghi, S., Graziano, V., Galavotti, S., Henriquez, N. V., Betts, J., Saxena, J., Minieri, V., A, D., Karlsson, A., Martins, L.M., et al. (2015). Inhibition of oxidative metabolism leads to p53 genetic inactivation and transformation in neural stem cells. Proc. Natl. Acad. Sci. *112*, 1059–1064.

Basu-Roy, U., Bayin, N.S., Rattanakorn, K., Han, E., Placantonakis, D.G., Mansukhani, A., and Basilico, C. (2015). Sox2 antagonizes the Hippo pathway to maintain stemness in cancer cells. Nat. Commun. *6*, 6411.

Batchelor, T.T., Reardon, D.A., de Groot, J.F., Wick, W., and Weller, M. (2014). Antiangiogenic therapy for glioblastoma: current status and future prospects. Clin. Cancer Res. *20*, 5612–5619.

Beck, B., and Blanpain, C. (2013). Unravelling cancer stem cell potential. Nat. Rev. Cancer *13*, 727–738.

Becker, P.B., and Workman, J.L. (2013). Nucleosome Remodeling and Epigenetics. Cold Spring Harb. Perspect. Biol. *5*, a017905.

Beier, D., Hau, P., Proescholdt, M., Lohmeier, A., Wischhusen, J., Oefner, P.J., Aigner, L., Brawanski, A., Bogdahn, U., and Beier, C.P. (2007). CD133+ and CD133- glioblastoma-derived cancer stem cells show differential growth characteristics and molecular profiles. Cancer Res. *67*, 4010–4015.

Ben-Porath, I., Thomson, M.W., Carey, V.J., Ge, R., Bell, G.W., Regev, A., and Weinberg, R.A. (2008). An embryonic stem cell–like gene expression signature in poorly differentiated aggressive human tumors. Nat. Genet. *40*, 499–507.

Bhat, K.P.L., Balasubramaniyan, V., Vaillant, B., Ezhilarasan, R., Hummelink, K., Hollingsworth, F., Wani, K., Heathcock, L., James, J.D., Goodman, L.D., et al. (2013). Mesenchymal Differentiation Mediated by NF-κB Promotes Radiation Resistance in Glioblastoma. Cancer Cell *24*, 331–346.

Blom, T., Tynninen, O., Puputti, M., Halonen, M., Paetau, A., Haapasalo, H., Tanner, M., and Nupponen, N.N. (2006). Molecular genetic analysis of the REST/NRSF gene in nervous system tumors. Acta Neuropathol. *112*, 483–490.

Bobola, M.S., Alnoor, M., Chen, J.Y.-S., Kolstoe, D.D., Silbergeld, D.L., Rostomily, R.C., Blank, A., Chamberlain, M.C., and Silber, J.R. (2015). O6-methylguanine-DNA methyltransferase activity is associated with response to alkylating agent therapy and withMGMTpromoter methylation in glioblastoma and anaplastic glioma. BBA Clin. *3*, 1–10.

Bonnet, D., and Dick, J.E. (1997). Human acute myeloid leukemia is organized as a hierarchy that originates from a primitive hematopoietic cell. Nat. Med. *3*, 730–737.

Brada, M., Ford, D., Ashley, S., Bliss, J.M., Crowley, S., Mason, M., Rajan, B., and Traish, D. (1992). Risk of second brain tumour after conservative surgery and radiotherapy for pituitary adenoma. BMJ *304*, 1343–1346.

Breemen, M.S.M., Rijsman, R.M., Taphoorn, M.J.B., Walchenbach, R., Zwinkels, H., and Vecht, C.J. (2009). Efficacy of anti-epileptic drugs in patients with gliomas and seizures. J. Neurol. *256*, 1519–1526.

Brennan, C.W., Verhaak, R.G.W., McKenna, A., Campos, B., Noushmehr, H., Salama, S.R., Zheng, S., Chakravarty, D., Sanborn, J.Z., Berman, S.H., et al. (2013). The Somatic Genomic Landscape of Glioblastoma. Cell *155*, 462–477.

Bronicki, L.M., and Jasmin, B.J. (2013). Emerging complexity of the HuD/ELAVl4 gene; implications for neuronal development, function, and dysfunction. RNA *19*, 1019–1037.

Bruce, A.W., Donaldson, I.J., Wood, I.C., Yerbury, S.A., Sadowski, M.I., Chapman, M., Gottgens, B., and Buckley, N.J. (2004). Genome-wide analysis of repressor element 1 silencing transcription factor/neuron-restrictive silencing factor (REST/NRSF) target genes. Proc. Natl. Acad. Sci. *101*, 10458–10463.

Bruce, A.W., López-contreras, A.J., Flicek, P., Down, T.A., Dhami, P., Dillon, S.C., Koch, C.M., Langford, C.F., Dunham, I., Andrews, R.M., et al. (2009). Functional diversity for REST (NRSF) is defined by in vivo binding affinity hierarchies at the DNA sequence level Functional diversity for REST (NRSF) is defined by in vivo binding affinity hierarchies at the DNA sequence level. Genome Res. 994–1005.

Buckley, N.J., Johnson, R., Sun, Y.M., and Stanton, L.W. (2009). Is REST a regulator of pluripotency? Nature *457*, 4–7.

Buckner, J.C., Brown, P.D., O'Neill, B.P., Meyer, F.B., Wetmore, C.J., and Uhm, J.H. (2007). Central Nervous System Tumors. Mayo Clin. Proc. *82*, 1271–1286.

Budhu, A.S., and Noy, N. (2002). Direct channeling of retinoic acid between cellular retinoic acid-binding protein II and retinoic acid receptor sensitizes mammary carcinoma cells to retinoic acid-induced growth arrest. Mol. Cell. Biol. *22*, 2632–2641.

Candelario, K.M., Shuttleworth, C.W., and Cunningham, L.A. (2013). Neural stem/progenitor cells display a low requirement for oxidative metabolism independent of hypoxia inducible factor-1alpha expression. J. Neurochem. *125*, 420–429.

Cattaneo, E., and McKay, R. (1990). Proliferation and differentiation of neuronal stem cells regulated by nerve

growth factor. Nature *347*, 762–765.

Cavadas, M.A.S., Mesnieres, M., Crifo, B., Manresa, M.C., Selfridge, A.C., Keogh, C.E., Fabian, Z., Scholz, C.C., Nolan, K.A., Rocha, L.M.A., et al. (2016). REST is a hypoxia-responsive transcriptional repressor. Sci. Rep. *6*, 31355.

Chaerkady, R., Kerr, C.L., Marimuthu, A., Kelkar, D.S., Kashyap, M.K., Gucek, M., Gearhart, J.D., and Pandey, A. (2009). Temporal Analysis of Neural Differentiation Using Quantitative Proteomics †. J. Proteome Res. *8*, 1315–1326.

Chaichana, K.L., Parker, S.L., Olivi, A., and Quiñones-Hinojosa, A. (2009). Long-term seizure outcomes in adult patients undergoing primary resection of malignant brain astrocytomas. J. Neurosurg. *111*, 282–292.

Chang, L., Zhang, P., Zhao, D., Liu, H., Wang, Q., Li, C., Du, W., Liu, X., Zhang, H., Zhang, Z., et al. (2016). The hedgehog antagonist HHIP as a favorable prognosticator in glioblastoma. Tumor Biol. *37*, 3979–3986.

Chatzispyrou, I.A., Held, N.M., Mouchiroud, L., Auwerx, J., and Houtkooper, R.H. (2015). Tetracycline antibiotics impair mitochondrial function and its experimental use confounds research. Cancer Res. *75*, 4446–4449.

Chen, D., Zuo, D., Luan, C., Liu, M., Na, M., Ran, L., Sun, Y., Persson, A., Englund, E., Salford, L.G., et al. (2014). Glioma Cell Proliferation Controlled by ERK Activity-Dependent Surface Expression of PDGFRA. PLoS One *9*, e87281.

Chen, J., Li, Y., Yu, T.-S., McKay, R.M., Burns, D.K., Kernie, S.G., and Parada, L.F. (2012). A restricted cell population propagates glioblastoma growth after chemotherapy. Nature *488*, 522–526.

Chen, Z.-F., Paquette, A.J., and Anderson, D.J. (1998). NRSF/REST is required in vivo for repression of multiple neuronal target genes during embryogenesis. Nat. Genet. *20*, 136–142.

Chojnacki, A., Mak, G., and Weiss, S. (2011). PDGFRα expression distinguishes GFAP-expressing neural stem cells from PDGF-responsive neural precursors in the adult periventricular area. J. Neurosci. *31*, 9503–9512.

Chomczynski, P., and Mackey, K. (1995). Short technical reports. Modification of the TRI reagent procedure for isolation of RNA from polysaccharide- and proteoglycan-rich sources. Biotechniques *19*, 942–945.

Chong, J.A., Tapia-Ramirez, J., Kim, S., Toledo-Aral, J.J., Zheng, Y., Boutros, M.C., Altshuller, Y.M., Frohman, M.A., Kraner, S.D., and Mandel, G. (1995). REST: A mammalian silencer protein that restricts sodium channel gene expression to neurons. Cell *80*, 949–957.

Cicchillitti, L., Penci, R., Di Michele, M., Filippetti, F., Rotilio, D., Donati, M.B., Scambia, G., and Ferlini, C. (2008). Proteomic characterization of cytoskeletal and mitochondrial class III -tubulin. Mol. Cancer Ther. *7*, 2070–2079.

Cisternas, F.A., Vincent, J.B., Scherer, S.W., and Ray, P.N. (2003). Cloning and characterization of human CADPS and CADPS2, new members of the Ca2+-dependent activator for secretion protein family. Genomics *81*, 279–291.

Clarke, M.F., Dick, J.E., Dirks, P.B., Eaves, C.J., Jamieson, C.H.M., Jones, D.L., Visvader, J., Weissman, I.L., and Wahl, G.M. (2006). Cancer Stem Cells—Perspectives on Current Status and Future Directions: AACR Workshop on Cancer Stem Cells. Cancer Res. *66*, 9339–9344.

Collins, A.T., Berry, P.A., Hyde, C., Stower, M.J., and Maitland, N.J. (2005). Prospective Identification of Tumorigenic Prostate Cancer Stem Cells. Cancer Res. *65*, 10946–10951.

Conaco, C., Otto, S., Han, J.-J., and Mandel, G. (2006). Reciprocal actions of REST and a microRNA promote neuronal identity. Proc. Natl. Acad. Sci. *103*, 2422–2427.

Conti, L., Pollard, S.M., Gorba, T., Reitano, E., Toselli, M., Biella, G., Sun, Y., Sanzone, S., Ying, Q.-L., Cattaneo, E., et al. (2005). Niche-Independent Symmetrical Self-Renewal of a Mammalian Tissue Stem Cell. PLoS Biol. *3*, e283.

Conti, L., Crisafulli, L., Caldera, V., Tortoreto, M., Brilli, E., Conforti, P., Zunino, F., Magrassi, L., Schiffer, D., and Cattaneo, E. (2012). REST Controls Self-Renewal and Tumorigenic Competence of Human Glioblastoma Cells. PLoS One *7*, e38486.

Coulson, J.M. (2005). Transcriptional Regulation: Cancer, Neurons and the REST. Curr. Biol. *15*, R665–R668.

Coulson, J.M., Fiskerstrand, C.E., Woll, P.J., and Quinn, J.P. (1999). Arginine vasopressin promoter regulation is mediated by a neuron-restrictive silencer element in small cell lung cancer. Cancer Res. *59*, 5123–5127.

Coulson, J.M., Edgson, J.L., Woll, P.J., and Quinn, J.P. (2000). A splice variant of the neuron-restrictive silencer factor repressor is expressed in small cell lung cancer: a potential role in derepression of neuroendocrine genes and a useful clinical marker. Cancer Res. *60*, 1840–1844.

Cowan, J.M., Powers, J., and Tischler, A.S. (1996). Assignment of the REST Gene to 4q12 by Fluorescencein SituHybridization. Genomics *34*, 260–262.

Cui, Y., Han, J., Xiao, Z., Chen, T., Wang, B., Chen, B., Liu, S., Han, S., Fang, Y., Wei, J., et al. (2016). The miR-20-Rest-Wnt signaling axis regulates neural progenitor cell differentiation. Sci. Rep. *6*, 23300.

Dai, C., Celestino, J.C., Okada, Y., Louis, D.N., Fuller, G.N., and Holland, E.C. (2001). PDGF autocrine stimulation dedifferentiates cultured astrocytes and induces oligodendrogliomas and oligoastrocytomas from neural progenitors and astrocytes in vivo. Genes Dev. *15*, 1913–1925.

Daily, K., Patel, V.R., Rigor, P., Xie, X., and Baldi, P. (2011). MotifMap: integrative genome-wide maps of regulatory motif sites for model species. BMC Bioinformatics *12*, 495.

Daynac, M., Tirou, L., Faure, H., Mouthon, M.-A., Gauthier, L.R., Hahn, H., Boussin, F.D., and Ruat, M. (2016). Hedgehog Controls Quiescence and Activation of Neural Stem Cells in the Adult Ventricular-Subventricular Zone. Stem Cell Reports *7*, 735–748.

Diekstra, F.P., Van Deerlin, V.M., van Swieten, J.C., Al-Chalabi, A., Ludolph, A.C., Weishaupt, J.H., Hardiman, O., Landers, J.E., Brown, R.H., van Es, M.A., et al. (2014). *C9orf72* and *UNC13A* are shared risk loci for amyotrophic lateral sclerosis and frontotemporal dementia: A genome-wide meta-analysis. Ann. Neurol. *76*, 120–133.

De Donato, M., Mariani, M., Petrella, L., Martinelli, E., Zannoni, G.F., Vellone, V., Ferrandina, G., Shahabi, S., Scambia, G., and Ferlini, C. (2012). Class III β-tubulin and the cytoskeletal gateway for drug resistance in ovarian cancer. J. Cell. Physiol. *227*, 1034–1041.

Drago, D., Cossetti, C., Iraci, N., Gaude, E., Musco, G., Bachi, A., and Pluchino, S. (2013). The stem cell secretome and its role in brain repair. Biochimie *95*, 2271–2285.

Eichhorn, P.J.A., Rodón, L., Gonzàlez-Juncà, A., Dirac, A., Gili, M., Martínez-Sáez, E., Aura, C., Barba, I., Peg, V., Prat, A., et al. (2012). USP15 stabilizes TGF-β receptor I and promotes oncogenesis through the activation of TGF-β signaling in glioblastoma. Nat. Med. *18*, 429–435.

Elmi, M., Matsumoto, Y., Zeng, Z., Lakshminarasimhan, P., Yang, W., Uemura, A., Nishikawa, S., Moshiri, A., Tajima, N., Agren, H., et al. (2010). TLX activates MASH1 for induction of neuronal lineage commitment of adult hippocampal neuroprogenitors. Mol. Cell. Neurosci. *45*, 121–131.

Eriksson, P.S., Perfilieva, E., Björk-Eriksson, T., Alborn, A.M., Nordborg, C., Peterson, D.A., and Gage, F.H. (1998). Neurogenesis in the adult human hippocampus. Nat. Med. *4*, 1313–1317.

Eyler, C.E., Wu, Q., Yan, K., MacSwords, J.M., Chandler-Militello, D., Misuraca, K.L., Lathia, J.D., Forrester, M.T., Lee, J., Stamler, J.S., et al. (2011). Glioma Stem Cell Proliferation and Tumor Growth Are Promoted by Nitric Oxide Synthase-2. Cell *146*, 53–66.

Falk, A., Koch, P., Kesavan, J., Takashima, Y., Ladewig, J., Alexander, M., Wiskow, O., Tailor, J., Trotter, M., Pollard, S., et al. (2012). Capture of Neuroepithelial-Like Stem Cells from Pluripotent Stem Cells Provides a Versatile System for In Vitro Production of Human Neurons. PLoS One *7*, e29597.

Faronato, M., and Coulson, J. (2011). REST (RE1-silencing transcription factor). Atlas Genet. Cytogenet. Oncol. Haematol. *3*, 208–213.

Faronato, M., Patel, V., Darling, S., Dearden, L., Michael, J., Urbé, S., Coulson, J., Faronato, M., Patel, V., Darling, S., et al. (2013). The deubiquitylase USP15 stabilizes newly synthesized REST and rescues its expression at mitotic exit The deubiquitylase USP15 stabilizes newly synthesized REST and rescues its expression at mitotic exit. *4101*.

Favaro, R., Appolloni, I., Pellegatta, S., Sanga, A.B., Pagella, P., Gambini, E., Pisati, F., Ottolenghi, S., Foti, M., Finocchiaro, G., et al. (2014). Sox2 Is Required to Maintain Cancer Stem Cells in a Mouse Model of High-Grade Oligodendroglioma. Cancer Res. *74*, 1833–1844.

Fecci, P.E., Heimberger, A.B., and Sampson, J.H. (2014). Immunotherapy for Primary Brain Tumors: No Longer a Matter of Privilege. Clin. Cancer Res. *20*, 5620–5629.

Ferrucci, M., Biagioni, F., Lenzi, P., Gambardella, S., Ferese, R., Calierno, M.T., Falleni, A., Grimaldi, A., Frati, A., Esposito, V., et al. (2017). Rapamycin promotes differentiation increasing βIII-tubulin, NeuN, and NeuroD while suppressing nestin expression in glioblastoma cells. Oncotarget *8*, 29574–29599.

Fitzsimons, C.P., Herbert, J., Schouten, M., Meijer, O.C., Lucassen, P.J., and Lightman, S. (2016). Circadian and ultradian glucocorticoid rhythmicity: Implications for the effects of glucocorticoids on neural stem cells and adult hippocampal neurogenesis. Front. Neuroendocrinol. *41*, 44–58.

Frederiksen, K., Jat, P.S., Valtz, N., Levy, D., and McKay, R. (1988). Immortalization of precursor cells from the mammalian CNS. Neuron *1*, 439–448.

Furnari, F.B., Fenton, T., Bachoo, R.M., Mukasa, A., Stommel, J.M., Stegh, A., Hahn, W.C., Ligon, K.L., Louis, D.N., Brennan, C., et al. (2007). Malignant astrocytic glioma: genetics, biology, and paths to treatment. Genes Dev. *21*, 2683–2710.

Gage, F.H., Coates, P.W., Palmer, T.D., Kuhn, H.G., Fisher, L.J., Suhonen, J.O., Peterson, D.A., Suhr, S.T., and Ray, J. (1995). Survival and differentiation of adult neuronal progenitor cells transplanted to the adult brain. Proc. Natl. Acad. Sci. U. S. A. *92*, 11879–11883.

Gaiano, N., Nye, J.S., and Fishell, G. (2000). Radial glial identity is promoted by Notch1 signaling in the murine forebrain. Neuron *26*, 395–404.

Galli, R., Binda, E., Orfanelli, U., Cipelletti, B., Gritti, A., De Vitis, S., Fiocco, R., Foroni, C., Dimeco, F., and Vescovi, A. (2004). Isolation and Characterization of Tumorigenic, Stem-like Neural Precursors from Human Glioblastoma. Cancer Res. *64*, 7011–7021.

Gan, P.P., Pasquier, E., and Kavallaris, M. (2007). Class III β-Tubulin Mediates Sensitivity to Chemotherapeutic Drugs in Non–Small Cell Lung Cancer. Cancer Res. *67*, 9356–9363.

Gao, Z., Ure, K., Ding, P., Nashaat, M., Yuan, L., Ma, J., Hammer, R.E., and Hsieh, J. (2011). The Master Negative Regulator REST/NRSF Controls Adult Neurogenesis by Restraining the Neurogenic Program in Quiescent Stem Cells. J. Neurosci. *31*, 9772–9786.

Ghersi, E., Noviello, C., and D'Adamio, L. (2004). Amyloid-β Protein Precursor (AβPP) Intracellular Domain-associated Protein-1 Proteins Bind to AβPP and Modulate Its Processing in an Isoform-specific Manner. J. Biol. Chem. *279*, 49105–49112.

Giachino, C., Basak, O., Lugert, S., Knuckles, P., Obernier, K., Fiorelli, R., Frank, S., Raineteau, O., Alvarez-Buylla, A., and Taylor, V. (2014). Molecular Diversity Subdivides the Adult Forebrain Neural Stem Cell Population. Stem Cells *32*, 70–84.

Gilbert, M.R., Dignam, J.J., Armstrong, T.S., Wefel, J.S., Blumenthal, D.T., Vogelbaum, M.A., Colman, H., Chakravarti, A., Pugh, S., Won, M., et al. (2014). A Randomized Trial of Bevacizumab for Newly Diagnosed Glioblastoma. N. Engl. J. Med. *370*, 699–708.

Gilbertson, R.J., and Rich, J.N. (2007). Making a tumour's bed: glioblastoma stem cells and the vascular niche. Nat. Rev. Cancer *7*, 733–736.

Goldman, S.A., and Nottebohm, F. (1983). Neuronal production, migration, and differentiation in a vocal control nucleus of the adult female canary brain. Proc. Natl. Acad. Sci. U. S. A. *80*, 2390–2394.

Grimes, J.A., Nielsen, S.J., Battaglioli, E., Miska, E.A., Speh, J.C., Berry, D.L., Atouf, F., Holdener, B.C., Mandel, G., and Kouzarides, T. (2000). The co-repressor mSin3A is a functional component of the REST-CoREST repressor complex. J. Biol. Chem. *275*, 9461–9467.

Gross, V., Andus, T., Castell, J., Vom Berg, D., Heinrich, P.C., and Gerok, W. (1989). O- and N-glycosylation lead to different molecular mass forms of human monocyte interleukin-6. FEBS Lett. *247*, 323–326.

Guardavaccaro, D., Frescas, D., Dorrello, N.V., Peschiaroli, A., Multani, A.S., Cardozo, T., Lasorella, A., Iavarone, A., Chang, S., Hernando, E., et al. (2008). Control of chromosome stability by the β-TrCP-REST-Mad2 axis. Nature *452*, 365–369.

Hägerstrand, D., He, X., Bradic Lindh, M., Hoefs, S., Hesselager, G., Östman, A., and Nistér, M. (2011). Identification of a SOX2-dependent subset of tumor- and sphere-forming glioblastoma cells with a distinct

tyrosine kinase inhibitor sensitivity profile. Neuro. Oncol. *13*, 1178–1191.

Hara, A., Sakai, N., Yamada, H., Niikawa, S., Ohno, T., Tanaka, T., and Mori, H. (1991). Proliferative assessment of GFAP-positive and GFAP-negative glioma cells by nucleolar organizer region staining. Surg. Neurol. *36*, 190–194.

Hegi, M.E., Diserens, A.-C., Gorlia, T., Hamou, M.-F., de Tribolet, N., Weller, M., Kros, J.M., Hainfellner, J.A., Mason, W., Mariani, L., et al. (2005). *MGMT* Gene Silencing and Benefit from Temozolomide in Glioblastoma. N. Engl. J. Med. *352*, 997–1003.

Herberich, S.E., Klose, R., Moll, I., Yang, W.-J., Wüstehube-Lausch, J., and Fischer, A. (2015). ANKS1B Interacts with the Cerebral Cavernous Malformation Protein-1 and Controls Endothelial Permeability but Not Sprouting Angiogenesis. PLoS One *10*, e0145304.

Heride, C., Urbé, S., and Clague, M.J. (2014). Ubiquitin code assembly and disassembly. Curr. Biol. *24*, R215–R220.

Holland, J.D., Klaus, A., Garratt, A.N., and Birchmeier, W. (2013). Wnt signaling in stem and cancer stem cells. Curr. Opin. Cell Biol. *25*, 254–264.

Huang, Y., Myers, S.J., and Dingledine, R. (1999). Transcriptional repression by REST: recruitment of Sin3A and histone deacetylase to neuronal genes. Nat. Neurosci. *2*, 867–872.

Huang, Z., Wu, Q., Guryanova, O.A., Cheng, L., Shou, W., Rich, J.N., and Bao, S. (2011). Deubiquitylase HAUSP stabilizes REST and promotes maintenance of neural progenitor cells. Nat. Cell Biol. *13*, 142–152.

Imayoshi, I., Isomura, A., Harima, Y., Kawaguchi, K., Kori, H., Miyachi, H., Fujiwara, T., Ishidate, F., and Kageyama, R. (2013). Oscillatory Control of Factors Determining Multipotency and Fate in Mouse Neural Progenitors. Science (80-.). *342*, 1203–1208.

Jang, M.-H., Bonaguidi, M.A., Kitabatake, Y., Sun, J., Song, J., Kang, E., Jun, H., Zhong, C., Su, Y., Guo, J.U., et al. (2013). Secreted Frizzled-Related Protein 3 Regulates Activity-Dependent Adult Hippocampal Neurogenesis. Cell Stem Cell *12*, 215–223.

Jessberger, S., Nakashima, K., Clemenson, G.D., Mejia, E., Mathews, E., Ure, K., Ogawa, S., Sinton, C.M., Gage, F.H., and Hsieh, J. (2007). Epigenetic modulation of seizure-induced neurogenesis and cognitive decline. J. Neurosci. *27*, 5967–5975.

Joensuu, H., Puputti, M., Sihto, H., Tynninen, O., and Nupponen, N.N. (2005). Amplification of genes encoding KIT, PDGFRα and VEGFR2 receptor tyrosine kinases is frequent in glioblastoma multiforme. J. Pathol. *207*, 224–231.

Johnson, J.D., and Young, B. (1996). Demographics of brain metastasis. Neurosurg. Clin. N. Am. *7*, 337–344.

Johnson, D.S., Mortazavi, A., Myers, R.M., and Wold, B. (2007). Genome-wide mapping of in vivo protein-DNA interactions. Science *316*, 1497–1502.

Johnson, R., Gamblin, R.J., Ooi, L., Bruce, A.W., Donaldson, I.J., Westhead, D.R., Wood, I.C., Jackson, R.M., and Buckley, N.J. (2006). Identification of the REST regulon reveals extensive transposable element-mediated binding site duplication. Nucleic Acids Res. *34*, 3862–3877.

Johnson, R., Teh, C.H., Kunarso, G., Wong, K.Y., Srinivasan, G., Cooper, M.L., Volta, M., Chan, S.S., Lipovich, L., Pollard, S.M., et al. (2008). REST Regulates Distinct Transcriptional Networks in Embryonic and Neural Stem Cells. PLoS Biol. *6*, e256.

Johnson, R., Samuel, J., Ng, C.K.L., Jauch, R., Stanton, L.W., and Wood, I.C. (2009). Evolution of the Vertebrate Gene Regulatory Network Controlled by the Transcriptional Repressor REST. Mol. Biol. Evol. *26*, 1491–1507.

Jones, M.J., Goodman, S.J., and Kobor, M.S. (2015). DNA methylation and healthy human aging. Aging Cell *14*, 924–932.

Jørgensen, H.F., and Fisher, A.G. (2010). Can controversies be put to REST? Nature *467*, E3–E4.

Jørgensen, H.F., Chen, Z.-F., Merkenschlager, M., and Fisher, A.G. (2009b). Is REST required for ESC pluripotency? Nature *457*, E4–E5.

Jørgensen, H.F., Terry, A., Beretta, C., Pereira, C.F., Leleu, M., Chen, Z.-F., Kelly, C., Merkenschlager, M., and Fisher, A.G. (2009a). REST selectively represses a subset of RE1-containing neuronal genes in mouse

embryonic stem cells. Development *136*, 715–721.

Jornayvaz, F.R., and Shulman, G.I. (2010). Regulation of mitochondrial biogenesis. Essays Biochem. *47*, 69–84.

Juillerat-Jeanneret, L., Celerier, J., Chapuis Bernasconi, C., Nguyen, G., Wostl, W., Maerki, H.P., Janzer, R.-C., Corvol, P., and Gasc, J.-M. (2004). Renin and angiotensinogen expression and functions in growth and apoptosis of human glioblastoma. Br. J. Cancer *90*, 1059–1068.

K.J., Z. (1979). Histological typing of tumours of the central nervous system (Geneva : World Health Organization,).

Kamal, M.M., Sathyan, P., Singh, S.K., Zinn, P.O., Marisetty, A.L., Liang, S., Gumin, J., El-Mesallamy, H.O., Suki, D., Colman, H., et al. (2012). REST regulates oncogenic properties of glioblastoma stem cells. Stem Cells *30*, 405–414.

Kaplan, M.S., and Hinds, J.W. (1977). Neurogenesis in the adult rat: electron microscopic analysis of light radioautographs. Science *197*, 1092–1094.

Karsy, M., Gelbman, M., Shah, P., Balumbu, O., Moy, F., and Arslan, E. (2012). Established and emerging variants of glioblastoma multiforme: review of morphological and molecular features. Folia Neuropathol. *4*, 301–321.

Katsetos, C.D., Draber, P., and Kavallaris, M. (2011). Targeting βIII-tubulin in glioblastoma multiforme: from cell biology and histopathology to cancer therapeutics. Anticancer. Agents Med. Chem. *11*, 719–728.

Keime-Guibert, F., Chinot, O., Taillandier, L., Cartalat-Carel, S., Frenay, M., Kantor, G., Guillamo, J.-S., Jadaud, E., Colin, P., Bondiau, P.-Y., et al. (2007). Radiotherapy for Glioblastoma in the Elderly. N. Engl. J. Med. *356*, 1527–1535.

Kemp, D.M., Lin, J.C., and Habener, J.F. (2003a). Regulation of Pax4 Paired Homeodomain Gene by Neuron-restrictive Silencer Factor. J. Biol. Chem. *278*, 35057–35062.

Kemp, D.M., Lin, J.C., and Habener, J.F. (2003b). Regulation of Pax4 paired homeodomain gene by neuron-restrictive silencer factor. J. Biol. Chem. *278*, 35057–35062.

Kerkhof, M., Dielemans, J.C.M., van Breemen, M.S., Zwinkels, H., Walchenbach, R., Taphoorn, M.J., and Vecht, C.J. (2013). Effect of valproic acid on seizure control and on survival in patients with glioblastoma multiforme. Neuro. Oncol. *15*, 961–967.

Killela, P.J., Reitman, Z.J., Jiao, Y., Bettegowda, C., Agrawal, N., Diaz, L.A., Friedman, A.H., Friedman, H., Gallia, G.L., Giovanella, B.C., et al. (2013). TERT promoter mutations occur frequently in gliomas and a subset of tumors derived from cells with low rates of self-renewal. Proc. Natl. Acad. Sci. *110*, 6021–6026.

Kim, M., and Costello, J. (2017). DNA methylation: an epigenetic mark of cellular memory. Exp. Mol. Med. *49*, e322–e322.

Kim, D.-Y., Rhee, I., and Paik, J. (2014). Metabolic circuits in neural stem cells. Cell. Mol. Life Sci. *71*, 4221–4241.

Kim, T.-M., Huang, W., Park, R., Park, P.J., and Johnson, M.D. (2011). A Developmental Taxonomy of Glioblastoma Defined and Maintained by MicroRNAs. Cancer Res. *71*, 3387–3399.

Kimiwada, T., Sakurai, M., Ohashi, H., Aoki, S., Tominaga, T., and Wada, K. (2009). Clock genes regulate neurogenic transcription factors, including NeuroD1, and the neuronal differentiation of adult neural stem/progenitor cells. Neurochem. Int. *54*, 277–285.

Knobloch, M., and Jessberger, S. (2017). Metabolism and neurogenesis. Curr. Opin. Neurobiol. *42*, 45–52.

Knobloch, M., Braun, S.M.G., Zurkirchen, L., von Schoultz, C., Zamboni, N., Araúzo-Bravo, M.J., Kovacs, W.J., Karalay, Ö., Suter, U., Machado, R.A.C., et al. (2012). Metabolic control of adult neural stem cell activity by Fasn-dependent lipogenesis. Nature *493*, 226–230.

Koenigsberger, C., Chicca Ii, J.J., Amoureux, M.-C., Edelman, G.M., and Jones, F.S. (1999). Differential regulation by multiple promoters of the gene encoding the neuron-restrictive silencer factor.

Kojima, T., Murai, K., Naruse, Y., Takahashi, N., and Mori, N. (2001). Cell-type non-selective transcription of mouse and human genes encoding neural-restrictive silencer factor. Brain Res. Mol. Brain Res. *90*, 174–186.

Kokaia, Z., Martino, G., Schwartz, M., and Lindvall, O. (2012). Cross-talk between neural stem cells and immune cells: the key to better brain repair? Nat. Neurosci. *15*, 1078–1087.

Kraner, S.D., Chong, J.A., Tsay, H.-J., and Mandel, G. (1992). Silencing the type II sodium channel gene: A model for neural-specific gene regulation. Neuron *9*, 37–44.

Kuwabara, T., Hsieh, J., Muotri, A., Yeo, G., Warashina, M., Lie, D.C., Moore, L., Nakashima, K., Asashima, M., and Gage, F.H. (2009). Wnt-mediated activation of NeuroD1 and retro-elements during adult neurogenesis. Nat. Neurosci. *12*, 1097–1105.

Kuwahara, K. (2013). Role of NRSF/REST in the regulation of cardiac gene expression and function. Circ. J. *77*, 2682–2686.

Kwon, J.-H., Shin, J.H., Kim, E.-S., Lee, N., Park, J.Y., Koo, B.S., Hong, S.M., Park, C.W., and Choi, K.Y. (2013). REST-dependent expression of TRF2 renders non-neuronal cancer cells resistant to DNA damage during oxidative stress. Int. J. Cancer *132*, 832–842.

Lai, A., Kharbanda, S., Pope, W.B., Tran, A., Solis, O.E., Peale, F., Forrest, W.F., Pujara, K., Carrillo, J.A., Pandita, A., et al. (2011). Evidence for Sequenced Molecular Evolution of *IDH1* Mutant Glioblastoma From a Distinct Cell of Origin. J. Clin. Oncol. *29*, 4482–4490.

Laigle-Donadey, F., Martin-Duverneuil, N., Lejeune, J., Crinière, E., Capelle, L., Duffau, H., Cornu, P., Broët, P., Kujas, M., Mokhtari, K., et al. (2004). Correlations between molecular profile and radiologic pattern in oligodendroglial tumors. Neurology *63*, 2360–2362.

Lan, X., Jörg, D.J., Cavalli, F.M.G., Richards, L.M., Nguyen, L. V, Vanner, R.J., Guilhamon, P., Lee, L., Kushida, M.M., Pellacani, D., et al. (2017). Fate mapping of human glioblastoma reveals an invariant stem cell hierarchy. Nature *549*, 227–232.

Laneve, P., Gioia, U., Andriotto, A., Moretti, F., Bozzoni, I., and Caffarelli, E. (2010). A minicircuitry involving REST and CREB controls miR-9-2 expression during human neuronal differentiation. Nucleic Acids Res. *38*, 6895–6905.

Lange, C., Turrero Garcia, M., Decimo, I., Bifari, F., Eelen, G., Quaegebeur, A., Boon, R., Zhao, H., Boeckx, B., Chang, J., et al. (2016). Relief of hypoxia by angiogenesis promotes neural stem cell differentiation by targeting glycolysis. EMBO J. *35*, 924–941.

de Lange, T. (2005). Shelterin: the protein complex that shapes and safeguards human telomeres. Genes Dev. *19*, 2100–2110.

Lapidot, T., Sirard, C., Vormoor, J., Murdoch, B., Hoang, T., Caceres-Cortes, J., Minden, M., Paterson, B., Caligiuri, M.A., and Dick, J.E. (1994). A cell initiating human acute myeloid leukaemia after transplantation into SCID mice. Nature *367*, 645–648.

Lawinger, P., Venugopal, R., Guo, Z.S., Immaneni, A., Sengupta, D., Lu, W., Rastelli, L., Marin Dias Carneiro, A., Levin, V., Fuller, G.N., et al. (2000). The neuronal repressor REST/NRSF is an essential regulator in medulloblastoma cells. Nat. Med. *6*, 826–831.

Lee, S.Y. (2016). Temozolomide resistance in glioblastoma multiforme. Genes Dis. *3*, 198–210.

Lee, B.R., and Kamitani, T. (2011). Improved immunodetection of endogenous ??-synuclein. PLoS One *6*.

Lee, J., Kotliarova, S., Kotliarov, Y., Li, A., Su, Q., Donin, N.M., Pastorino, S., Purow, B.W., Christopher, N., Zhang, W., et al. (2006). Tumor stem cells derived from glioblastomas cultured in bFGF and EGF more closely mirror the phenotype and genotype of primary tumors than do serum-cultured cell lines. Cancer Cell *9*, 391–403.

Lee, J.H., Shimojo, M., Chai, Y.G., and Hersh, L.B. (2000). Studies on the interaction of REST4 with the cholinergic repressor element-1/neuron restrictive silencer element. Brain Res. Mol. Brain Res. *80*, 88–98.

Lee, M.G., Wynder, C., Cooch, N., and Shiekhattar, R. (2005). An essential role for CoREST in nucleosomal histone 3 lysine 4 demethylation. Nature *437*, 432–435.

Lee, N., Park, S.J., Haddad, G., Kim, D.-K., Park, S.-M., Park, S.K., Kwan, &, and Choi, Y. (2016). Interactomic analysis of REST/ NRSF and implications of its functional links with the transcription suppressor TRIM28 during neuronal differentiation. Nat. Publ. Gr.

Leung, T.H., Hoffmann, A., and Baltimore, D. (2004). One Nucleotide in a κB Site Can Determine Cofactor Specificity for NF-κB Dimers. Cell *118*, 453–464.

Li, A., Lin, X., Tan, X., Yin, B., Han, W., Zhao, J., Yuan, J., Qiang, B., and Peng, X. (2013). Circadian gene Clock contributes to cell proliferation and migration of glioma and is directly regulated by tumor-suppressive miR-124. FEBS Lett. *587*, 2455–2460.

Li, C., Heidt, D.G., Dalerba, P., Burant, C.F., Zhang, L., Adsay, V., Wicha, M., Clarke, M.F., and Simeone, D.M. (2007). Identification of Pancreatic Cancer Stem Cells. Cancer Res. *67*, 1030–1037.

Li, J., Zhu, S., Kozono, D., Ng, K., Futalan, D., Shen, Y., Akers, J.C., Steed, T., Kushwaha, D., Schlabach, M., et al. (2014). Genome-wide shRNA screen revealed integrated mitogenic signaling between dopamine receptor D2 (DRD2) and epidermal growth factor receptor (EGFR) in glioblastoma. Oncotarget *5*, 882–893.

Li, S., Sun, G., Murai, K., Ye, P., and Shi, Y. (2012). Characterization of TLX Expression in Neural Stem Cells and Progenitor Cells in Adult Brains. PLoS One *7*, e43324.

Li, Y., Wang, W., Wang, F., Wu, Q., Li, W., Zhong, X., Tian, K., Zeng, T., Gao, L., Liu, Y., et al. (2017). Paired related homeobox 1 transactivates dopamine D2 receptor to maintain propagation and tumorigenicity of glioma-initiating cells. J. Mol. Cell Biol. *9*, 302–314.

Liang, J., Tong, P., Zhao, W., Li, Y., Zhang, L., Xia, Y., and Yu, Y. (2014). The REST Gene Signature Predicts Drug Sensitivity in Neuroblastoma Cell Lines and Is Significantly Associated with Neuroblastoma Tumor Stage. Int. J. Mol. Sci. *15*, 11220–11233.

Liang, J., Meng, Q., Zhao, W., Tong, P., Li, P., Zhao, Y., Zhao, X., and Li, H. (2016). An expression based REST signature predicts patient survival and therapeutic response for glioblastoma multiforme. Sci. Rep. *6*, 1–9.

Lie, D.-C., Colamarino, S.A., Song, H.-J., Désiré, L., Mira, H., Consiglio, A., Lein, E.S., Jessberger, S., Lansford, H., Dearie, A.R., et al. (2005). Wnt signalling regulates adult hippocampal neurogenesis. Nature *437*, 1370–1375.

Lie, D.C., Dziewczapolski, G., Willhoite, A.R., Kaspar, B.K., Shults, C.W., and Gage, F.H. (2002). The adult substantia nigra contains progenitor cells with neurogenic potential. J. Neurosci. *22*, 6639–6649.

Liebelt, B.D., Shingu, T., Zhou, X., Ren, J., Shin, S.A., and Hu, J. (2016). Glioma Stem Cells: Signaling, Microenvironment, and Therapy. Stem Cells Int. *2016*, 1–10.

Lipstein, N., Verhoeven-Duif, N.M., Michelassi, F.E., Calloway, N., van Hasselt, P.M., Pienkowska, K., van Haaften, G., van Haelst, M.M., van Empelen, R., Cuppen, I., et al. (2017). Synaptic UNC13A protein variant causes increased neurotransmission and dyskinetic movement disorder. J. Clin. Invest. *127*, 1005–1018.

Liu, M., Xia, Y., Ding, J., Ye, B., Zhao, E., Choi, J.-H., Alptekin, A., Yan, C., Dong, Z., Huang, S., et al. (2016). Transcriptional Profiling Reveals a Common Metabolic Program in High-Risk Human Neuroblastoma and Mouse Neuroblastoma Sphere-Forming Cells. Cell Rep. *17*, 609–623.

Liu, X.-Y., Gerges, N., Korshunov, A., Sabha, N., Khuong-Quang, D.-A., Fontebasso, A.M., Fleming, A., Hadjadj, D., Schwartzentruber, J., Majewski, J., et al. (2012). Frequent ATRX mutations and loss of expression in adult diffuse astrocytic tumors carrying IDH1/IDH2 and TP53 mutations. Acta Neuropathol. *124*, 615–625.

Loh, Y.-H., Wu, Q., Chew, J.-L., Vega, V.B., Zhang, W., Chen, X., Bourque, G., George, J., Leong, B., Liu, J., et al. (2006). The Oct4 and Nanog transcription network regulates pluripotency in mouse embryonic stem cells. Nat. Genet. *38*, 431–440.

Louis, D.N., Ohgaki, H., Wiestler, O.D., Cavenee, W.K., Burger, P.C., Jouvet, A., Scheithauer, B.W., and Kleihues, P. (2007). The 2007 WHO classification of tumours of the central nervous system. Acta Neuropathol. *114*, 97–109.

Louis, D.N., Perry, A., Burger, P., Ellison, D.W., Reifenberger, G., von Deimling, A., Aldape, K., Brat, D., Collins, V.P., Eberhart, C., et al. (2014). International Society of Neuropathology-Haarlem Consensus Guidelines for Nervous System Tumor Classification and Grading. Brain Pathol. *24*, 429–435.

Lowe, M.T.J., Kim, E.H., Faull, R.L.M., Christie, D.L., and Waldvogel, H.J. (2013). Dissociated expression of mitochondrial and cytosolic creatine kinases in the human brain: a new perspective on the role of creatine in brain energy metabolism. J. Cereb. Blood Flow Metab. *33*, 1295–1306.

Lunyak, V. V., and Rosenfeld, M.G. (2005). No Rest for REST: REST/NRSF Regulation of Neurogenesis. Cell *121*,

499–501.

Lunyak, V. V., Burgess, R., Prefontaine, G.G., Nelson, C., Sze, S.-H., Chenoweth, J., Schwartz, P., Pevzner, P.A., Glass, C., Mandel, G., et al. (2002). Corepressor-Dependent Silencing of Chromosomal Regions Encoding Neuronal Genes. Science (80-.). *298*, 1747–1752.

Mao, D.D., Gujar, A.D., Mahlokozera, T., Chen, I., Pan, Y., Luo, J., Brost, T., Thompson, E.A., Turski, A., Leuthardt, E.C., et al. (2015). A CDC20-APC/SOX2 Signaling Axis Regulates Human Glioblastoma Stem-like Cells. Cell Rep. *11*, 1809–1821.

Marisetty, A.L., Singh, S.K., Nguyen, T.N., Coarfa, C., Liu, B., and Majumder, S. (2017). REST represses miR-124 and miR-203 to regulate distinct oncogenic properties of glioblastoma stem cells. Neuro. Oncol. *19*, 514–523.

Martin, D., and Grapin-Botton, A. (2017). The Importance of REST for Development and Function of Beta Cells. Front. Cell Dev. Biol. *5*, 12.

Martin, D., Kim, Y.-H., Sever, D., Mao, C.-A., Haefliger, J.-A., and Grapin-Botton, A. (2015). REST represses a subset of the pancreatic endocrine differentiation program. Dev. Biol. *405*, 316–327.

Martínez-Balbás, M.A., Dey, A., Rabindran, S.K., Ozato, K., and Wu, C. (1995). Displacement of sequence-specific transcription factors from mitotic chromatin. Cell *83*, 29–38.

Mashimo, T., Pichumani, K., Vemireddy, V., Hatanpaa, K.J., Singh, D.K., Sirasanagandla, S., Nannepaga, S., Piccirillo, S.G., Kovacs, Z., Foong, C., et al. (2014). Acetate Is a Bioenergetic Substrate for Human Glioblastoma and Brain Metastases. Cell *159*, 1603–1614.

McLendon, R., Friedman, A., Bigner, D., Van Meir, E.G., Brat, D.J., M. Mastrogianakis, G., Olson, J.J., Mikkelsen, T., Lehman, N., Aldape, K., et al. (2008). Comprehensive genomic characterization defines human glioblastoma genes and core pathways. Nature *455*, 1061–1068.

Meerbrey, K.L., Hu, G., Kessler, J.D., Roarty, K., Li, M.Z., Fang, J.E., Herschkowitz, J.I., Burrows, A.E., Ciccia, A., Sun, T., et al. (2011). The pINDUCER lentiviral toolkit for inducible RNA interference in vitro and in vivo. Proc. Natl. Acad. Sci. *108*, 3665–3670.

Merico, D., Isserlin, R., Stueker, O., Emili, A., and Bader, G.D. (2010). Enrichment Map: A Network-Based Method for Gene-Set Enrichment Visualization and Interpretation. PLoS One *5*, e13984.

Minniti, G., Traish, D., Ashley, S., Gonsalves, A., and Brada, M. (2005). Risk of Second Brain Tumor after Conservative Surgery and Radiotherapy for Pituitary Adenoma: Update after an Additional 10 Years. J. Clin. Endocrinol. Metab. *90*, 800–804.

Mukherjee, S., Brulet, R., Zhang, L., and Hsieh, J. (2016). REST regulation of gene networks in adult neural stem cells. Nat. Commun. *7*, 13360.

Murai, K., Naruse, Y., Shaul, Y., Agata, Y., and Mori, N. (2004). Direct interaction of NRSF with TBP: chromatin reorganization and core promoter repression for neuron-specific gene transcription. Nucleic Acids Res. *32*, 3180–3189.

Murphy, M., Drago, J., and Bartlett, P.F. (1990). Fibroblast growth factor stimulates the proliferation and differentiation of neural precursor cells in vitro. J. Neurosci. Res. *25*, 463–475.

Naruse, Y., Aoki, T., Kojima, T., and Mori, N. (1999). Neural restrictive silencer factor recruits mSin3 and histone deacetylase complex to repress neuron-specific target genes. Proc. Natl. Acad. Sci. U. S. A. *96*, 13691–13696.

Nechiporuk, T., McGann, J., Mullendorff, K., Hsieh, J., Wurst, W., Floss, T., and Mandel, G. (2016). The REST remodeling complex protects genomic integrity during embryonic neurogenesis. Elife *5*, 1–28.

Neglia, J.P., Robison, L.L., Stovall, M., Liu, Y., Packer, R.J., Hammond, S., Yasui, Y., Kasper, C.E., Mertens, A.C., Donaldson, S.S., et al. (2006). New Primary Neoplasms of the Central Nervous System in Survivors of Childhood Cancer: a Report From the Childhood Cancer Survivor Study. JNCI J. Natl. Cancer Inst. *98*, 1528–1537.

Negrini, S., Prada, I., D'Alessandro, R., and Meldolesi, J. (2013). REST: an oncogene or a tumor suppressor? Trends Cell Biol. *23*, 289–295.

Ning, H., Li, T., Zhao, L., Li, T., Li, J., Liu, J., Liu, Z., and Fan, D. (2006). TRF2 promotes multidrug resistance in

gastric cancer cells. Cancer Biol. Ther. *5*, 950–956.

Nishihara, S., Tsuda, L., and Ogura, T. (2003). The canonical Wnt pathway directly regulates NRSF/REST expression in chick spinal cord. Biochem. Biophys. Res. Commun. *311*, 55–63.

Nobusawa, S., Watanabe, T., Kleihues, P., and Ohgaki, H. (2009). IDH1 Mutations as Molecular Signature and Predictive Factor of Secondary Glioblastomas. Clin. Cancer Res. *15*, 6002–6007.

Noushmehr, H., Weisenberger, D.J., Diefes, K., Phillips, H.S., Pujara, K., Berman, B.P., Pan, F., Pelloski, C.E., Sulman, E.P., Bhat, K.P., et al. (2010). Identification of a CpG Island Methylator Phenotype that Defines a Distinct Subgroup of Glioma. Cancer Cell *17*, 510–522.

Ohgaki, H., and Kleihues, P. (2013). The Definition of Primary and Secondary Glioblastoma. Clin. Cancer Res. *19*, 764–772.

Ohgaki, H., Dessen, P., Jourde, B., Horstmann, S., Nishikawa, T., Di Patre, P.-L., Burkhard, C., Schüler, D., Probst-Hensch, N.M., Maiorka, P.C., et al. (2004). Genetic Pathways to Glioblastoma. Cancer Res. *64*, 6892–6899.

Ohtsuka, T., Shimojo, H., Matsunaga, M., Watanabe, N., Kometani, K., Minato, N., and Kageyama, R. (2011). Gene expression profiling of neural stem cells and identification of regulators of neural differentiation during cortical development. Stem Cells *29*, 1817–1828.

Ooi, L., and Wood, I.C. (2007). Chromatin crosstalk in development and disease: Lessons from REST. Nat. Rev. Genet. *8*, 544–554.

Ooi, L., Belyaev, N.D., Miyake, K., Wood, I.C., and Buckley, N.J. (2006). BRG1 Chromatin Remodeling Activity Is Required for Efficient Chromatin Binding by Repressor Element 1-silencing Transcription Factor (REST) and Facilitates REST-mediated Repression. J. Biol. Chem. *281*, 38974–38980.

Ostrom, Q.T., and Barnholtz-Sloan, J.S. (2011). Current State of Our Knowledge on Brain Tumor Epidemiology. Curr. Neurol. Neurosci. Rep. *11*, 329–335.

Ostrom, Q.T., Gittleman, H., Liao, P., Rouse, C., Chen, Y., Dowling, J., Wolinsky, Y., Kruchko, C., and Barnholtz-Sloan, J. (2014). CBTRUS Statistical Report: Primary Brain and Central Nervous System Tumors Diagnosed in the United States in 2007-2011. Neuro. Oncol. *16*, iv1-iv63.

Ostrom, Q.T., de Blank, P.M., Kruchko, C., Petersen, C.M., Liao, P., Finlay, J.L., Stearns, D.S., Wolff, J.E., Wolinsky, Y., Letterio, J.J., et al. (2015). Alex's Lemonade Stand Foundation Infant and Childhood Primary Brain and Central Nervous System Tumors Diagnosed in the United States in 2007–2011. Neuro. Oncol. *16*, x1–x36.

Otto, S.J., McCorkle, S.R., Hover, J., Conaco, C., Han, J.-J., Impey, S., Yochum, G.S., Dunn, J.J., Goodman, R.H., and Mandel, G. (2007). A new binding motif for the transcriptional repressor REST uncovers large gene networks devoted to neuronal functions. J. Neurosci. *27*, 6729–6739.

Ottoboni, L., Merlini, A., and Martino, G. (2017). Neural Stem Cell Plasticity: Advantages in Therapy for the Injured Central Nervous System. Front. Cell Dev. Biol. *5*, 52.

Packer, A.N., Xing, Y., Harper, S.Q., Jones, L., and Davidson, B.L. (2008). The bifunctional microRNA miR-9/miR-9* regulates REST and CoREST and is downregulated in Huntington's disease. J. Neurosci. *28*, 14341–14346.

Palm, K., Belluardo, N., Metsis, M., and Timmusk, T. onis (1998). Neuronal Expression of Zinc Finger Transcription Factor REST/NRSF/XBR Gene. J. Neurosci. *18*, 1280–1296.

Palm, K., Metsis, M., and Timmusk, T. (1999). Neuron-specific splicing of zinc finger transcription factor REST/NRSF/XBR is frequent in neuroblastomas and conserved in human, mouse and rat. Brain Res. Mol. Brain Res. *72*, 30–39.

Palmer, T.D., Ray, J., and Gage, F.H. (1995). FGF-2-responsive neuronal progenitors reside in proliferative and quiescent regions of the adult rodent brain. Mol. Cell. Neurosci. *6*, 474–486.

Palmer, T.D., Markakis, E.A., Willhoite, A.R., Safar, F., and Gage, F.H. (1999). Fibroblast growth factor-2 activates a latent neurogenic program in neural stem cells from diverse regions of the adult CNS. J. Neurosci. *19*, 8487–8497.

Pance, A., Livesey, F.J., and Jackson, A.P. (2006). A role for the transcriptional repressor REST in maintaining

the phenotype of neurosecretory-deficient PC12 cells. J. Neurochem. *99*, 1435–1444.

Park, H.J., Hong, M., Bronson, R.T., Israel, M.A., Frankel, W.N., and Yun, K. (2013). Elevated *Id2* Expression Results in Precocious Neural Stem Cell Depletion and Abnormal Brain Development. Stem Cells *31*, 1010–1021.

Parsons, D.W., Jones, S., Zhang, X., Lin, J.C.-H., Leary, R.J., Angenendt, P., Mankoo, P., Carter, H., Siu, I.-M., Gallia, G.L., et al. (2008). An Integrated Genomic Analysis of Human Glioblastoma Multiforme. Science (80-.). *321*, 1807–1812.

Patel, A.P., Tirosh, I., Trombetta, J.J., Shalek, A.K., Gillespie, S.M., Wakimoto, H., Cahill, D.P., Nahed, B. V., Curry, W.T., Martuza, R.L., et al. (2014). Single-cell RNA-seq highlights intratumoral heterogeneity in primary glioblastoma. Science (80-.). *344*, 1396–1401.

Paton, J.A., and Nottebohm, F.N. (1984). Neurons generated in the adult brain are recruited into functional circuits. Science *225*, 1046–1048.

Peiris-Pagès, M., Martinez-Outschoorn, U.E., Pestell, R.G., Sotgia, F., and Lisanti, M.P. (2016). Cancer stem cell metabolism. Breast Cancer Res. *18*, 55.

Pérez-Larraya, J.G., Ducray, F., Chinot, O., Catry-Thomas, I., Taillandier, L., Guillamo, J.-S., Campello, C., Monjour, A., Cartalat-Carel, S., Barrie, M., et al. (2011). Temozolomide in Elderly Patients With Newly Diagnosed Glioblastoma and Poor Performance Status: An ANOCEF Phase II Trial. J. Clin. Oncol. *29*, 3050–3055.

Pevny, L.H., and Nicolis, S.K. (2010). Sox2 roles in neural stem cells. Int. J. Biochem. Cell Biol. *42*, 421–424.

Pollard, S., Clarke, I.D., Smith, A., and Dirks, P. (2009a). Brain Cancer Stem Cells: A Level Playing Field. Cell Stem Cell *5*, 468–469.

Pollard, S.M., Conti, L., Sun, Y., Goffredo, D., and Smith, A. (2006). Adherent Neural Stem (NS) Cells from Fetal and Adult Forebrain. Cereb. Cortex *16*, i112–i120.

Pollard, S.M., Yoshikawa, K., Clarke, I.D., Danovi, D., Stricker, S., Russell, R., Bayani, J., Head, R., Lee, M., Bernstein, M., et al. (2009b). Glioma Stem Cell Lines Expanded in Adherent Culture Have Tumor-Specific Phenotypes and Are Suitable for Chemical and Genetic Screens. Cell Stem Cell *4*, 568–580.

Pozzi, D., Lignani, G., Ferrea, E., Contestabile, A., Paonessa, F., D'Alessandro, R., Lippiello, P., Boido, D., Fassio, A., Meldolesi, J., et al. (2013). REST/NRSF-mediated intrinsic homeostasis protects neuronal networks from hyperexcitability. EMBO J. *32*, 2994–3007.

Qian, X.-L., Li, Y.-Q., Gu, F., Liu, F.-F., Li, W.-D., Zhang, X.-M., and Fu, L. (2012). Overexpression of ubiquitous mitochondrial creatine kinase (uMtCK) accelerates tumor growth by inhibiting apoptosis of breast cancer cells and is associated with a poor prognosis in breast cancer patients. Biochem. Biophys. Res. Commun. *427*, 60–66.

Qin, S., Niu, W., Iqbal, N., Smith, D.K., and Zhang, C.-L. (2014). Orphan nuclear receptor TLX regulates astrogenesis by modulating BMP signaling. Front. Neurosci. *8*, 74.

Qu, Q., Sun, G., Li, W., Yang, S., Ye, P., Zhao, C., Yu, R.T., Gage, F.H., Evans, R.M., and Shi, Y. (2010). Orphan nuclear receptor TLX activates Wnt/beta-catenin signalling to stimulate neural stem cell proliferation and self-renewal. Nat. Cell Biol. *12*, 31-40; sup pp 1-9.

Qureshi, I.A., and Mehler, M.F. (2009). Regulation of non-coding RNA networks in the nervous system—What's the REST of the story? Neurosci. Lett. *466*, 73–80.

Raj, B., O'Hanlon, D., Vessey, J.P., Pan, Q., Ray, D., Buckley, N.J., Miller, F.D., and Blencowe, B.J. (2011). Cross-regulation between an alternative splicing activator and a transcription repressor controls neurogenesis. Mol. Cell *43*, 843–850.

Ray, J., Peterson, D.A., Schinstine, M., and Gage, F.H. (1993). Proliferation, differentiation, and long-term culture of primary hippocampal neurons. Proc. Natl. Acad. Sci. U. S. A. *90*, 3602–3606.

Restrepo, A., Smith, C.A., Agnihotri, S., Shekarforoush, M., Kongkham, P.N., Seol, H.J., Northcott, P., and Rutka, J.T. (2011). Epigenetic regulation of glial fibrillary acidic protein by DNA methylation in human malignant gliomas. Neuro. Oncol. *13*, 42–50.

Reuss, D., and von Deimling, A. (2009). Hereditary Tumor Syndromes and Gliomas. In Recent Results in Cancer Research. Fortschritte Der Krebsforschung. Progres Dans Les Recherches Sur Le Cancer, pp. 83–102.

Reya, T., Morrison, S.J., Clarke, M.F., and Weissman, I.L. (2001). Stem cells, cancer, and cancer stem cells. Nature *414*, 105–111.

Reynolds, B.A., and Vescovi, A.L. (2009). Brain Cancer Stem Cells: Think Twice before Going Flat. Cell Stem Cell *5*, 466–467.

Reynolds, B.A., and Weiss, S. (1992). Generation of neurons and astrocytes from isolated cells of the adult mammalian central nervous system. Science *255*, 1707–1710.

Ricci-Vitiani, L., Lombardi, D.G., Pilozzi, E., Biffoni, M., Todaro, M., Peschle, C., and De Maria, R. (2007). Identification and expansion of human colon-cancer-initiating cells. Nature *445*, 111–115.

Riemenschneider, M., Konta, L., Friedrich, P., Schwarz, S., Taddei, K., Neff, F., Padovani, A., Kölsch, H., Laws, S.M., Klopp, N., et al. (2006). A functional polymorphism within plasminogen activator urokinase (PLAU) is associated with Alzheimer's disease. Hum. Mol. Genet. *15*, 2446–2456.

Roa, W., Brasher, P.M.A., Bauman, G., Anthes, M., Bruera, E., Chan, A., Fisher, B., Fulton, D., Gulavita, S., Hao, C., et al. (2004). Abbreviated Course of Radiation Therapy in Older Patients With Glioblastoma Multiforme: A Prospective Randomized Clinical Trial. J. Clin. Oncol. *22*, 1583–1588.

Rockowitz, S., and Zheng, D. (2015). Significant expansion of the REST/NRSF cistrome in human versus mouse embryonic stem cells: Potential implications for neural development. Nucleic Acids Res. *43*, 5730–5743.

Rockowitz, S., Lien, W.-H., Pedrosa, E., Wei, G., Lin, M., Zhao, K., Lachman, H.M., Fuchs, E., and Zheng, D. (2014). Comparison of REST Cistromes across Human Cell Types Reveals Common and Context-Specific Functions. PLoS Comput. Biol. *10*, e1003671.

Ron, E., Modan, B., Boice, J.D., Alfandary, E., Stovall, M., Chetrit, A., and Katz, L. (1988). Tumors of the Brain and Nervous System after Radiotherapy in Childhood. N. Engl. J. Med. *319*, 1033–1039.

Roopra, A., Sharling, L., Wood, I.C., Briggs, T., Bachfischer, U., Paquette, A.J., and Buckley, N.J. (2000). Transcriptional repression by neuron-restrictive silencer factor is mediated via the Sin3-histone deacetylase complex. Mol. Cell. Biol. *20*, 2147–2157.

Roopra, A., Qazi, R., Schoenike, B., Daley, T.J., and Morrison, J.F. (2004). Localized Domains of G9a-Mediated Histone Methylation Are Required for Silencing of Neuronal Genes. Mol. Cell *14*, 727–738.

De Rosa, A., Pellegatta, S., Rossi, M., Tunici, P., Magnoni, L., Speranza, M.C., Malusa, F., Miragliotta, V., Mori, E., Finocchiaro, G., et al. (2012). A radial glia gene marker, fatty acid binding protein 7 (FABP7), is involved in proliferation and invasion of glioblastoma cells. PLoS One *7*, e52113.

Rozpedek, W., Pytel, D., Mucha, B., Leszczynska, H., Diehl, J.A., and Majsterek, I. (2016). The Role of the PERK/eIF2α/ATF4/CHOP Signaling Pathway in Tumor Progression During Endoplasmic Reticulum Stress. Curr. Mol. Med. *16*, 533–544.

Sadakata, T., Shinoda, Y., Oka, M., Sekine, Y., Sato, Y., Saruta, C., Miwa, H., Tanaka, M., Itohara, S., and Furuichi, T. (2012). Reduced axonal localization of a Caps2 splice variant impairs axonal release of BDNF and causes autistic-like behavior in mice. Proc. Natl. Acad. Sci. *109*, 21104–21109.

Sadetzki, S., Chetrit, A., Freedman, L., Stovall, M., Modan, B., and Novikov, I. (2005). Long-term follow-up for brain tumor development after childhood exposure to ionizing radiation for tinea capitis. Radiat. Res. *163*, 424–432.

Saito, K., Dubreuil, V., Arai, Y., Wilsch-Brauninger, M., Schwudke, D., Saher, G., Miyata, T., Breier, G., Thiele, C., Shevchenko, A., et al. (2009). Ablation of cholesterol biosynthesis in neural stem cells increases their VEGF expression and angiogenesis but causes neuron apoptosis. Proc. Natl. Acad. Sci. *106*, 8350–8355.

Salven, P., Mustjoki, S., Alitalo, R., Alitalo, K., and Rafii, S. (2003). VEGFR-3 and CD133 identify a population of CD34+ lymphatic/vascular endothelial precursor cells. Blood *101*, 168–172.

Sandmann, T., Bourgon, R., Garcia, J., Li, C., Cloughesy, T., Chinot, O.L., Wick, W., Nishikawa, R., Mason, W., Henriksson, R., et al. (2015). Patients With Proneural Glioblastoma May Derive Overall Survival Benefit From the Addition of Bevacizumab to First-Line Radiotherapy and Temozolomide: Retrospective Analysis of the AVAglio Trial. J. Clin. Oncol. *33*, 2735–2744.

Sasai, Y., Kageyama, R., Tagawa, Y., Shigemoto, R., and Nakanishi, S. (1992). Two mammalian helix-loop-helix factors structurally related to Drosophila hairy and Enhancer of split. Genes Dev. *6*, 2620–2634.

Sathyan, P., Zinn, P.O., Marisetty, A.L., Liu, B., Kamal, M.M., Singh, S.K., Bady, P., Lu, L., Wani, K.M., Veo, B.L., et al. (2015). Mir-21-Sox2 Axis Delineates Glioblastoma Subtypes with Prognostic Impact. J. Neurosci. *35*, 15097–15112.

Schmidt, F., van den Eijnden, M., Pescini Gobert, R., Saborio, G.P., Carboni, S., Alliod, C., Pouly, S., Staugaitis, S.M., Dutta, R., Trapp, B., et al. (2012). Identification of VHY/Dusp15 as a Regulator of Oligodendrocyte Differentiation through a Systematic Genomics Approach. PLoS One *7*, e40457.

Schnell, A., Chappuis, S., Schmutz, I., Brai, E., Ripperger, J.A., Schaad, O., Welzl, H., Descombes, P., Alberi, L., and Albrecht, U. (2014). The Nuclear Receptor REV-ERBα Regulates Fabp7 and Modulates Adult Hippocampal Neurogenesis. PLoS One *9*, e99883.

Schoenherr, C.J., and Anderson, D.J. (1995). The neuron-restrictive silencer factor (NRSF): a coordinate repressor of multiple neuron-specific genes. Science *267*, 1360–1363.

Schweitzer, T., Vince, G.H., Herbold, C., Roosen, K., and Tonn, J.C. (2001). Extraneural metastases of primary brain tumors. J. Neurooncol. *53*, 107–114.

Seita, J., and Weissman, I.L. (2010). Hematopoietic stem cell: Self-renewal versus differentiation. Wiley Interdiscip. Rev. Syst. Biol. Med. *2*, 640–653.

Selcuk Unal, E., Zhao, R., Qiu, A., and Goldman, I.D. (2008). N-linked glycosylation and its impact on the electrophoretic mobility and function of the human proton-coupled folate transporter (HsPCFT). Biochim. Biophys. Acta - Biomembr. *1778*, 1407–1414.

Shaheen, N., Kobayashi, K., Terazono, H., Fukushige, T., Horiuchi, M., and Saheki, T. (1995). Characterization of human wild-type and mutant argininosuccinate synthetase proteins expressed in bacterial cells. Enzyme Protein *48*, 251–264.

Shao, Q., Yang, T., Huang, H., Alarmanazi, F., and Liu, G. (2017). Uncoupling of UNC5C with Polymerized TUBB3 in Microtubules Mediates Netrin-1 Repulsion. J. Neurosci. *37*, 5620–5633.

Shihabuddin, L.S., Ray, J., and Gage, F.H. (1997). FGF-2 is sufficient to isolate progenitors found in the adult mammalian spinal cord. Exp. Neurol. *148*, 577–586.

Shimojo, M. (2006). Characterization of the nuclear targeting signal of REST/NRSF. Neurosci. Lett. *398*, 161–166.

Shimojo, M. (2008). Huntingtin Regulates RE1-silencing Transcription Factor / Neuron-restrictive Silencer Factor (REST / NRSF) Nuclear Trafficking Indirectly through a Complex with REST / NRSF-interacting LIM Domain Protein (RILP) and Dynactin p150 Glued *. *283*, 34880–34886.

Shimojo, M., and Hersh, L.B. (2003). REST / NRSF-Interacting LIM Domain Protein , a Putative Nuclear Translocation Receptor. *23*, 9025–9031.

Shimojo, M., Paquette, A.J., Anderson, D.J., and Hersh, L.B. (1999). Protein kinase A regulates cholinergic gene expression in PC12 cells: REST4 silences the silencing activity of neuron-restrictive silencer factor/REST. Mol. Cell. Biol. *19*, 6788–6795.

Shimojo, M., Lee, J.H., and Hersh, L.B. (2001). Role of zinc finger domains of the transcription factor neuron-restrictive silencer factor/repressor element-1 silencing transcription factor in DNA binding and nuclear localization. J. Biol. Chem. *276*, 13121–13126.

Shin, J., Gu, C., Park, E., and Park, S. (2007). Identification of phosphotyrosine binding domain-containing proteins as novel downstream targets of the EphA8 signaling function. Mol. Cell. Biol. *27*, 8113–8126.

Shin, J., Berg, D.A., Zhu, Y., Shin, J.Y., Song, J., Bonaguidi, M.A., Enikolopov, G., Nauen, D.W., Christian, K.M., Ming, G., et al. (2015). Single-Cell RNA-Seq with Waterfall Reveals Molecular Cascades underlying Adult Neurogenesis. Cell Stem Cell *17*, 360–372.

Sidaway, P. (2017). CNS cancer: Glioblastoma subtypes revisited. Nat. Rev. Clin. Oncol. 2017 1410.

Silber, J., Lim, D.A., Petritsch, C., Persson, A.I., Maunakea, A.K., Yu, M., Vandenberg, S.R., Ginzinger, D.G., James, C.D., Costello, J.F., et al. (2008). miR-124 and miR-137 inhibit proliferation of glioblastoma multiforme

cells and induce differentiation of brain tumor stem cells. BMC Med. *6*, 14.

Singh, A., Rokes, C., Gireud, M., Fletcher, S., Baumgartner, J., Fuller, G., Stewart, J., Zage, P., and Gopalakrishnan, V. (2011). Retinoic acid induces REST degradation and neuronal differentiation by modulating the expression of SCF(β-TRCP) in neuroblastoma cells. Cancer *117*, 5189–5202.

Singh, S.K., Clarke, I.D., Terasaki, M., Bonn, V.E., Hawkins, C., Squire, J., and Dirks, P.B. (2003). Identification of a cancer stem cell in human brain tumors. Cancer Res. *63*, 5821–5828.

Singh, S.K., Hawkins, C., Clarke, I.D., Squire, J.A., Bayani, J., Hide, T., Henkelman, R.M., Cusimano, M.D., and Dirks, P.B. (2004). Identification of human brain tumour initiating cells. Nature *432*, 396–401.

Singh, S.K., Kagalwala, M.N., Parker-Thornburg, J., Adams, H., and Majumder, S. (2008). REST maintains self-renewal and pluripotency of embryonic stem cells. Nature *453*, 223–227.

Singh, S.K., Kagalwala, M.N., Parker-Thornburg, J., Adams, H., and Majumder, S. (2010). Singh et al. reply. Nature *467*, E5–E5.

Singh, S.K., Marisetty, A., Sathyan, P., Kagalwala, M., Zhao, Z., and Majumder, S. (2015). REST-miR-21-SOX2 axis maintains pluripotency in E14Tg2a.4 embryonic stem cells. Stem Cell Res. *15*, 305–311.

Sirard, C., Lapidot, T., Vormoor, J., Cashman, J.D., Doedens, M., Murdoch, B., Jamal, N., Messner, H., Addey, L., Minden, M., et al. (1996). Normal and leukemic SCID-repopulating cells (SRC) coexist in the bone marrow and peripheral blood from CML patients in chronic phase, whereas leukemic SRC are detected in blast crisis. Blood *87*, 1539–1548.

Smart, I., and Leblond, C.P. (1961). Evidence for division and transformations of neuroglia cells in the mouse brain, as derived from radioautography after injection of thymidine-H3. J. Comp. Neurol. *116*, 349–367.

Smith, J.S., Wang, X.Y., Qian, J., Hosek, S.M., Scheithauer, B.W., Jenkins, R.B., and James, C.D. (2000). Amplification of the platelet-derived growth factor receptor-A (PDGFRA) gene occurs in oligodendrogliomas with grade IV anaplastic features. J. Neuropathol. Exp. Neurol. *59*, 495–503.

Smith, T.H., Blume, L.C., Straiker, A., Cox, J.O., David, B.G., McVoy, J.R.S., Sayers, K.W., Poklis, J.L., Abdullah, R.A., Egertová, M., et al. (2015). Cannabinoid receptor-interacting protein 1a modulates CB1 receptor signaling and regulation. Mol. Pharmacol. *87*, 747–765.

Song, X., Allen, R.A., Dunn, S.T., Fung, K.M., Farmer, P., Gandhi, S., Ranjan, T., Demopoulos, A., Symons, M., Schulder, M., et al. (2011). Glioblastoma with PNET-like components has a higher frequency of isocitrate dehydrogenase 1 (IDH1) mutation and likely a better prognosis than primary glioblastoma. Int. J. Clin. Exp. Pathol. *4*, 651–660.

Spalding, K.L., Bergmann, O., Alkass, K., Bernard, S., Salehpour, M., Huttner, H.B., Boström, E., Westerlund, I., Vial, C., Buchholz, B.A., et al. (2013). Dynamics of Hippocampal Neurogenesis in Adult Humans. Cell *153*, 1219–1227.

Stockhammer, F., Misch, M., Helms, H.-J., Lengler, U., Prall, F., von Deimling, A., and Hartmann, C. (2012). IDH1/2 mutations in WHO grade II astrocytomas associated with localization and seizure as the initial symptom. Seizure *21*, 194–197.

Stoll, E.A., Makin, R., Sweet, I.R., Trevelyan, A.J., Miwa, S., Horner, P.J., and Turnbull, D.M. (2015). Neural Stem Cells in the Adult Subventricular Zone Oxidize Fatty Acids to Produce Energy and Support Neurogenic Activity. Stem Cells *33*, 2306–2319.

Stupp, R., Mason, W.P., van den Bent, M.J., Weller, M., Fisher, B., Taphoorn, M.J.B., Belanger, K., Brandes, A.A., Marosi, C., Bogdahn, U., et al. (2005). Radiotherapy plus concomitant and adjuvant temozolomide for glioblastoma. N. Engl. J. Med. *352*, 987–996.

Subramanian, A., Harris, A., Piggott, K., Shieff, C., and Bradford, R. (2002). Metastasis to and from the central nervous system--the “relatively protected site”. Lancet. Oncol. *3*, 498–507.

Subramanian, A., Tamayo, P., Mootha, V.K., Mukherjee, S., Ebert, B.L., Gillette, M.A., Paulovich, A., Pomeroy, S.L., Golub, T.R., Lander, E.S., et al. (2005). Gene set enrichment analysis: a knowledge-based approach for interpreting genome-wide expression profiles. Proc. Natl. Acad. Sci. U. S. A. *102*, 15545–15550.

Sulli, G., Rommel, A., Wang, X., Kolar, M.J., Puca, F., Saghatelian, A., Plikus, M. V., Verma, I.M., and Panda, S. (2018). Pharmacological activation of REV-ERBs is lethal in cancer and oncogene-induced senescence. Nature

553, 351–355.

Sun, L., Hui, A.-M., Su, Q., Vortmeyer, A., Kotliarov, Y., Pastorino, S., Passaniti, A., Menon, J., Walling, J., Bailey, R., et al. (2006). Neuronal and glioma-derived stem cell factor induces angiogenesis within the brain. Cancer Cell *9*, 287–300.

Sun, Y.-M., Greenway, D.J., Johnson, R., Street, M., Belyaev, N.D., Deuchars, J., Bee, T., Wilde, S., and Buckley, N.J. (2005). Distinct profiles of REST interactions with its target genes at different stages of neuronal development. Mol. Biol. Cell *16*, 5630–5638.

Sun, Y., Pollard, S., Conti, L., Toselli, M., Biella, G., Parkin, G., Willatt, L., Falk, A., Cattaneo, E., and Smith, A. (2008a). Long-term tripotent differentiation capacity of human neural stem (NS) cells in adherent culture. Mol. Cell. Neurosci. *38*, 245–258.

Sun, Y.M., Cooper, M., Finch, S., Lin, H.H., Chen, Z.F., Williams, B.P., and Buckley, N.J. (2008b). Rest-mediated regulation of extracellular matrix is crucial for neural development. PLoS One *3*.

Suzuki, T., Maruno, M., Wada, K., Kagawa, N., Fujimoto, Y., Hashimoto, N., Izumoto, S., and Yoshimine, T. (2004). Genetic analysis of human glioblastomas using a genomic microarray system. Brain Tumor Pathol. *21*, 27–34.

Tabuchi, A., Yamada, T., Sasagawa, S., Naruse, Y., Mori, N., and Tsuda, M. (2002). REST4-Mediated Modulation of REST/NRSF-Silencing Function during BDNF Gene Promoter Activation. Biochem. Biophys. Res. Commun. *290*, 415–420.

Taphoorn, M.J., Stupp, R., Coens, C., Osoba, D., Kortmann, R., van den Bent, M.J., Mason, W., Mirimanoff, R.O., Baumert, B.G., Eisenhauer, E., et al. (2005). Health-related quality of life in patients with glioblastoma: a randomised controlled trial. Lancet Oncol. *6*, 937–944.

Tapia-Ramrez, J., Eggen, B.J.L., Peral-Rubio, M.J., Toledo-Aral, J.J., and Mandel, G. (1997). A single zinc finger motif in the silencing factor REST represses the neural-specific type II sodium channel promoter. Biochemistry *94*, 1177–1182.

Tawadros, T., Martin, D., Abderrahmani, A., Leisinger, H.-J., Waeber, G., and Haefliger, J.-A. (2005). IB1/JIP-1 controls JNK activation and increased during prostatic LNCaP cells neuroendocrine differentiation. Cell. Signal. *17*, 929–939.

Temple, S. (1989). Division and differentiation of isolated CNS blast cells in microculture. Nature *340*, 471–473.

Tetreault, M.-P., Yang, Y., and Katz, J.P. (2013). Krüppel-like factors in cancer. Nat. Rev. Cancer *13*, 701–713.

Thiel, G., Lietz, M., and Cramer, M. (1998). Biological activity and modular structure of RE-1-silencing transcription factor (REST), a repressor of neuronal genes. J. Biol. Chem. *273*, 26891–26899.

Tindi, J.O., Chávez, A.E., Cvejic, S., Calvo-Ochoa, E., Castillo, P.E., and Jordan, B.A. (2015). ANKS1B Gene Product AIDA-1 Controls Hippocampal Synaptic Transmission by Regulating GluN2B Subunit Localization. J. Neurosci. *35*, 8986–8996.

Tivnan, A., Zhao, J., Johns, T.G., Day, B.W., Stringer, B.W., Boyd, A.W., Tiwari, S., Giles, K.M., Teo, C., and McDonald, K.L. (2014). The tumor suppressor microRNA, miR-124a, is regulated by epigenetic silencing and by the transcriptional factor, REST in glioblastoma. Tumor Biol. *35*, 1459–1465.

Tripathi, S., Pohl, M.O., Zhou, Y., Rodriguez-Frandsen, A., Wang, G., Stein, D.A., Moulton, H.M., DeJesus, P., Che, J., Mulder, L.C.F., et al. (2015). Meta- and Orthogonal Integration of Influenza "OMICs" Data Defines a Role for UBR4 in Virus Budding. Cell Host Microbe *18*, 723–735.

Tropepe, V., Coles, B.L., Chiasson, B.J., Horsford, D.J., Elia, A.J., McInnes, R.R., and van der Kooy, D. (2000). Retinal stem cells in the adult mammalian eye. Science *287*, 2032–2036.

Tusher, V.G., Tibshirani, R., and Chu, G. (2001). Significance analysis of microarrays applied to the ionizing radiation response. Proc. Natl. Acad. Sci. *98*, 5116–5121.

Uhrbom, L., Hesselager, G., Nistér, M., and Westermark, B. (1998). Induction of brain tumors in mice using a recombinant platelet-derived growth factor B-chain retrovirus. Cancer Res. *58*, 5275–5279.

Urbán, N., and Guillemot, F. (2014). Neurogenesis in the embryonic and adult brain: same regulators,

different roles. Front. Cell. Neurosci. *8*, 396.

Urbán, N., van den Berg, D.L.C., Forget, A., Andersen, J., Demmers, J.A.A., Hunt, C., Ayrault, O., and Guillemot, F. (2016). Return to quiescence of mouse neural stem cells by degradation of a proactivation protein. Science *353*, 292–295.

Verhaak, R.G.W., Hoadley, K.A., Purdom, E., Wang, V., Qi, Y., Wilkerson, M.D., Miller, C.R., Ding, L., Golub, T., Mesirov, J.P., et al. (2010). Integrated Genomic Analysis Identifies Clinically Relevant Subtypes of Glioblastoma Characterized by Abnormalities in PDGFRA, IDH1, EGFR, and NF1. Cancer Cell *17*, 98–110.

Wagoner, M.P., and Roopra, A. (2012). A REST derived gene signature stratifies glioblastomas into chemotherapy resistant and responsive disease. BMC Genomics *13*.

Wagoner, M.P., Gunsalus, K.T.W., Schoenike, B., Richardson, A.L., Friedl, A., and Roopra, A. (2010). The Transcription Factor REST Is Lost in Aggressive Breast Cancer. PLoS Genet. *6*, e1000979.

Wang, Q., Hu, B., Hu, X., Kim, H., Squatrito, M., Scarpace, L., deCarvalho, A.C., Lyu, S., Li, P., Li, Y., et al. (2017). Tumor Evolution of Glioma-Intrinsic Gene Expression Subtypes Associates with Immunological Changes in the Microenvironment. Cancer Cell *32*, 42–56.e6.

Watanabe, K., Tachibana, O., Sata, K., Yonekawa, Y., Kleihues, P., and Ohgaki, H. (1996). Overexpression of the EGF receptor and p53 mutations are mutually exclusive in the evolution of primary and secondary glioblastomas. Brain Pathol. *6*, 217-23; discussion 23-4.

Watanabe, T., Yokoo, H., Yokoo, M., Yonekawa, Y., Kleihues, P., and Ohgaki, H. (2001). Concurrent inactivation of RB1 and TP53 pathways in anaplastic oligodendrogliomas. J. Neuropathol. Exp. Neurol. *60*, 1181–1189.

Weiss, S., Dunne, C., Hewson, J., Wohl, C., Wheatley, M., Peterson, A.C., and Reynolds, B.A. (1996). Multipotent CNS stem cells are present in the adult mammalian spinal cord and ventricular neuroaxis. J. Neurosci. *16*, 7599–7609.

Weller, M., van den Bent, M., Hopkins, K., Tonn, J.C., Stupp, R., Falini, A., Cohen-Jonathan-Moyal, E., Frappaz, D., Henriksson, R., Balana, C., et al. (2014). EANO guideline for the diagnosis and treatment of anaplastic gliomas and glioblastoma. Lancet Oncol. *15*, e395–e403.

Weller, M., Wick, W., Aldape, K., Brada, M., Berger, M., Pfister, S.M., Nishikawa, R., Rosenthal, M., Wen, P.Y., Stupp, R., et al. (2015). Glioma. Nat. Rev. Dis. Prim. *1*, 15017.

Wen, P.Y., and Kesari, S. (2008). Malignant Gliomas in Adults. N. Engl. J. Med. *359*, 492–507.

Westbrook, T.F., Martin, E.S., Schlabach, M.R., Leng, Y., Liang, A.C., Feng, B., Zhao, J.J., Roberts, T.M., Mandel, G., Hannon, G.J., et al. (2005). A genetic screen for candidate tumor suppressors identifies REST. Cell *121*, 837–848.

Westbrook, T.F., Hu, G., Ang, X.L., Mulligan, P., Pavlova, N.N., Liang, A., Leng, Y., Maehr, R., Shi, Y., Harper, J.W., et al. (2008). SCFβ-TRCP controls oncogenic transformation and neural differentiation through REST degradation. Nature *452*, 370–374.

Wick, W., Menn, O., Meisner, C., Steinbach, J., Hermisson, M., Tatagiba, M., and Weller, M. (2005). Pharmacotherapy of epileptic seizures in glioma patients: who, when, why and how long? Onkologie *28*, 391–396.

Wick, W., Gorlia, T., Bendszus, M., Taphoorn, M., Sahm, F., Harting, I., Brandes, A.A., Taal, W., Domont, J., Idbaih, A., et al. (2017). Lomustine and Bevacizumab in Progressive Glioblastoma. N. Engl. J. Med. *377*, 1954–1963.

Wirsching, H.-G., Galanis, E., and Weller, M. (2016). Glioblastoma. In Handbook of Clinical Neurology, pp. 381–397.

Wood, I.C., Belyaev, N.D., Bruce, A.W., Jones, C., Mistry, M., Roopra, A., and Buckley, N.J. (2003). Interaction of the repressor element 1-silencing transcription factor (REST) with target genes. J. Mol. Biol. *334*, 863–874.

Woolard, K., and Fine, H.A. (2009). Glioma Stem Cells: Better Flat Than Round. Cell Stem Cell *4*, 466–467.

Wu, J., and Xie, X. (2006). Comparative sequence analysis reveals an intricate network among REST, CREB and miRNA in mediating neuronal gene expression. Genome Biol. *7*, R85.

Xie, X., Rigor, P., and Baldi, P. (2009). MotifMap: a human genome-wide map of candidate regulatory motif

sites. Bioinformatics *25*, 167–174.

Xie, Z., Jones, A., Deeney, J.T., Hur, S.K., and Bankaitis, V.A. (2016). Inborn Errors of Long-Chain Fatty Acid β-Oxidation Link Neural Stem Cell Self-Renewal to Autism. Cell Rep. *14*, 991–999.

Yamada, Y., Aoki, H., Kunisada, T., and Hara, A. (2010). Rest Promotes the Early Differentiation of Mouse ESCs but Is Not Required for Their Maintenance. Cell Stem Cell *6*, 10–15.

Yan, G.-N., Lv, Y.-F., Yang, L., Yao, X.-H., Cui, Y.-H., and Guo, D.-Y. (2013). Glioma stem cells enhance endothelial cell migration and proliferation via the Hedgehog pathway. Oncol. Lett. *6*, 1524–1530.

Yang, M., Gocke, C.B., Luo, X., Borek, D., Tomchick, D.R., Machius, M., Otwinowski, Z., and Yu, H. (2006). Structural Basis for CoREST-Dependent Demethylation of Nucleosomes by the Human LSD1 Histone Demethylase. Mol. Cell *23*, 377–387.

Yang, W., Soares, J., Greninger, P., Edelman, E.J., Lightfoot, H., Forbes, S., Bindal, N., Beare, D., Smith, J.A., Thompson, I.R., et al. (2013). Genomics of Drug Sensitivity in Cancer (GDSC): a resource for therapeutic biomarker discovery in cancer cells. Nucleic Acids Res. *41*, D955-61.

Yeo, M., Lee, S.-K., Lee, B., Ruiz, E.C., Pfaff, S.L., and Gill, G.N. (2005). Small CTD Phosphatases Function in Silencing Neuronal Gene Expression. Science (80-.). *307*, 596–600.

Yi, L., Cui, Y., Xu, Q., and Jiang, Y. (2016). Stabilization of LSD1 by deubiquitinating enzyme USP7 promotes glioblastoma cell tumorigenesis and metastasis through suppression of the p53 signaling pathway. Oncol. Rep. *36*, 2935–2945.

Yin, A.H., Miraglia, S., Zanjani, E.D., Almeida-Porada, G., Ogawa, M., Leary, A.G., Olweus, J., Kearney, J., and Buck, D.W. (1997). AC133, a novel marker for human hematopoietic stem and progenitor cells. Blood *90*, 5002–5012.

Yuile, P., Dent, O., Cook, R., Biggs, M., and Little, N. (2006). Survival of glioblastoma patients related to presenting symptoms, brain site and treatment variables. J. Clin. Neurosci. *13*, 747–751.

Zhang, D., Li, Y., Wang, R., Li, Y., Shi, P., Kan, Z., and Pang, X. (2016). Inhibition of REST Suppresses Proliferation and Migration in Glioblastoma Cells. Int. J. Mol. Sci. *17*, 664.

Zhang, P., Pazin, M.J., Schwartz, C.M., Becker, K.G., Wersto, R.P., Dilley, C.M., and Mattson, M.P. (2008). Nontelomeric TRF2-REST Interaction Modulates Neuronal Gene Silencing and Fate of Tumor and Stem Cells. Curr. Biol. *18*, 1489–1494.

Zhang, P., Lathia, J.D., Flavahan, W.A., Rich, J.N., and Mattson, M.P. (2009). Squelching glioblastoma stem cells by targeting REST for proteasomal degradation. Trends Neurosci. *32*, 559–565.

Zhang, X., Zhang, R., Zheng, Y., Shen, J., Xiao, D., Li, J., Shi, X., Huang, L., Tang, H., Liu, J., et al. (2013). Expression of gamma-aminobutyric acid receptors on neoplastic growth and prediction of prognosis in non-small cell lung cancer. J. Transl. Med. *11*, 102.

Zhu, T.S., Costello, M.A., Talsma, C.E., Flack, C.G., Crowley, J.G., Hamm, L.L., He, X., Hervey-Jumper, S.L., Heth, J.A., Muraszko, K.M., et al. (2011). Endothelial cells create a stem cell niche in glioblastoma by providing NOTCH ligands that nurture self-renewal of cancer stem-like cells. Cancer Res. *71*, 6061–6072.

Zhu, Z., Khan, M.A., Weiler, M., Blaes, J., Jestaedt, L., Geibert, M., Zou, P., Gronych, J., Bernhardt, O., Korshunov, A., et al. (2014). Targeting Self-Renewal in High-Grade Brain Tumors Leads to Loss of Brain Tumor Stem Cells and Prolonged Survival. Cell Stem Cell *15*, 185–198.

Zuccato, C., Tartari, M., Crotti, A., Goffredo, D., Valenza, M., Conti, L., Cataudella, T., Leavitt, B.R., Hayden, M.R., Timmusk, T., et al. (2003). Huntingtin interacts with REST/NRSF to modulate the transcription of NRSE-controlled neuronal genes. Nat. Genet. *35*, 76–83.

Side Project

Inducible Alpha-Synuclein Expression Affects Human Neural Stem Cells' Behavior

Contents

PREFACE	170
AUTHORS CONTRIBUTION	170
INDUCIBLE ALPHA-SYNUCLEIN EXPRESSION AFFECTS HUMAN NEURAL STEM CELLS' BEHAVIOR	171

Preface

The following manuscript is the result of a side project I carried out during my PhD. Aim of this work was to establish a novel hNSC model to study α-Synuclein (aSyn) pathogenesis *in vitro* and characterise the effect of aSyn on hNSCs multipotency and dopaminergic differentiation capabilities.

Authors contribution

The following research has been carried out exclusively by the persons working in the Laboratory of Stem Cell Biology, Centre for Integrative Biology, Università degli Studi di Trento, Trento, Italy. In particular: Jacopo Zasso (PhD Student), Ahmed Mastad (Master Student), Alessandro Cutarelli (Post-doctoral fellow), and Prof. Luciano Conti (Laboratory head).

L.C. conceived the idea. L.C. and J.Z. designed the experiments. J.Z., M.A., and A.C. performed the experiments. L.C., J.Z., and A.M. analysed the data and prepared the figures. L.C. and J.Z. wrote the manuscript. L.C. supervised the project.

STEM CELLS AND DEVELOPMENT
Volume 27, Number 14, 2018

DOI: 10.1089/scd.2018.0011

Inducible Alpha-Synuclein Expression Affects Human Neural Stem Cells' Behavior

Jacopo Zasso, Mastad Ahmed, Alessandro Cutarelli, and Luciano Conti

Converging evidence suggest that levels of alpha-synuclein (aSyn) expression play a critical role in Parkinson's disease (PD). Several mutations of the SNCA gene, encoding for aSyn have been associated to either the familial or the sporadic forms of PD. Nonetheless, the mechanism underlying wild-type aSyn-mediated neurotoxicity in neuronal cells as well as its specific driving role in PD pathogenesis has yet to be fully clarified. In this view, the development of proper in vitro cellular systems is a crucial step. In this study, we present a novel human Tet-on human neural stem cell (hNSC) line, in which aSyn timing and level of expression can be tightly experimentally tuned. Induction of aSyn in self-renewing hNSCs leads to progressive formation of aSyn aggregates and impairs their proliferation and cell survival. Furthermore, aSyn induction during the neuronal differentiation process results in reduced neuronal differentiation and increased number of astrocytes and undifferentiated cells in culture. Finally, acute aSyn induction in hNSC-derived dopaminergic neuronal cultures results in cell toxicity. This novel conditional in vitro cell model system may be a valuable tool for dissecting of aSyn pathogenic effects in hNSCs and neurons and in developing new potential therapeutic strategies.

Keywords: alpha-synuclein, human neural stem cells, Parkinson's disease, neurons, inducible expression

Introduction

Lewy bodies (LBs) are considered a capital hallmark of Parkinson's disease (PD). They consist of cytoplasmic inclusions mainly composed of fibrillar misfolded alpha-synuclein (aSyn) aggregates within the brain parenchyma [1]. aSyn is a small 140-residue protein highly abundant in neurons and particularly localized at the presynaptic terminals, where it is thought to play roles in vesicle trafficking and in the assembling of the SNARE complex for neurotransmitter release [2].

Mutations of the *SNCA* gene, encoding for aSyn, are either associated to rare familial PD or represent risk factors for sporadic PD [3,4]. Furthermore, increased *SCNA* copy number variation has been shown to be causal for PD, thus suggesting that increased aSyn protein levels are sufficient to trigger the disease [5]. In PD patients, aggregation of aSyn in LBs has been shown, resulting in its mislocalization and loss of function, ultimately leading to the loss of dopaminergic neurons. Besides its role in mature neurons, in vivo aSyn overexpression has been shown to affect proliferative potential of mouse hippocampal neural stem cells (NSCs), resulting in a reduction of the pool of neural progenitors and decreased neuronal differentiation and maturation [6–9]. Also, ectopic expression of aSyn was shown to affect the migration of NSCs in mouse subventricular zone [10].

Despite the association to PD has been known for decades, aSyn function in human neural stem cells (hNSCs) and neurons as well as its involvement in PD are still poorly understood. So far, the main limitations have been due to the inaccessibility of adequate in vitro cellular models. Indeed, most of the studies aimed at defining a clear role for aSyn in normal and PD neurons have been so far carried out using either non-human systems, including rodent culture [6,7,10], non-neuronal transformed cell lines [11], or noncentral nervous system (CNS)-derived neuronal-like cells [12,13].

More recently, the advent of human-induced pluripotent stem cells (hiPSCs)' technology has widened opportunities to model human conditions, including the possibility to generate *bona fide* hNSCs and mature neurons and consequently matching the affected cells in neurodegenerative disorders [14]. hiPSC lines derived from PD patients carrying triplication of the *SNCA locus* have been reported [15]. These cells were proven to efficiently differentiate and mature into TH^{+ve} dopaminergic neurons while showing a twofold increase in aSyn protein levels with respect to hiPSCs derived from unaffected relatives and recapitulating some aspects of the patient physiology. Interestingly, neuronal precursor cells derived from these PD hiPSCs have been reported to exhibit significant deficiencies in growth, viability, cellular energy metabolism, and stress resistance [16], thus indicating that aSyn may play important roles in hNSC physiology.

Similarly, wild-type (wt) aSyn overexpression in fetal cortex-derived hNSCs has been shown to impair cell growth and neuronal versus glial lineage commitment [17]. Finally,

Centre for Integrative Biology-CIBIO, Università degli Studi di Trento, Trento, Italy

aSyn overexpression has been described to reduce the number of mouse secondary neurospheres formed and to affect NSC morphology and cell cycle progression, leading to their accelerated differentiation [10]. These studies suggest that there is a link between neurogenesis, aSyn, and neurodegenerative diseases [18].

In this study, we report the generation of a novel in vitro cell system in which levels and timing of human wt aSyn expression can be experimentally tightly controlled in hiPSC-derived long-term expandable NSCs. Following induction, a progressive increase of aSyn levels can be achieved, leading to the formation of aSyn cytoplasmic aggregates. This versatile system allows to investigate the effects of aSyn expression on hNSCs behavior, including self-renewal and differentiation programs.

Our results show that induction of aSyn leads to a reduction in hNSCs growth accompanied by an increased susceptibility to apoptosis. During neuronal differentiation process, aSyn induction affects neurogenic potential and induces an increase in the number of astrocytes and undifferentiated cells in culture. Furthermore, acute aSyn induction resulted in enhanced apoptotic cell death in hNSC-derived dopaminergic neurons.

This novel in vitro cell system may represent a valuable tool for studying aSyn-driven pathogenic-relevant mechanisms in hNSCs and their mature derivatives, and for screening potential therapeutics.

Materials and Methods

Cell cultures

AF22 cells (kindly donated by Prof. Austin Smith, Cambridge Stem Cell Institute, University of Cambridge, UK) were previously described [19]. Cells were routinely passaged every 2–3 days at a density of $2.5–3.5 \times 10^4$ cells/cm^2 in hNSCs Self-renewal medium composed of Dulbecco's modified Eagle's medium/Nutrient Mixture F-12 (DMEM/F-12; Thermo Fisher Scientific), N2 supplement (1%; Thermo Fisher Scientific), B27 supplement (1%; Thermo Fisher Scientific), EGF (10 ng/mL; PeproTech), bFGF (10 ng/mL; PeproTech), and GlutaMAX (2 mM; Thermo Fisher Scientific). Briefly, before seeding the cells, plastic culture vessels were treated with 3 μg/mL Laminin (Thermo Fisher Scientific) at 37°C for 3–5 h. For passaging, cells were incubated for 1–2 min with StemPro Accutase (Thermo Fisher Scientific) and centrifuged at 260 *g* for 3 min. Pellet was resuspended in fresh medium and plated onto the laminin-coated vessels.

For general neuronal differentiation, cells were seeded on laminin-coated cell culture-grade plasticware at a density of 8×10^3 cells/cm^2 in self-renewal medium. The following day, medium was shifted to self-renewal medium deprived of EGF and bFGF. After 3 additional days, medium was replaced with neuronal differentiation medium composed of a 1:1 mix of Neurobasal (Thermo Fisher Scientific), and DMEM/F-12, N2 supplement 1%, B27 supplement 1%, cAMP 300 ng/mL, and GlutaMAX. For aSyn induction during differentiation process, a medium supplemented with doxycycline was replaced every 24 h.

For dopaminergic neuronal differentiation, self-renewing cultures were maintained in the presence of 200 ng/mL of both FGF8 and SHH for 2–3 weeks to specify a ventral midbrain dopaminergic fate, before differentiating them as in the general neuronal differentiation. Seven hundred and fifty nanograms per milliliter of doxycycline were added at 21 days in vitro (DIV) every 24 h for 4 DIV before fixing the cells for immunocytochemistry.

Lentiviral particle preparation and AF22 cell infection

Lentiviral particles carrying the pLVX-TetOne-Puro-human aSyn vector (kindly donated by Dr. Tilo Kunath, University of Edinburgh, UK) were prepared. This vector, based on the pLVX-TetOn-Puro plasmid (Clontech) is specifically designed to carry on a single vector the complementary DNA (cDNA) for a tetracycline transactivator (Tet-on 3G) and a tetracycline responsive promoter (TREGS promoter) containing seven tetracycline-responsive elements (TRE) controlling the expression of the cDNA for human aSyn. The vector also carries a puromycin resistance cassette for selection of infected cells.

For lentiviral particle preparation, 6×10^4 HEK 293T cells/cm^2 were seeded in DMEM containing 10% fetal bovine serum (FBS) and left undisturbed overnight. The following day, cells were transfected by $CaPO_4$ method with 20 μg of pLVX-TetOne-Puro-human aSyn, 15 μg of psPAX2 vector (kindly provided by Prof. M. Pizzato, University of Trento, Italy), and 5 μg of VSV-G. Two days after transfection, the supernatant was collected and concentrated using the Lenti-X concentrator reagent (Clontech) following the manufacturer's recommendation.

For AF22 cell infection, 10 μL of concentrated lentiviral particles were used to infect 2×10^4 cells/cm^2. After 8 h, the medium was completely changed, and 72 h later, positive selection of the transduced cells was started with 0.3 μg/mL puromycin (Thermo Fisher Scientific) until the noninfected control cells died completely. Cultures were subsequently selected with higher doses of puromycin as discussed in the Results section.

Cell growth assay

For growth assay, 2×10^3 cells/cm^2 were seeded onto laminin-coated 24-well plates. aSyn induction was achieved by treatment with 750 ng/mL doxycycline added to the cultures and the medium was renewed every day. Cells were fixed at specific time points by using 4% paraformaldehyde for 15 min at room temperature (RT) and then nuclei were stained with Hoechst 33258 (Thermo Fisher Scientific). Cell counting was performed using Operetta High-Content Imaging System (PerkinElmer). Images were collected with a 10× long working distance objective considering technical quadruplicate for each time point and the cell number was determined using the software Harmony 4.1 (PerkinElmer) by the segmentation of the nuclear region.

Immunocytochemistry and evaluation of aSyn aggregates

For immunofluorescence assay, cells were fixed with 4% paraformaldehyde for 15 min at RT, then permeabilized with 0.5% Triton X-100 in phosphate-buffered saline (PBS) for 15 min at RT and blocked with a blocking solution (5% FBS, 0.3% Triton X-100 in PBS) for 2 h at RT. Cultures were then incubated over-night at 4°C with specific primary

antibodies (Supplementary Table S1; Supplementary Data are available online at www.liebertpub.com/scd) diluted in a blocking solution. After three rinses with PBS, cells were incubated with the appropriate secondary antibodies (Supplementary Table S1) for 2 h and nuclei counterstained with Hoechst 33258 before imaging with a Leica DMIL inverted fluorescent microscope. For the quantification of specific immunopositive cells, at least 3,000 cells per condition for every antigen were counted. Data were normalized on the total number of cells in every field.

For evaluation of aSyn aggregation, cells were treated with 750 ng/mL of doxycycline for 12 days. Cultures were fixed with 4% paraformaldehyde for 15 min at RT and stained with anti-aSyn antibody. Nuclei and cytoplasm were counterstained using Hoechst 33258 and CellMask Deep Red (Molecular Probes). Cells were analyzed using the Operetta High-Content Imaging System. Images were collected using a 20× long WD objective considering technical quadruplicate and analyzed with Harmony 4.1 software. Briefly, cells were identified by the segmentation of the nuclear region based on the Hoechst 33258 signal and cytoplasm region of interest (ROI) was defined based on the CellMask signal. aSyn aggregates were detected as fluorescent spots inside the ROI. Number of objects, area, and intensity of the signal were calculated for each well and normalized on the number of $aSyn^{low/Med-}$ and $aSyn^{high}$-intensity aSyn immunoreactive cells.

For the quantitative evaluation of the effect of aSyn induction on mitochondrial number, cells were treated with 750 ng/mL of doxycycline for 5 days, before fixing with 4% paraformaldehyde for 15 min at RT and stained with Mitotracker (Molecular Probes) to image mitochondria as recommended by the manufacturer. Nuclei and cytoplasm were counterstained using Hoechst 33258 and CellMask Deep Red (Molecular Probes). Cells were analyzed using the Operetta High-Content Imaging System. Images were collected and analyzed as described above. Briefly, cells were identified by the segmentation of the nuclear region based on the Hoechst 33258 signal and cytoplasm. ROI was defined based on the CellMask signal. Mitochondria were detected as fluorescent spots inside the ROI. Area and number of objects were calculated for each well and normalized on the number of cells.

Western blot analysis

Cells were lysed using the sodium dodecyl sulfate (SDS) sample buffer (62.5 mM Tris-HCl pH 6.8, 2% SDS, 10% Glycerol, 50 mM DTT) and boiled for 5 min at 95°C before loading into a 15% polyacrylamide gel run at 15 mA. After transfer on PVDF membrane at 100 V constant for 2 h, proteins were incubated in 0.4% paraformaldehyde in PBS solution for 30 min at RT as previously reported [20] and then in blocking solution (10% milk) in TBS-T for 1 h. Membranes were further incubated O/N at 4°C in agitation with primary antibody. After the washing step with TBS-T, membranes were incubated with the secondary antibody for 2 h. Both primary and secondary antibodies were prepared in TBS-T supplemented with 5% non-fat milk diluted in TBS-T. Signal was detected using Clarity ECL reagents (Bio-Rad) in a dark chamber Uvitec Alliance (Uvitec) and the manufacturer software to acquire and analyze the data.

Statistical analysis

Statistical significance was assayed using a two-sided unpaired Student's *t*-test or two-way analysis of variance with Bonferroni post hoc test using the GraphPad Prism software. Data distribution was assessed for normality using the Shapiro–Wilk test. $P < 0.05$ was considered statistically significant.

Results

Modulation of wt aSyn expression in AF22 Tet-On aSyn cells

To generate a hNSC line for the inducible expression of wt aSyn, hiPSC-derived AF22 cells were infected with lentiviral particles carrying the pLVX-TetOn-Puro-human αSyn vector. Following infection, cultures were exposed to 1 μg/mL puromycin, chosen as optimal puromycin dose that allows for effective selection without altering the normal self-renewal potential of the resistant cells (Supplementary Fig. S1A). AF22 Tet-On aSyn cells selected with this puromycin dose exhibited low aSyn basal expression levels that increased 7.7-fold following treatment with doxycycline for 72 h (Supplementary Fig. S1B). Based on our previous experience with Tet-On systems, the abovementioned induction experiments were performed using a 750 ng/mL dose of doxycycline.

To test if AF22 Tet-On aSyn cells show a dose-dependent level of induction and to test at which dose of doxycycline it reached the maximum level of induction, we treated the cultures for 72 h with different concentrations of doxycycline (0, 100, 250, 500, 750, and 1,000 ng/mL). A clear dose-response relationship in the induction of aSyn expression levels was found, reaching a maximum plateau of eightfold induction already at 750 ng/mL doxycycline treatment (Supplementary Fig. S2A). Higher doses of doxycycline did not lead to a significant increase of aSyn induction levels. Based on these results, we confirmed 750 ng/mL doxycycline as the optimal dose for further analyses reported in this study.

Short-term time-course analysis of doxycycline induction on AF22 Tet-On aSyn cells (Fig. 1A) showed a progressive increase of aSyn expression levels along with time of doxycycline treatment (2.2-, 5.3-, and 7.9-fold induction at 24, 48, and 72 h of doxycycline treatment, respectively) (Fig. 1B). Immunofluorescence assay performed on these cultures showed that not all of the aSyn immunoreactive cells exhibited the same levels of expression, with even a fraction of the cells that barely showed any transgene expression (Fig. 1C). Quantitative analysis revealed that $72.21\% \pm 16.64\%$ of cells in culture were $aSyn^{+ve}$, the remaining showing very low or undetectable aSyn immunoreactivity (Fig. 1D). Furthermore, the pool of $aSyn^{+ve}$ cells can be divided in $30.3\% \pm 8.21\%$ cells exhibiting high aSyn immunoreactivity ($aSyn^{high}$ cells) and $69.67\% \pm 8.05\%$ cells exhibiting low/medium aSyn immunoreactivity ($aSyn^{low/Med}$ cells) (Fig. 1E).

Longer time-course analysis of doxycycline induction on AF22 Tet-On aSyn cells (Supplementary Fig. S2B) confirmed the progressive increase of transgene expression levels from 48 to 72 h of doxycycline induction and a strong immunoreactive band at 12 days of induction (2.0-, 7.4-, and 13.4-fold induction at 48 and 72 h and 12 days of doxycycline treatment,

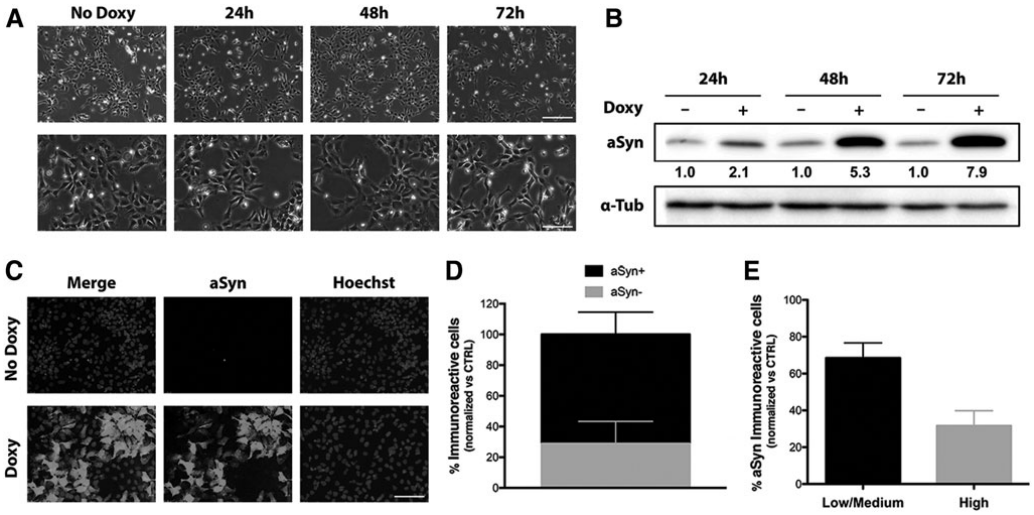

FIG. 1. Modulation of wt aSyn expression in AF22 Tet-On aSyn cells. **(A, B)** Time course of aSyn induction in AF22 Tet-On aSyn cells treated with 750 ng/mL doxycycline. **(A)** Phase contrast pictures of AF22 Tet-On aSyn cells during time-course induction of aSyn. Scale bars: *upper panels* 200 μm; *lower panels* 100 μm. **(B)** Representative image of western blot assays of time-course induction of aSyn. Densitometric quantification was normalized on α-tubulin expression versus untreated cells. **(C–E)** Immunocytochemistry analysis for aSyn on AF22 Tet-On aSyn cells untreated and treated with 750 ng/mL doxycycline for 72 h and quantification of immunopositive cells. **(C)** Representative immunofluorescent images showing $aSyn^{+ve}$ cells in AF22 Tet-On aSyn cultures. Hoechst was used for nuclear staining. Scale bar: 100 μm. **(D)** Quantification of the total number of $aSyn^{+ve}$ cells in basal and induced conditions. **(E)** Quantification of the percentage of $aSyn^{high}$ cells and $aSyn^{low/Med}$ cells among the overall population of $aSyn^{+ve}$ cells in induced AF22 Tet-On aSyn cells. aSyn, alpha-synuclein; wt, wild-type.

respectively) (Supplementary Fig. S2C). On the whole, these results indicate that aSyn induction in AF22 Tet-On aSyn cells is maintained long-term and progressive in aSyn accumulation.

wt aSyn overexpression affects cell division and cell viability in AF22 Tet-On aSyn cells

To test if aSyn induction in the cultures results in phenotypic abnormalities on hNSCs growth, we performed a cell growth assay on AF22 Tet-On aSyn cells. Since aSyn has been described to influence mitochondrial activity, we decided to avoid mitochondrial activity-based growth assays. We thus performed an automated high-throughput screening (HTS) cell count of stained cell nuclei on cultures fixed at defined time points.

aSyn induction produced a slight reduction in cell growth already after 72 h and this effect was more marked at later time points (Figs. 1A and 2A), where a strong impairment in the growth occurred (% reduction in cell number: 34.12 and 44.74 at 5 and 7 days, respectively) (Fig. 2A). These data could be interpreted by possible effects elicited by aSyn either on (1) cell division, (2) cell death, (3) change of fate by induction of differentiation, or (4) a combination of the abovementioned effects.

To dissect out which of these possibilities was prominent, we performed specific assays. Analysis of phospho-Histone $H3^{+ve}$ cells present in the cultures at different time points (Supplementary Fig. S3) showed a reduction, although not statistically significant, of phospho-Histone $H3^{+ve}$ cells occurring both at 72 and 96 h of induction (Fig. 2B). A statistically significant 47.16% reduction was appreciated at 120 h (Fig. 2B). Furthermore, a stronger statistically significant reduction of phospho-Histone $H3^{+ve}$ cells in $aSyn^{+ve}$ cells compared with $aSyn^{-ve}$ cells was visible, at all the time points considered (% of reduction of phospho-Histone $H3^{+ve}$ cells in $aSyn^{+ve}$ cells in culture: 82.3, 96.79, and 91.54 at 3, 4, and 5 days, respectively) (Fig. 2C). These results indicate that aSyn induction affects cell division in AF22 Tet-On aSyn cells.

Furthermore, immunofluorescent analysis for NSC markers (Nestin and Sox2), neurons (β3-Tubulin), and astrocytes (GFAP) indicated that more than 97% of the cells retain their normal NSC identity without any significant induction of neuronal or glial cells (not shown), thus indicating that aSyn overexpression in self-renewing conditions does not force differentiation.

To test if aSyn induction could also impact on cell survival, we performed an immunofluorescent analysis for cleaved Caspase-3 at different time points following doxycycline treatment (Supplementary Fig. S4). aSyn induction led to a marked increase in the number of apoptotic cells in culture (fold increase of cleaved $Caspase\text{-}3^{+ve}$ cells in culture: 3.31, 2.03, and 2.19 at 3, 4, and 5 days, respectively) (Fig. 2D). Mitochondrial impairments have been explored in many aSyn assays both in vivo and in vitro. Besides impaired mitochondrial function, aSyn has been demonstrated to induce severe mitochondrial fragmentation in a number of

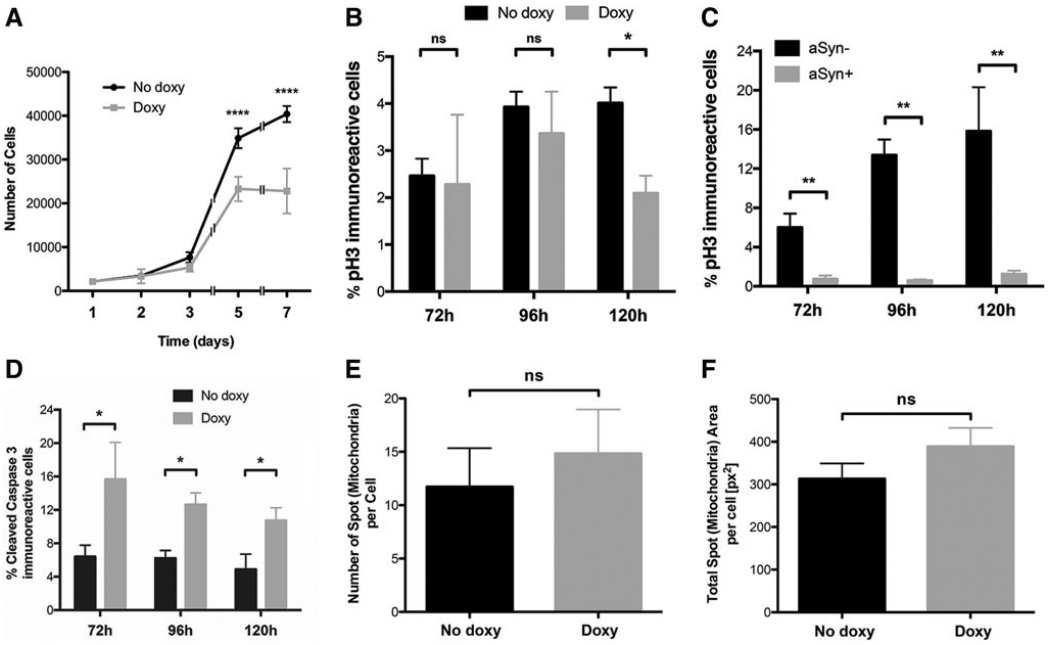

FIG. 2. wt aSyn expression affects proliferation and cell viability of AF22 Tet-On aSyn cells. **(A)** Cell growth assay on basal or induced AF22 Tet-On aSyn cells. **(B, C)** Quantification of time-course immunofluorescent analysis for phospho-Histone H3 on AF22 Tet-On aSyn cells untreated or treated with 750 ng/mL doxycycline. **(B)** Quantification of the total number of phospho-Histone H3 immunopositive cells at defined time points. **(C)** Quantification of the percentage of phospho-Histone H3 immunopositive cells in induced AF22 Tet-On aSyn cells. **(D)** Quantification of time-course immunofluorescent analysis for cleaved Caspase 3 on AF22 Tet-On aSyn cells treated or not with 750 ng/mL doxycycline and relative quantification of immunoreactive cells. **(E, F)** Mitotracker staining on AF22 Tet-On aSyn cells treated with or without 750 ng/mL doxycycline for 120 h and relative quantification of mitochondrial spots. **(E)** Quantification of the number of spots (mitochondria) per cell. **(F)** Quantification of the total spot (mitochondria) area per cell. Normalization was performed on the populations of $aSyn^{+ve}$ and $aSyn^{-ve}$ cells **(B, C)** or on the total number of cells **(D)**. $*P<0.05$, $**P<0.01$, $****P<0.0001$. ns, non-significant.

cell culture studies. We thus explored by automated analysis, mitochondria number in basal and doxycycline-treated (5 days) cells in self-renewal condition (Fig. 2E, F and Supplementary Fig. S5). We did not find any significant variation on this parameter and also on mitochondrial size (not shown) in relation to aSyn induction.

On the whole, these results indicate that aSyn overexpression in hNSCs leads to a reduced cell growth by a double action, both by affecting proliferation capability and by enhancing cell death occurrence. Importantly, further analysis is required to dissect the contribution of mitochondrial dysfunction to these events.

Conditional overexpression of wt aSyn leads to the formation of intracellular aggregates in AF22 Tet-On aSyn cells

aSyn has been shown to generate aggregates inside of the cells and that these may contribute to cellular dysfunctions. Immunofluorescence analysis for aSyn in AF22 Tet-On aSyn cells following 12 days of doxycycline treatment showed that a fraction of $aSyn^{+ve}$ cells exhibited punctate immunoreactive dots in the cytoplasm (arrows in Fig. 3A). aSyn aggregates were present both in $aSyn^{high}$ cells and $aSyn^{low/Med}$ cells, although the former presented higher number of aggregates with respect to the latter (number of aggregates: 0.48 ± 0.19 and 3.14 ± 0.32 in $aSyn^{low/Med}$ and $aSyn^{high}$ cells, respectively) (Fig. 3B). Also, aggregates in $aSyn^{high}$ cells exhibited a 5.8-fold increase in the immunoreactive signal with respect to the ones present in $aSyn^{mod/low}$ cells (Fig. 3C). Furthermore, $aSyn^{high}$ cells showed a 3.1-fold increase in the parameter of area of aggregated spots with respect to $aSyn^{mod/low}$ cells (Fig. 3D).

To exclude that the $aSyn^{+ve}$ spots we detect in our cultures might be the result of nonspecific apoptosis-related structures instead of aggregation process, we performed a double immunofluorescent staining for Cleaved Caspase-3 (Supplementary Fig. S6). The presence of $aSyn^{+ve}$ spots in Cleaved Caspase-3^{-ve} cells (Supplementary Fig. S6) excluded this possibility, nevertheless, additional biochemical analyses will be required to deeper investigate the properties of these structures.

These results indicate that aSyn overexpression produces aggregation on long-term induced AF22 Tet-On aSyn cells and that the occurrence of aggregation is dependent on the level of aSyn overexpression, with $aSyn^{high}$ cells producing

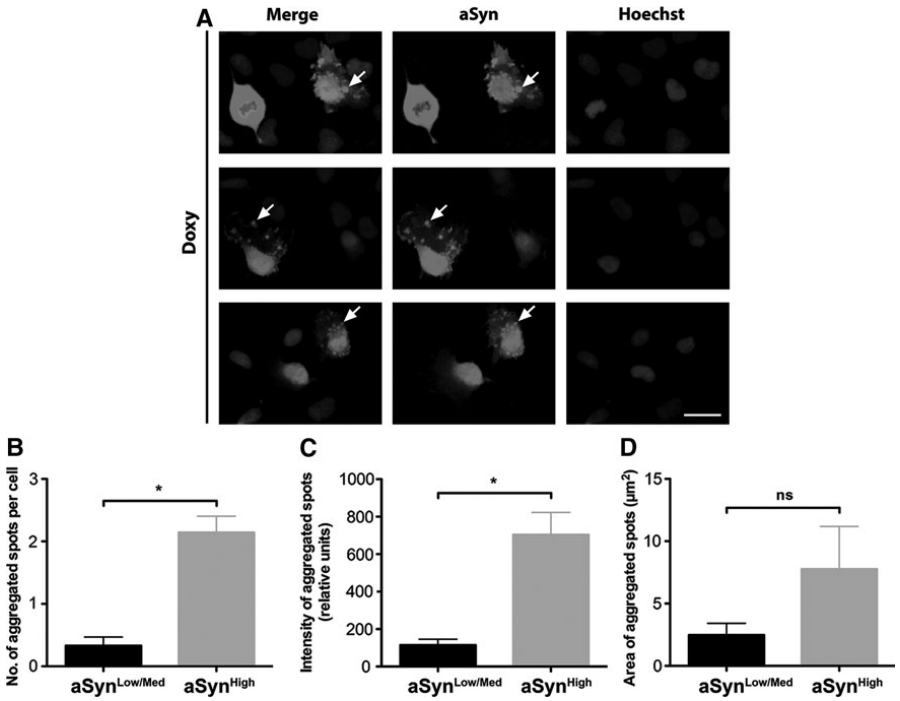

FIG. 3. Conditional overexpression of wt aSyn leads to the formation of intracellular $aSyn^{+ve}$ aggregates in AF22 Tet-On aSyn cells. **(A–D)** Immunocytochemistry analysis for aSyn on AF22 Tet-On aSyn cells treated with 750 ng/mL doxycycline for 12 days and relative evaluation of aSyn aggregates. **(A)** Representative pictures of AF22 aSyn Tet-On treated with 750 ng/mL doxycycline for 12 days and stained for aSyn and Hoechst. *Arrows* indicate aSyn aggregates. Scale bar: 25 µm. **(B)** Quantification of the number of aSyn aggregates per cell in $aSyn^{Low/Medium}$ and $aSyn^{High}$ cells. **(C)** Quantification of the intensity of the fluorescent signal of the aSyn aggregated spots in $aSyn^{Low/Medium-}$ and $aSyn^{High}$-expressing cells. **(D)** Quantification of the area of aSyn aggregated spots in $aSyn^{Low/Medium-}$ and $aSyn^{High}$-expressing cells. $*P < 0.05$.

more aggregated spots with greater intensity with respect to $aSyn^{mod/low}$ cells.

aSyn overexpression impairs neuronal differentiation in AF22 Tet-On aSyn cells

aSyn overexpression has been indicated as a main player in neuronal dysfunction. To test if aSyn induction in AF22 Tet-On aSyn cells could induce defects in the neuronal differentiation potential of the cultures, AF22 Tet-On aSyn cells (CTRL and cells maintained in doxycycline for the entire differentiation procedure) were exposed to a 2-week neuronal differentiation protocol. In these conditions, cells started to show morphological changes indicative of their progressive neuronal maturation. Immunofluorescence analysis on 14-day induced cultures showed that $73.25\% \pm 1.97\%$ of the cells in culture were $aSyn^{+ve}$ (not shown). As expected, at this stage, not induced cultures were mainly composed of β3-$tubulin^{+ve}$ neurons (% of β3-$tubulin^{+ve}$ cells: 87.52 ± 6.09) (Supplementary Fig. S7A) with only a fraction of the cells in the culture positive for Map2, a marker for mature neurons (% of $Map2^{+ve}$ cells: 21.14 ± 4.35) (Supplementary Fig. S7B). On the contrary, doxycycline-treated cultures showed a 51.85% and 38.45% reduction in the overall number of β3-$tubulin^{+ve}$ cells and $Map2^{+ve}$ cells, respectively (Fig. 4B). These results indicate that aSyn overexpression partially affects neuronal differentiation capability of hNSCs.

We next asked if the reduction in the number of neuronal cells is mainly due to (1) induced competence to differentiate toward non-neuronal fates (ie, shift from neurogenic versus gliogenic fate) or (2) to an impaired competence of the cells to start the neuronal differentiation process. In this respect, we found that aSyn overexpression induced a 7.61-fold increase in the number of $GFAP^{+ve}$ cells (% of $GFAP^{+ve}$ cells: 0.46 ± 0.23 and 3.57 ± 0.61 in not induced and doxycycline-induced cells, respectively) (Fig. 4B and Supplementary Fig. S7C) in the cultures, thus indicating a possible enhanced propensity of the cells to differentiate toward the astrocytic lineage. Furthermore, Sox2 immunofluorescence showed the presence of large clusters of $Sox2^{+ve}$ cells in the doxycycline-treated culture with a 12-fold increase in the number of $Sox2^{+ve}$ cells, thus indicating that aSyn overexpression increased the percentage of the cell's refractory to undergo neuronal differentiation process (Fig. 4B and Supplementary Fig. S8).

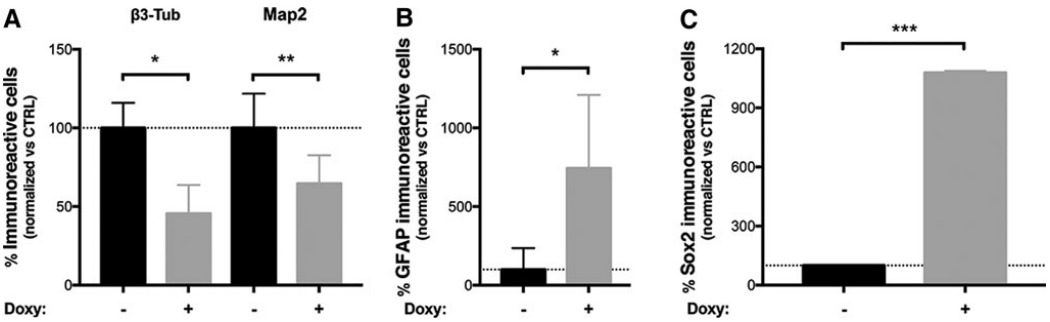

FIG. 4. aSyn expression impairs neuronal differentiation of AF22 Tet-On aSyn cells. **(A–C)** Effects of aSyn expression on neuronal differentiation of AF22 Tet-On aSyn cells treated or not with 750 ng/mL of doxycycline for the entire differentiation process (14 DIV). **(A)** Quantification of the total number of β3-Tubulin^{+ve} and Map2^{+ve} cells on basal and induced conditions. Values are normalized over the basal condition. **(B)** Quantification of the total number of GFAP^{+ve} cells on basal and induced conditions. **(C)** Quantification of the total number of Sox2^{+ve} cells on basal and induced conditions. Values are normalized over the number of immunoreactive cells in basal condition. $*P < 0.05$, $**P < 0.01$, $***P < 0.001$.

On the whole, these results indicate that there is a combined effect of aSyn overexpression in disturbing hNSC neuronal or neurogenic process.

aSyn overexpression affects cell viability in AF22 Tet-On aSyn cell-derived dopaminergic neurons

AF22 cells have the competence to differentiate toward dopaminergic neuronal fate in defined in vitro conditions [19]. Thus, we next analyzed the possible effects elicited by aSyn acute induction in long-term differentiated hNSC-derived dopaminergic neuronal cultures. To this aim, self-renewing AF22 Tet-On aSyn cells were patterned for 3 weeks with FGF8/SHH and then induced to differentiate to dopaminergic neurons for 3 weeks as previously reported [19,21]. After 3 weeks of dopaminergic neuronal maturation, cultures were mainly composed of neurons (% of β3-tubulin^{+ve} cells: 86.53 ± 7.17), most of which were dopaminergic neurons positive for Nurr-1 (% of Nurr-1^{+ve}/β3-tubulin^{+ve} neurons: 74.43% ± 8.26%) (Supplementary Fig. S9A) and tyrosine hydroxylase (TH) (Supplementary Fig. S9B).

At this stage, acute aSyn overexpression was achieved by treating the cultures for 4 days with 750 ng/mL doxycycline. aSyn overexpression produced an acute toxic effect resulting in the degeneration of the neuronal cells in culture (% reduction of the total number of neurons in aSyn-induced cultures: 24.72 ± 6.13) (Supplementary Fig. S9A) and by a 1.94-fold increase in the number of cleaved Caspase-3^{+ve} cells (Fig. 5A and Supplementary Fig. S9C). Quantitative analysis showed that the fraction of Nurr-1^{+ve}/β3-tubulin^{+ve} neurons was significantly decreased following aSyn induction (% reduction of the number of Nurr-1^{+ve}/β3-tubulin^{+ve} neurons in aSyn-induced cultures: 31.72 ± 4.36) (Fig. 5B) with only a minor effect on the Nurr-1^{-ve}/β3-tubulin^{+ve} neurons, that were not significantly affected by acute aSyn overexpression (Fig. 5C). Thus, aSyn overexpression impairs the survival of hNSC-derived neurons, with dopaminergic neurons being differentially affected with respect to nondopaminergic neuronal subtypes.

Discussion

Although aSyn is considered of relevance for PD pathogenic process, the molecular mechanism triggering PD

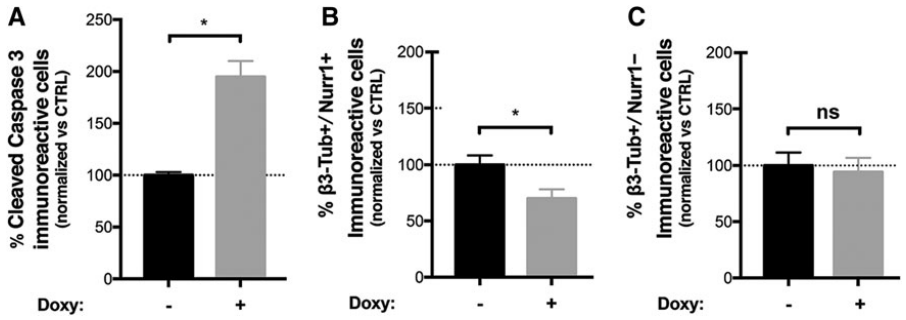

FIG. 5. aSyn overexpression affects cell viability in AF22 Tet-On aSyn cell-derived dopaminergic neurons. **(A–C)** Effects of acute aSyn induction (21–25 DIV) on AF22 Tet-On aSyn cell-derived dopaminergic neurons. **(B)** Quantification of the total number of Cleaved Caspase 3^{+ve} cells on basal and induced conditions. Values are normalized over the basal condition. **(C)** Quantification of the total number of β3-Tubulin^{+ve}/Nurr1^{-ve} cells on basal and induced conditions. Values are normalized over the basal condition. $*P < 0.05$.

starting from aSyn homeostasis alteration is still a matter of debate. In this study, we report the generation of a novel cellular model based on the overexpression of wt human aSyn in NSCs. The system is characterized by the controlled expression of wt human aSyn by means of a Tet-On inducible mechanism and represents a valuable tool to study the effects of aSyn overexpression in hNSCs and neurons.

The AF22 Tet-On aSyn cell model developed in this study has several features that make it attractive for studying the biological and molecular effects elicited by aSyn in different developmental paradigms. These include the hNSC nature of the parental AF22 cells. Originally, described by Falk et al. [19], these cells have been obtained from normal hiPSCs and show features that make them ideal as parental cells to be engineered. Indeed, they are homogeneously composed of self-renewing NSCs characterized by genomic stability and high amenability to genetic manipulation. Importantly, these cells maintain a stable high neurogenic capability along long-term in vitro expansion and the competence to respond to specific patterning cues that allows generating defined neuronal subtype populations, including dopaminergic neurons.

The inducible nature of aSyn expression coupled to the NSC system opens to the possibility to study both acute and chronic aSyn-mediated effects in defined relevant cell populations, that is, neural progenitors and mature neurons. Also, this is instrumental to sort out specific effects in several processes, including self-renewing, lineage commitment, and neuronal maturation and/or maintenance.

aSyn inducible systems have been reported from different immature parental cell lines, mainly PC12 cells and human neuroblastoma lines [12,13,22–24]. Nonetheless, these systems have some intrinsic limitations that are overcome in AF22 Tet-On aSyn cell model. Indeed, PC12 cells are of rodent origin and species-specific differences in aSyn sequence and roles have been reported [25–27]. Additionally, both PC12 cells and neuroblastoma lines are transformed and share a non-CNS origin. Noteworthy, their neurogenic potential is limited in terms of efficiency and quality of neuronal-like cells that can be obtained following their differentiation, thus limiting their physiological relevance for studies aimed at dissecting aSyn roles in human CNS neurons.

AF22 Tet-On aSyn cells show a clear dose–response transgene expression with a robust aSyn induction up to seven- to eightfold; also, induction can be maintained long term leading to a progressive increase in aSyn levels. When we tried to induce aSyn aggregation in AF22 Tet-On aSyn cells, we found that this process requires a prolonged induction period allowing to aSyn levels to increase progressively. The appearance of aSyn aggregates in AF22 Tet-On aSyn cells occurs after 12 days of induction. Other studies performed on PC12/TetOn aSyn inducible systems failed to observe wt aSyn aggregates in proliferating cells [22]. This could be due to the different origins of the parental cells or to the fact that levels of aSyn induction are lower or due to the quite reduced time of induction with respect to our study. Also, several reports have shown different oligomeric aSyn forms and prion-like transmission of aSyn in vitro and in vivo. Further investigation is required to dissect these aspects in our cellular system, both in self-renewal and differentiating conditions.

It is interesting to note that wt aSyn overexpression induces phenotypic defects in hNSCs in the self-renewing state. Other studies have reported that overexpression of aSyn in the proliferating state fails to induce any cell death in proliferating neural-like cells, despite the prominent accumulation of aSyn aggregates [12]. The factors accounting for the differential death effects could include differences in clearance mechanisms, or involvement of cell cycle molecules or other proteins differentially expressed in the two states.

An increasing number of studies reveal that aSyn may play an important role in neurogenesis. When the SNCA gene is differentially expressed or bears mutations, the in vivo NSC pool is negatively regulated and both neurogenesis and survival of newly generated neurons are decreased [9]. These studies suggest that a link might exist among neurogenesis, aSyn, and neurodegenerative diseases [18].

In vitro, aSyn overexpression has been described to reduce the number of mouse secondary neurospheres formed and to affect NSC morphology and cell cycle progression, leading to their accelerated differentiation [10]. hiPSC-derived neuronal precursor cells from a PD patient carrying a genomic triplication of the SNCA gene showed substantial impairments in growth, viability, cellular energy metabolism, and stress resistance. These effects were exacerbated when the cultures were challenged by starvation or toxic stimuli [16]. Also, overexpression of wt aSyn in expanded populations of progenitors derived from the human fetal cortex showed a slight effect on cell growth and a progressive impairment of lineage commitment competence [17]. Similarly, studies on human embryonic stem cell (hESC)-derived neural progenitors overexpressing wt aSyn and on neural progenitors obtained from hiPSCs from a PD patient with a *SCNA* locus triplication, showed an increased cell death and reduced neurogenic capacity compared with control cultures [17,28].

Our results confirm that overexpression of human wt aSyn impairs the process of differentiation of hNSCs into neuronal cells. In particular, we have seen a marked reduction on the efficiency of the cells to generate neurons when exposed to neuronal differentiative cues with a parallel increase in the number of astrocytes and undifferentiated cells.

Further studies are required to dissect the molecular mechanisms triggering these specific defects. PSC-derived long-term expandable hNSCs, including the AF 22 cells, are highly responsive to efficiently undergo neuronal differentiation when exposed to the neuronal differentiation protocol employed in this study[19,21]. Additional investigation is required to define if this defect is maintained when exposing the cultures to other proneuronal differentiation conditions. Furthermore, exposure to non-neuronal (ie, gliogenic) differentiation cues could help to understand if the observed refractoriness to exit self-renewal is specific for the transition toward the neuronal lineage or is a more general aSyn-mediated effect. Finally, we cannot exclude aSyn-selective toxicity toward specific cell types might contribute to these alterations. Besides this, we have in this study reported an aSyn-driven effect on hNSCs neurogenic process that results in increased number of astrocytes found in neuronally differentiating cultures.

Other studies have reported that wt aSyn overexpression in human neural progenitors derived from fetal cortex

preserved the neurogenic competence of the cells following long-term expansion [17]. To this respect, we can speculate that this discrepancy might be related to the different nature and identity between our and the abovementioned cell system. Indeed, differently from fetal brain-derived cell systems that are representative of late developmental neural stages and in which the neurogenic competence quickly declines with in vitro passages, the PSC-derived hNSCs we employed are representative of earlier developmental neural stages and are extremely stable also following extensive long-term expansion [29].

Finally, we have observed an aSyn-mediated acute toxicity in hNSC-derived neurons, being dopaminergic neurons selectively affected. These results are in agreement with a previous study reporting acute aSyn toxicity in hESC-derived neuronal cultures [17]. Those authors showed that hESC-derived neuronal cultures are highly vulnerable to expression of both wt aSyn or mutant aSyn forms, with dopaminergic neurons exhibiting higher toxic susceptibility with respect to nondopaminergic (GABAergic) neurons. It is yet unclear the reason of this neuronal subtype's selective cytotoxicity. The factors accounting for this differential death effects in different neuronal subtypes are unknown but could include differences in clearance mechanisms or other proteins differentially expressed in the two states. Interestingly, aSyn overexpression has been shown to directly affect TH expression, suggesting possible direct TH effects [30]. Regardless of the exact reason, this fact further validates the current model as one in which toxic effects occur preferentially in dopaminergic neurons.

In conclusion, we have developed a cell system for controlled expression of wt aSyn in hNSCs that exhibit defined aSyn-driven phenotypes both in self-renewal and differentiating/differentiated stages. This novel inducible model may prove valuable in the deciphering of aSyn-mediated pathogenic effects and in the assessment and screening of potential therapeutic strategies.

Acknowledgments

The authors wish to thank Prof. Austin Smith (Cambridge Stem Cell Institute, University of Cambridge) for providing the AF22 cell line, Dr. Tilo Kunath (MRC Center for Regenerative Medicine, University of Edinburgh, UK) for the pLVX-TetOn-Puro-human aSyn vector, and Prof. Massimo Pizzato for the psPax2 vector. They also thank the personnel of Cibio HTS Core Facility and of Advanced Imaging Core Facility. This work was supported by the intramural funding from the University of Trento.

Author Disclosure Statement

No competing financial interests exist.

References

1. Spillantini MG, ML Schmidt, VM Lee, JQ Trojanowski, R Jakes and M Goedert. (1997). Alpha-synuclein in Lewy bodies. Nature 388:839–840.
2. Bendor JT, TP Logan and RH Edwards. (2013). The function of alpha-synuclein. Neuron 79:1044–1066.
3. Simon-Sanchez J, C Schulte, JM Bras, M Sharma, JR Gibbs, D Berg, C Paisan-Ruiz, P Lichtner, SW Scholz, et al. (2009). Genome-wide association study reveals genetic risk underlying Parkinson's disease. Nat Genet 41:1308–1312.
4. Singleton AB, M Farrer, J Johnson, A Singleton, S Hague, J Kachergus, M Hulihan, T Peuralinna, A Dutra, et al. (2003). Alpha-synuclein locus triplication causes Parkinson's disease. Science 302:841.
5. Ibanez P, AM Bonnet, B Debarges, E Lohmann, F Tison, P Pollak, Y Agid, A Durr and A Brice. (2004). Causal relation between alpha-synuclein gene duplication and familial Parkinson's disease. Lancet 364:1169–1171.
6. Crews L, H Mizuno, P Desplats, E Rockenstein, A Adame, C Patrick, B Winner, J Winkler and E Masliah. (2008). Alpha-synuclein alters Notch-1 expression and neurogenesis in mouse embryonic stem cells and in the hippocampus of transgenic mice. J Neurosci 28:4250–4260.
7. Desplats P, B Spencer, L Crews, P Pathel, D Morvinski-Friedmann, K Kosberg, S Roberts, C Patrick, B Winner, J Winkler and E Masliah. (2012). Alpha-synuclein induces alterations in adult neurogenesis in Parkinson disease models via p53-mediated repression of Notch1. J Biol Chem 287:31691–31702.
8. Kohl Z, N Ben Abdallah, J Vogelgsang, L Tischer, J Deusser, D Amato, S Anderson, CP Muller, O Riess, et al. (2016). Severely impaired hippocampal neurogenesis associates with an early serotonergic deficit in a BAC alpha-synuclein transgenic rat model of Parkinson's disease. Neurobiol Dis 85:206–217.
9. Winner B, DC Lie, E Rockenstein, R Aigner, L Aigner, E Masliah, HG Kuhn and J Winkler. (2004). Human wild-type alpha-synuclein impairs neurogenesis. J Neuropathol Exp Neurol 63:1155–1166.
10. Tani M, H Hayakawa, T Yasuda, T Nihira, N Hattori, Y Mizuno and H Mochizuki. (2010). Ectopic expression of alpha-synuclein affects the migration of neural stem cells in mouse subventricular zone. J Neurochem 115: 854–863.
11. Domert J, C Sackmann, E Severinsson, L Agholme, J Bergstrom, M Ingelsson and M Hallbeck. (2016). Aggregated alpha-synuclein transfer efficiently between cultured human neuron-like cells and localize to lysosomes. PLoS One 11:e0168700.
12. Ko LW, HH Ko, WL Lin, JG Kulathingal and SH Yen. (2008). Aggregates assembled from overexpression of wild-type alpha-synuclein are not toxic to human neuronal cells. J Neuropathol Exp Neurol 67:1084–1096.
13. Vekrellis K, M Xilouri, E Emmanouilidou and L Stefanis. (2009). Inducible over-expression of wild type alpha-synuclein in human neuronal cells leads to caspase-dependent non-apoptotic death. J Neurochem 109:1348–1362.
14. Corti S, I Faravelli, M Cardano and L Conti. (2015). Human pluripotent stem cells as tools for neurodegenerative and neurodevelopmental disease modeling and drug discovery. Expert Opin Drug Discov 10:615–629.
15. Devine MJ, M Ryten, P Vodicka, AJ Thomson, T Burdon, H Houlden, F Cavaleri, M Nagano, NJ Drummond, et al. (2011). Parkinson's disease induced pluripotent stem cells with triplication of the alpha-synuclein locus. Nat Commun 2:440.
16. Flierl A, LM Oliveira, LJ Falomir-Lockhart, SK Mak, J Hesley, F Soldner, DJ Arndt-Jovin, R Jaenisch, JW Langston, TM Jovin and B Schule. (2014). Higher vulnerability

and stress sensitivity of neuronal precursor cells carrying an alpha-synuclein gene triplication. PLoS One 9:e112413.
17. Schneider BL, CR Seehus, EE Capowski, P Aebischer, SC Zhang and CN Svendsen. (2007). Over-expression of alpha-synuclein in human neural progenitors leads to specific changes in fate and differentiation. Hum Mol Genet 16:651–666.
18. Le Grand JN, L Gonzalez-Cano, MA Pavlou and JC Schwamborn. (2015). Neural stem cells in Parkinson's disease: a role for neurogenesis defects in onset and progression. Cell Mol Life Sci 72:773–797.
19. Falk A, P Koch, J Kesavan, Y Takashima, J Ladewig, M Alexander, O Wiskow, J Tailor, M Trotter, et al. (2012). Capture of neuroepithelial-like stem cells from pluripotent stem cells provides a versatile system for in vitro production of human neurons. PLoS One 7:e29597.
20. Lee BR and T Kamitani. (2011). Improved immunodetection of endogenous alpha-synuclein. PLoS One 6:e23939.
21. Koch P, T Opitz, JA Steinbeck, J Ladewig and O Brüstle. (2009). A rosette-type, self-renewing human ES cell-derived neural stem cell with potential for in vitro instruction and synaptic integration. Proc Natl Acad Sci U S A 106:3225–3230.
22. Batelli S, E Peverelli, S Rodilossi, G Forloni and D Albani. (2011). Macroautophagy and the proteasome are differently involved in the degradation of alpha-synuclein wild type and mutated A30P in an in vitro inducible model (PC12/TetOn). Neuroscience 195:128–137.
23. Larsen KE, Y Schmitz, MD Troyer, E Mosharov, P Dietrich, AZ Quazi, M Savalle, V Nemani, FA Chaudhry, et al. (2006). Alpha-synuclein overexpression in PC12 and chromaffin cells impairs catecholamine release by interfering with a late step in exocytosis. J Neurosci 26:11915–11922.
24. Tanaka Y, S Engelender, S Igarashi, RK Rao, T Wanner, RE Tanzi, A Sawa, V Dawson L, TM Dawson and CA Ross. (2001). Inducible expression of mutant alpha-synuclein decreases proteasome activity and increases sensitivity to mitochondria-dependent apoptosis. Hum Mol Genet 10:919–926.
25. Hamilton BA. (2004). Alpha-synuclein A53T substitution associated with Parkinson disease also marks the divergence of Old World and New World primates. Genomics 83:739–742.
26. Lee M, D Hyun, B Halliwell and P Jenner. (2001). Effect of the overexpression of wild-type or mutant alpha-synuclein on cell susceptibility to insult. J Neurochem 76:998–1009.
27. Xu J, SY Kao, FJ Lee, W Song, LW Jin and BA Yankner. (2002). Dopamine-dependent neurotoxicity of alpha-synuclein: a mechanism for selective neurodegeneration in Parkinson disease. Nat Med 8:600–606.
28. Oliveira LM, LJ Falomir-Lockhart, MG Botelho, KH Lin, P Wales, JC Koch, E Gerhardt, H Taschenberger, TF Outeiro, et al. (2015). Elevated alpha-synuclein caused by SNCA gene triplication impairs neuronal differentiation and maturation in Parkinson's patient-derived induced pluripotent stem cells. Cell Death Dis 6:e1994.
29. Conti L and E Cattaneo. (2010). Neural stem cell systems: physiological players or in vitro entities? Nat Rev Neurosci 11:176–187.
30. Baptista MJ, C O'Farrell, S Daya, R Ahmad, DW Miller, J Hardy, MJ Farrer and MR Cookson. (2003). Co-ordinate transcriptional regulation of dopamine synthesis genes by alpha-synuclein in human neuroblastoma cell lines. J Neurochem 85:957–968.

Address correspondence to:
Dr. Luciano Conti
Centre for Integrative Biology—CIBIO
Università degli Studi di Trento
Via Sommarive 9, Povo
38123 Trento
Italy

E-mail: luciano.conti@unitn.it

Received for publication January 15, 2018
Accepted after revision April 18, 2018
Prepublished on Liebert Instant Online April 19, 2018

Supplementary Data

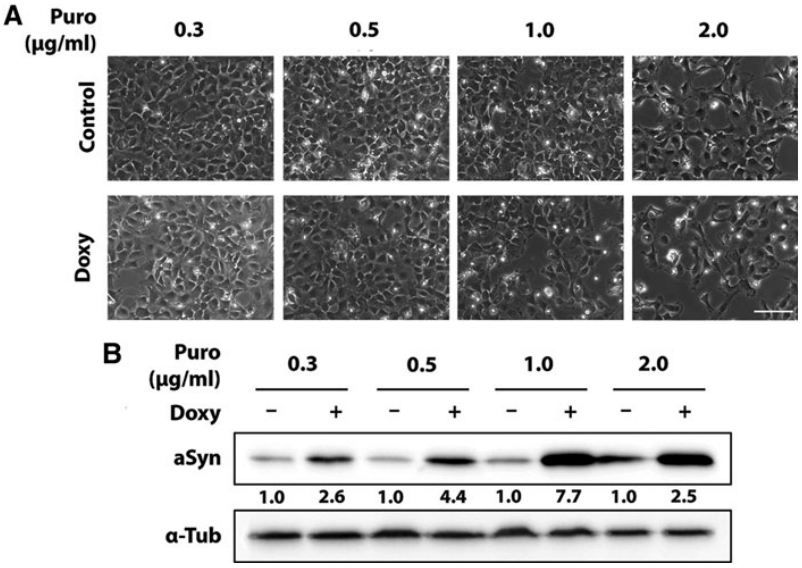

SUPPLEMENTARY FIG. S1. Evaluation of aSyn induction in AF22 Tet-On aSyn cultures selected by means of different doses of puromycin (*upper panel*). Phase contrast images of AF22 Tet-On aSyn cells selected with different doses of puromycin and treated or not with 750 ng/mL of doxycycline for 72 h. Scale bar: 100 μm (*lower panel*). Representative image of a western blot analysis of the cells in **(A)**. Densitometric quantification was normalized on α-tubulin expression and versus untreated cells. aSyn, alpha-synuclein.

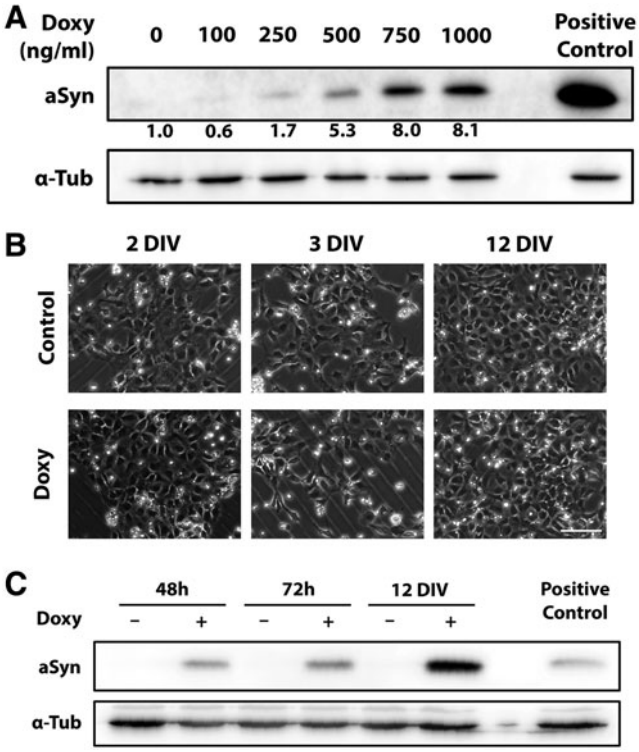

SUPPLEMENTARY FIG. S2. Evaluation of dose–response and long-term aSyn induction in AF22 Tet-On aSyn cultures. **(A)** Dose-dependent αSyn induction in AF22 Tet-On aSyn cells treated with or without doxycycline for 72 h and relative densitometric quantification normalized on α-tubulin expression and versus untreated control. **(B)** Phase contrast pictures of AF22 Tet-On aSyn cultures treated with or without 750 ng/mL doxycycline for the indicated time. Scale bar: 100 μm. **(C)** Kinetics of αSyn induction of AF22 Tet-On aSyn cells treated with 750 ng/mL doxycycline for the indicated time showing a time-dependent accumulation of αSyn levels. Expression is maintained in long-term induced (12 DIV) cultures.

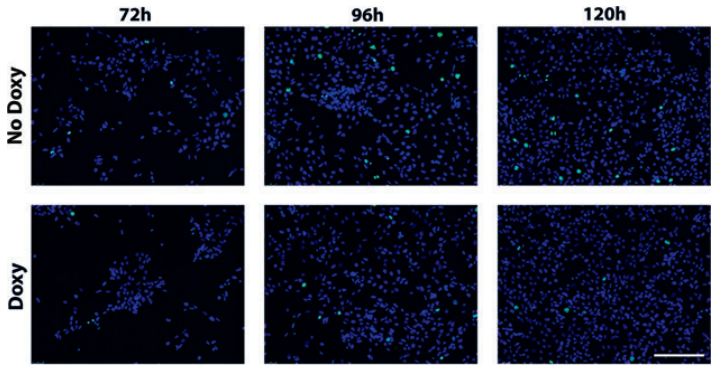

SUPPLEMENTARY FIG. S3. wt aSyn overexpression affects proliferation of AF22 Tet-On aSyn cells. Time course immunofluorescent analysis for phospho-Histone H3 on doxycycline-treated AF22 Tet-On aSyn cells with 750 ng/mL doxycycline and relative quantification of immunopositive cells. Representative pictures of AF22 Tet-On aSyn cells stained for phospho-Histone H3. Hoechst was used for nuclear staining. Scale bar: 200 μm. wt, wild-type.

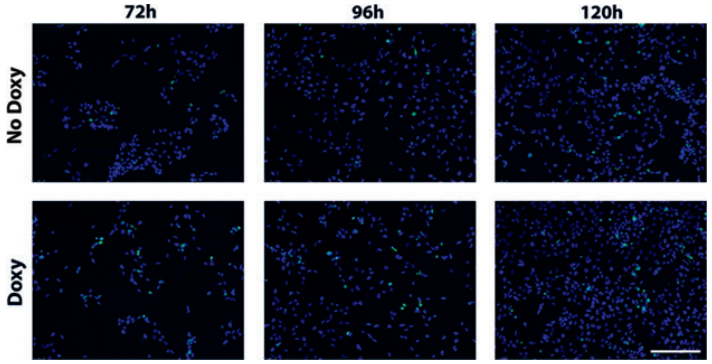

SUPPLEMENTARY FIG. S4. wt aSyn overexpression affects cell viability in AF22 Tet-On aSyn cells. Representative pictures of uninduced or induced AF22 Tet-On aSyn cells stained for cleaved Caspase-3. Hoechst was used for nuclear staining. Scale bar: 200 μm.

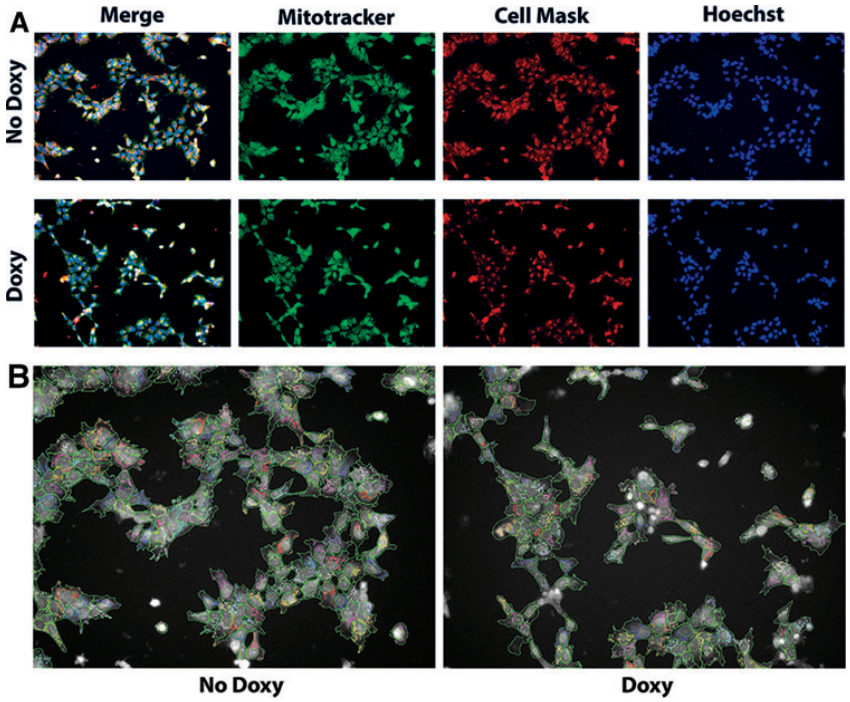

SUPPLEMENTARY FIG. S5. wt aSyn overexpression does not affect mitochondrial number in self-renewing AF22 Tet-On aSyn cells. Mitotracker staining of AF22 Tet-On αSyn cells treated with or without 750 ng/mL doxycycline for 120 h and relative quantification of mitochondrial spots. **(A)** Representative pictures of cultures stained for Mitotracker, Cell Mask, and nuclei. **(B)** Overlay of stained cells with ROIs for quantifying mitochondria. ROIs, regions of interest.

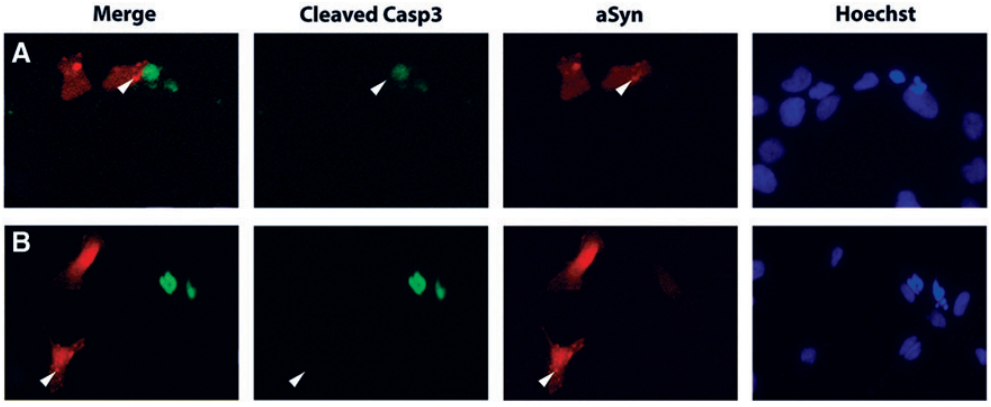

SUPPLEMENTARY FIG. S6. aSyn immunoreactive aggregates do not colocalize with cleaved Caspase-3. Immunocytochemistry analysis for αSyn and cleaved Caspase-3 of AF22 Tet-On αSyn cells treated with or without 750 ng/mL doxycycline for 72 h. **(A, B)** Representative pictures of cultures stained for αSyn, cleaved Caspase-3, and nuclei. *Arrowheads* indicates $aSyn^{+ve}$ aggregates that are negative for cleaved Caspase-3.

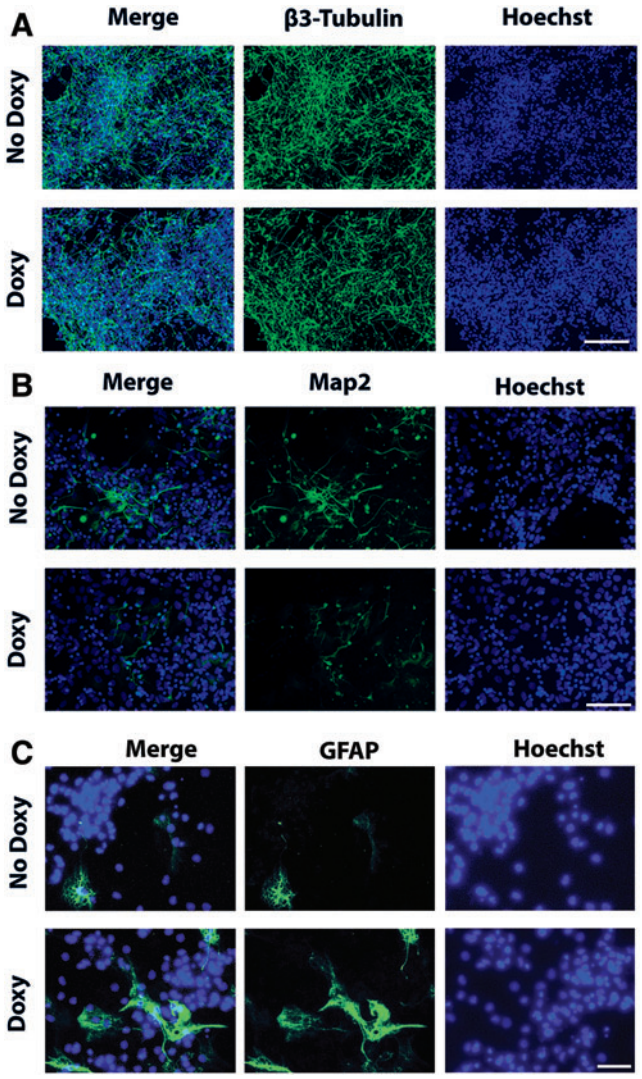

SUPPLEMENTARY FIG. S7. Expression of aSyn disturbs neuronal differentiation of AF22 Tet-On aSyn cells. **(A–C)** Effects of aSyn expression on neuronal differentiation of AF22 Tet-On aSyn cells treated or not with 750 ng/mL of doxycycline for the entire differentiation process (14 DIV). **(A)** Representative pictures of β3-Tubulin^{+ve} cells on 14 DIV cultures of basal and induced AF22 Tet-On aSyn cultures. **(B)** Representative pictures of Map2^{+ve} cells on 14 DIV cultures of basal and induced AF22 Tet-On aSyn cultures. **(C)** Representative pictures of GFAP^{+ve} astrocytes on 14 DIV cultures of basal and induced AF22 Tet-On aSyn cultures. Hoechst was used for nuclear staining. Scale bar: 100 μm **(C)**.

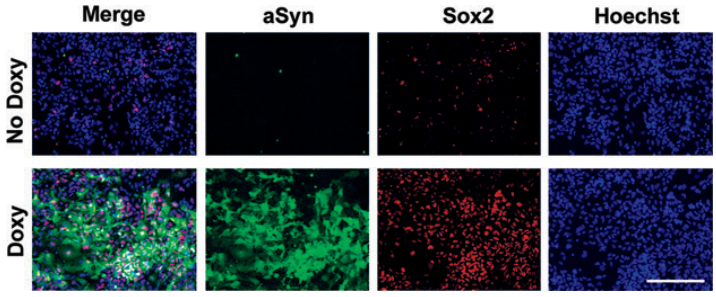

SUPPLEMENTARY FIG. S8. aSyn induction increases the number of undifferentiated cells in AF22 Tet-On aSyn cells undergoing neuronal differentiation process. Effects of aSyn expression on neuronal differentiation of AF22 Tet-On aSyn cells treated or not with 750 ng/mL of doxycycline for the entire differentiation process (14 DIV). Representative pictures of $sox2^{+ve}$ cells on DIV 14 cultures of basal and induced AF22 Tet-On aSyn cultures. The presence of clusters of $sox2^{+ve}$ cells is visible in induced cultures. Hoechst was used for nuclear staining. Scale bar: 100 µm.

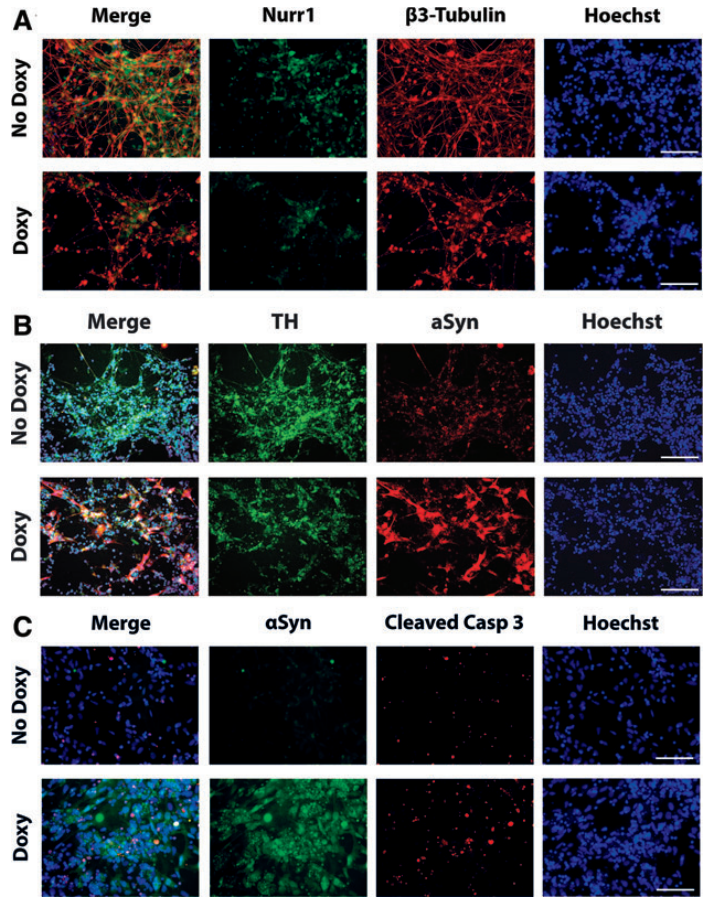

SUPPLEMENTARY FIG. S9. Acute aSyn induction impairs AF22 Tet-On aSyn cell-derived dopaminergic neuron viability. Effects of acute aSyn induction (21–25 DIV) on AF22 Tet-On aSyn cell-derived dopaminergic neurons. **(A)** Representative pictures of β3-$Tubulin^{+ve}$ and $Nurr1^{+ve}$ cells in 25 DIV cultures. **(B)** Representative pictures of TH^{+ve} and $aSyn^{+ve}$ cells in 25 DIV cultures. **(C)** Representative pictures of Cleaved Caspase 3^{+ve} and $aSyn^{+ve}$ cells in 25 DIV cultures. Hoechst was used for nuclear staining. Hoechst was used for nuclear staining. Scale bar: 100 µm.

Supplementary Table S1. List of Primary and Secondary Antibodies Used in the Study

Antigen	*Company*	*Dilution*	*Species*
Alpha-synuclein	Sigma	1:1,000–1:500	Mouse
β3-Tubulin	Promega	1:1,000	Mouse
GFAP	DAKO	1:1,000	Mouse
Sox2	Millipore	1:300	Rabbit
Phospho-histone H3	Chemicon/Millipore	1:500	Rabbit
Cleaved caspase 3	Cell Signaling Technology	1:1,000	Rabbit
Map2	Millipore	1:300	Rabbit
Nurr-1	Santa Cruz Biotechnologies	1:100	Rabbit
TH	Sigma	1:500	Rabbit
Alexa Fluor IgG anti-rabbit 568	Molecular Probes	1:500	Goat
Alexa Fluor IgG anti-rabbit 488	Molecular Probes	1:500	Goat
Immunostar anti-mouse HRP	Bio-Rad	1:2,000	Goat
Immunostar anti-rabbit HRP	Bio-Rad	1:2,000	Goat

HRP, horseradish peroxidase.